The Spectroscopy and Quenching of Some Ion-Pair States of I_2, Br_2 and IBr

by

Michael Alistair MacDonald

A thesis presented for the degree of
Doctor of Philosophy in the
Faculty of Science at the
University of Edinburgh, 1984

Acknowledgements

I begin by expressing my thanks to my two supervisors, Professor R.J. Donovan and Dr. K.P. Lawley. Without their help and encouragement much of the work presented here could not have been carried out. Stimulating discussions with my supervisors helped, on many occasions, to clarify the interpretation of experimental results and ideas for further work. I also wish to thank Dr. C. Fotakis and Dr. J.P.T. Wilkinson for their generous help. Discussions with the four people mentioned above helped to create and maintain my interest in ultra-violet spectroscopy and gas kinetics.

I must also express my gratitude to all members of the research group, past and present, for creating a friendly and interesting working environment. Particular thanks must also go to Mr. J. Broom for glass-blowing the pyrex cells used and for the use of his oven to bake out and clean the cells used.

During the past three years, I have been fortunate enough to visit the S.E.R.C. Rutherford Appleton Laboratory's Ultra-Violet Radiation Facility and the S.E.R.C. Synchrotron Radiation Source at Daresbury. The staff at these two laboratories were most helpful. In particular thanks must be expressed to Dr. M.C. Gower, Ms. J. Szechi and Mr. G. Hogg (R.A.L.) and Dr. I. Munro, Dr. M. Kelly, Dr. D. Shaw and Dr. D. Holland (S.R.S.).

Finally, thanks must be expressed to Mr. I. MacDonald for his help in proof-reading the typescript.

Abstract

The potentials of the ion-pair states of the halogens are dominated by the attraction of the two charges in the ion-pair (of the form r^{-1}). As a result these ion-pair states have large values of r_e and are formed in highly vibrationally excited states by the absorption of a single ultra-violet photon. The resulting fluorescence from these excited states consists mainly of oscillatory continuum fluorescence. Such spectra of I_2 (excited at 193 nm), IBr (excited at 193 nm) and Br_2 (excited at 158 nm) are presented in this thesis. In each case, two spectra are presented under medium (0.35 nm) resolution, one consisting of oscillatory fluorescence to the ground electronic state of the halogen and the other of fluorescence to a repulsive state. For the cases of $I_2(D)$ and $Br_2(K)$ these spectra were inverted by the method of direct spectral simulation to produce potentials for both the ion-pair state and the lower repulsive state probed. The ion-pair state potential was assumed to be in the form of a Rittner potential:

$$U(r) = A \exp(-br) - {}^{C_1}/_{r} + {}^{C_3}/_{r^3} - {}^{C_4}/_{r^4} - {}^{C_6}/_{r^6} + T_\infty$$

For I_2 and Br_2, experiments were carried out to determine how these oscillatory continuum spectra alter when the excitation wavelength producing them is changed. It is also suggested that the existance of mixed isotopic pairs in IBr and Br_2 has a marked effect on the "washing in" of the interference structure.

For all three molecules the ion-pair state accessed belonged to the lowest manifold of ion-pair states for that molecule. That is its diabatic dissociation products were $X^-(^1S) + X^+(^3P_2)$. The states accessed were readily quenched to the lower few vibrational levels of the lowest ion-pair state, the D' state. In studying the process, the total rate of removal of excited $Br_2(K)$ and IBr(D) molecules by quenching with various non-reactive gases was measured. In all cases the quenching was found to be rapid with $k \cong 1\text{-}4 \times 10^{-10}$ cm^3 molecule^{-1}s^{-1}. The pure radiative lifetime of IBr(D) (excited at 188 nm) was measured and found to be 27 ± 4 ns.

The reaction IBr(D) + Xe → XeBr* + I was also studied, it being found that the reaction has a photochemical threshold of 198.5 ± 5 nm, which is the same as the energetic threshold for the reaction. This implies there is no barrier involved in the reaction pathway.

CONTENTS

Chapter 1 - Introduction 1

1.1 General Introduction 2

1.2 The form of Ion-Pair States and the Rittner Potential 4

1.3 Oscillatory Continuum Emission 8

1.4 Nesting of Ion-Pair States and their Physical Quenching 24

1.5 References 28

Chapter 2 - Experimental 29

2.1 General 30

2.2 F_2 Lasers 30

2.3 Broad Band ArF Laser 32

2.4 Line Narrowed ArF Laser 32

2.5 Scanning Monochromator/Photomultiplier Detection System 34

2.6 The Optical Multichannel Analyser (O.M.A.)/Polychromator Detection System 36

2.7 The Sychrotron Radiation Source (SRS) 37

2.8 The Absorption Spectra from Port V.U.V. 3 37

2.9 Time Resolved Measurements on the S.R.S. 41

2.10 Description of Cells used in Experiments 43

2.11 Materials Used 44

2.12 Reference 45

Chapter 3 - The Simulation of Oscillatory Spectra 46

3.1 Introduction 47

3.2 Double Frequency (Interference) Type Spectra 48

3.3 Single Frequency (Reflection) Type Spectra 55

3.4 References 61

Chapter 4 - The Spectroscopy of I_2 $D(O_u^+)$ 62

4.1 Introduction 63

4.2 Experimental 64

4.3 The Absorption Spectrum 67

4.4 Results 71

4.5 References 85

Chapter 5 - The Spectroscopy and Quenching of $Br_2(K)$ 87

5.1 Introduction 88

5.2 Experimental 91

5.3 The Absorption Spectrum 92

5.4 Low Resolution Fluorescence Spectra 95

5.5 Medium Resolution Fluorescence Spectra 98

5.6 The Potentials and Simulated Spectra 103

5.7 Discussion 112

5.8 Quenching of the Upper State 116

5.9 References 122

Chapter 6 - Iodine Monobromide 123

The Spectroscopy and Quenching of IBr(D)

6.1 Introduction 124

6.2 Experimental 126

6.3 The Absorption Spectrum of IBr 127

6.4 The Fluorescence Spectrum of IBr Excited at $\lambda \cong 190$ nm 130

6.5 Physical Quenching of the D state of IBr 143

6.6 The Formation of XeBr(B) from IBr(D) + Xe 157

6.7 References 166

Appendix 1 - An Annotated Copy of the Computer Programme used for Calculating Simulated Spectra

Appendix 2 - Publications

Appendix 3 - Conferences and Lectures Attended

CHAPTER 1

Introduction

1.1 General Introduction

The electronic states of the halogens can be divided into three distinct groups: the low lying valence states, the ion-pair states and the Rydberg states. A diagram showing some selected states from each group for I_2 is reproduced as Figure 1.1. The low lying valence states dissociate to either ground state halogen atoms ($^2P_{3/2}$) or spin orbit excited atoms ($^2P_{\frac{1}{2}}$). They may be either bound or repulsive states. Next, in terms of energy, come the ion-pair states, which, as their name suggests dissociate (diabatically) to form an ion-pair, e.g. $X^-(^1S) + X^+(^3P_2)$. This thesis is mainly concerned with these ion-pair states and they will be discussed in more detail later. The Rydberg states resemble the low lying valence states of the halogens as they are formed by the promotion of a non-bonding (or a very weakly anti-bonding/bonding) electron into an orbit, with a higher principal quantum number, that is too diffuse to exhibit any strong bonding or anti-bonding character. Diabatically, these states dissociate to a highly excited halogen atom (e.g. for I $n \geqslant 6$, ^2P_J) plus a ground state halogen atom.

The potential minima of the lowest group of ion-pair states lie below the potential minimum of the lowest of the Rydberg states, but the ion-pair state diabatic dissociation limit lies above that for the Rydberg states, implying that the potentials will cross at large inter-nuclear separations. In general, the Rydberg and ion-pair

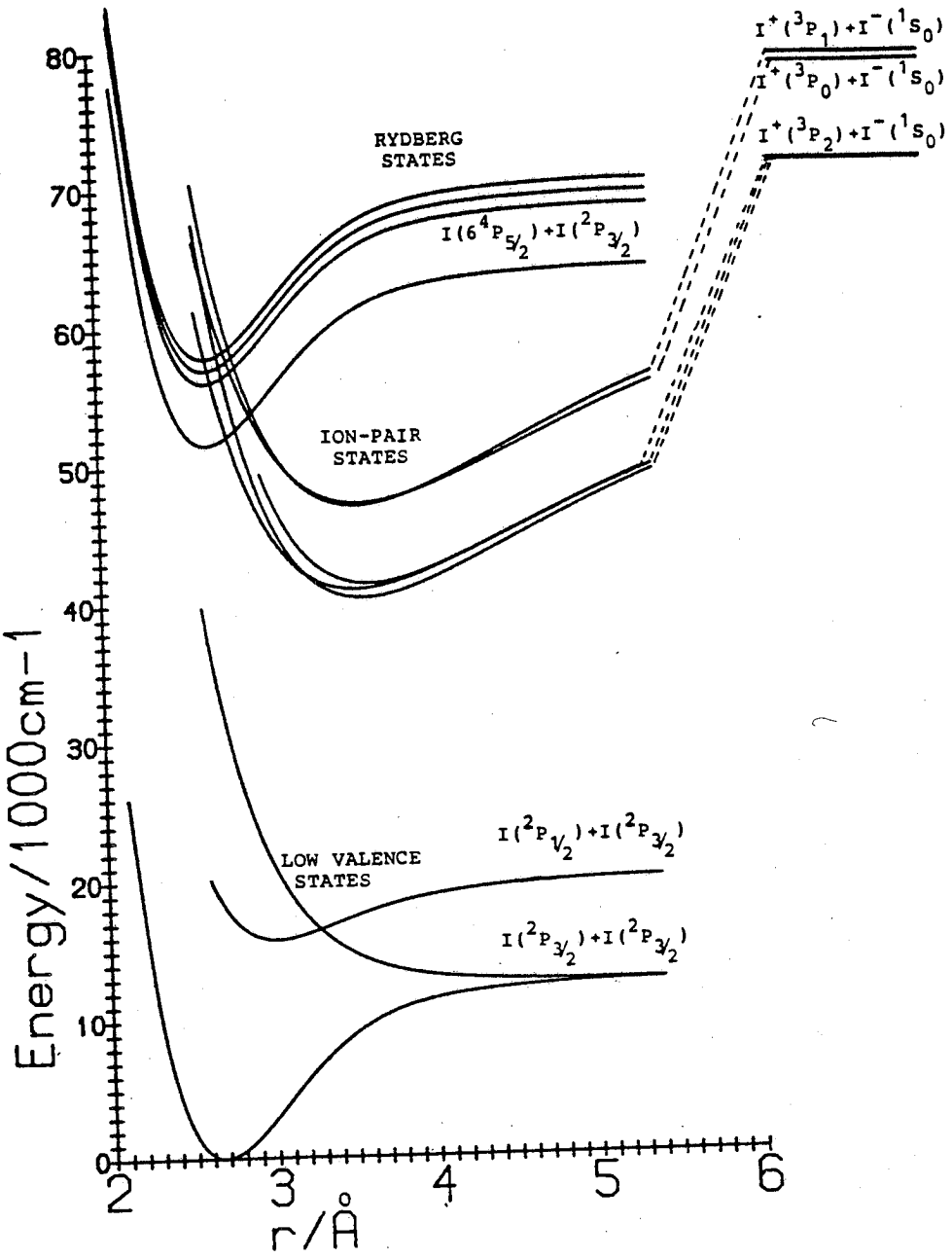

Figure 1.1 Selected low-lying valence states, ion-pair states and Rydberg states of I_2 with their dissociation limits

states will mix at these crossings, meaning that the adiabatic limits for the ion-pair states will correspond to the diabatic dissociation limits for the Rydberg states and vice versa. In this thesis the area of the ion-pair states probed lies below the energy of these avoided crossings and the extrapolations used are diabatic extrapolations.

The ion-pair states of the heavier halogens (e.g. I_2, Br_2, IBr) are lower and thus more accessible than the ion-pair states of other diatomic molecules (e.g. H_2) because of the relatively low ionisation potential and relatively high electron affinity of the halogens. It is not general that the adiabatic dissociation limit of ion-pair states lies below that of Rydberg states.

In this chapter most of the examples will be taken from I_2, although, unless it is specifically stated otherwise, they could equally well be taken from Br_2 or IBr.

1.2 The form of ion-pair states and the Rittner potential

The diabatic dissociation products of an ion-pair state are a pair of singly charged ions. At large separation the attractive force between these two ions will mainly be the charge/charge electrostatic force, acting with the form $\frac{-e^2}{4\pi\varepsilon_o r}$. This term is of much longer range than the r^{-6} term normally dominant at large internuclear separation in the low lying valence states. This has several important

consequences which will be fully discussed below. The attractive limb of the ion-pair states may be represented more fully by including higher multipole expansion terms as follows: the charge/quadrupole term C_3/r^3, the charge/induced dipole term C_4/r^4 and finally the induced dipole/induced dipole term C_6/r^6. Theoretically, the term C_4 is represented as

$$\frac{e^2}{4\pi\varepsilon_o}\left(\frac{\alpha_A + \alpha_B}{2}\right)$$

where e is the electronic charge and α_A and α_B are the polarisabilities of the two ions concerned. The C_6 term is represented, to a fairly good approximation by

$$\frac{3}{2}\alpha_A\alpha_B\left(\frac{\omega_A\omega_B}{\omega_A + \omega_B}\right) \quad (1)$$

where, using the notation of Brand and Hoy,[1] ω_A and ω_B are the ionisation potentials of the two ions involved. Thus, of the terms to be included in the attractive limb of the ion-pair potential, only the C_3 (charge/quadrupole) term is dependent on the exact quantum states of the ions involved, in sign as well as in magnitude. In fact, as the negatively charged ion will normally be ^1S and thus will normally possess no quadrupole moment, only the quantum state of the positive ion will be important.

In order to represent these ion-pair states a repulsive limb has to be added to the multipole expansion terms.

A simple exponential, of the form Aexp(-br), was chosen for this, making the combined potential a Rittner type of potential, which is given fully in equation 1.1.

$$U(r) = Aexp(-br) - {}^{C_1}/_{r} + {}^{C_3}/_{r^3} - {}^{C_4}/_{r^4} - {}^{C_6}/_{r^6} + T_\infty \qquad (1.1)$$

The term T_∞ represents the diabatic dissociation limit of the ion-pair state, which is given by the sum of the ionisation potential and the electron affinity required to produce the separated ions. The term C_3 is given a positive sign because it may be either attractive or repulsive, whereas the terms C_1, C_4 and C_6 must be attractive and so are given a negative sign in equation 1.1.

Only three of the terms in the Rittner potential are generally unknown before any attempt is made to analyse the ion-pair state potential, reducing the job of formulating the potential to that of finding the terms A, b and C_3.

The dominating term for most bondlengths of the ion-pair potential is the ${}^{1}/_{r}$ electrostatic attraction, which has two important effects on the potential. The first effect is that ion-pair potentials are deeply bound with a long range attractive limb, meaning that the existence of highly vibrationally excited levels is possible and that $\langle r^2 \rangle_v$ is very large, even well below dissociation.

The second main effect of this term is that the equilibrium bondlengths of these states tend to be significantly larger than those for the low lying valence states. This, taken with the above, means that absorption from the minimum of the ground state is to areas high up on the repulsive limb of the ion-pair potential, but because these potential wells are so deep the absorption is to bound, but highly excited, vibrational levels. Also the potential well in this area will be very wide and only slowly flattening out to reach the dissociation limit of the state concerned, which will affect the absorption spectrum as follows. Such ion-pair states will, in general, have close vibrational spacing in the region of the state accessible through the absorption spectrum (e.g. a vibrational spacing of 40-50 cm^{-1} for $I_2(D), v \cong 140$). Also, the vibrational spacing in the ion-pair state will only slowly converge to the continuum. Thus, the absorption spectrum will consist of a series of closely spaced vibrational peaks, whose spacing decreases only slowly as one scans the spectrum to shorter wavelengths.

The result of such absorption is to produce a highly vibrationally excited molecule. The combination of such a high level of excitation (e.g. $v \cong 140$ for $I_2(D)$ excited at 193 nm) and the typically large r_e of the ion-pair states has important effects on the fluorescence spectra produced by such excitation and particularly on the production of oscillatory continuum spectra. In particular, it should be noted that a wide range of r is probed in either bound→free or bound→bound fluorescence.

1.3 Oscillatory Continuum Emission

The classical Franck-Condon principle states that when an electronic transition occurs the positions and momenta of the nuclei are unaffected by the transition. The conservation of momentum means that kinetic energy must be conserved too. On this basis a difference potential can be constructed for a transition from an upper electronic state with a given amount of vibrational energy to a lower state. The difference potential, simply, is the locus of points where an electronic transition can conserve both the position and the kinetic energy of the nuclei involved. Figure 1.2 shows the difference potential constructed for the case of a bound upper state and a repulsive lower state. Thus according to the classical Franck-Condon principle, any emission from a diatomic molecule must "land" on the difference potential and in so doing must give out a photon of energy equal to the difference in energy between the initial energy of excitation of the molecule and the energy of the difference potential at the point where the transition "landed". From this a classical spectrum can be predicted. A classical spectrum being the fluorescence spectrum calculated using classica mechanics but taking only the idea that the energy and wavelength of light are connected by $E = h\nu$ from quantum mechanics.

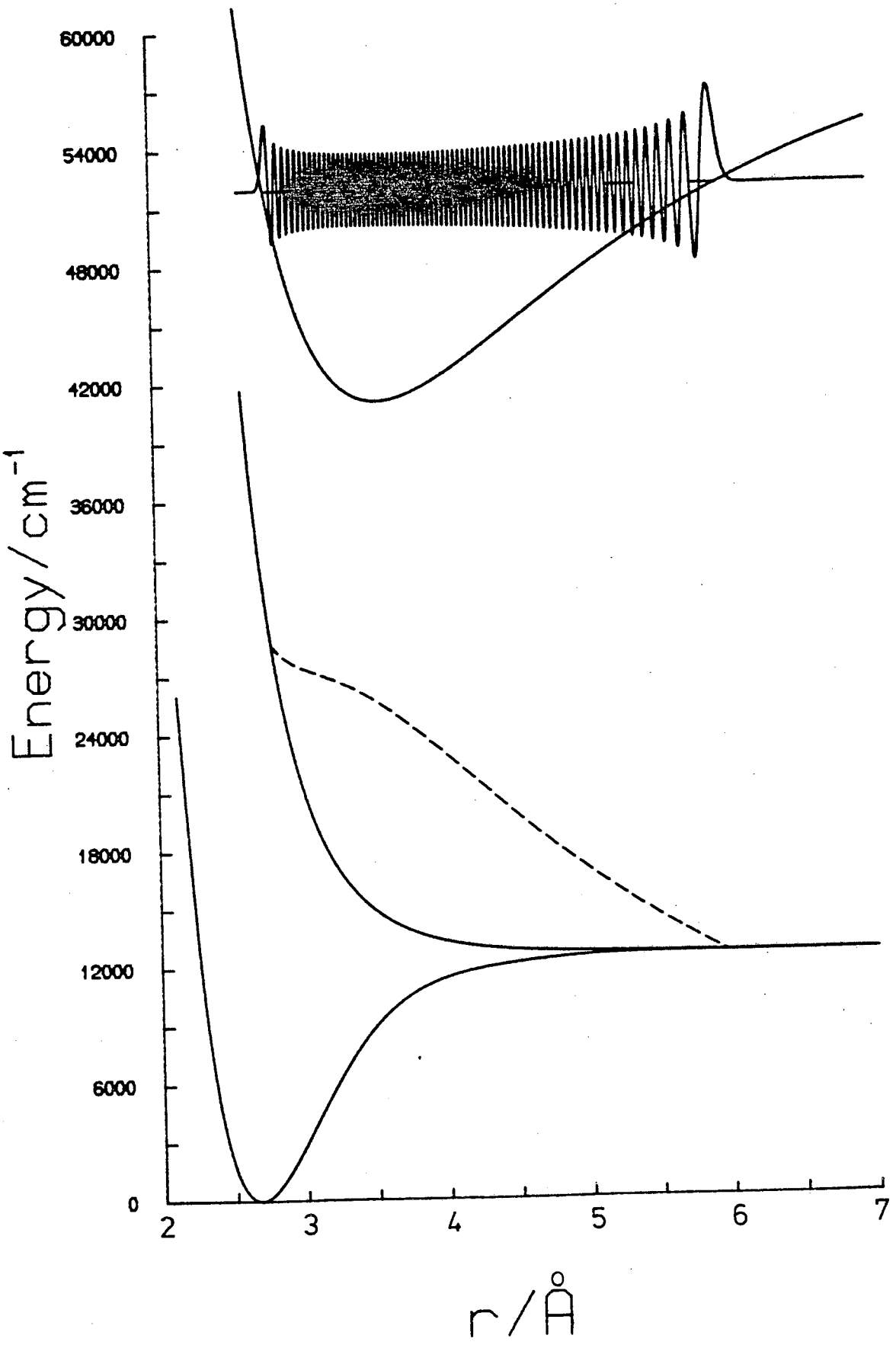

Figure 1.2 The difference potential for fluorescence from $I_2(DO_u^+, v = 144)$ to a repulsive lower state

The probability of an electronic transition from the upper state to the lower state emitting a photon of energy in the range E_f, $E_f + dE_f$ depends on two factors. The first factor is the probability of the oscillator being in the relevant range r, r + dr, that corresponds to the transition and the second is the square of the transition dipole moment function, $\mu_{12}(r)$. For a given dE_f the length of the segment dr will depend on the shape of the difference potential, the steeper the slope the smaller dr will be, leading to a reduced intensity of fluorescence in the range E_f, $E_f + dE_f$ because of the lower probability of the upper state being in the relevant range r, r + dr when dr is small. For a given dr the probability of the upper state being in the range r , r + dr will be inversely proportional to the square root of the kinetic energy (or the local velocity) of the upper state in the range r, r + dr. Mathematically, this can be expressed as follows:

$$E_f = U_2(r) - U_1(r); \quad \nu_f = E_f/h \qquad (1.2)$$

As stated above, the intensity of fluorescence from the bond-length range, dr, is proportional to $\mu_{12}(r)^2$ and inversely proportional to the speed in traversing the range r, r + dr

$$1/v(r) = \left[\frac{2(E - U_2(r))}{m}\right]^{-\frac{1}{2}} = \rho(r) \qquad (1.3)$$

m is the reduced mass of the molecule.

$$dI \propto \left[\frac{m}{2(E - U_2(r))}\right]^{\frac{1}{2}} \mu_{12}^2(r)\, dr \qquad (1.4)$$

Now the magnitude of dr is dependent on the slope of the difference potential at the point of fluorescence

$$\frac{d\nu_f}{dr} = \frac{d[U_2(r) - U_1(r)]}{h\, dr} \qquad (1.5)$$

so that

$$|dr| = h\left|\frac{dr}{d[U_2(r) - U_1(r)]}\right| d\nu_f \qquad (1.6)$$

Combining equations 1.4 and 1.6, one gets:

$$\frac{dI}{d\nu_f} \propto \mu_{12}^2(r).h.\left[\frac{m}{2(E - U_2(r))}\right]^{\frac{1}{2}} . \left|\frac{dr}{d[U_2(r) - U_1(r)]}\right| \qquad (1.7)$$

which is the same as the situation described in the preceding paragraph.

In the case of the potentials shown in Figure 1.2 and a typical transition dipole moment function which decays exponentially in going from small r to large r, the spectrum produced would be expected to peak at long wavelengths and then decay as the probability function $\rho(r)$ of the upper state decreases and the transition dipole moment function, $\mu_{12}(r)$ decreases. If the decay of μ_{12} is fast enough there will not be a peak at the short wavelength limit of the spectrum. If however $\mu_{12}(r)$ has an

appreciable magnitude at the outer turning-point of the upper state then there will be a peak at the short wavelength limit of the fluorescence spectrum.

Figure 1.3 shows a different fluorescence system, in that the difference potential of this system possesses a maximum. However in the classical case the same arguments apply to the production of the fluorescence spectrum and a little thought should show that the classical fluorescence spectrum of such a system will be as depicted in Figure 1.4. In this case, the long wavelength fluorescence maximum is not due to fluorescence from a turning-point in the upper state, but is due to fluorescence to the turning-point of the difference potential. This is because at this point the term $\frac{dr}{d[U_2(r) - U_1(r)]}$ in equation 1.7 diverges because of the maximum in the difference potential. In other words, at this point there is a range of bondlengths that gives rise to the same fluorescence wavelength. In scattering theory this type of classical catastrophe is quite common so the term "rainbow point" is sometimes borrowed to describe an extremum in the difference potential. The peaks in the fluorescence spectrum due to fluorescence at the turning-points of the upper state are still present in the fluorescence spectrum of Figure 1.4.

In the quantum mechanical theory, the intensity of a transition between two levels, bound or free, is determined by $| \langle \chi_1 | \mu_{12}(r) | \chi_2 \rangle |^2$, that is, the square of the

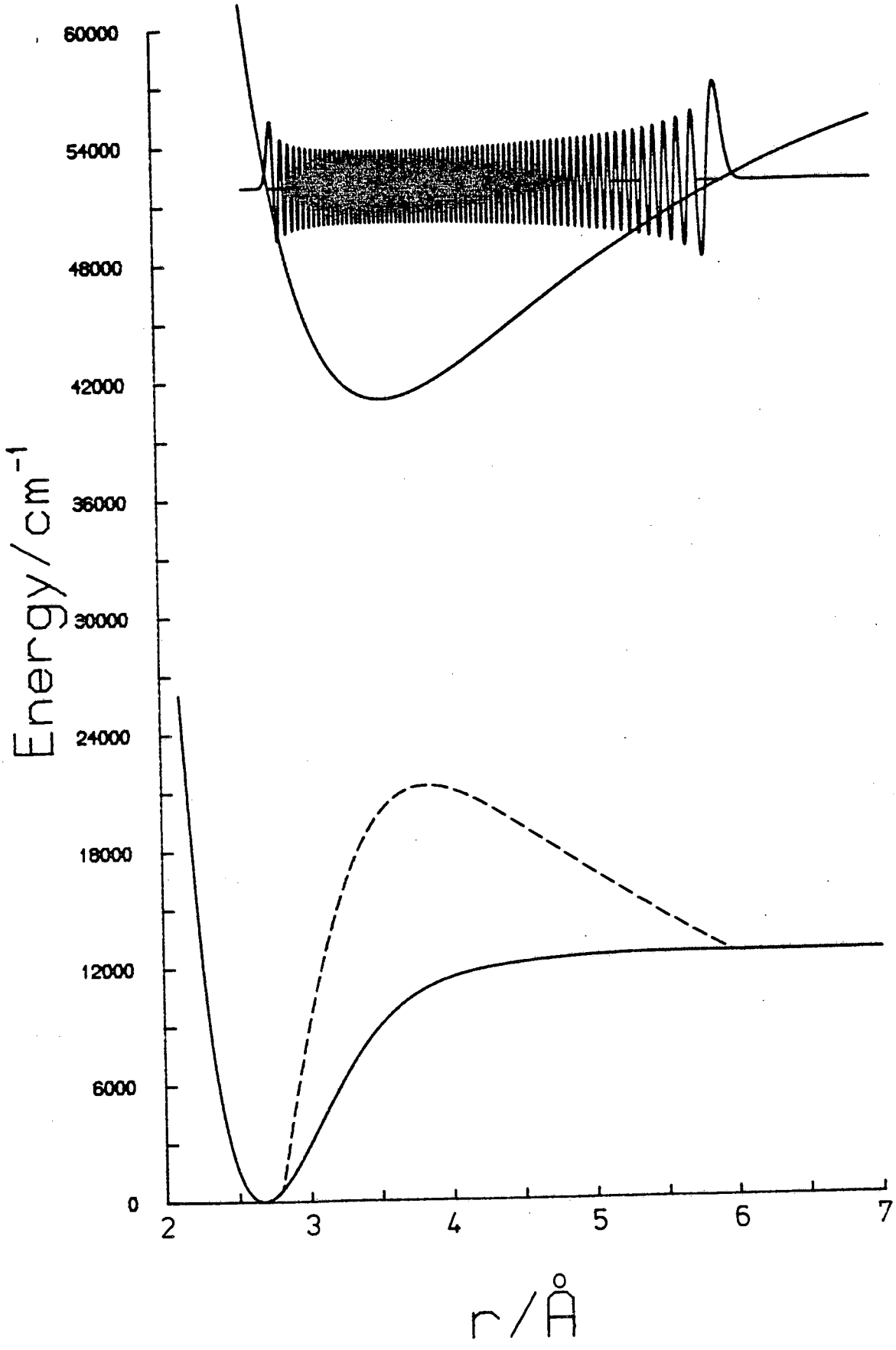

Figure 1.3 The difference potential for fluorescence from $I_2(DO_u^+, v = 144)$ to $I_2(X)$

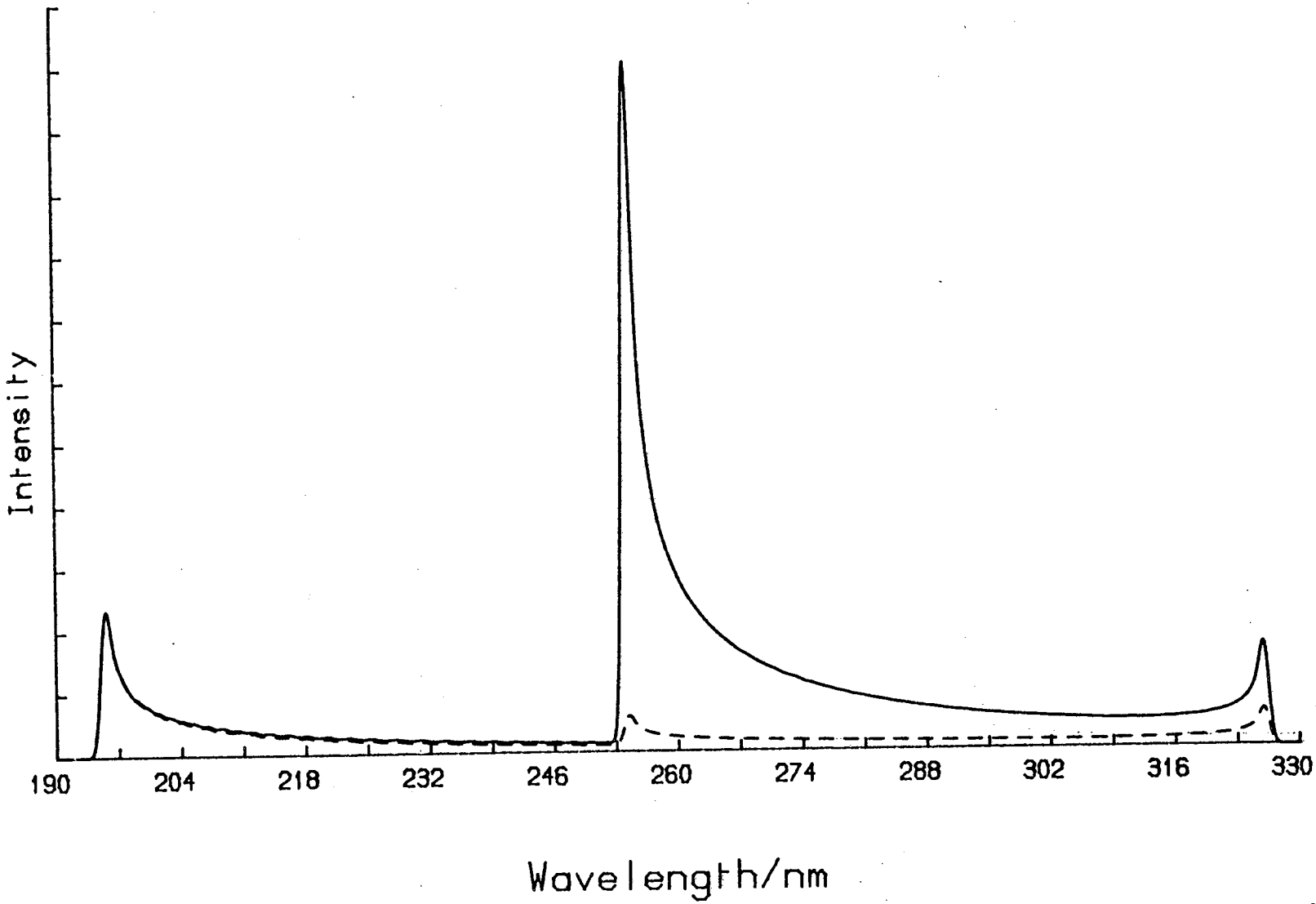

Figure 1.4 The classical fluorescence spectrum produced from the potentials shown in Figure 1.3. The solid line represents $\mu_{12}(r) = 1$ and the dashed line represents $\mu_{12}(r) = \exp(-0.5r)$. The two spectra were normalised to the peak at 195 nm. A resolution of 1 nm was assumed in calculating the spectra.

integrated overlap of the upper state and the lower state wave functions taking into account the transition dipole moment function, $\mu_{12}(r)$. If $\mu_{12}(r)$ is omitted, this just reduces to a Franck-Condon factor. In the examples given the integral has to be run over the entire range of the upper state. However for most of the range of this integral the local wavelengths of the upper state and lower state wave functions will be different so that the integral will be zero.

The difference potential, as described earlier, is the set of points where the position and momentum of the nuclei are conserved in a radiative transition. The importance of the difference potential in the quantum theory of these transitions is that, because of the conservation of momentum, and because the local wavelength of a wave function is only dependent on the nuclear momentum of the state, the difference potential can be regarded as the set of points where the upper and lower state wave functions possess equal local wavelengths so that there is a region of stationary phase in the overlap of the two wave functions. The integral in the bondlength regions close to the difference potential, then, will not necessarily integrate to zero. As $\mu_{12}(r)$ is a slowly varying function of r, it will not have a dramatic effect on the integral and if it is regarded as constant over the small r-range which contributes to this integral, one can simply do the integration and then multiply by the value of $\mu_{12}(r)$ at

the bondlength where the upper and lower wave functions have identical local wavelengths. This is known as the r-centroid approximation.

Again starting with the potentials shown in Figure 1.2, the evaluation of the resulting oscillatory continuum fluorescence spectrum will be described. Starting at the top of the difference potential in Figure 1.2 (long wavelength fluorescence) the bound upper vibrational state wave function and free lower state wave function will both have the same phase and local wavelength, so that the integral $|\langle \chi_1 | \mu_{12}(r) | \chi_2 \rangle|^2$ will give rise to a peak in the fluorescence spectrum. Some way further down the difference potential there will be an area where both the upper and lower wave functions, although having the same local wavelength , will be $\pi/2$ out of phase with each other and the integral will be zero leading to a minimum in the fluorescence spectrum. Further down the difference potential (going to shorter wavelengths of fluorescence) there will again be constructive interference between the two wave functions in the region of the difference potential, leading to another peak in the fluorescence spectrum. This process continues until either the end of the difference potential is reached, corresponding to the outer turning-point of the upper state, or until the transition dipole moment function becomes so weak that the fluorescence dies away. A computed example of this type of fluorescence spectrum, taken from the potentials in Figure 1.2,

is shown in Figure 1.5. Throughout the rest of this thesis such a spectrum, arising from a monotonic difference potential, will be termed a "single frequency" type of oscillatory continuum, although it is also known as a "reflection" type of spectrum.

For the system described in Figure 1.3, the above argument applies but with one further complication. In the energy region between the maximum of the difference potential and the dissociation energy of the bound lower state, there are two limbs of the difference potential and in classical terminology there are two separations at which fluorescence of a particular wavelength can occur. In quantum mechanical language there are two regions of stationary phase in $\chi_1\chi_2$. The integrals over these two regions of stationary phase may, depending on their relative phases, either augment or cancel each other, which will superimpose another frequency of oscillation onto the fluorescence system. This second frequency is generally lower than the first. The destructive interference between the two branches of the difference potential will only be complete if the intensities of fluorescence from the two branches of the difference potential are equal. This would only accidentally be true. As one moves down the difference potential (going to shorter fluorescence wavelengths) the two branches of the difference potential separate and the fluorescence from both branches becomes less and less equal. There are three main reasons for this. Firstly, the

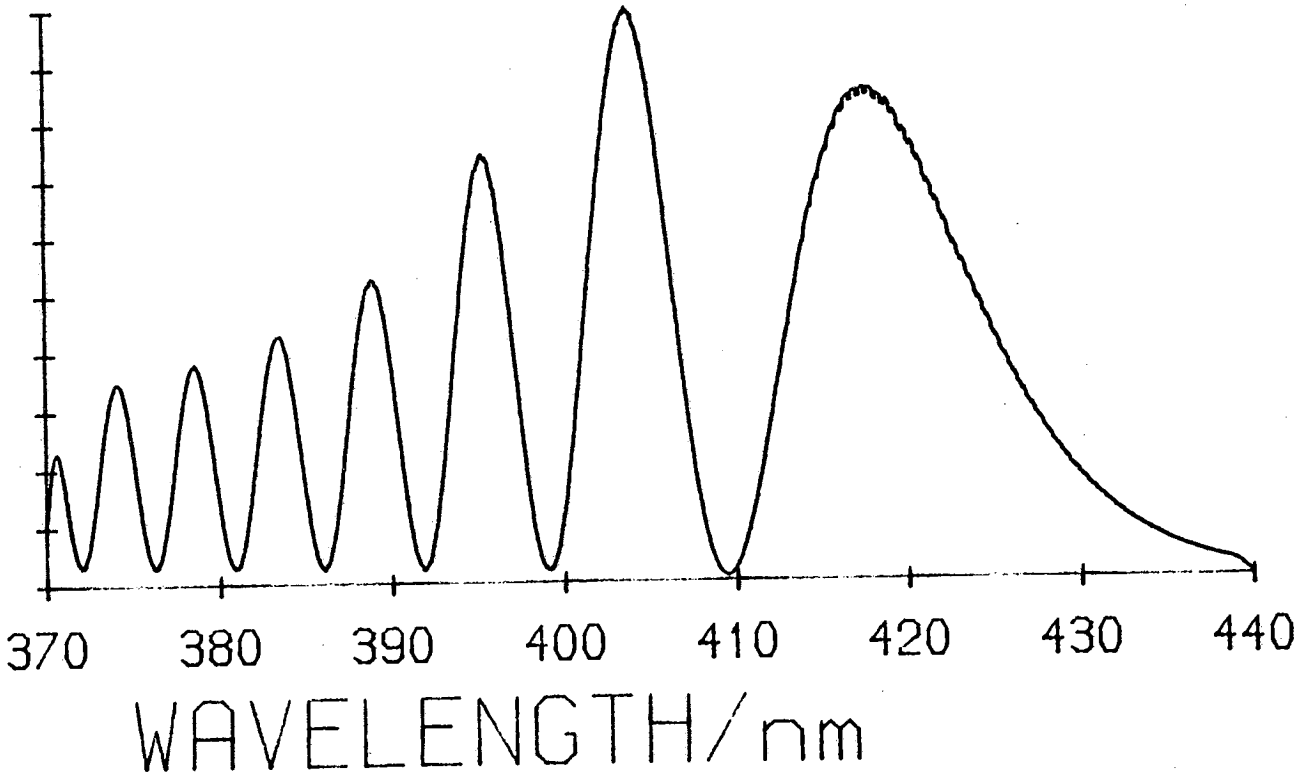

Figure 1.5 The quantum mechanical spectrum produced from the potentials in Figure 1.2. (This figure is identical to Figure 4.7).

transition dipole moment function, $\mu_{12}(r)$, will, although it is a slowly varying function of r, in general, be different at the transition points to the two different branches; secondly, the slope of the difference potential will, in general, be different at the transition points to the two different branches and finally the probability function $\rho(r)$ of the upper state having the right bond length for fluorescence to each branch of the difference potential will, in general, be different. Thus in Equation 1.7, the three variable terms, $\mu_{12}(r)$, $[\frac{m}{2(E - U_2(r))}]^{\frac{1}{2}}$ and $\frac{dr}{d[U_2(r) - U_1(r)]}$, will be different for transitions to each branch of the difference potential. For the reasons above one would expect the importance of this low frequency or rainbow structure to decrease as one moves further away from the long wavelength band head in the fluorescence spectrum. A computed spectrum for the potentials shown in Figure 1.3 is shown as Figure 1.6. The type of spectrum just described will, in the rest of this thesis, be termed a "double frequency" type of oscillatory continuum, although elsewhere it is also known as an "interference" oscillatory spectrum. In Figure 1.3 the region below the dissociation limit of the lower state is, by definition, bound, and fluorescence to this region will consist of discrete transitions corresponding to the bound vibrational levels of the lower state. Just below the dissociation energy the vibrational levels of the lower state will be closely spaced so that for fluorescence to this region the structure imposed by the discrete vibrational levels will be finer than the structure

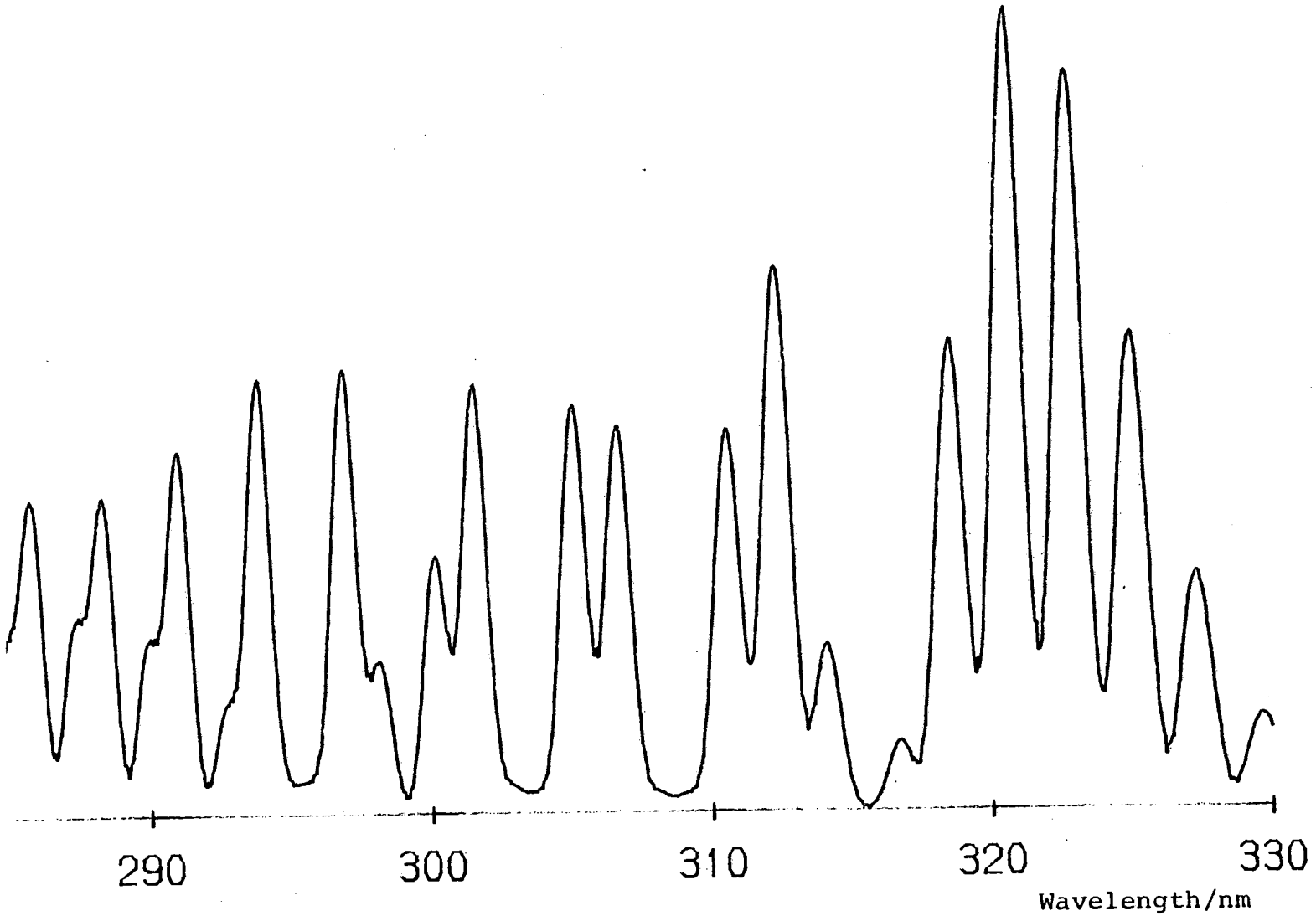

Figure 1.6 The quantum mechanical spectrum produced by the potentials in Figure 1.3. (This figure is identical to Figure 4.5).

from the oscillatory emission in this region. Thus an oscillatory envelope may be expected to appear over the discrete fluorescence to the bound levels of the lower state in Figure 1.3. Such fluorescence will have the characteristics of single frequency oscillatory spectra as there is only one branch of the difference potential in this energy range.

The above has been described in papers by Mulliken[2] and Tellinghuisen[3].

The two different types of oscillatory structure behave differently when the level of excitation of the bound upper state is changed. The behaviour of a double frequency oscillatory spectrum is easiest to describe in as much as the position of the long wavelength fluorescence maximum is independent of the level of excitation of the upper state. At the maximum of the difference potential, the gradients of the upper and lower potentials are equal. This is a unique point that is independent of the excitation energy so that at this point $U_2 - U_1$ will be independent of the level of excitation of the upper state. As the energy of an emitted photon is $U_2(r) - U_1(r)$ the long wavelength fluorescence limit of the spectrum will be also independent of the level of excitation of the upper state. In spectroscopic terms this means that, for a double frequency type of oscillatory continuum spectrum the long wavelength fluorescence maximum is independent of the wavelength of excitation of the fluorescence system. Tellinghuisen has published a nice example of this[4].

Because an extremum in the difference potential (if one exists) occurs at a position where the gradients of the upper and lower states are equal, it can be stated that for a system with a monotonic difference potential, giving rise to a single frequency type of oscillatory continuum, the gradient of the lower potential in the fluorescence region is either always larger or always smaller than that of the upper state. In either case, at the top end of the difference potential, the lower state will always be steeper than the upper state. In the situation shown in Figure 1.2 at the bondlength corresponding to the inner turning-point of the upper state the gradient of the lower state is more negative than the gradient of the upper state, although it is still true that $|\frac{dU_1(r)}{dr}| > |\frac{dU_2(r)}{dr}|$. This region is shown in diagrammatic form in Figure 1.7. If the level of excitation of the upper state is increased in energy by ΔU_2 this will shift the inner turning-point to shorter bondlengths by an amount Δr. The difference in the potential energy of the repulsive state between the points corresponding to the old and new inner turning-points will be ΔU_1. As at this point $|\frac{dU_1(r)}{dr}| > |\frac{dU_2(r)}{dr}|$, then $\Delta U_1 > \Delta U_2$. This means that as extra energy is added to the system $U_2(r) - U_1(r)$, with r corresponding to the inner turning-point of the upper state and being a function of excitation energy, will decrease. Thus the energy of fluorescence at the long wavelength limit of the spectrum will also decrease. This can be expressed in spectroscopic language in

$$\Delta E_f = \Delta U_1 - \Delta U_2$$

if λ_e decreases λ_{fmax} increases

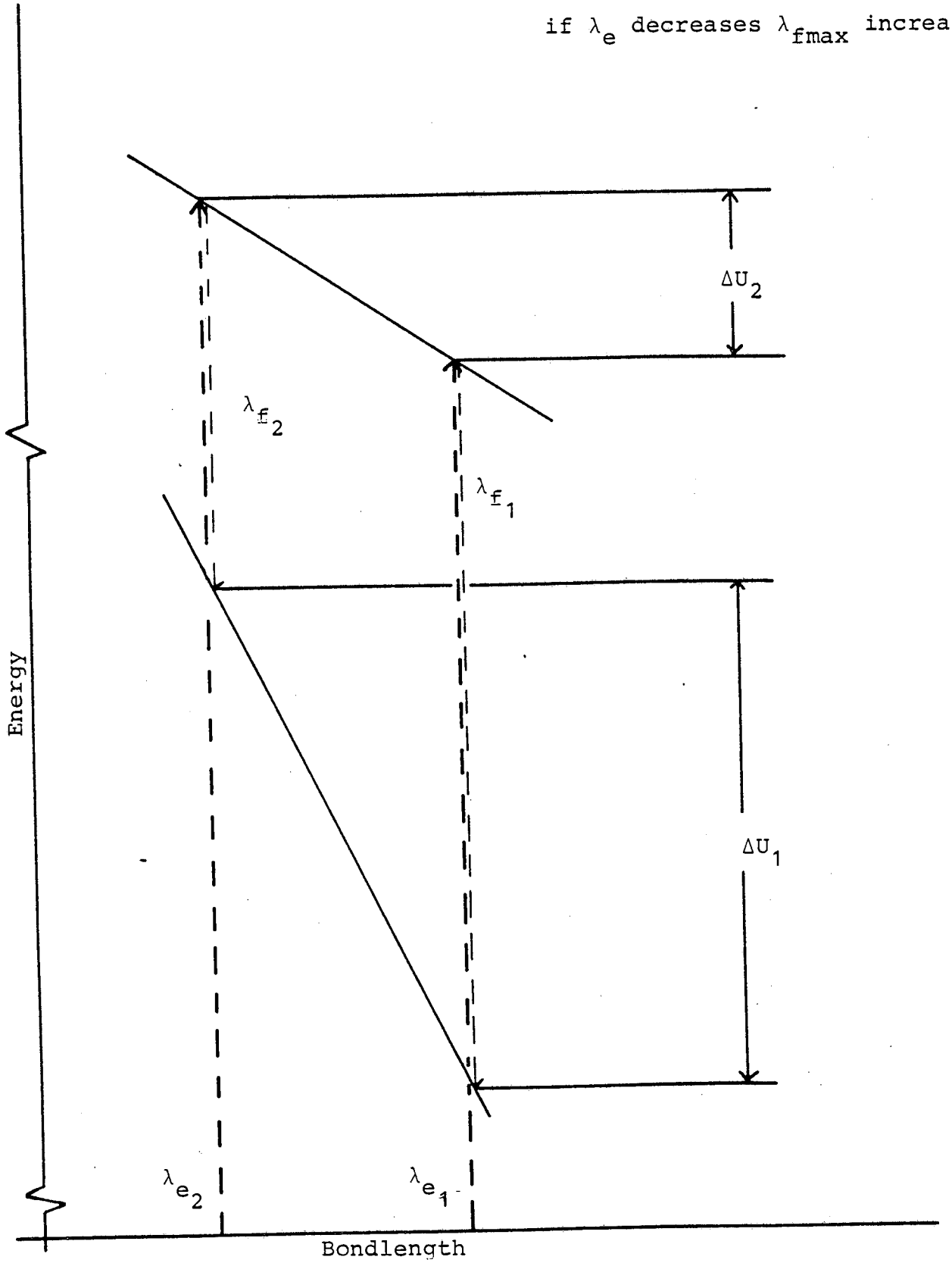

Figure 1.7 An expansion of Figure 1.2 concentrating on the area near the inner turning point of the upper state to show what happens when the wavelength of excitation is decreased.

the following way: in a situation giving rise to a single frequency type of oscillatory continuum, if the wavelength of excitation is decreased, the wavelength of the long wavelength fluorescence limit will increase. An experimental example of this is shown in Chapter 4, Figure 4.9. This rule still applies in the case where the difference potential always has a positive slope and the long wavelength fluorescence originates at the outer turning-point of the upper state.

A parallel argument to the above can be used to show that in cases where a monotonic difference potential is involved the short wavelength limit of the fluorescence spectrum decreases when the wavelength of excitation of the fluorescence spectrum is decreased. Unfortunately, this does not provide a unique test as to whether a system is a single or double frequency type of oscillatory continuum, as fluorescence from either turning-point of an upper state potential to a flat lower potential would possess the same characteristics.

1.4 Nesting of Ion-Pair States and their Physical Quenching

For iodine and the other homonuclear diatomic halogens there should be six ion-pair states diabatically dissociating to $I^-(^1S) + I^+(^3P_2)$, these states being 0_g^+, 0_u^+, 1_g, 1_u, 2_g and 2_u. There should also be six

states correlating to $I^-(^1S) + I^+(^3P_{1,0})$ (0_g^-, 0_u^-, 0_g^+, 0_u^+, 1_g and 1_u). In the heteronuclear diatomics there will be three members per group but there will be twice as many groups. For example, in IBr there will be three electronic states diabatically dissociating to $I^-(^1S)$ + $Br^+(^3P_2)$ the states being 0^+, 1 and 2 and three diabatically dissociating to $Br^-(^1S)$ + $I^+(^3P_2)$ (0^+, 1 and 2). Energetically, these states will be well separated from each other. This in effect replaces the gerade/ungerade pairs.

The members of each group will all have similar term values to the other members of the same group, but the term values of states in different groups will be separated by approximately the energy difference of the spin orbit splitting in the positive ion. The reason for the similarity in the shapes and binding energies of all the ion pair states is that for all of the attractive limb of the states, from the minimum to the diabatic dissociation limit, the ionic attraction term $\frac{e^2}{4\pi\varepsilon_o r}$ dominates the potentials and is identical for all the ion-pair states. This has two main consequences: firstly that the attractive limbs of all the ion-pair states of one group will, at large r, be identical, and secondly that the term values and equilibrium bond distances of all the members of one group of ion-pair states will be similar. For iodine the difference in term values between successive members of the lowest group is of the order of kT.

This has important consequences for the appearance of the fluorescence spectra of the ion-pair excited halogens in the presence of an excess of buffer gas. It seems reasonable to assume that there is rapid collisionally induced coupling between the similar members of an ion-pair manifold, but very weak quenching from ion-pair states to valence states, very different in character and energy, or to Rydberg states. Thus it would be expected that, in the presence of buffer gas, the ion-pair states of a manifold would assume a Boltzmann population distribution regardless of which member had originally been excited and, with enough buffer gas present, however highly excited that member was. In this way it would be expected that the lowest energy ion-pair state, normally the $2_{(g)}$ state and usually designated D', will be the most heavily populated state. Guy et al[5] have found that for I_2 excited by a tesla discharge in the presence of a high pressure of buffer gas (He, Ar, Ne or N_2) 85% of the total fluorescence in the region 200-500 nm is due to D' → A' fluorescence, implying that the D' state is the lowest ion-pair state of iodine. They also saw fluorescence at 288 nm which they attributed to F → X emission. The F state, being in the second manifold of iodine ion-pair states, would not be expected to be quenched very efficiently into the lowest manifold.

Tellinghuisen et al[6] have analysed the emission spectrum of bromine, again excited by a tesla discharge, in the presence of argon and found that at an argon pressure of 20 kNm^{-2} the dominant fluorescence system is

again the D' → A' system. Diegelmann et al[7] have produced quenched spectra for F_2, Cl_2, ClF, ICl, IF, BrF, BrCl and IBr and analysed them on the assumption that, as with Br_2 and I_2, at high pressure the D' → A' system dominates. Their analyses and calculations seem to indicate that the assumption of the D' → A' transition dominating the fluorescence spectrum is correct.

In this thesis rate data for the quenching of population from highly vibrationally excited ion-pair states of Br_2 and IBr will be presented. In both cases, with an inert gas as the quencher, the population seems to be transfered to the D' state giving rise to the D' → A' transition. This is to be expected with the D' state being the least energetic of the ion-pair states. This is the first time such rate data has been measured for the Br_2(K) state or the IBr(D) state.

Similar quenching rates for $I_2(DO_u^+)$ have been published by Donovan et al[8].

1.5 References

(1) J.C.D. Brand and A.R. Hoy, J.Mol.Spec., 97 (1983), 379.

(2) R.S. Mulliken, J.Chem.Phys., 55 (1971), 309.

(3) J. Tellinghuisen, J.Mol.Spec., 103 (1984), 455.

(4) J. Tellinghuisen, Chem.Phys.Letts., 29 (1974), 359.

(5) A.L. Guy, K.S. Viswanathan, A. Sur and J. Tellinghuisen, Chem.Phys.Lett., 73 (1980), 582.

(6) J. Tellinghuisen, P. Berwanger, T.G. Ashmore and K.S. Viswanathan, Chem.Phys.Letts., 84 (1981), 528.

(7) M. Diegelmann, K. Hohla, F. Rebentrost and K.L. Kompa, J.Chem.Phys., 76 (1982), 1233.

(8) R.J. Donovan, B.V. O'Grady, L. Lain and C. Fotakis, J.Chem.Phys., 78 (1983), 3727.

CHAPTER 2

Experimental Details

2.1 General

In all the fluorescence experiments the excitation source and the detection equipment were set at right angles to each other as shown in Figure 2.1, which shows the general layout of laser fluorescence experiments. In this chapter the properties of the various pieces of equipment that fit into the "boxes" in Figure 2.1 are described. The experimental set-up for recording the absorption spectra at the S.E.R.C. Synchrotron Radiation Source at Daresbury is also described.

2.2 F_2 Lasers

Two lasers were used for operating on the F_2 transition, the first was a Lambda Physik EMG200 and the second an Oxford Lasers KX2 Multigas Excimer Laser. The F_2 laser transition occurs at a wavelength of 157.8 nm ($\Delta\lambda < 0.05$ nm[1]) and is thus in the vacuum ultra-violet region of the spectrum. With the Lambda Physik laser the beam path was purged with a flow of oxygen free nitrogen from a B.O.C. cylinder for about 20 minutes before use and during use. Whereas with the Oxford laser system the beam path was evacuated.

The pulse energy of the Oxford Laser was $\sim$40 mJ while the average pulse energy of the Lambda Physik laser, as set up, was <5 mJ. For both systems the pulse life-time was $\sim$6 ns.

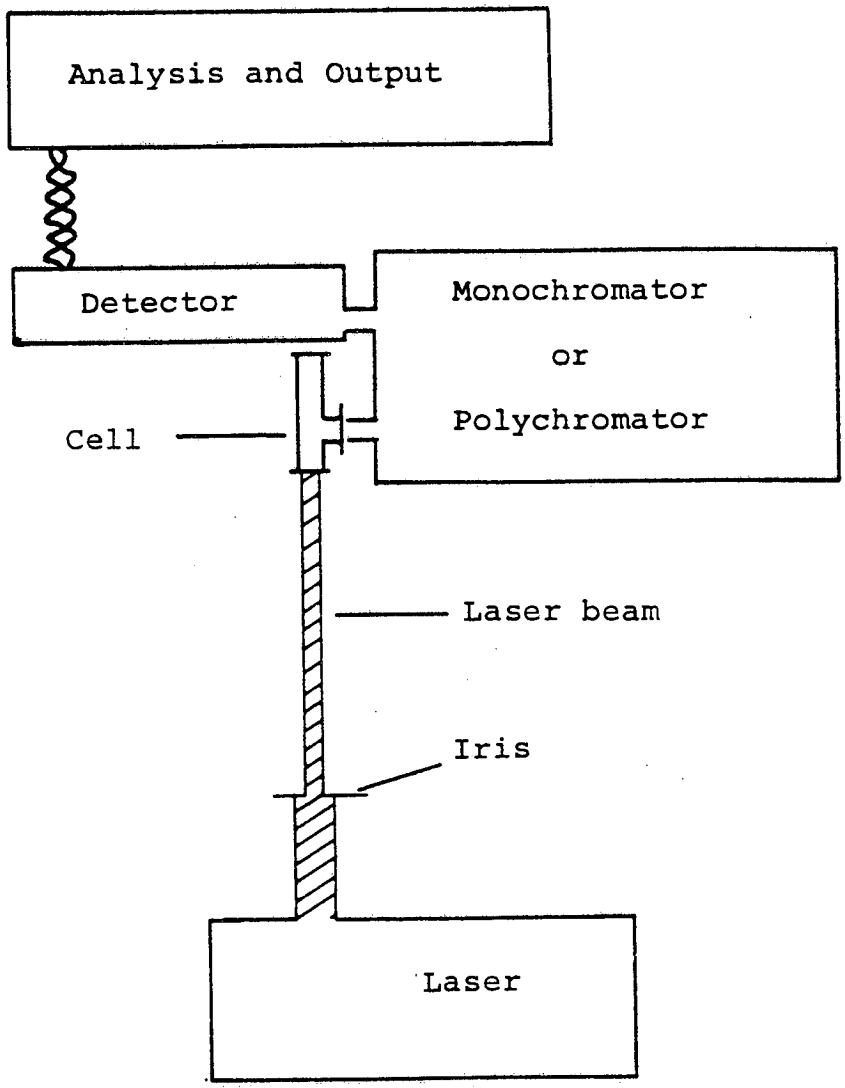

Figure 2.1 A diagram showing the experimental lay-out of all laser induced fluorescence experiments described.

2.3 Broad Band ArF Laser (Lambda Physik EMG200 and EMG500)

When operating on the ArF laser transition (λ = 193 nm), the Lambda Physik EMG200 gave out pulses of $\sim$400 mJ energy and $\sim$14 ns duration. In the experiments which are described here the laser beam was not focussed but it was passed through an iris of 10 mm diameter so that only the central portion of the 15 mm high x 32 mm wide output beam was used. The spectral distribution of the laser output is shown in Figure 2.2. The beam path was open to the atmosphere causing the minima in the spectrum. These minima were due to absorption by oxygen.

The EMG500 had similar characteristics to the EMG200 but gave much less energy per pulse. After passing the beam through a 10 mm diameter iris its energy was found to be typically 2 mJ per pulse. The other major difference was that the output beam dimensions were 32 mm high x 15 mm wide. The spectral profile of the laser was the same as that of the EMG200.

2.4 Line Narrowed ArF Laser (Lambda Physik EMG150)

The Lambda Physik EMG150 laser operates by firing one laser (the oscillator) into another laser cavity (the amplifier). This technique is known as injection locking.

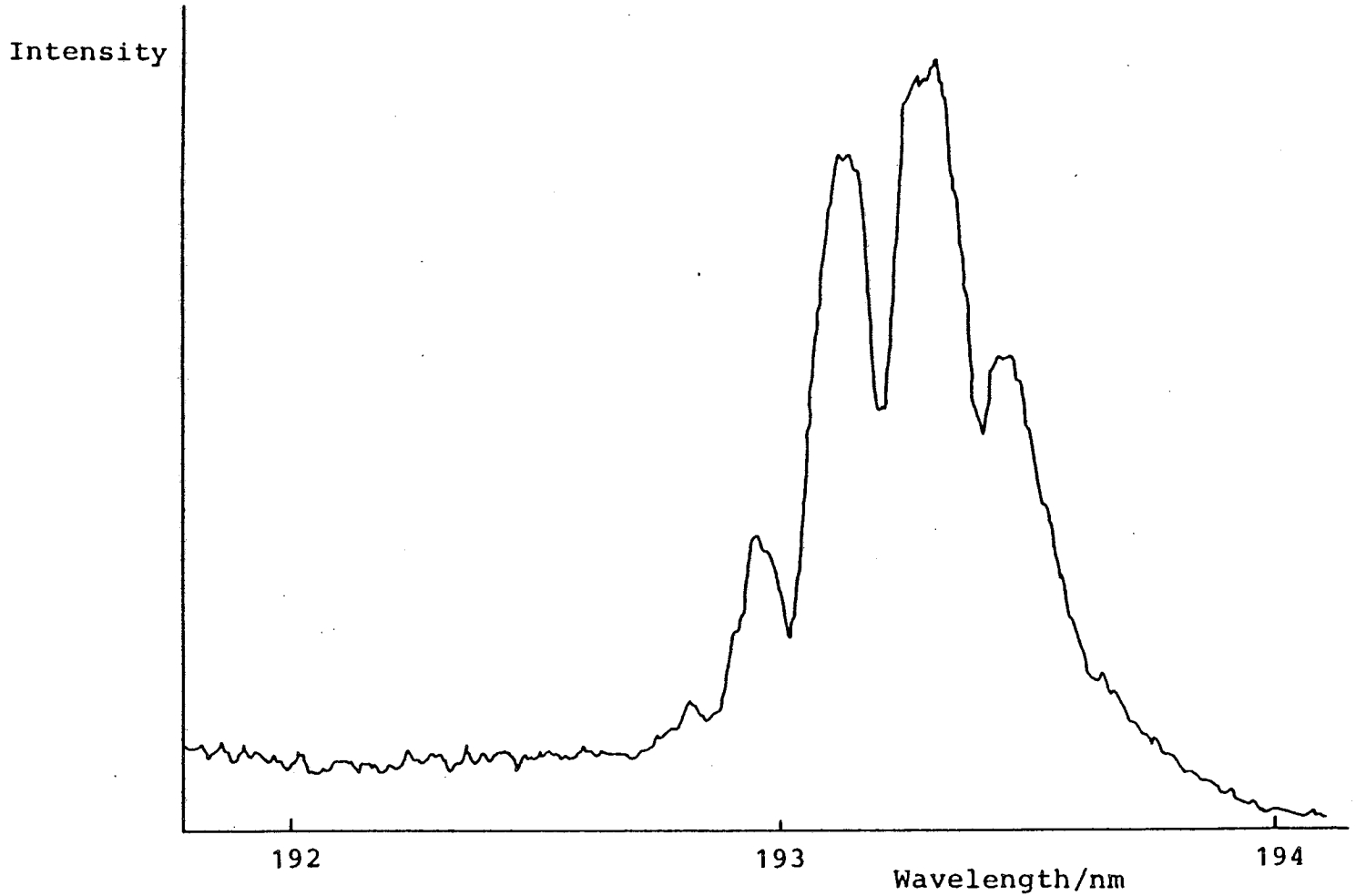

Figure 2.2 The spectral profile of the output from a normal (not line-narrowed) ArF laser.

The oscillator , which is a slightly modified Lambda Physik EMG100 laser, consists of a cavity with a stable resonator and, to alter the gain characteristics of the cavity leading to the spectral line narrowing, a set of expansion prisms and a grating. The oscillator output is fired into the amplifier cavity which is basically a Lambda Physik EMG200 laser with unstable resonator optics leading to triple pass amplification and beam expansion.

As used, the laser gave a usable pulse energy of $\sim$10 mJ in a pulse of $\sim$20 ns duration. The output of the EMG150 was tunable across the gain profile of a normal ArF laser (Figure 2.2) giving a narrow line of less than 10 cm^{-1} bandwidth. The locking efficiency of the system was usually greater than 85%. The spectral profile of a typical laser output is shown in Figure 2.3.

2.5 Scanning Monochromator/Photomultiplier Detection System

In experiments which used a scanning monochromator/ photomultiplier combination the monochromator was a McKee-Pederson MP1018B monochromator with a dispersion of 2 nm/mm. A slit width of 120 μm was typically used giving a spectral resolution of 0.24 nm. The photomultiplier tube used was an EMI 9661B photomultiplier run at 1010V, the signal from which was sent to an ORTEC-Brookdeal Linear Gate model 9415 and then on to a chart recorder. This system was usually used with the Lambda Physik EMG500 laser operating at 2 Hz and with linear gate set for a time constant of 3 s.

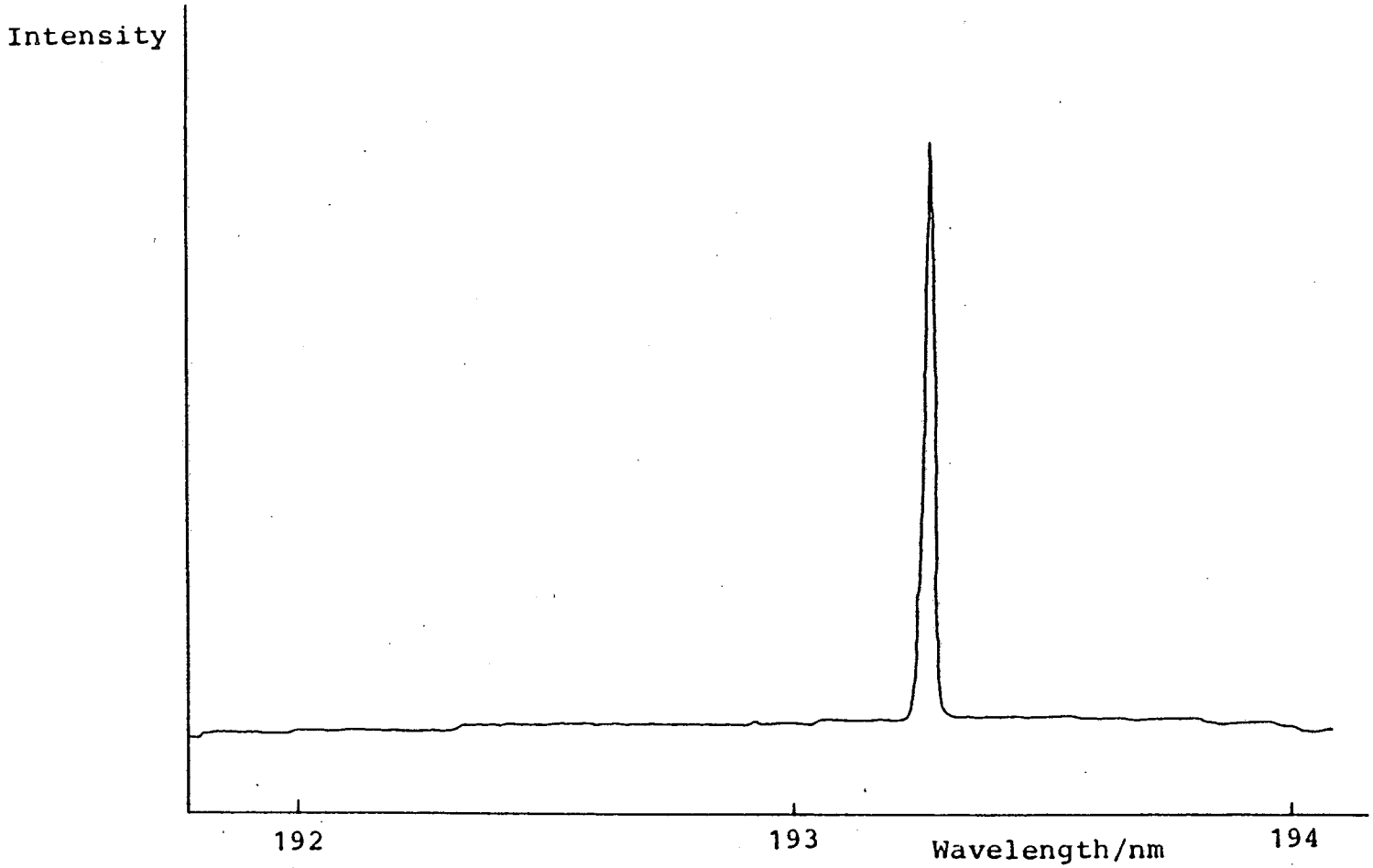

Figure 2.3 The spectral profile of the output from a line narrowed ArF laser (Lambda Physik EMG150).

2.6 The Optical Multichannel Analyser (O.M.A.)/ Polychromator Detection System

In this combination the sample fluorescence was observed at right angles to the laser excitation and was dispersed with a Jobin-Yvon (HRS 2) 0.3 m polychromator (monochromator with exit slit removed) with interchangeable gratings to give low (∿2.6 nm) and medium (∿0.35 nm) resolution spectra. The O.M.A. detection head was placed over the exit aperture of the polychromator. The detector consists of a row of equally spaced photosensitive diodes. A histogram of the amount of light detected by each diode against the diode position then produces the spectrum. To a first approximation, the width of each diode element will have the same effect on resolution as the exit slitwidth of a monochromator. In using the Optical Multichannel Analyser system (EG&G PAR OMAII) two different detector heads were used. One detector, referred to as a vidicon detector (type 1254 SIT) was used for work above 400 nm as it has a poor response much below this wavelength. For wider spectral coverage, a second detector, referred to as a diode array detector (type 1420) was used. Each detector was run by its own, dedicated, microprocessor controller, with in turn, a microcomputer controlling it and recording and analysing the spectra produced. After recording each spectrum, a second spectrum was recorded with the excitation source blocked. This acted as a background and took account of

the "dark current" from each diode. The background spectrum was then subtracted from the real spectrum on the microcomputer. It is these background subtracted spectra that are reproduced as figures and were used for analysis. The exact conditions used for recording each spectrum are given in the figure captions.

2.7 The Synchrotron Radiation Source (S.R.S.)

The Synchrotron Radiation Source (S.R.S.) at the S.E.R.C. Daresbury Laboratory produces light by accelerating electrons around a storage ring. In the Daresbury S.R.S., electrons normally circulate round the storage ring in 160 discrete bunches of 3.6 cm length, which corresponds to a light pulse of ∿120 ps duration. The time between bunches is normally 2.0 ns. If the S.R.S. is being used for time resolved work, it is possible for it to be filled with only one electron bunch circulating to provide a 120 ps light pulse every 320 ns. This is known as the "single bunch mode" of operation. Light is collected from the S.R.S. at various ports at the magnets that form the storage ring. For the absorption work described in this thesis, port VUV3 was used while for all other work carried out at the S.R.S. port HA12 was used.

2.8 The Absorption Spectra from Port VUV3

In these experiments the synchrotron radiation was dispersed using a McPherson 5m monochromator. The dispersion of the instrument was 0.16 nm/mm. The mono-

chromatic light was then shone through a cell of 10 cm path length with LiF front and back windows. The rear face of the exit window was coated with sodium salicylate, the fluorescence from which was detected by a photomultiplier. The output from the photomultiplier was fed into a current integrator. The output of the current integrator along with the wavelength setting of the monochromator were recorded by a microcomputer (PDP 11/04) before being transferred with the rest of the data points of the spectrum to an AS7000 mainframe computer for analysis. The microcomputer controlled the stepping of the monochromator grating as well as the data collection. The sample cell was filled from a conventional gas line. Typical conditions for the S.R.S. during these experiments were a beam energy of 1.8 GeV and a current of $\sim$180 mA. During these experiments, the S.R.S. was always run in multi-bunch mode.

The monochromator was initially calibrated using the Schumann-Runge bands of O_2 and also from the known Rydberg absorption bands in the halogen absorption spectra. To show the best resolution achievable with the instrument an absorption spectrum of the 8,0 Schumann-Runge system is presented as Figure 2.4. Also shown, as Figure 2.5, is the "absorption" spectrum taken with the sample cell empty. This is to show how the sensitivity of the system varies across the spectrum.

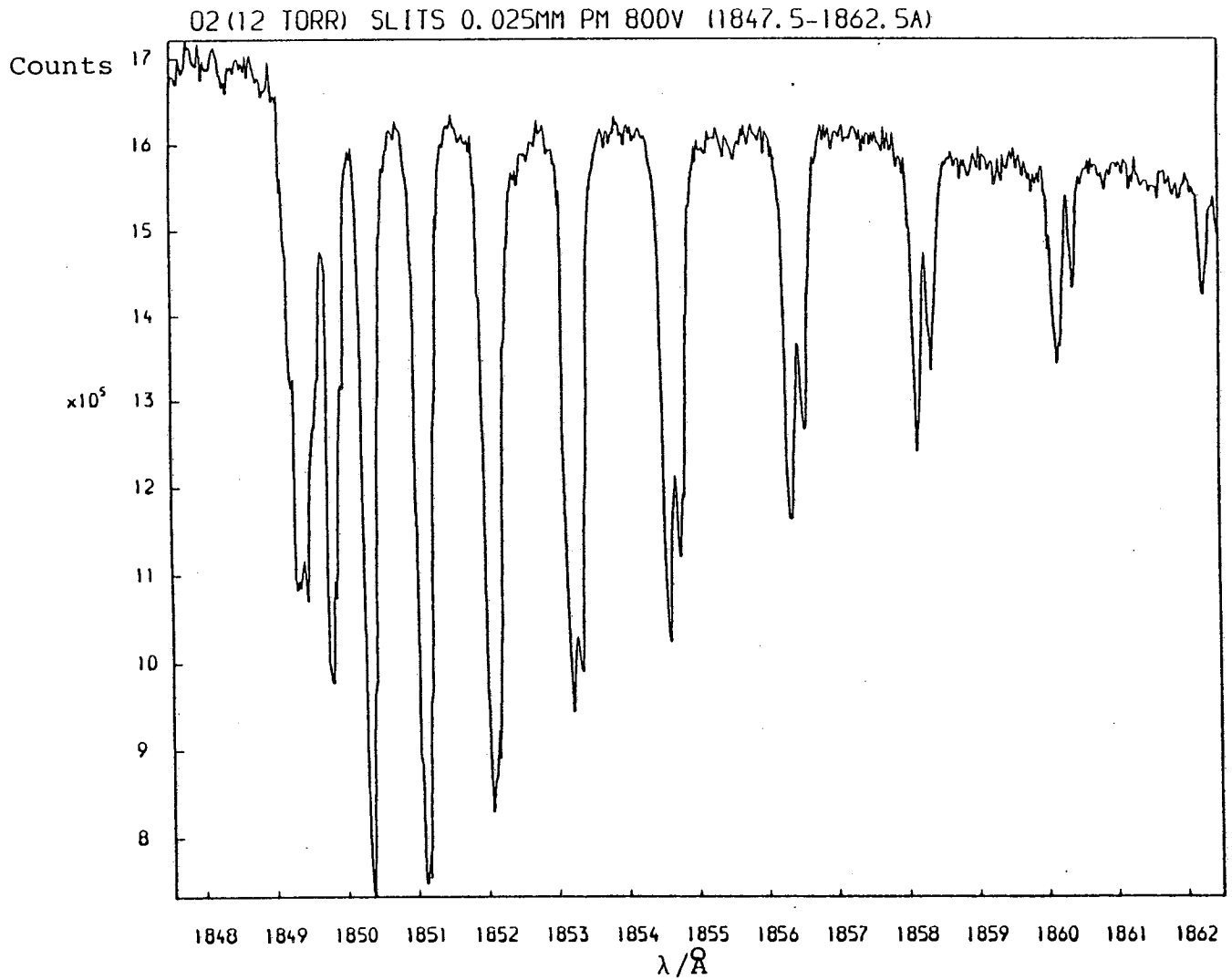

Figure 2.4 The 8,0 Schumann-Runge absorption of O_2, recorded under a resolution of 0.004 nm. The scale reads high by 2.8 Å.

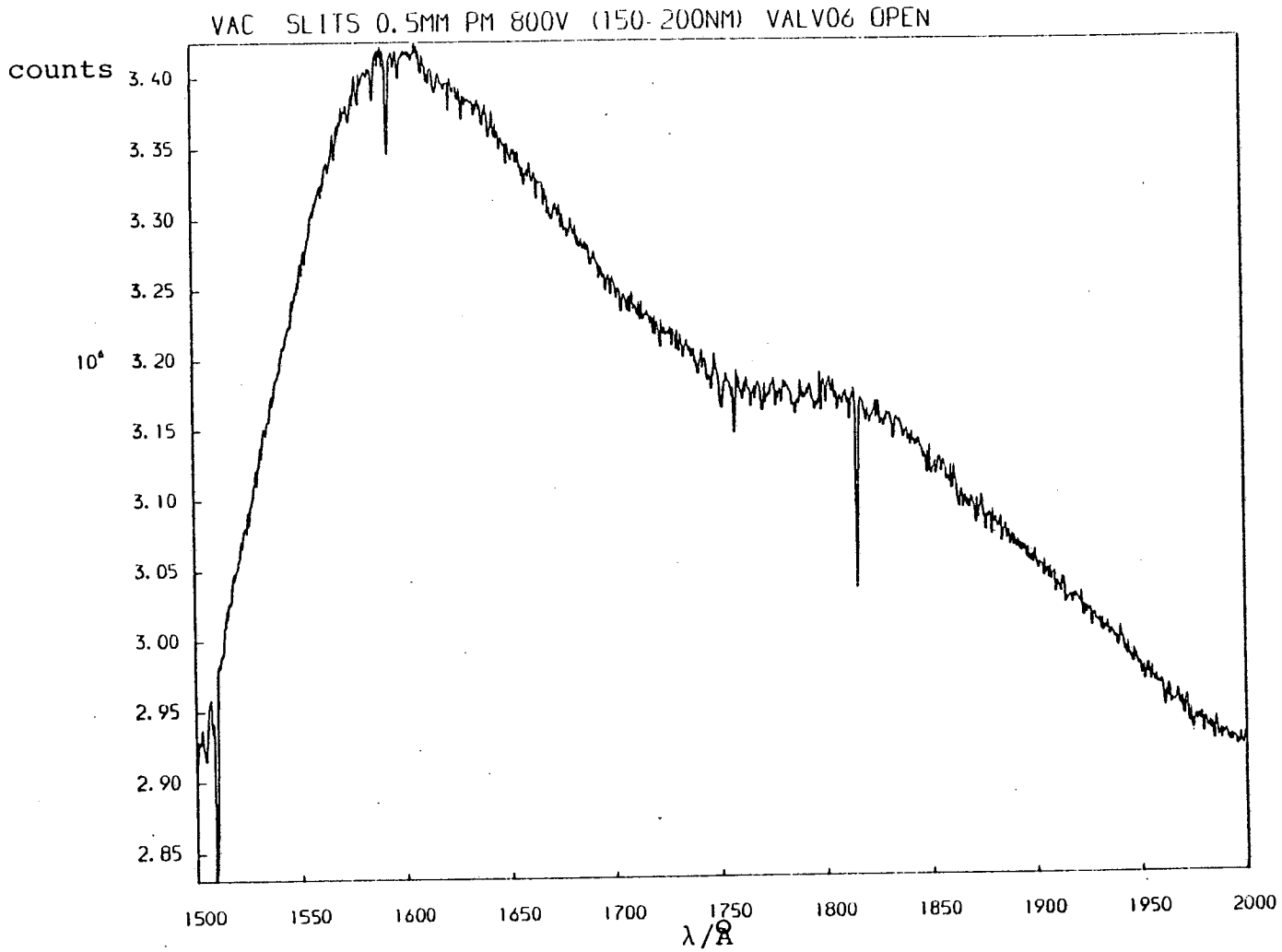

Figure 2.5 The absorption spectrum of an evacuated cell to show the response of the instrumentation

2.9 Time Resolved Measurements at the S.R.S.

For these experiments the S.R.S. was operated in single bunch mode as described above. The synchrotron radiation was dispersed by a Spex 1500 SP Czerny-Turner monochromator to give an excitation wavelength of 188 nm with a bandpass of 3 nm. This radiation was then used to excite samples of IBr contained in a standard 1 cm^2 Spectrosil fluorescence cell fitted with a greaseless tap (to enable filling from a standard vacuum line). The fluorescence collected at right angles to the excitation beam from the IBr sample was then passed through an LF30 filter (λ > 300 nm) and detected by a Mullard XP2020Q photomultiplier. The fluorescence lifetime was determined by measuring many times the interval between the photomultiplier pulse (after constant fraction discrimination) and the zero time reference signal from the strip line on the storage ring, using a time to amplitude converter (TAC). Output pulses from the TAC were accumulated in a multichannel analyser. The lifetime spectra were recorded locally on a PDP11/04 and also transferred to the AS7000 mainframe computer for analysis. A schematic diagram of the experimental set-up is shown as Figure 2.6. This time resolved work was carried out in collaboration with my colleague, Mr. G. Gilbert.

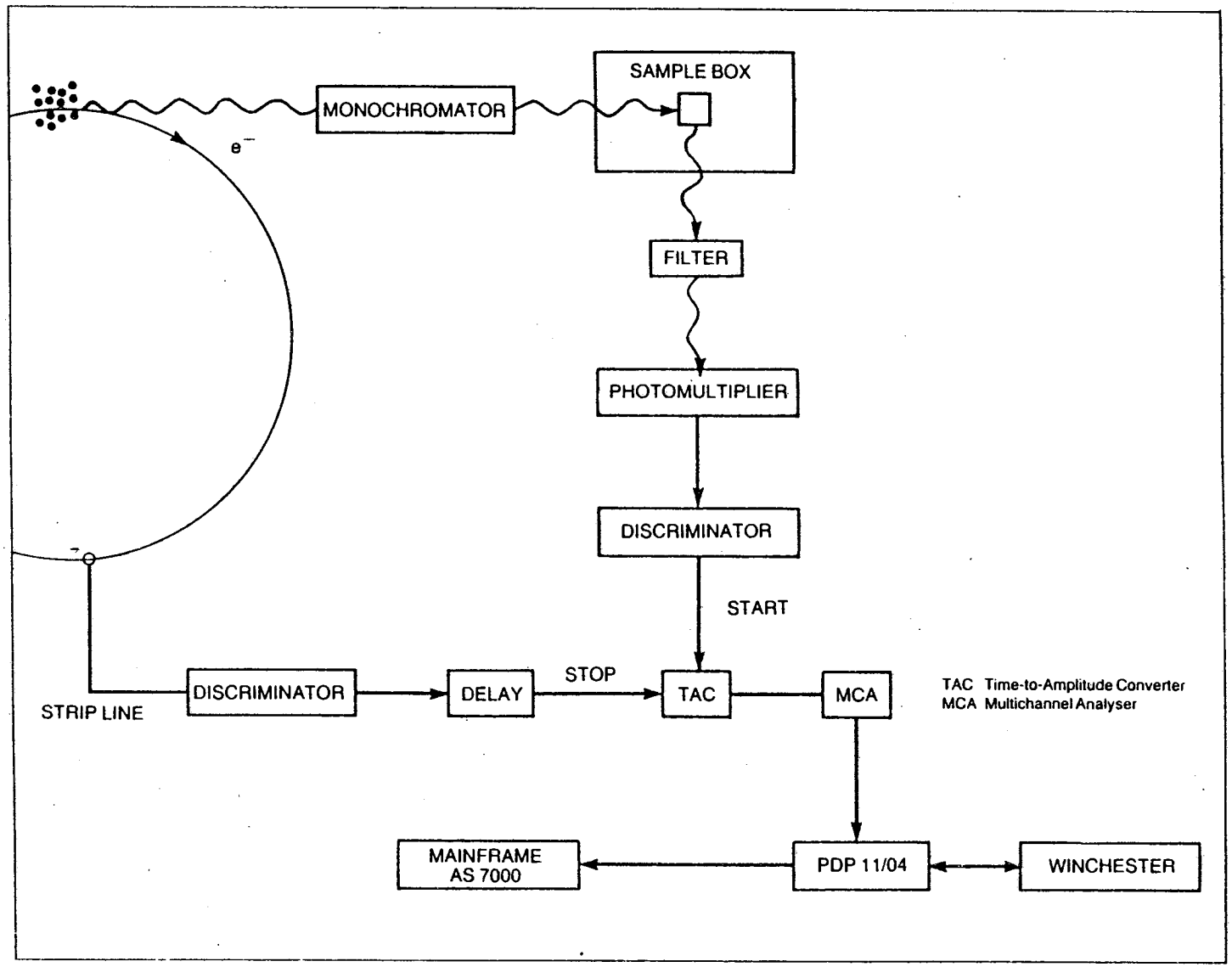

Figure 2.6 Schematic diagram of the timing apparatus used at the S.E.R.C. Daresbury Laboratory

2.10 Description of Cells used in Experiments

The standard cell used for the ArF laser induced fluorescence experiments was an all-quartz cell. This consisted of a hollow cylinder of Spectrosil quartz 100 mm long and 10 mm in diameter. Two Spectrosil windows (10 mm diameter) had been fused on to the ends of the cell. A "Young's Greaseless" tap was attached to the cell through a B10 size ground glass joint using black wax. The cell was filled from a standard vacuum line using this tap.

The cell used for F_2 laser induced experiments was a Pyrex cylinder (100 mm long, 10 mm diameter) with a "Young's Greaseless" tap fused half way down the cell. An opening had been blown 15 mm from the front of the cell so that a 15 mm diameter side window could be fixed in place. A MgF_2 window (10 mm diameter) was black waxed onto the front of the cell. A 10 mm Spectrosil window was black waxed onto the rear of the cell. The observation window was a 15 mm diameter Spectrosil quartz window attached to the side of the cell using black wax.

For the experiments involving work with a spectrofluorimeter or time resolved experiments using the Synchrotron Radiation Source, the cell used was a standard 1 cm^2 Spectrosil fluorescence cell with a "Young's Greaseless" tap fitted with black wax. This allowed gas handling using a conventional vacuum line.

Finally, the cell used in the absorption experiments using the Synchrotron at Daresbury consisted of a Pyrex cylinder 100 mm long and 10 mm in diameter with a "Young's Greaseless" tap fused on to allow gas handling. 10 mm diameter MgF_2 windows were attached at either end of the cell using Araldite. The rear surface of the exit window was coated with sodium salicylate to a surface density of 2 mg cm^{-2}.

2.11 Materials Used

The iodine used was Analar quality I_2 (99.9% pure), supplied by BDH Ltd., and was thoroughly de-gassed before use. The bromine used was S.L.R. quality Br_2 (99% pure) supplied by Fisons Ltd. This was transferred to a vacuum line and the middle boiling fraction of the sample was then transferred to a sample tube for later use. The sample of Br_2 used was thoroughly de-gassed before use.

The IBr used in the experiments described in this thesis was made by mixing equimolar amounts of the I_2 and Br_2 described above in a 1 dm^3 evacuated glass (Pyrex) bulb. The mixture was left for several days in order to reach complete equilibrium. Again this sample was thoroughly de-gassed before use.

The gases used for the quenching experiments were as follows:

B.O.C. spectroscopic grade xenon, B.O.C. high purity grade argon, B.O.C. white spot grade nitrogen, B.O.C. research grade helium and Matheson C.P. Grade sulphur hexafluoride. All gases that could be condensed by liquid nitrogen were de-gassed before use.

2.12 Reference

(1) H. Pummer, K. Hohla, M. Diegelmann and J.P. Reilly, Opt.Commun., 28 (1979), 104.

CHAPTER 3

The Simulation of Oscillatory Spectra

3.1 Introduction

In general, there are three approaches to extracting information on potential curves from experimental spectra. These are: analytical approximations to U(r) that lead to a solution in a closed form (e.g. the harmonic oscillator potential), unfolding or transform techniques and direct spectral simulation. In the present case, it should be possible to derive an approximate formula that connects the spacing of the high frequency peaks in an oscillatory fluorescence spectrum with the slope of the difference potential or a formula to connect the spacing of the low frequency structure (supernumerary rainbows) with the curvature of the difference potential. However, such formulae would only be approximate and would in any case have to be checked by direct simulation. Therefore it was decided that the method of direct simulation would be used with such formulae only occurring implicitly in the choice of trial potentials.

In calculating oscillatory spectra by direct simulation, both the upper and lower potentials need to be input to the simulation programme. In general one of the potentials is well known while the other is merely a guess. The result of the calculation is then compared to the original experimental spectrum and alterations are judiciously made to the trial potential. This process is followed iteratively until the calculated spectrum resembles the experimental spectrum sufficiently for the trial

potential to be a reasonable representation of the actual molecular potential involved. Once all the peaks in the calculated fluorescence spectrum have been fixed, the general intensity envelope of the spectrum is altered to fit the experimental data by the use of the transition dipole moment function, $\mu_{12}(r)$. It is this process of altering the trial potentials and $\mu_{12}(r)$, and in particular how it was used in the case of halogen ion-pair state fluorescence, that is described in this chapter, rather than the workings of the simulation programme itself. An annotated copy of the simulation programme appears as Appendix 1. The programme was originally written by K.P. Lawley[1] and has been only slightly modified in the last three years. A description of the programme can be found in reference 1.

3.2 Double Frequency (Interference) Type Spectra

The McLennan bands of I_2 and the similar fluorescence system from Br_2 were analysed in order to obtain information on the bound ion-pair state from which the fluorescence originated. That is, in analysing the double frequency type of oscillatory spectra, the ground state was known and the upper state had to be determined. In the absence of any information on the upper state other than the fluorescence spectrum, the method outlined below would be recommended, although it was not the only method used in the three years of research on which this thesis is based.

Two properties of the difference potential have the most effect on the appearance of the fluorescence spectrum: the position and curvature of the maximum of the difference potential. These two properties should be fixed first. The energy at which the rainbow point occurs mainly affects the position of the long wavelength maximum in the fluorescence spectrum, while the curvature at this point has most effect on the spacing of the peaks of the fluorescence spectrum. The energy of the rainbow point is easy to calculate and is found by subtracting the energy of a photon emitted at the long wavelength fluorescence maximum from the energy of the excitation photon. The curvature of the difference potential at the rainbow point has to be found by trial and error.

The procedure for this is as follows: First, choose the bondlength at which the rainbow point is likely to occur – it is not important to guess this very accurately but a good guess will help later on. A value of the r_e of the D' state of the molecule concerned plus $\sim$0.3 Å would be reasonable. The position of the rainbow point should then be fixed using the position of the long wavelength fluorescence maximum of the spectrum, and a value for the curvature of the difference potential at this point should be guessed. Since, by definition, the gradient of the difference potential at the rainbow point is zero, this process fixes three pieces of information on the difference potential and, because the ground state is known, on the upper potential as well.

These three pieces of information can be used to determine the three unknown constants in the Rittner potential (equation 3.1), A, b and C_3. The mathematics of this is described later. The potential so determined

$$U(r) = A \exp(-br) - {}^{C_1}/_{r} + {}^{C_3}/_{r3} - {}^{C_4}/_{r4} - {}^{C_6}/_{r6} + T_\infty \qquad (3.1)$$

is used as the first trial upper state in the simulation procedures. This process is repeated with various curvatures until the best trial potential is found. In general, the greater the curvature of the difference potential, the greater is the spacing of the peaks in the calculated spectrum. Using this rule the best value for the curvature of the difference potential can be found quite easily. Once the best guess at the curvature of the difference potential has been found and the energy of the rainbow point fixed, the next stage is to shift the bondlength at which the rainbow point occurs in order to improve the fit of the calculated spectrum to the experimental spectrum, keeping the energy of the rainbow point and the curvature constant. The first stage of this process should simulate the last group of peaks in the experimental spectrum fairly well while the last stage should extend the fit to shorter fluorescence wavelengths. Once the best bondlength for the rainbow point has been found the curvature should then be re-examined. This process should be carried out iteratively until a satisfactory fit to the original experimental spectrum has been obtained.

As this point, the transition dipole moment function, $\mu_{12}(r)$, should be introduced. The computer programme which calculates the spectra only allows $\mu_{12}(r)$ to be an exponential function, i.e. $\exp(-\alpha r)$. Therefore, the final stage in simulating an experimental spectrum is to try various values of α to find the best $\mu_{12}(r)$. A flow diagram of the above is presented as Figure 3.1 as a summary of the method of simulation described above.

The mathematics for calculating the Rittner potential from the position and curvature of the rainbow point in the difference potential will now be described. In forming the Rittner potential it is important that the point at which the fitting is carried out contains information on A, b and C_3. That is, the point must not be at a bondlength sufficiently large that $A \exp(-br)$ is negligible or sufficiently small that $A \exp(-br)$ totally dominates C_3. In practice, this condition rarely prevents values being obtained for A, b or C_3 but does mean that the physical interpretation of the value of the term C_3 is suspect. This is because, typically, the C_3 term never contributes more than $\sim$5% to the binding energy of the upper state so that this method will only fix its value with poor precision. Also the values for all the coefficients are only appropriate to the particular functional form chosen for $U_2(r)$. Thus, if a potential with switching functions were chosen the importance of the term C_3 would vary with bondlength. However, even if

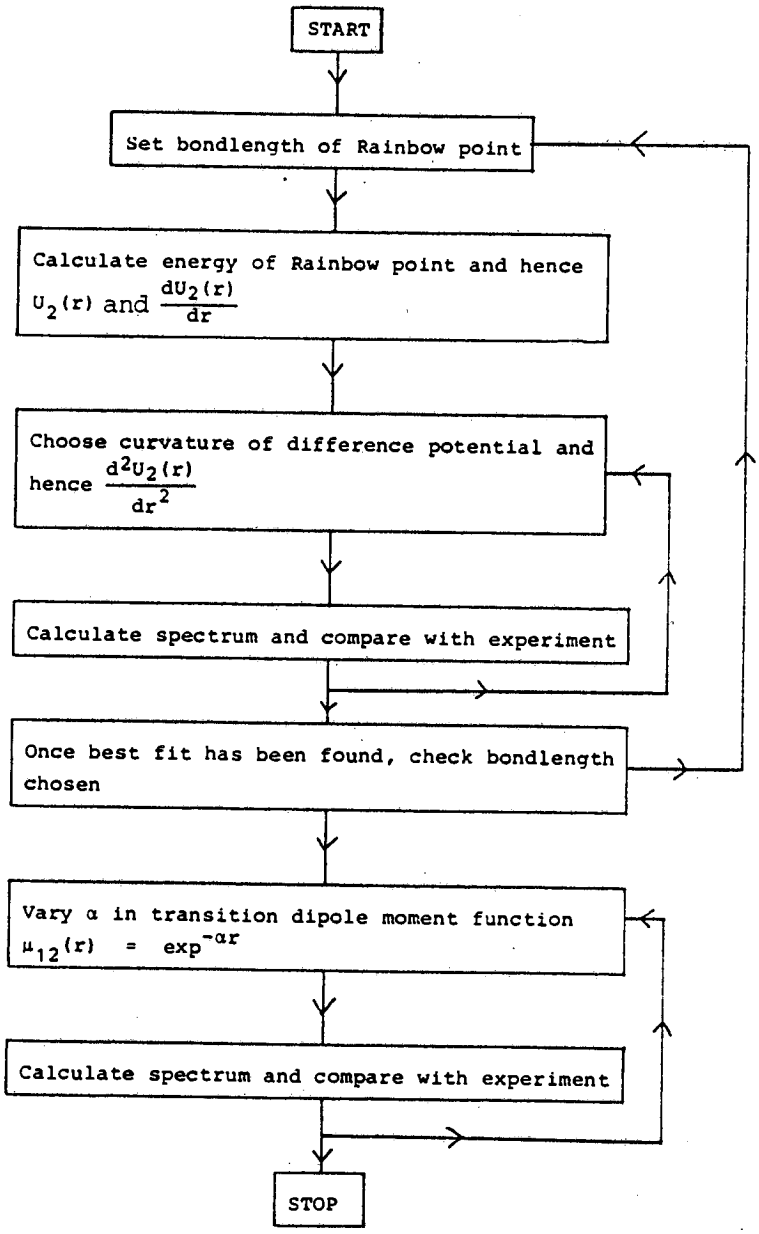

Figure 3.1 A schematic of the simulation process for finding the upper state of a two frequency type of oscillatory emission

the value found for C_3 does not agree with the strength of the charge-quadrupole interaction for the ions concerned, the combination of values for A, b and C_3 does fix the potential properly at the point of interest and the Rittner potential does extrapolate properly to the dissociation limit of the ion-pair states. The values of A, b and C_3 are found as follows:

$$U_2(r) = A \exp(-br) - {}^{C_1}/_{r} + {}^{C_3}/_{r^3} - {}^{C_4}/_{r^4} - {}^{C_6}/_{r^6} + T_\infty \qquad (3.1)$$

$$\frac{dU_2(r)}{dr} = -Ab \exp(-br) + {}^{C_1}/_{r^2} - {}^{3C_3}/_{r^4} + {}^{4C_4}/_{r^5} + {}^{6C_6}/_{r^7} \qquad (3.2)$$

$$\frac{d^2U_2(r)}{dr^2} = Ab^2 \exp(-br) - {}^{2C_1}/_{r^3} + {}^{12C_3}/_{r^5} - {}^{20C_4}/_{r^6} - {}^{42C_6}/_{r^8} \qquad (3.3)$$

Collecting known terms together in equations 3.1, 3.2 and 3.3:

$$A \exp(-br) + {}^{C_3}/_{r^3} = K(r) = U_2(r) + {}^{C_1}/_{r} + {}^{C_4}/_{r^4} + {}^{C_6}/_{r^6} - T_\infty \qquad (3.4)$$

$$-Ab \exp(-br) - {}^{3C_3}/_{r^4} = L(r) = \frac{dU_2(r)}{dr} - {}^{C_1}/_{r^2} - {}^{4C_4}/_{r^5} - {}^{6C_6}/_{r^7} \qquad (3.5)$$

$$Ab^2 \exp(-br) + {}^{12C_3}/_{r^5} = M(r) = \frac{d^2U_2(r)}{dr^2} + {}^{2C_1}/_{r^3} + {}^{20C_4}/_{r^6} + {}^{42C_6}/_{r^8} \qquad (3.6)$$

From equations 3.4 and 3.5:

$$C_3 = [K(r) - A \exp(-br)] \cdot r^3 = -\frac{1}{3}[L(r) + Ab \exp(-br)] \cdot r^4 \qquad (3.7)$$

$$\Rightarrow A = [K(r) + \frac{1}{3}L(r) \cdot r] / \{[1 - \frac{1}{3}br][\exp(-br)]\} \qquad (3.8)$$

Again from equations 3.4 and 3.5:

$$A = [K(r) - {}^{C_3}/_{r^3}] / [\exp(-br)] = -[L(r) + {}^{3C_3}/_{r^4}] / [b \exp(-br)] \qquad (3.9)$$

$$\Rightarrow b = -[L(r) + {}^{3C_3}/_{r^4}] / [K(r) - {}^{C_3}/_{r^3}] \qquad (3.10)$$

and combining equations 3.5 and 3.6:

$$A = -[L(r) + {}^{3C_3}/_{r^4}] / [b \exp(-br)] = [M(r) - {}^{12C_3}/_{r^5}] / [b^2 \exp(-br)] \qquad (3.11)$$

$$\Rightarrow b = -[M(r) - {}^{12C_3}/_{r^5}] / [L(r) + {}^{3C_3}/_{r^4}] \qquad (3.12)$$

Combining equations 3.10 and 3.12 gives:

$$b = -[L(r) + {}^{3C_3}/_{r^4}] / [K(r) - {}^{C_3}/_{r^3}] = -[M(r) - {}^{12C_3}/_{r^5}] / [L(r) + {}^{3C_3}/_{r^4}] \qquad (3.13)$$

$$\Rightarrow {}^{3C_3^2}/_{r^8} - C_3[12K(r)/r^5 + 6L(r)/r^4 + M(r)/r^3] + M(r)K(r) - L^2(r) = 0 \qquad (3.14)$$

The final step is to solve equation 3.14 as a quadratic equation in C_3.

$$\alpha C_3^2 + \beta C_3 + \gamma = 0 \qquad (3.15)$$

where

$\alpha = {}^3/r^8$; $\beta = -[12K(r)/r^5 + 6L(r)/r^4 + M(r)/r^3]$;

$\gamma = M(r)K(r) - L^2(r)$

Solving equation 3.15 and substitution back through equations 3.10 and 3.8, gives values of A, b and C_3 if a point on a Rittner potential and the first two derivatives at that point are known. These are trivial to calculate from a knowledge of the difference potential and $U_1(r)$.

3.3 Single Frequency (Reflection) Type Spectra

In analysing these spectra it is the upper state that is known and the lower state that has to be found. The lower states of I_2 and Br_2 were found in the following way. It was assumed that the lower state was purely repulsive and in the two cases analysed dissociated to two ground state halogen atoms (e.g. $I^2P_{3/2} + I^2P_{3/2}$) and the analysis involved fitting the potential to a sum of exponential terms $A_i \exp(-b_i r)$. The spectrum was analysed by extending the fit from the long wavelength fluorescence limit to shorter wavelengths as far as the experimental spectrum would allow.

The first step in the simulation process was to find $U_1(r)$ at the bondlength corresponding to the inner turning-point of the upper state which was relatively easy because at this point the molecule in the upper state possesses no kinetic energy. $U_1(r)$, where r is the inner turning-point of the upper state, was found by subtracting the energy of a photon emitted at the long wavelength fluorescence limit from the energy of the photon used to excite the system. Once this point had been fixed, the process used to fit the rest of the spectrum was one of trial and error. Initially, a single exponential (equation 3.16) was used.

$$U_1(r) = A \exp(-br) + D_e \qquad (3.16)$$

This exponential was fitted to the first few peaks of the fluorescence spectrum by systematically altering the slope of this potential at the reference point calculated above. Only the peak positions were fitted, with no effort having been put into matching peak intensities. It was relatively easy to iterate to the correct slope as the effect of steepening the slope increased the spacings between peaks on the calculated spectrum. Once the calculated spectrum fitted the experimental spectrum over the first few peaks, it was necessary to calculate the bondlength range over which $U_1(r)$ was valid. This was best done by determining the fluorescence wavelength at which the calculated spectrum began to deviate from the experimental spectrum and then the point on the classical

difference potential at which this fluorescence landed and the corresponding point on $U_1(r)$. This last point on the single exponential potential was used as the first point of an exponential extension to the potential. The original potential was kept intact up to this point, at which the second exponential section was added. The slope of this second exponential was systematically varied until the positions of the next few peaks in the experimental fluorescence spectrum were properly fitted. The next step in this process was to find the last point at which this new $U_1(r)$ was valid. In general, a third or fourth extension to the lower potential may be necessary until the complete experimental fluorescence spectrum has been successfully simulated. At this stage, $U_1(r)$ was not a smooth function. In order to make $U_1(r)$ smooth, it was fitted to a sum of exponential decays (equation 3.17), using as few exponentials as possible; i.e. N was kept as small as possible as was consistent with obtaining a good fit.

$$U_1(r) = \sum_{i=1}^{N} [A_i \exp(-b_i r)] + D_e \qquad (3.17)$$

Once a smooth lower potential was found, effort was put into finding the transition dipole moment function, $\mu_{12}(r)$. As with the case of a double frequency type of oscillatory spectrum, the computer programme used only allows $\mu_{12}(r)$ to be of the form $\exp(-\alpha r)$ so that finding the best value of α was simply a matter of systematically varying α until

the best fit of peak intensities was obtained. Increasing the value of α makes the fluorescence spectrum die away more rapidly as one moves towards shorter fluorescence wavelengths. A schematic of this simulation process is presented as Figure 3.2.

The spectra studied involved transitions from an ion-pair state to a valence state. At large internuclear separations, the transition dipole moment function must tend to zero as such transitions involve a large electron jump from the negative ion to the positive ion. As the electron cloud overlap decreases exponentially as the two nuclei separate, $\mu_{12}(r)$ should also decrease exponentially with r, at least for all but very short bondlengths. For this reason it was decided to introduce $\mu_{12}(r)$ into the simulation programme as a simple exponential decay. This function worked well for the two spectra of iodine simulated.

In the case of a single frequency type of oscillatory spectrum $\mu_{12}(r)$ can be found in a more general form by using the r-centroid approximation. The r-centroid approximation states that, as $\mu_{12}(r)$ is a slowly varying function of r, it may be taken out of the integral $< \chi_1 \mid \mu_{12} \mid \chi_2 >^2$ and replaced by the nearly constant value it possesses in the small bondlength region where this integral accumulates (see Chapter 1 for a fuller discussion of this). In other words, $\mu_{12}(r)$ may be replaced by its value at the classical point of transition. In practice this means finding the points on the classical

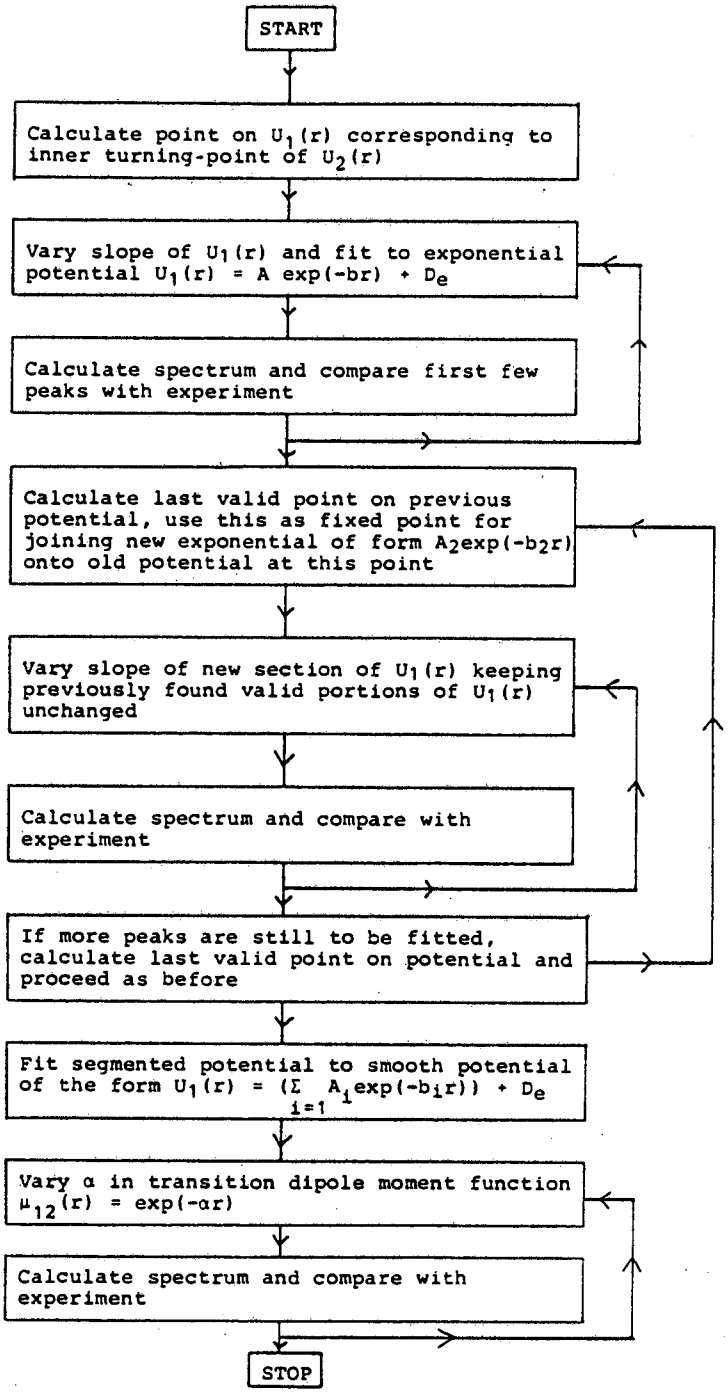

Figure 3.2 A schematic of the simulation process for finding the lower state involved in a single frequency oscillatory continuum emission

difference potential where fluorescence from each peak lands and setting $\mu_{12}(r)$ at each point to correct the calculated fluorescence intensity. This, with interpolation between the points, should lead to a smooth, slowly varying function for $\mu_{12}(r)$. More explicitly, this process is carried out as follows.

Suppose an experimental spectrum, $I_E(\nu)$, is simulated using a constant for $\mu_{12}(r)$, giving as a result a simulated spectrum $I_S(\nu)$. If the peaks occuring in the spectrum are numbered from i = 0, N and if both the spectra are normalised to the intensity of the first peak (i = 0) then equation 3.18 can be used. This equation states that the ratio of the value of $\mu_{12}(r)$ at the classical point of

$$\mu_{12}^{(1)}(r_i)/\mu_{12}(r_o) = (I_E(\nu_i(r))/I_S(\nu_i(r)))^{\frac{1}{2}} \qquad (3.18)$$

transition giving rise to peak O and the value of $\mu_{12}(r)$ used to obtain the first simulated spectrum $I(\nu)$ is equal to the square root of the ratio of the intensity of peak i in the experimental spectrum and the intensity of peak i in the simulated spectrum. In this way, $\mu_{12}^{(1)}(r_i)$ can be calculated for all the peaks in the experimental spectrum. These $\mu_{12}^{(1)}(r_i)$ can then be fitted to a smooth function $\mu_{12}^{(1)}(r)$, which can be inserted in the simulation programme to obtain $I_S^{(1)}$. This process can be repeated using the recurrence relation of equation 3.19 to further refine $\mu_{12}(r)$.

$$\mu_{12}^{(j+1)}(r_i)/\mu_{12}^{(j)}(r_i) = (I_E(\nu_i(r))/I_S^{(j)}(\nu_i(r)))^{\frac{1}{2}} \qquad (3.19)$$

If the peak positions in the simulated spectrum shift as each improved $\mu_{12}^{(j)}(r)$ is used, then $\mu_{12}(r)$ is classified as a rapidly varying function of r. In this case the potential parameters originally derived will have to be re-optimised to bring the simulated peak positions back into alignment with the experimental peak positions each time an improved $\mu_{12}^{(j)}(r)$ is used. This will slow down the rate of convergence of the iteration.

3.4 Reference

(1) K.P. Lawley and R. Wheeler, J.Chem.Soc., Faraday Trans. II, 77 (1981), 1133.

CHAPTER 4

The Spectroscopy of $I_2D(O_u^+)$

4.1 Introduction

Iodine is the best studied of all the halogens: in fact, there is experimental information on nine of the twelve ion-pair states of I_2 that diabatically dissociate to $I^-(^1S) + I^+(^3P_{2,1,0})$ while calculated parameters are quoted in the literature for all twelve states. The present position has been summarised by Viswanathan and Tellinghuisen[1]. A table taken from their paper is presented here, with minor alterations, as Table 4.1. In this table, Tellinghuisen's more recent analysis[2] of the $D(O_u^+)$ state of I_2 has been substituted for his earlier analysis[3]. The results described in this chapter have been added to the table.

Recently, Ishiwata et al[4] have analysed one of the ion-pair states of I_2 diabatically dissociating to $I^-(^1S)$ and $I^+(^1D)$. This state, the $F^1(O_u^+)$ state , has a T_e of 51707 cm^{-1} which, as expected, is higher than the T_e s of the states described in Table 4.1. The ω_e value of the $F^1(O_u^+)$ state is 131 cm^{-1} which is approximately 30% higher than for the ion-pair states dissociating to $I^-(^1S) + I^+(^3P_{2,1,0})$. An equilibrium bond distance of 3.48 Å is given in the paper.

To obtain the information in Table 4.1 the experimenters used either high resolution tunable dye lasers or high resolution spectrographs, whereas the techniques used for the present work require neither a

very narrow bandwidth of excitation to probe the excited state nor high resolution dispersion of the resulting fluorescence. In the work described here a high vibrational level ($v' = 144$) of the $I_2 D(O_u^+)$ state was excited by the absorption of a single ultra-violet photon and the resulting fluorescence spectra were recorded with a resolution of a few angstroms. The D→X portion of the fluorescence spectrum was then inverted to produce a Rittner type of potential for the $D(O_u^+)$ state. It is the spectroscopic constants which were derived from this potential that are presented in Table 4.1. A second fluorescence system was also analysed and inverted. This produced a repulsive lower state. Some of the preliminary work carried out for this chapter has previously been published[5].

4.2 Experimental

The experimental set-up to produce the laser induced fluorescence spectra was of standard design, with fluorescence being observed at right angles to the excitation beam (see Figure 2.1). Work done at Edinburgh used a Lambda Physik EMG500 laser, filled to operate on the ArF transition (193 nm), as the excitation source. Signal detection was achieved by using a scanning McKee Pederson 0.5 m monochromator with photomultiplier (EMI 9661B).

Table 4.1 (adapted from reference 1)

Summary of experimentally known ion-pair states of I_2 which diabatically dissociate to $I^-(^1S) + I^+(^3P_{2,1,0})$. Theoretically predicted spectroscopic constants for these states are also included.

State	R_e/Å Experiment/theory (15)		T_e/cm^{-1} Experiment/theory (15)		ω_e/cm^{-1} Experiment/theory (15)		Ref.
corresponding to $I^-(^1S) + I^+(^3P_2)$							
$D'\ ^2_g$	3.61	3.61	40388	41950	104.0	101.8	6,7
$\beta\ ^1_g$	3.61	3.60	40821	42400	105.0	102.6	8
$D\ O^+_u$	3.60	3.60	41027	42600	95.0	96.3	2
$E\ O^+_g$	3.65	3.63	41412	42700	101.4	101.5	9,8
$\gamma\ ^1_u$	3.68	3.68	41621	43050	95.0	95.1	10
$\delta\ ^2_u$	~4.0	3.77	41789	43050	100.2	97.8	10
corresponding to $I^-(^1S) + I^+(^3P_{1,0})$							
$f\ O^+_g$	3.57	3.62	47026	48550	104.2	102.9	11
$g\ O^-_g$		3.61	47070	48950	105.7	101.5	1
$F\ O^+_u$	3.59	3.73	47218	49450	96.0	89.9	12,13
$G\ ^1_g$	3.53	3.61	47559	49700	106.6	103.6	14
O^-_u		3.79		50100		99.4	
^1_u		3.69		50100		102.6	
Results from this chapter for I_2 DO^+_u							
$D\ O^+_u$	3.56		41011		98.8		

At the S.E.R.C. Rutherford Appleton Laboratory the excitation source was a line narrowed ArF laser (Lambda Physik EMG150) giving a linewidth of only a few wavenumbers (<10 cm^{-1}). The fluorescence signal was dispersed using a Jobin-Yvon 0.3 m monochromator equipped with a medium resolution grating to give ∿0.3 nm F.W.H.M. resolution. The detection system used was an optical multichannel analyser (EG & G/PAR OMA II) fitted with an intensified diode array head. The recorded spectra were the result of accumulating the fluorescence produced from several laser shots directly on the diode array head. The figure captions will state the exact conditions used.

A Perkin-Elmer 650-40 spectrofluorimeter, on loan from the S.E.R.C. Daresbury Laboratory, was also used to obtain fluorescence spectra. To obtain excitation below 200 nm, the excitation monochromator had to be used in 2nd order. A 250 nm cut-off filter was used to prevent scattered light from the excitation source reaching the detection photomultiplier. Light from the excitation source passing through the excitation monochromator in 1st order (i.e. light with λ ∿400 nm) could not be filtered out. The excitation source was blocked while the detector scanned these 1st order wavelengths in order to protect the detection photomultiplier from scattered light, leading to the gaps in the fluorescence spectra shown in Figure 4.9. The iodine sample was contained in a standard 1 cm^2 quartz spectrofluorimeter cell fitted with a greaseless tap.

Absorption spectra of I_2 were obtained using the S.E.R.C. synchrotron radiation source at Daresbury in conjunction with a McPherson 5 m monochromator and a standard photomultiplier detector.

In all cases the iodine sample consisted of a few crystals of iodine placed in a cell which was then evacuated. Thus all spectra are of iodine vapour at its room temperature vapour pressure ($\sim$27 Nm^{-2}). Further experimental details can be found in Chapter 2.

4.3 The Absorption Spectrum

Two absorption spectra of iodine are presented here, the first covering the region from 160 nm to 200 nm (Figure 4.1), while the second concentrates on the region between 180 nm and 200 nm (Figure 4.2). In Figure 4.1 one can see ion-pair state absorption running from 178 nm out to longer wavelengths, while below 178 nm the spectrum consists mainly of Rydberg absorption systems. These Rydberg bands have previously been analysed by Venkateswarlu[16] and were used for calibration. The vibrational spacing measured from Figure 4.2 in the region of ArF laser excitation (193 nm) is 55 cm^{-1} ± 5 cm^{-1}; this increases to 60 cm^{-1} ± 5 cm^{-1} by 198 nm and decreases to 48 cm^{-1} ± 5 cm^{-1} by 188 nm. The close vibrational spacing observed and the relatively slow rate of convergence of these levels is indicative of ion-pair state absorption. This is a consequence of the ion-pair

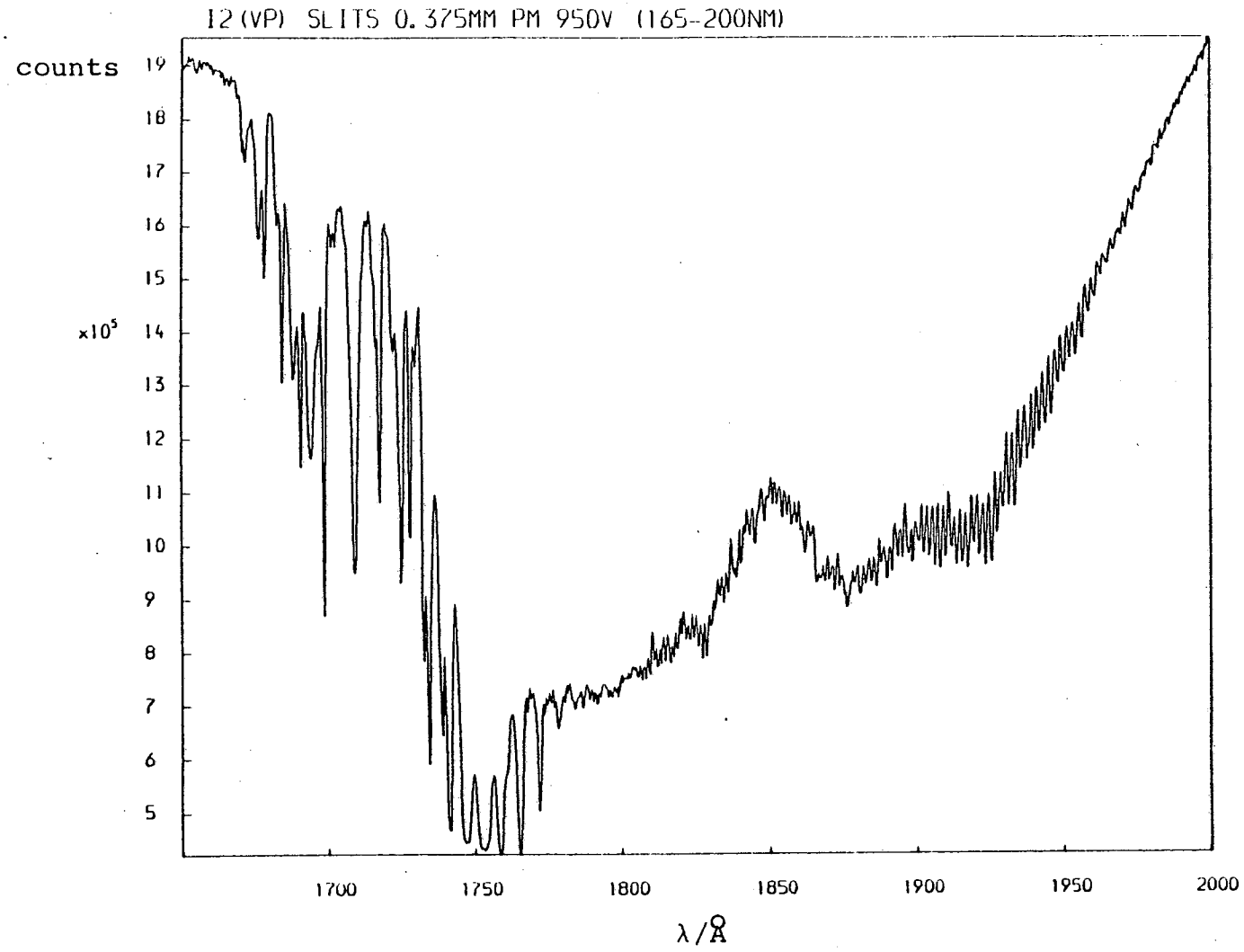

Figure 4.1 Absorption spectrum of I_2 (27 Nm^{-2}) showing both Rydberg absorption (165 - 177 nm) and ion-pair absorption (177 - 200 nm). The Rydberg bands were used to calibrate the spectrum, it being found that the scale reads high by 2.8 Å. The spectrum was recorded with a resolution of 0.06 nm.

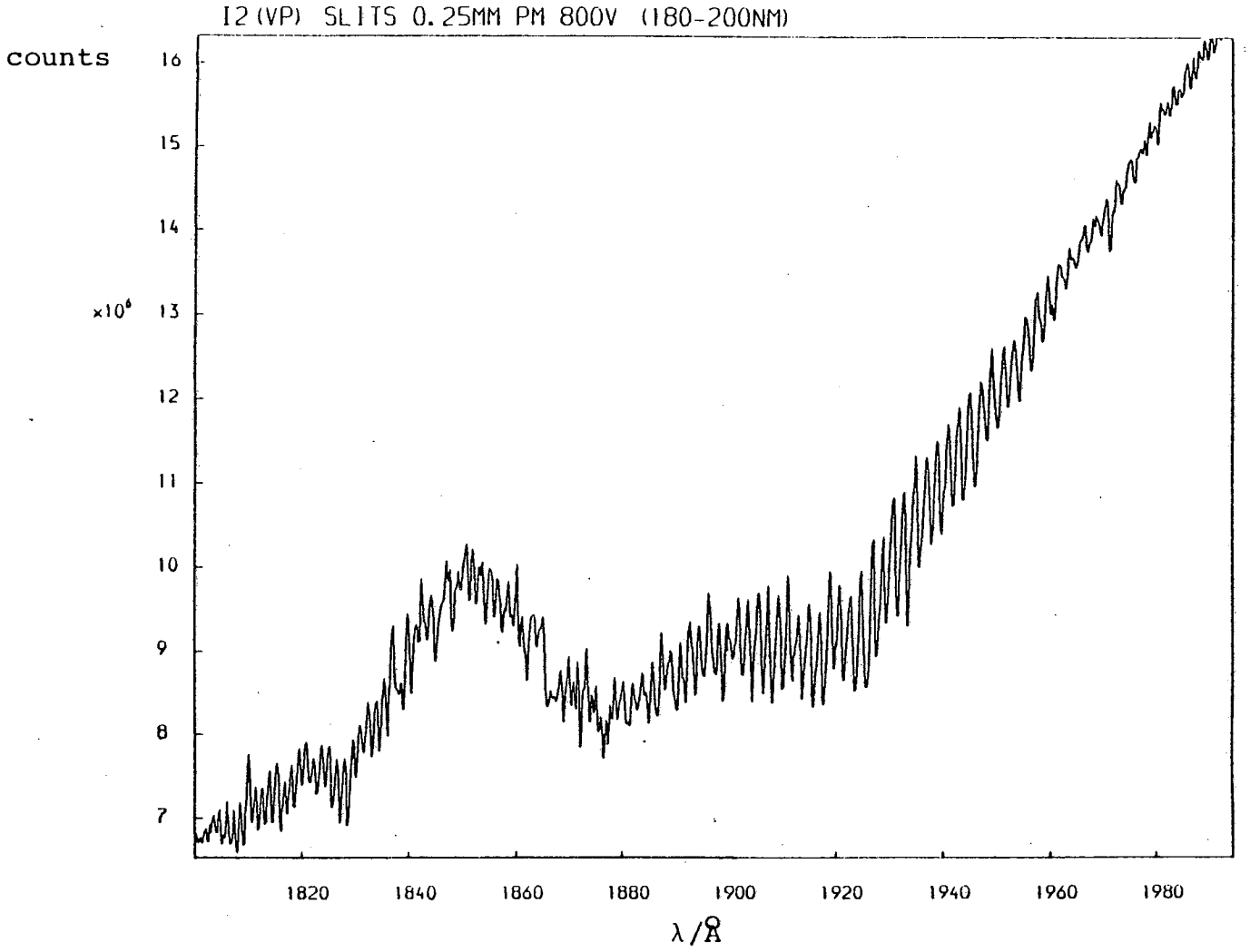

Figure 4.2 Absorption spectrum of I_2 (27 Nm^{-2}) showing ion-pair absorption. The scale reads high by 2.8 Å. The spectrum was recorded with a resolution of 0.04 nm.

potential being dominated by the long range r^{-1} term as opposed to the r^{-5} or r^{-6} terms normally expected to dominate valence state potentials.

The absorption structure appears simple between 180 nm and 184 nm but then becomes complex between 184 nm and 188 nm. After 188 nm the absorption spectrum again simplifies, remaining simple until 197 nm. Between 197 nm and 200 nm the spectrum once more appears complex, while beyond 200 nm the spectrum is again simple. A possible explanation for this is that the regions where the absorption spectrum appears simple correspond to regions where the absorption is dominantly from a single vibrational level in the ground state. In regions where the spectrum appears complex the absorption is from two vibrational levels of the ground state. Because part of the ion-pair state absorption is obscured by the stronger Rydberg absorption system the assignment of the v'' levels involved cannot be certain. One possible assignment is absorption between 180 nm and 184 nm is from v'' = 1, absorption between 188 nm and 197 nm is from v'' = 0 and absorption above 200 nm is again from v'' = 1. However a second possible assignment is that absorption between 180 nm and 184 nm is from v'' = 0, absorption between 188 nm and 197 nm is from v'' = 1 and absorption above 200 nm is from v'' = 2. Both these assignments are possible as, at room temperature approximately 30% of the molecules in a sample of I_2 vapour will posses one quantum of vibrational energy while approximately 10% will possess two quanta of vibrational energy.

4.4 Results

Figure 4.3 is a low resolution fluorescence spectrum of iodine, excited at 193 nm, recorded by Martin, Donovan and Fotakis[17] and shows the two main fluorescence systems with which this chapter is concerned. The spectrum was recorded using a standard ArF laser and a polychromator/optical multichannel analyser combination. The first system, peaking at a wavelength of 322 nm, consists of fluorescence from the $D(0_u^+)$ state back to both bound and unbound regions of the ground $X(0_g^+)$ state. All fluorescence with a wavelength below 254 nm must be bound-bound fluorescence, while D→X fluorescence at wavelengths longer than 254 nm is bound-free oscillatory continuum fluorescence. The peaks which make up the long wavelength maximum of this fluorescence system, occuring at $\lambda \sim 322$ nm, are known as the McLennan bands. These are shown under higher resolution in Figure 4.4.

The McLennan bands were simulated in order to fix the $D(0_u^+)$ state, the resulting simulated spectrum being shown as Figure 4.5. The ground state potential of iodine used in the simulation was based on the R.K.R. analysis of LeRoy[18]. The repulsive limb of the potential was extended by fitting a curve of the form r^{-12} to the last two points of LeRoy's analysis, while the attractive limb was fixed by ensuring that at very large r the gradient of the potential was zero and the potential energy was equal

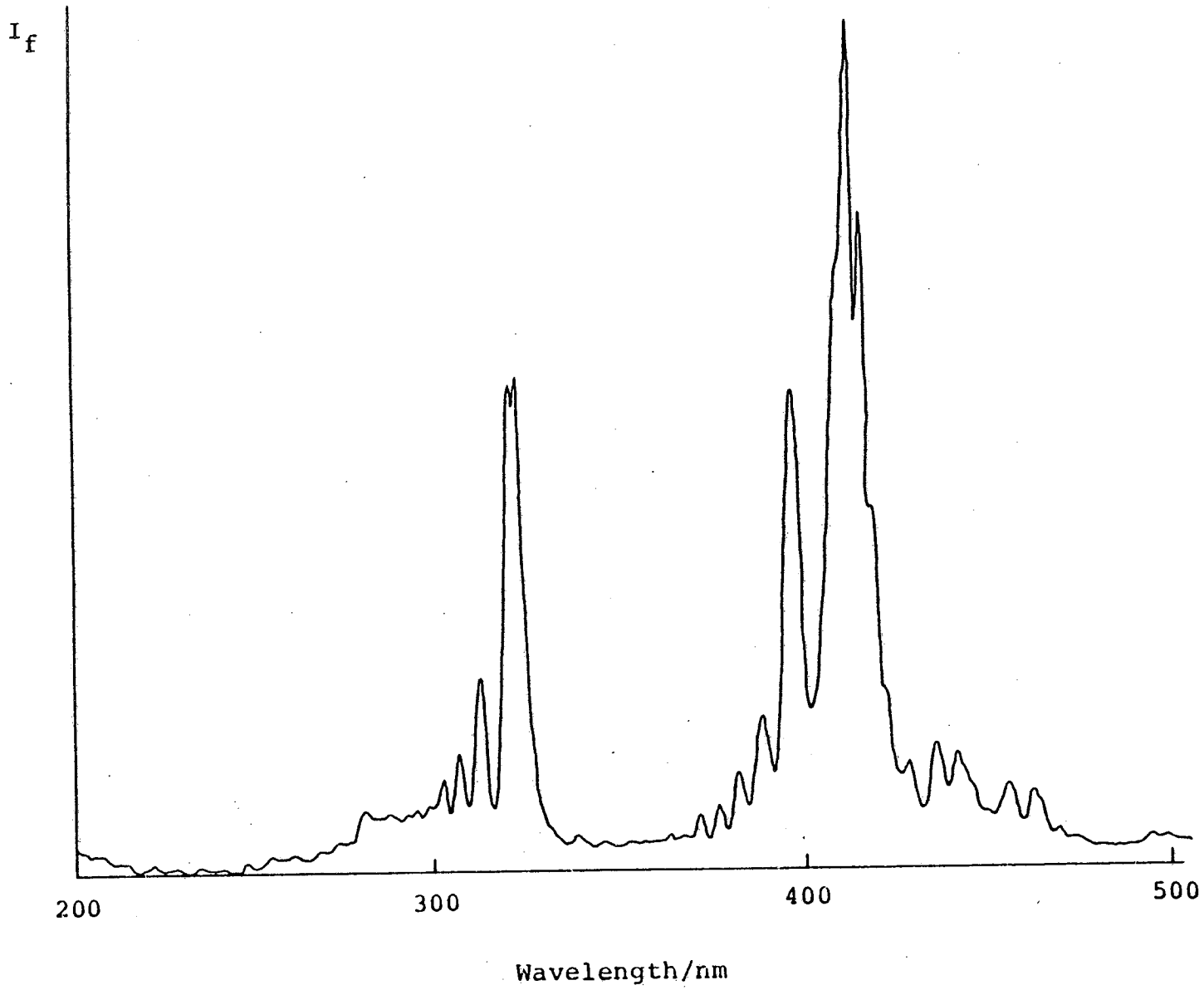

Figure 4.3 Low resolution fluorescence spectrum of iodine excited at 193 nm (ArF laser), taken from Martin, Donovan and Fotakis[17].

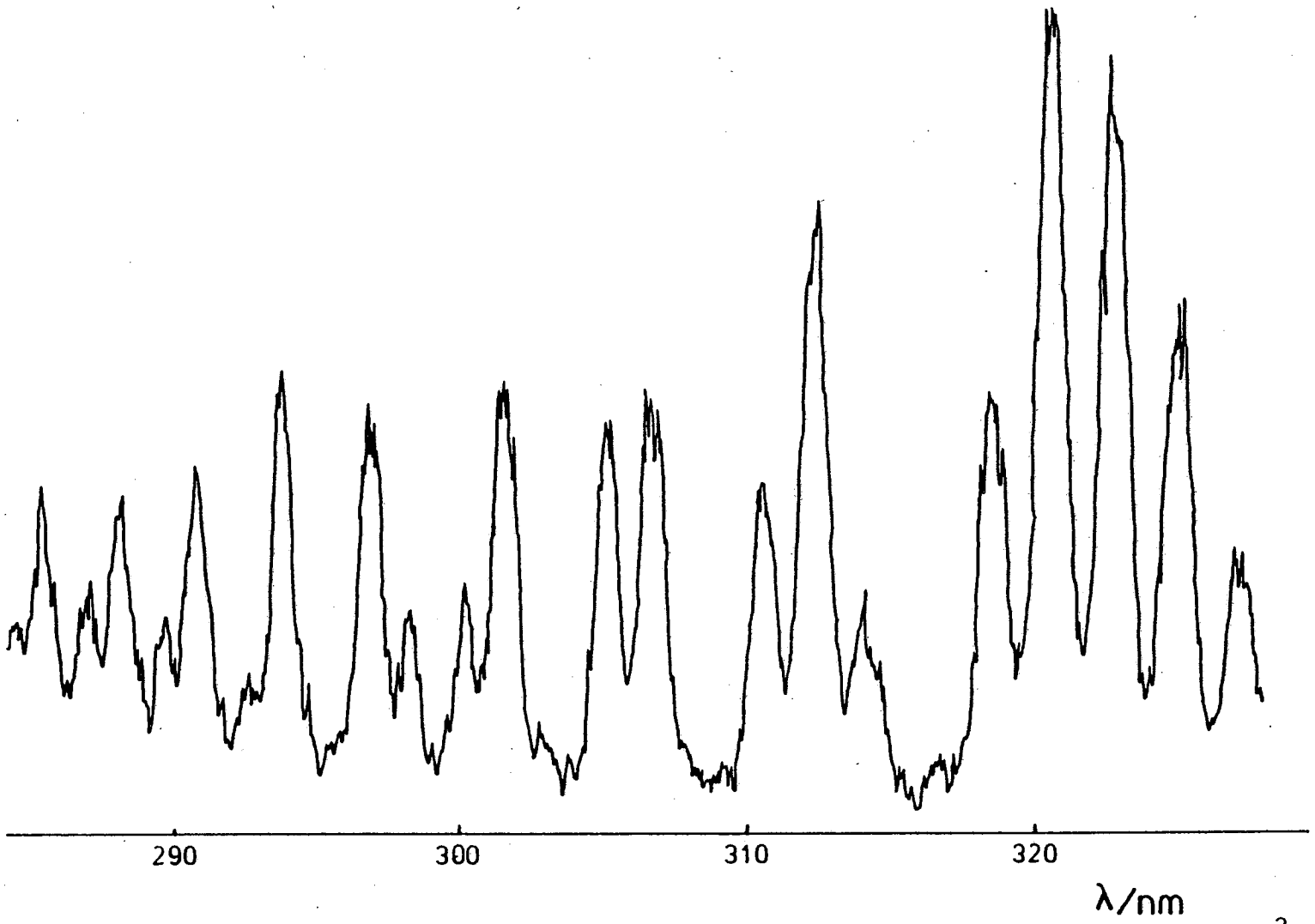

Figure 4.4 Medium resolution fluorescence spectrum of iodine ($p \cong 30\ Nm^{-2}$) excited at 193 nm using a Lambda Physik EMG500 ArF laser. The spectrum was recorded using a scanning monochromator and photomultiplier combination as the detection system

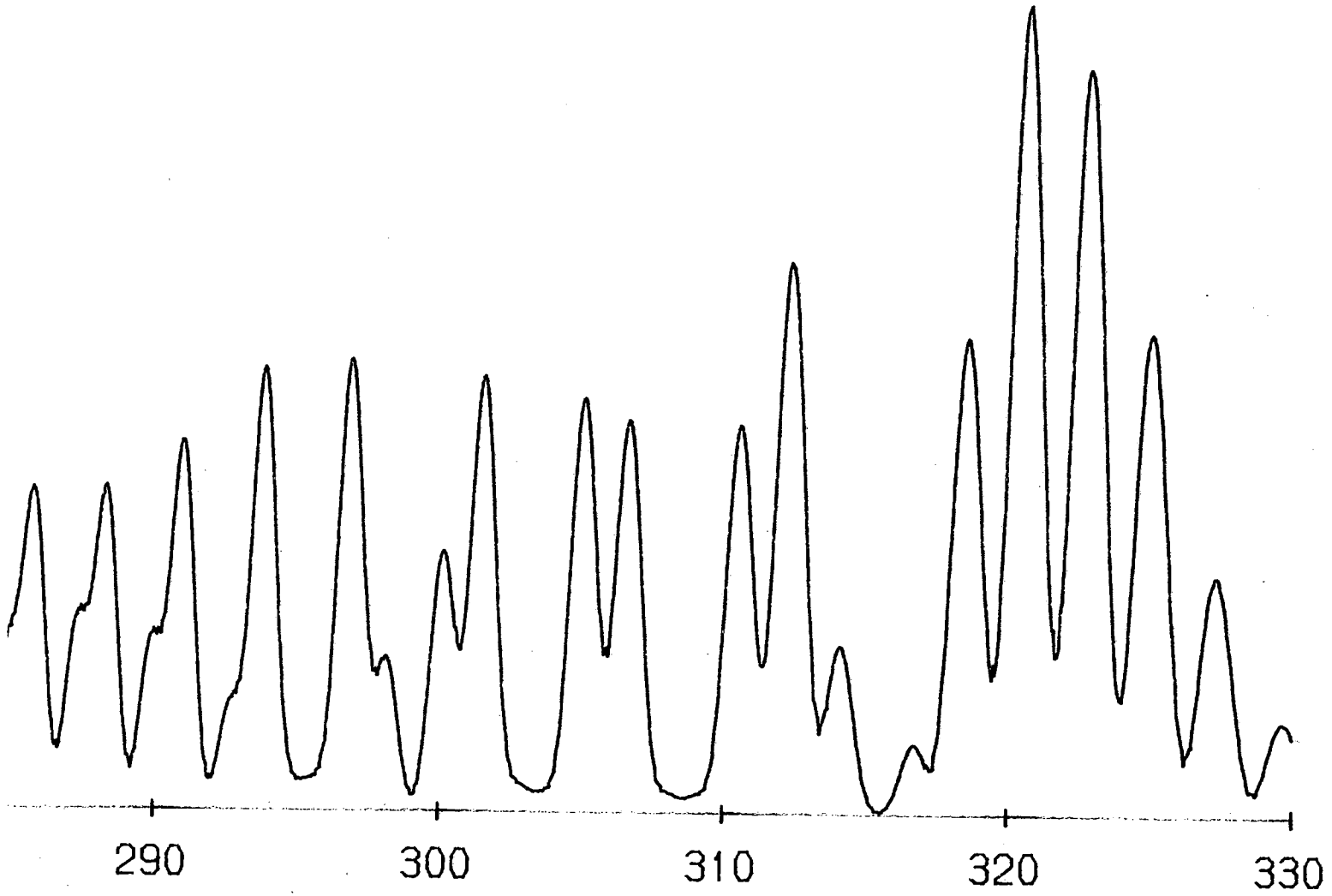

Figure 4.5 A simulation of the data shown in Figure 4.4 using the Rittner potential given in Table 4.2 and α = 0.5 in the transition dipole moment function $\mu_{12}(r) = \exp(-\alpha r)$

to the dissociation energy of I_2 (12548 cm^{-1}). More precisely a spline interpolation was carried out on the R.K.R. data points of LeRoy with the extra stipulation that the potential must have reached the dissociation limit and have zero gradient at r = 13.0 Å.

The upper $D(O_u^+)$ state potential was assumed to be in the form of a Rittner potential (equation 3.1). The final values of the constants used are given in Table 4.2.

Table 4.2 The coefficients of the Rittner potential for the $D(O_u^+)$ state of I_2, found by the simulation of the D→X fluorescence system (the McLennan bands).

Coefficient	Value	Theoretical form	Ref.
A/cm^{-1}	1.2977×10^7	found from simulation	
$b/Å^{-1}$	2.0664	found from simulation	
C_1/cm^{-1} Å	1.16142×10^5	$e^2/4\pi\varepsilon_o$	
C_3/cm^{-1} $Å^3$	-2.3462×10^4	found from simulation	
C_4/cm^{-1} $Å^4$	9.0×10^5	$e^2/4\pi\varepsilon_o(\frac{\alpha_A + \alpha_B}{2})$	19
C_6/cm^{-1} $Å^6$	1.4×10^6	$\frac{3}{2}\alpha_A\alpha_B\omega_A\omega_B/(\omega_A + \omega_B)$	19
T_∞/cm^{-1}	72,161	$I^+ = {}^3P_2$	20

This potential, with the constants in Table 4.2, yields values of 98.8 cm^{-1} for ω_e, 41011.6 cm^{-1} for T_e and 3.565 Å for r_e. These spectroscopic constants agree well

with the values quoted by Tellinghuisen[2] from his analysis of emission from the lower vibrational levels of the $I_2D(O_u^+)$ state. Tellinghuisen's results were $\omega_e = 95.0 \pm 0.3\ cm^{-1}$, $T_e = 41027.3 \pm 0.5\ cm^{-1}$ and $r_e = 3.60 \pm 0.03$ Å

The second fluorescence system shown in Figure 4.3, peaking at a wavelength of 420 nm, is shown under higher resolution in Figure 4.6. Figure 4.7 shows a simulation of the spectrum in Figure 4.6. The experimental spectrum was recorded using a line-narrowed ArF laser, at the S.E.R.C. Rutherford Appleton Laboratory, to ensure that only a single vibrational level of $I_2D(O_u^+)$ was excited. This did not change the fluorescence spectrum appreciably from that produced by standard (i.e. not line-narrowed) ArF laser excitation, implying that "washing in" of peaks, due to the excitation of several vibrational levels in the upper state, is negligible in "standard" ArF laser induced fluorescence spectra.

The fluorescence spectrum in Figure 4.6 was judged to be a single frequency type of oscillatory continuum. Therefore in analysing this spectrum the lower potential was assumed to be repulsive and sufficiently steep that the difference potential produced did not possess a maximum. The upper state potential used was that described above. The final form of the lower state potential used to generate Figure 4.7 consisted of a double exponential as no single exponential was found to

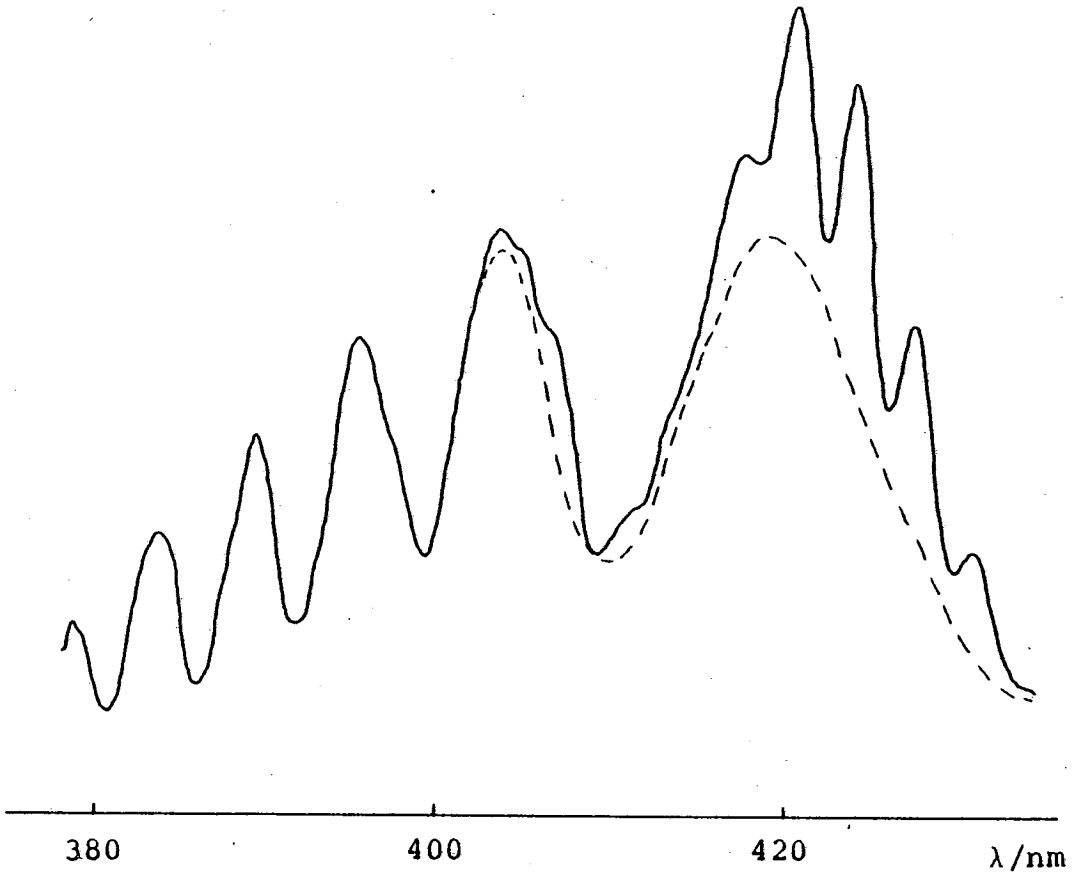

Figure 4.6 Medium resolution spectrum of I_2 ($p \cong 30\ Nm^{-2}$) recorded by averaging 20 shots of a line narrowed ArF laser (Lambda Physik EMG150) on an intensified diode array detector connected to an optical multichannel analyser. A pyrex filter was used to remove wavelengths below 300 nm

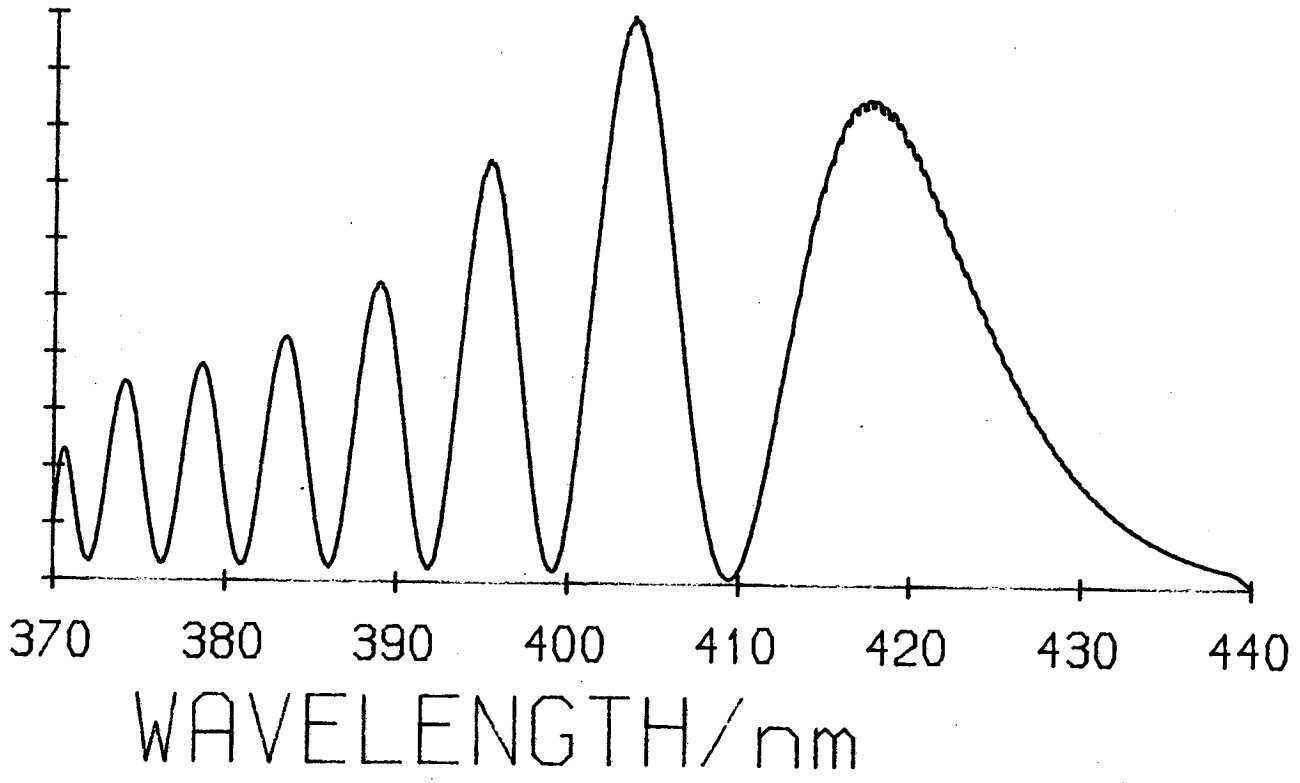

Figure 4.7 A simulation of the spectrum in Figure 4.6. The potentials used are described in the text.

be adequate. The form of this curve was $U(r) = 6.744 \times 10^6 \exp(-2.300r) + 2.644 \times 10^9 \exp(-4.687r) + 12548.0$ where energies are expressed in cm^{-1} and bond-lengths in Å.

In comparing Figures 4.6 and 4.7, it should be noted that no attempt was made to simulate the structure present on top of the 420 nm peak of the fluorescence spectrum. This is because that structure was assumed to be part of another fluorescence system (i.e. not part of the system being investigated). If this structure were part of the main fluorescence system, the system would possess two frequencies of oscillation like the McLennan bands. In this case the low frequency structure (peaks at 420 nm, 403 nm etc.) would be caused by interference between fluorescence to two branches of the difference potential (remembering that to produce a double frequency, the difference potential involved must possess an extremum). One would then expect the high frequency structure to dominate the spectrum at short wavelengths. This is because, as explained in the introduction, the strength of the low frequency interference must be reduced as transitions to one limb of the difference potential begin to dominate over those to the other limb (as the two Condon points move further apart). On the other hand, there is no comparable mechanism by which the high frequency structure can fade across the spectrum. The low frequency structure would be expected to fade quickly because the transition dipole moment function, $\mu_{12}(r)$, must vanish at large r.

This is so because to make a transition from an ion-pair to a valence state the electron must jump a large distance, the probability of which must fall off in the same manner as the overlap between the two atomic electron distributions (i.e. it must fall off exponentially). As can be seen from Figure 4.6, the low frequency "structure" is dominant at short fluorescence wavelengths, which is the opposite of what one would expect. Thus the fluorescence system is not a double frequency or McLennan type system but must be a simple single frequency type of oscillatory continuum with another system superimposed on it at 420 nm. This interpretation makes the analysed system look similar to the 360 nm, F_2 (157.8 nm) laser induced, fluorescence system of bromine described in Chapter 5. This interpretation is also backed up by evidence, which is described below, obtained from work carried out with the spectrofluorimeter.

The two distinct types of oscillatory continuum behave differently when the wavelength of excitation producing them is changed. The position of the long wavelength maximum (band head) of a double frequency oscillatory spectrum like the McLennan bands, would not be expected to shift with a change of excitation wavelength. Figure 4.8 shows McLennan band fluorescence from iodine at a variety of excitation wavelengths between 185 nm and 205 nm.

A single frequency oscillatory spectrum produced by a monotonic difference potential, would be expected to change as the excitation wavelength is changed. In particular, the position of the long wavelength band head of the spectrum,

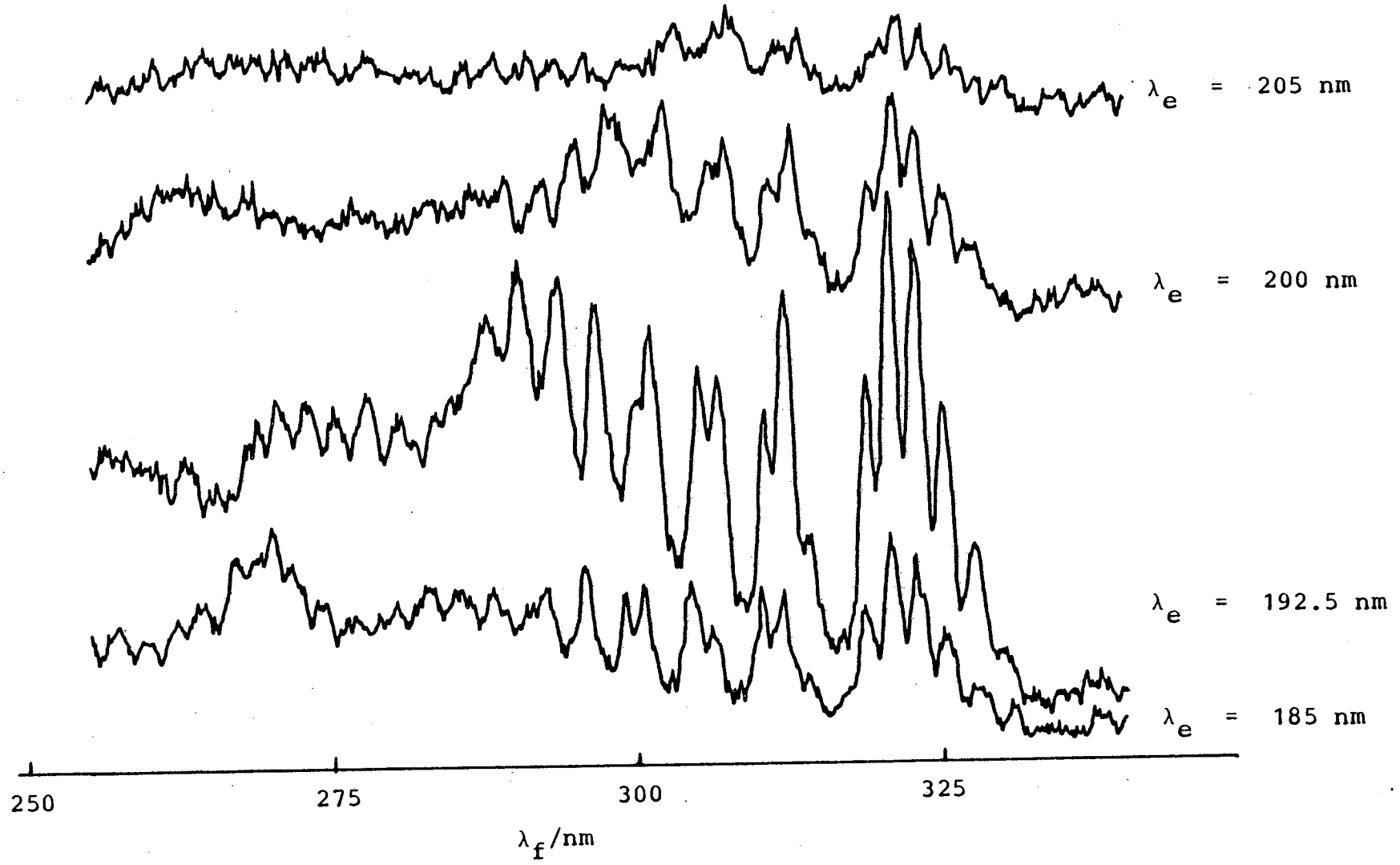

Figure 4.8 The McLennan bands of iodine recorded using various excitation wavelengths as indicated. The spectra were recorded on a Perkin Elmer 650-40 spectrofluorimeter using an excitation monochromator resolution of 5 nm and an emission monochromator resolution of 0.8 nm.

produced by fluorescence from the inner turning-point of the upper state, should move to longer wavelengths as the excitation wavelength is decreased. Figure 4.9 shows that the 420 nm fluorescence system behaves as if it were a single frequency type of oscillatory spectrum.

The nature of the system sitting on top of the 420 nm fluorescence system of iodine already analysed is at present unknown, but Figure 4.9 tends to suggest that the position of the system is independent of the excitation wavelength producing the fluorescence. This implies that it is a double frequency type of oscillatory spectrum. Although the peaks of this extra system are not quite resolved in Figure 4.9, there is evidence that they do not move. The last peak of the analysed system, recorded with an excitation wavelength (λ_e) of 190 nm, seems to have this extra structure superimposed upon it, whereas the corresponding peak for λ_e = 197.5 nm seems to be extended to the red, possibly again by the extra system. The spectra with intermediate λ_e seem to fall between these two extreme cases. Thus it appears that this third system is a double frequency (interference) type of oscillatory continuum emission.

As a summary of the results of this chapter, the two potentials analysed and the ground state potential are drawn out in Figure 4.10.

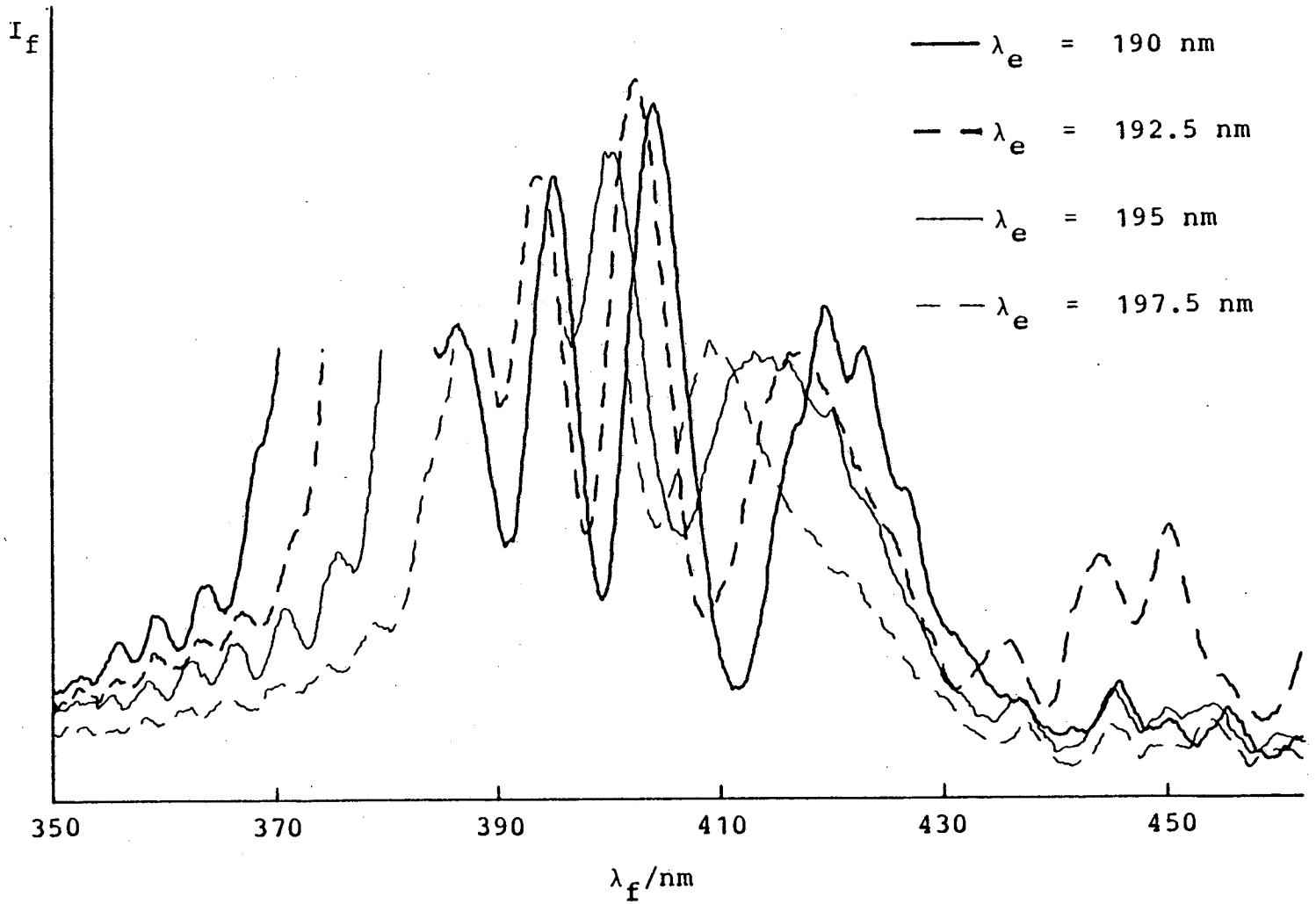

Figure 4.9 The 420 nm fluorescence system of I_2 recorded at various excitation wavelengths, as indicated, using a Perkin Elmer 650-40 spectrofluorimeter. ($\Delta\lambda_e = \Delta\lambda_f = 2$ nm).

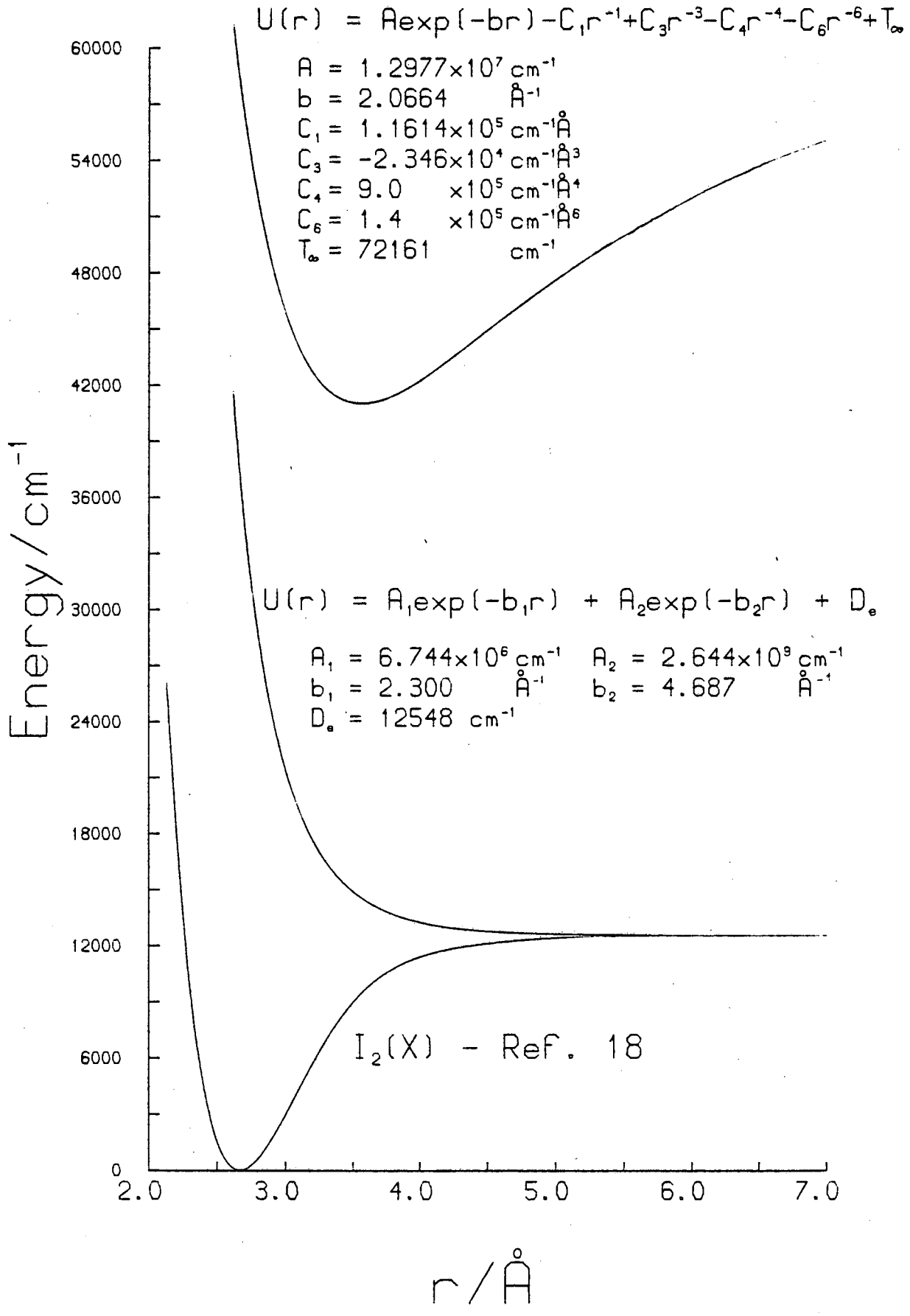

Figure 4.10 A summary of the potentials of I_2 derived in this work.

4.5 References

(1) K.S. Viswanathan and J. Tellinghuisen, J.Mol.Spec., 101 (1983), 285.

(2) J. Tellinghuisen, Chem.Phys. Letters, 99 (1983), 373.

(3) J. Tellinghuisen, Chem.Phys. Letters, 29 (1974), 359.

(4) T. Ishiwata, H. Ohtoshi, M. Sokaki and I. Tanaka, J.Chem.Phys., 80 (1984), 1411.

(5) K.P. Lawley, M.A. MacDonald, R.J. Donovan and A. Kvaran, Chem.Phys. Letters, 92 (1982), 322.

(6) J. Tellinghuisen, J.Mol.Spec., 94 (1982), 231.

(7) J. Tellinghuisen, J.Chem.Phys., 78 (1983), 2374.

(8) J.P. Perrot, M. Brayer, J. Chevaleyre and B. Femelat, J.Mol.Spec., 98 (1983), 161.

(9) J.C.D. Brand, A.R. Hoy, A.K. Kalkar and A.B. Yamashita, J.Mol.Spec., 95 (1982), 350.

(10) G.W. King, I.M. Littlewood and J.R. Robins,Chem.Phys., 56 (1981), 145.

(11) J.C.D. Brand and A.R. Hoy, J.Mol.Spec., 97 (1983), 379.

(12) K. Wieland, J. Tellinghuisen and A. Nobbs, J.Mol.Spec., 41 (1972), 69.

(13) K.S. Viswanathan and J. Tellinghuisen, quoted in reference 1.

(14) K.S. Viswanathan, A. Sur and J. Tellinghuisen, J.Mol.Spec., 86 (1981), 393.

(15) R.L. Jaffe, quoted in reference 1.

(16) P. Venkateswarlu, Can.J.Phys., 48 (1970), 1055.

(17) M. Martin, C. Fotakis, R.J. Donovan and M.J. Shaw, Nuovo Cimento, 63 (1981), 300.

(18) R.J. LeRoy, J.Chem.Phys., 52 (1970), 2683.

(19) J. Tellinghuisen, J.Phys.Chem., 87 (1983), 5136.

(20) C.E. Moore, "Atomic Energy Levels", N.B.S. Monographs.

CHAPTER 5

The Spectroscopy and Quenching of $Br_2(K)$

5.1 Introduction

Of the twelve ion-pair states of Br_2, correlating with $Br^-(^1S)$ and $Br^+(^3P_{2,1,0})$, molecular constants are known for only five — these are the D (2_g), $E(0_g^+)$, $D(0_u^+)$, $f(0_g^+)$ and $F(0_u^+)$ states. A summary of these molecular constants is given in Table 5.1.

Various methods have been used to obtain this information, the most important of which are described briefly below. To study the D' and E states, Tellinghuisen and co-workers[1,2] excited bromine vapour (133 Nm^{-2}), both in the presence and absence of argon (up to 27 kNm^{-2}), using a tesla discharge. The resulting fluorescence spectra were recorded under high resolution (0.003 Å). An analysis of the vibrational and rotational structure in the D'→A' and E→B fluorescence systems gave information on the D' and E states. This method has the advantage that the fluorescence is relatively easily produced but has the disadvantage that a high resolution spectrometer is required. To study the $F(0_u^+)$ ion-pair state, Shinzawa et al[3] used the method of optical-optical double resonance. The B state of bromine was pumped with one tunable dye laser while a second dye laser was scanned over the (two-photon) B → $F(0_u^+)$ transition. Fluorescence from the $F(0_u^+)$ state was collected at right angles to the laser radiation through a band-pass filter. They also recorded fluorescence spectra from the $F(0_u^+)$ state following one-colour, three-photon excitation of that state via the B state. Analysis of the excitation and

fluorescence spectra provided the information on the $F(O_u^+)$ state given in Table 5.1.

Table 5.1 Summary of experimentally known ion-pair states of Br_2 dissociating to $Br^-(^1S)$ and $Br^+(^3P_{2,1,0})$

State	R_e/Å	T_e/cm^{-1}	ω_e/cm^{-1}	Reference
Dissociating to $Br^-(^1S)$ & $Br^+(^3P_2)$				
D' 2_g	3.17	48,930	150.86	1
E O_g^+	3.197	49,780	150.46	4,2
D O_u^+	3.19	49,925	135.7	5
Dissociating to $Br^-(^1S)$ & $Br^+(^3P_{1,0})$				
f O_g^+	3.17	53,102	152.8	6
F O_u^+	3.28	53,900	155.8	3
Results from this chapter (dissociating to $Br^-(^1S)$ & $Br^+(^3P_2)$)				
K (1_u)	3.31	50,048	131.6	

Brand et al[4] recorded rotationally resolved E ← B spectra using the method of polarization-labelling spectroscopy. Again a dye laser was used to populate the B state, although in this experiment it was circularly polarized. The probe used was a XeCl excimer laser. The

output from this was then blocked from a spectrograph, by crossed polarizers, at all frequencies except those corresponding to the E↔B transition. Analysis of this E↔B system yielded information on the $E(0_g^+)$ state of Br_2. The disadvantage of this method is that it requires a tunable dye laser and suffers from the problems of timing involved in all two-colour experiments. All the above experiments probed the lower vibrational levels of the ion-pair states.

In 1969 Venkateswarlu[7] reported an extensive system of absorption bands in the region 59,000-67,000 cm^{-1}. Although there was no analysis of the state involved he called the upper state the K state. In this chapter laser induced fluorescence from this K state, excited using an F_2 laser (157.8 nm), will be described. This method of probing an ion-pair state of bromine has the advantages of requiring neither high resolution spectrometers nor the use of multi-colour laser techniques. However, it has the disadvantage that the laser pump operates in the vacuum ultra-violet region of the spectrum. In recording these laser induced fluorescence spectra a high vibrational level of the K state ($v \cong 120$) is accessed and oscillatory continuum spectra are produced. The spectra can then be inverted to produce molecular potentials; the molecular constants obtained by this method, for the K state, are presented in Table 5.1. Collisional quenching of the bromine K state will also be discussed. Some of the work presented here has been published[8].

5.2 Experimental

The experimental set-up for obtaining the fluorescence spectra presented here, was of standard design (see Figure 2.1). The early work done for this chapter used a Lambda Physik EMG200 laser operating on the F_2 (157.8 nm) transition. The laser beam was passed through a cylinder that was flushed with nitrogen and into a standard T-shaped cell with a LiF front window and quartz side and end windows. Later work was carried out using an excimer laser, built by Oxford Lasers, and an evacuated beam path. The fluorescence signal was dispersed using a Jobin-Yvon 0.3 m monochromator with its exit slit removed and with interchangeable gratings giving low (2.5 nm) and medium (0.3 nm F.W.H.M.) resolution. The detection system was an optical multichannel analyser (EG&G/PAR OMAII) fitted with either an intensified diode array head or a vidicon head. The recorded spectra were the result of averaging a number of laser shots at 0.25 Hz. The figure captions state the conditions used in the recording of each spectrum presented, while more detail on the experimental apparatus can be found in Chapter 2. A description of the set-up for recording absorption spectra can also be found in Chapter 2.

All experimental work described in this chapter was carried out at the S.E.R.C. Rutherford and Appleton Laboratory's Ultra-Violet Radiation Facility except for

the recording of absorption spectra which took place at the S.E.R.C. Synchrotron Radiation Source at Daresbury, using the McPherson 5 m monochromator there. In this case the detector was a standard photomultiplier.

5.3 The Absorption Spectrum

The absorption spectra presented in this section need little additional comment to understand them. Because similar spectra were produced for iodine and iodine monobromide the details of the experimental procedure used to obtain these spectra can be found in Chapter 2.

Two absorption spectra are presented here, as Figures 5.1 and 5.2. Figure 5.1 shows the whole absorption spectrum from 147 nm to 167 nm, which covers the region studied by Venkateswarlu[7] who assigned the Rydberg bands present. His published data proved extremely useful for calibrating these spectra. The second figure (5.2) concentrates on the vibrational levels of the ion-pair state accessed by the F_2 laser. Preliminary study of these data yields the vibrational spacings of this state. In the region around 158 nm this spacing is 67 cm^{-1} ± 5 cm^{-1}, reducing to 60 cm^{-1} ± 5 cm^{-1} by the time the Rydberg absorption bands start to obscure the ion-pair spectrum at around 152 nm. This narrow vibrational spacing and slow convergence is consistent with the absorbing state being an ion-pair state, dominated by the long range r^{-1} term in the potential, as opposed to a valence state which converges far more quickly, with a leading term of r^{-5} or r^{-6}.

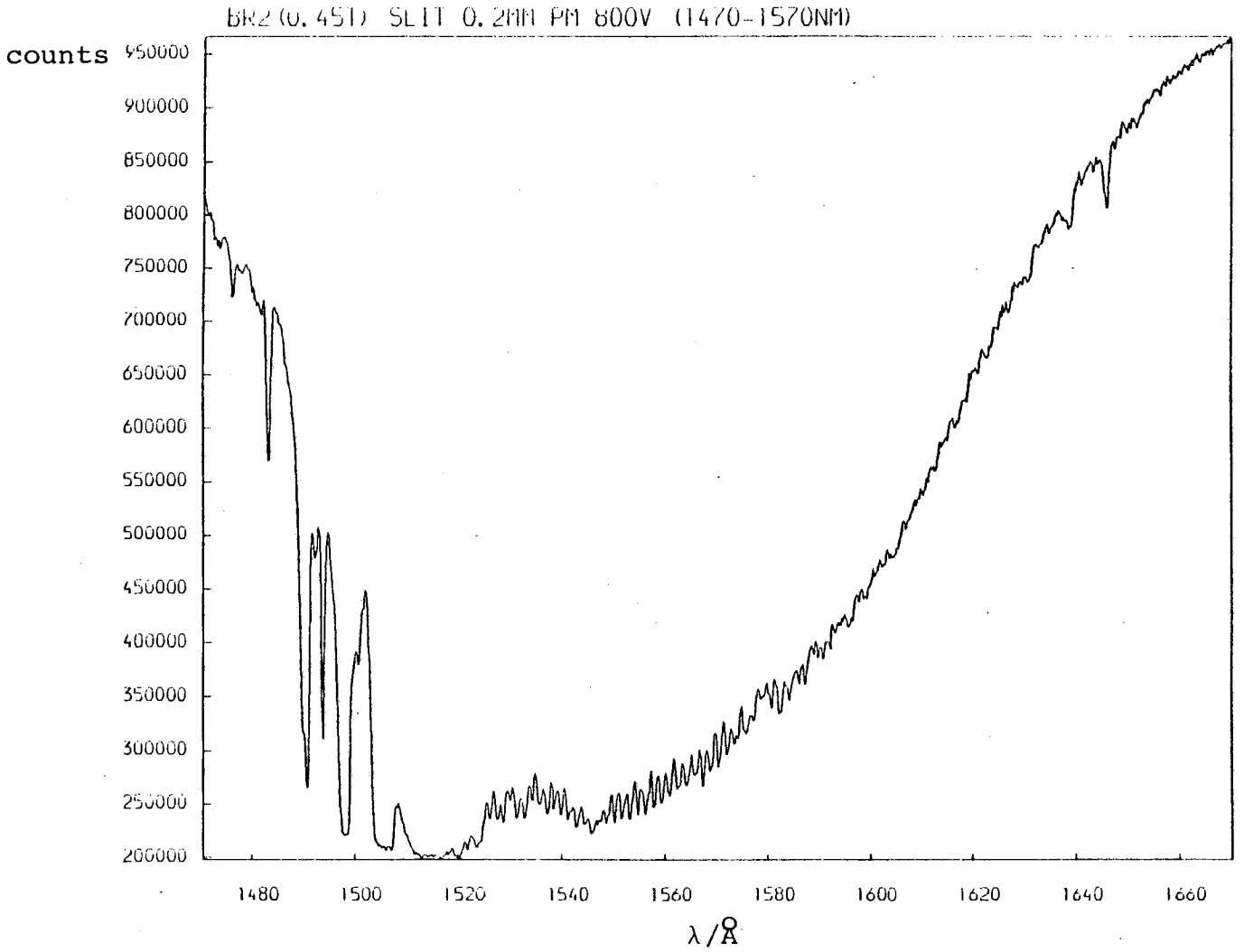

Figure 5.1 Absorption spectrum of Br_2 (66.5 Nm^{-2}) showing both Rydberg absorption (147 - 153 nm) and ion pair abosrption (153 - 162 nm). The Rydberg bands were used to calibrate the spectrum, it being found that the scale reads high by 2.5 Å. The spectrum was recorded with a resolution of 0.035 nm.

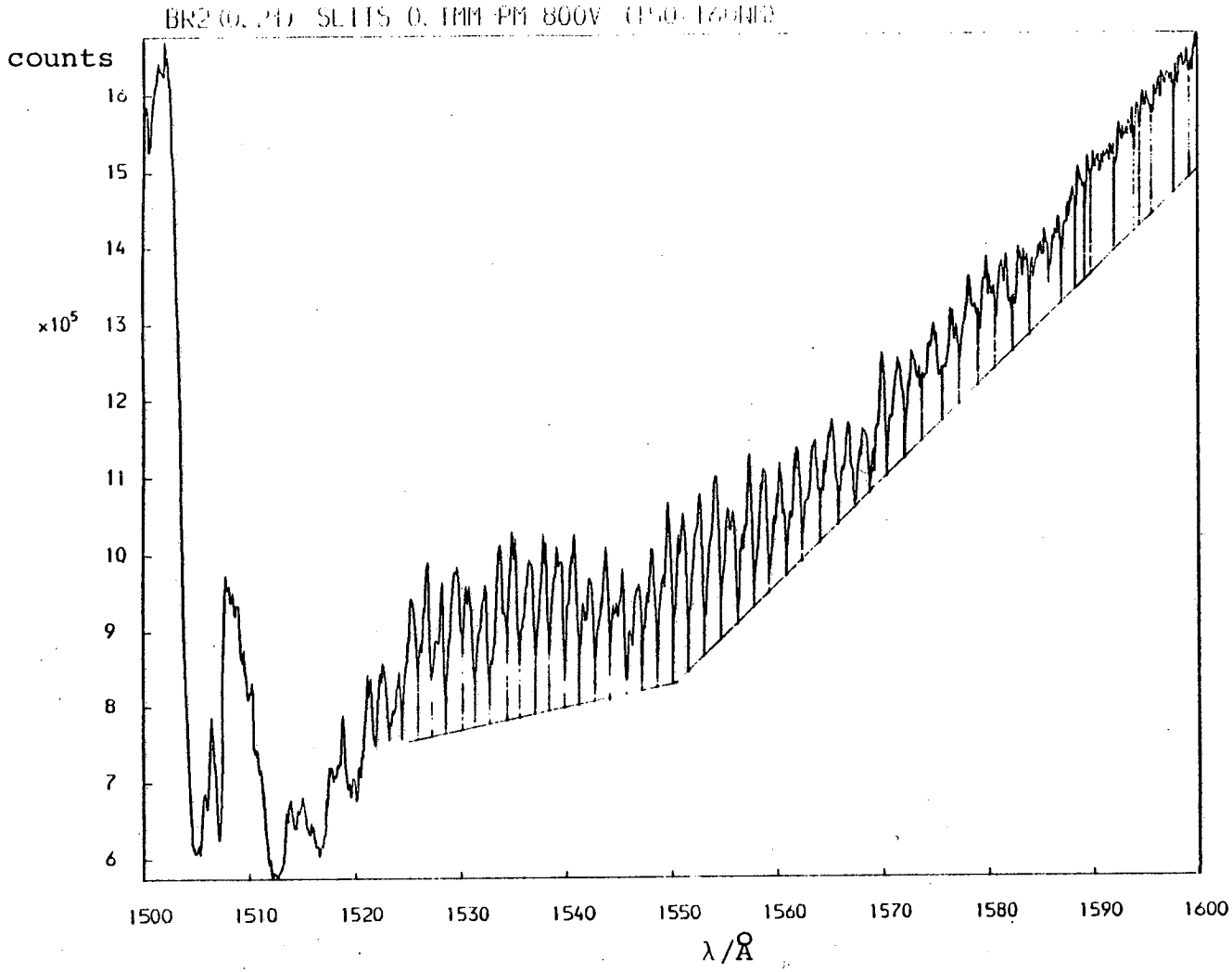

Figure 5.2 Absorption spectrum of Br_2 (27 Nm^{-2}) showing ion-pair absorption (152 - 160 nm). The scale reads high by 2.5 Å. The spectrum was recorded with a resolution of 0.016 nm.

The absorption spectrum is particularly valuable in determining the repulsive limb of the upper state potential. This is because the attractive limb of the potential is fixed by the electrostatic terms and is relatively well known and because the density of vibrational levels is quite sensitive to the width of the potential. Thus the vibrational energy level spacings can be used in the determination of the repulsive limb of the potential. Finally, as 157.8 nm is towards the long wavelength end of the clearly structured absorption it is likely that the absorption is occurring from near the outer turning-point of the ground state ($v'' = 0$) vibrational level. This information could be used to fix a point on the repulsive wall of the K state potential.

These absorption spectra were recorded at the very end of the three years of this project so there was not time to incorporate this information into the reported potentials.

5.4 Low Resolution Fluorescence Spectra

Absorption of a photon of wavelength 157.8 nm should excite Br_2 to the K state[7]. This state must be of ungerade symmetry and is a member of the group of the six lowest ion-pair states of Br_2. Figure 5.3 shows the fluorescence from this K state dispersed under low resolution, while Figure 5.4 shows the same spectrum but with a 250 nm cut-off filter in place. The spectrum was

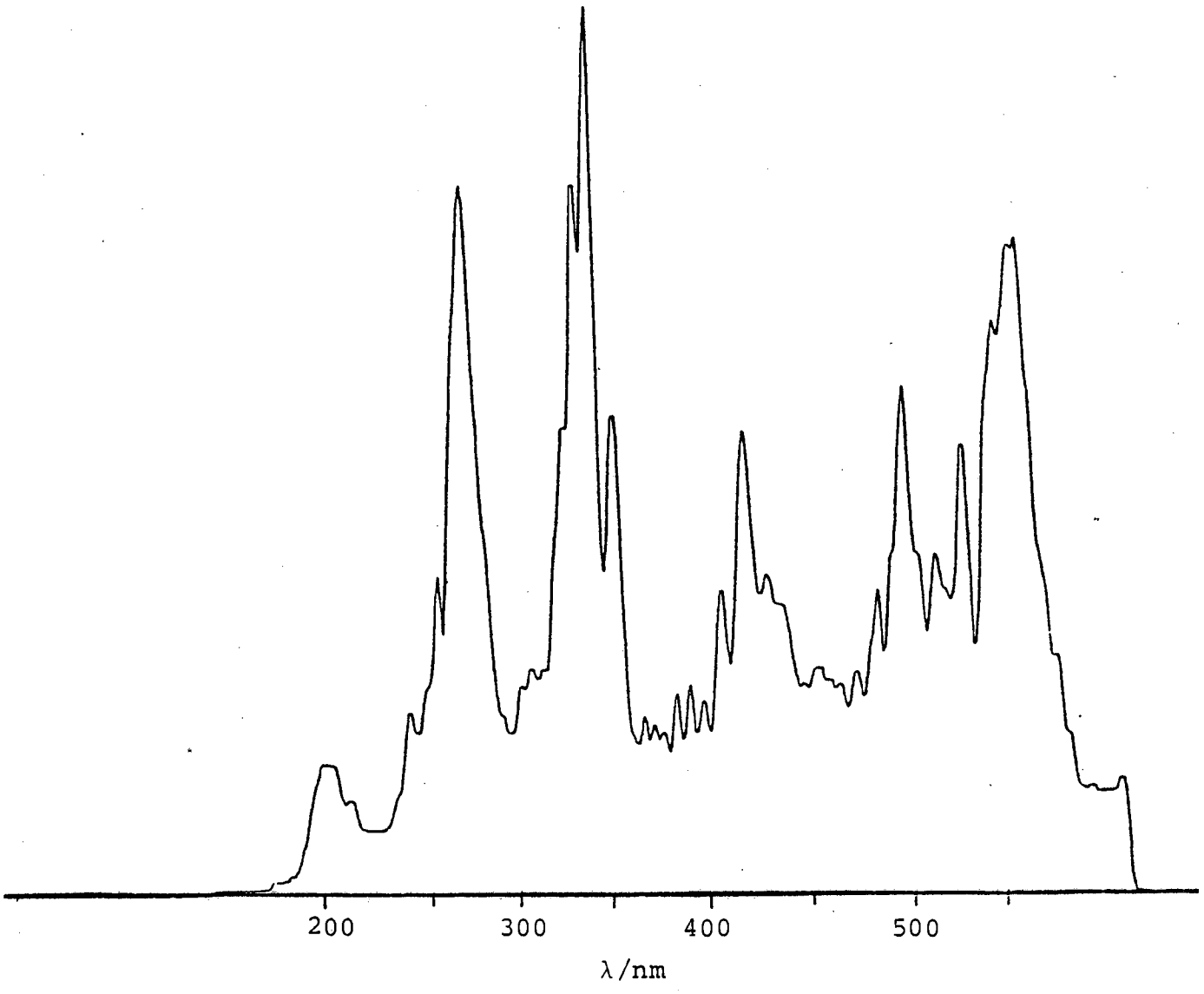

Figure 5.3 Low resolution spectrum of Br_2 (133 Nm^{-2}) recorded by averaging 500 shots of an F_2 laser (157.8 nm) onto a diode array detector at 0.25 Hz. No filter was used. The laser used was an Oxford Lasers KX2 multigas laser.

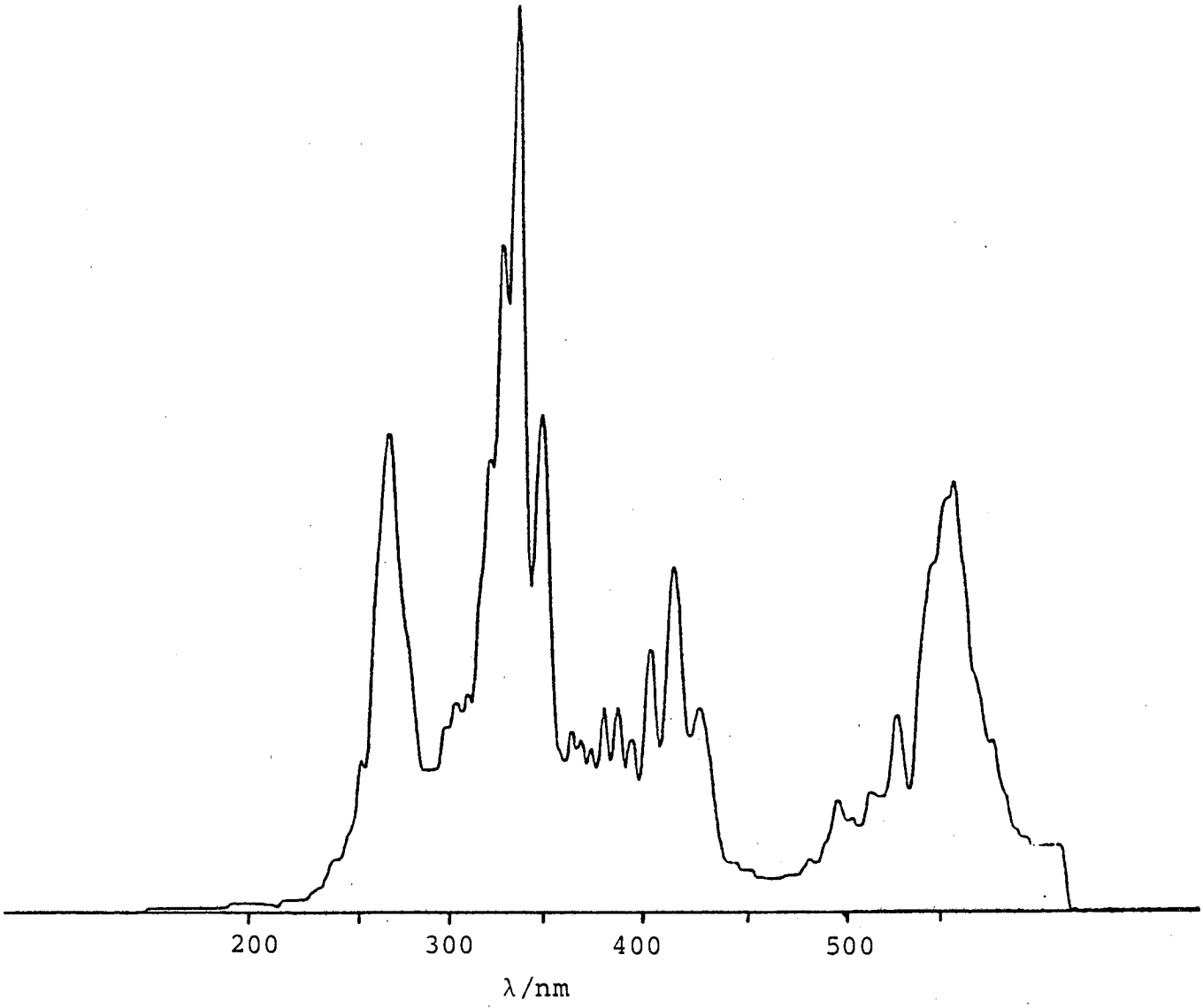

Figure 5.4 Low resolution spectrum of Br_2 (133 Nm^{-2}), recorded by averaging 100 shots with an F_2 (157.8 nm) laser (Oxford Lasers) onto an intensified diode array detector at 0.25 Hz. A 250 nm cut-off filter was used.

also recorded using other cut-off filters and it was found that there was no intense fluorescence beyond 450 nm.

The main guide in analysing these spectra was that of comparison with the known spectra of iodine (see Chapter 4). It appears that the spectrum shown in Figure 5.3 consists of three main electronic systems. The first extending from the atmospheric cut-off at 185 nm up to 290 nm with a maximum at 275 nm. This is interpreted as fluorescence back to the ground state of Br_2 (K → X emission), with that portion below 210 nm being bound→bound and that above 210 nm being emission to continuum levels of the ground state (analogous to the McLennan bands of I_2).

The next system, from 300-360 nm is also an oscillatory continuum and, using the analogy with iodine, probably terminates on a repulsive lower state. The final system is again oscillatory bound→free emission. The above assignments are summarised in Table 5.2.

5.5 Medium Resolution Fluorescence Spectra

The fluorescence spectrum of bromine was analysed in further detail between 180 nm and 360 nm. That is, the first two systems in Table 5.2 were recorded under medium resolution. The results are shown in Figures 5.5 and 5.6.

Table 5.2 Emission systems observed following F_2 laser (158 nm) excitation of Br_2

Designation	Wavelength Range	Comments
$K \rightarrow X^1\Sigma_g^+$ (system 1)	180 - 290 nm	Bound to bound emission below 210 nm and bound to free emission between 210 and 290 nm
K → ? (system 2)	300 - 360 nm	Bound to free emission. The lower state is probably purely repulsive in the region spanned by the fluorescence
K → ? (system 3)	360 - 440 nm	Bound to free emission. The lower state is probably purely repulsive in the region spanned by the fluorescence

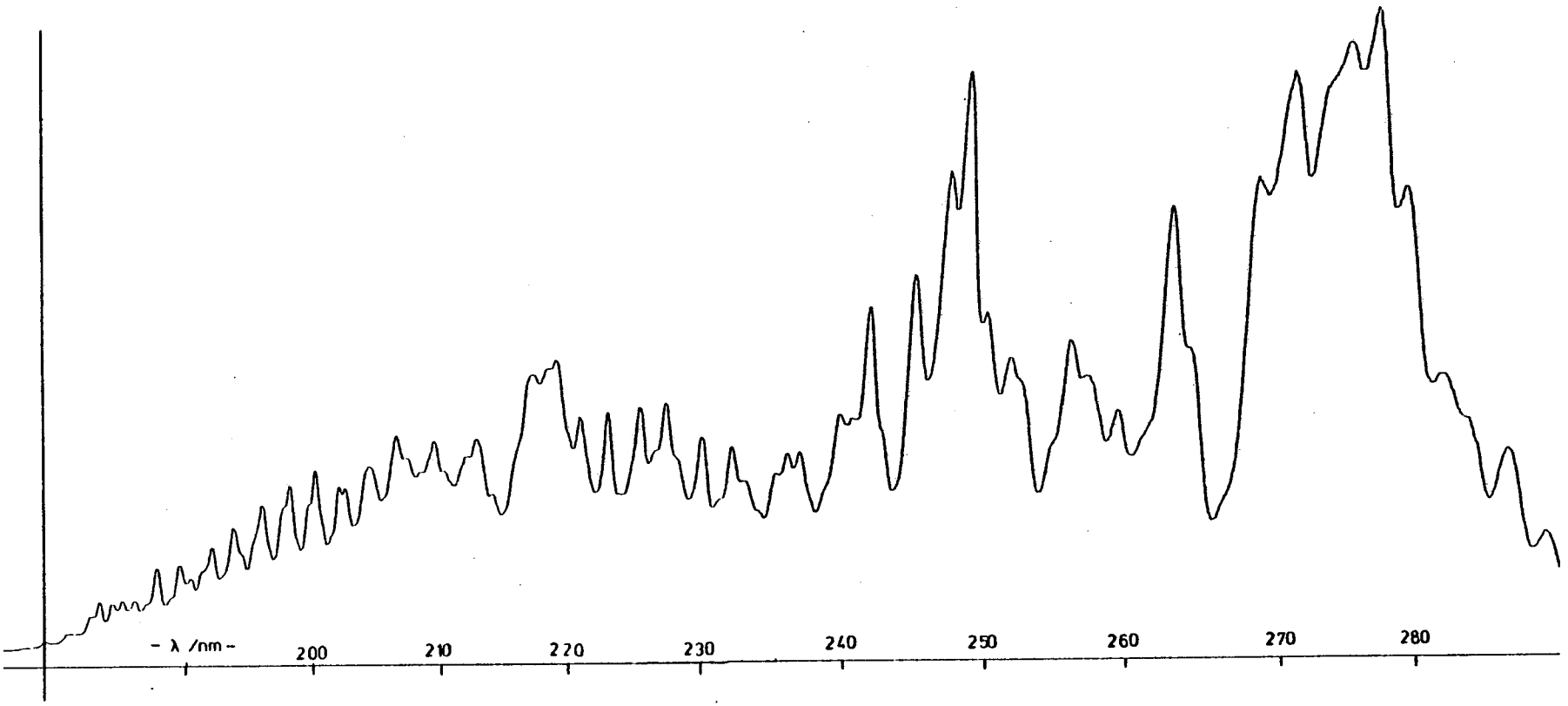

Figure 5.5 Medium resolution spectrum of Br_2 (133 Nm^{-2}) recorded by averaging 500 shots of an Oxford Lasers F_2 (157.8 nm) laser onto a diode array detector at 0.25 Hz. No filter was used.

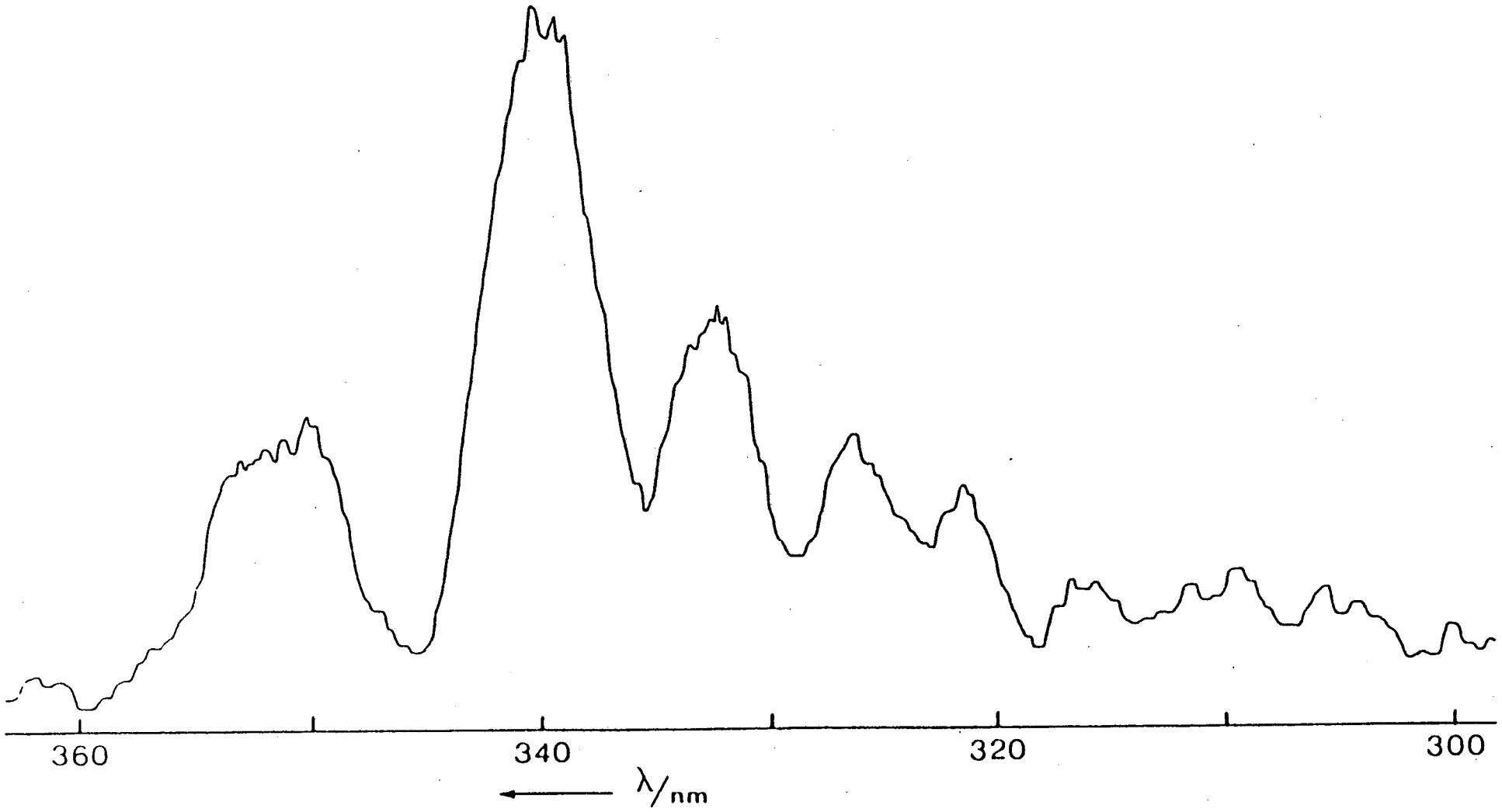

Figure 5.6 Medium resolution spectrum of Br_2 (13.3 Nm^{-2}) recorded by averaging 5 shots of a Lambda Physik EMG200 laser operating on the F_2 transition (157.8 nm) onto a diode array detector at 0.5 Hz. No filter was used.

It should be noted that in Figure 5.5, there are two frequencies of oscillation as in a McLennan type system. This implies that the difference potential involved in creating this spectrum has an extremum, i.e. a rainbow point. The high frequency structure in this spectrum seems to be "washed in" by more than can be accounted for by the resolution of the monochromator. An explanation of this is that more than one isotopic pair of the three present in natural Br_2 ($^{79}Br_2$, $^{79,81}Br_2$, $^{81}Br_2$) seems to be excited, with each isotopic pair giving a different phase to the oscillations in the fluorescence spectrum. Simulations show that when a superposition of spectra, from individual isotopic pairs, is carried out the result is a filling in of the minima in the spectrum (see Section 5.6).

Figure 5.6 shows the second system that was recorded under medium resolution. The most obvious difference is that this spectrum has only one frequency of oscillation, implying that the electronic transition concerned terminates on a potential steep enough to exclude an extremum appearing in the difference potential for the system. The above two systems were analysed using the method of computer simulation described earlier (Chapter 3).

5.6 The Potentials and Simulated Spectra

The potential used for the ground state of Br_2, and thus as the starting point for all the simulations, was that given by J.A. Coxon[9]. This R.K.R. analysis covers $Br_2(^1\Sigma_g^+)$ up to v = 36 with an energy of 10302.1 cm^{-1}. The repulsive wall of the ground state was then extended by fitting a curve with the functional form r^{-12} to the first two points of the analysis. To extend the attractive limb of the potential to the known dissociation energy of Br_2 (16057 cm^{-1}), the last four points of Coxon's analysis were fitted to

$$U(r) = T_\infty - {}^{C_5}/_{r5} - {}^{C_6}/_{r6}; \quad r > 2.90 \text{ Å} \qquad (5.1)$$

This fitting gave $C_5 = (-2.15 \pm 0.1) \times 10^6$ cm^{-1} Å^5 and $C_6 = (1.017 \pm 0.005) \times 10^7$ cm^{-1} Å^6. As the coefficient C_5 is negative the potential must rise above the dissociation energy and then fall back down to T_∞ from above, but in this case it only exceeds T_∞ by a few wave numbers at a bondlength of 5 Å which is beyond the main area of interest. This was felt to be a minor problem and no action was taken to rectify it. The potential produced by the above process was then interpolated to 0.001 Å intervals and used as data in the simulations.

The upper state was assumed to have the form of a Rittner potential (equation 5.2), the unknown constants of which were found by simulating the fluorescence spectrum

$$U(r) = A \exp(-br) - {}^{C_1}/_{r} + {}^{C_3}/_{r3} - {}^{C_4}/_{r4} - {}^{C_6}/_{r6} + T_\infty \qquad (5.2)$$

of bromine in the region 240 - 290 nm. Elementary calculation shows that the rainbow point in the difference potential must be at 35,850 cm^{-1}. By definition, the first gradient of the difference potential at this point must be equal to zero, while trial and error analysis showed that the second derivative at this point was 17,060 cm^{-1} $Å^{-2}$. The bondlength (r) of the rainbow point was then shifted until the best fit to the experimental spectrum was found. The results of this are shown in Table 5.3 and Figure 5.7.

Table 5.3 The coefficients of the Rittner potential for the K-state of bromine found by simulating the K → X fluorescence spectrum

Coefficient	Value	Theoretical form
A/cm^{-1}	5.383×10^7	Found from simulation
$b/Å^{-1}$	2.7386	Found from simulation
C_1/cm^{-1} Å	1.16142×10^5	$e^2/4\Pi\varepsilon_o$
C_3/cm^{-1} $Å^3$	7.027×10^4	Found from simulation
C_4/cm^{-1} $Å^4$	4.030×10^5	$e^2/4\pi\varepsilon_o(\frac{\alpha_A + \alpha_B}{2})$
C_6/cm^{-1} $Å^6$	3.607×10^5	$^3/_2\ \alpha_A\alpha_B\ \omega_A\omega_B/(\omega_A + \omega_B)$
T_∞/cm^{-1}	84480	$Br^+ = {}^3P_2$

The potential described above has r_e = 3.3 Å, which is larger than the r_e values published for the other Br_2 ion-pair states. (A summary of these other data is given in Table 5.1).

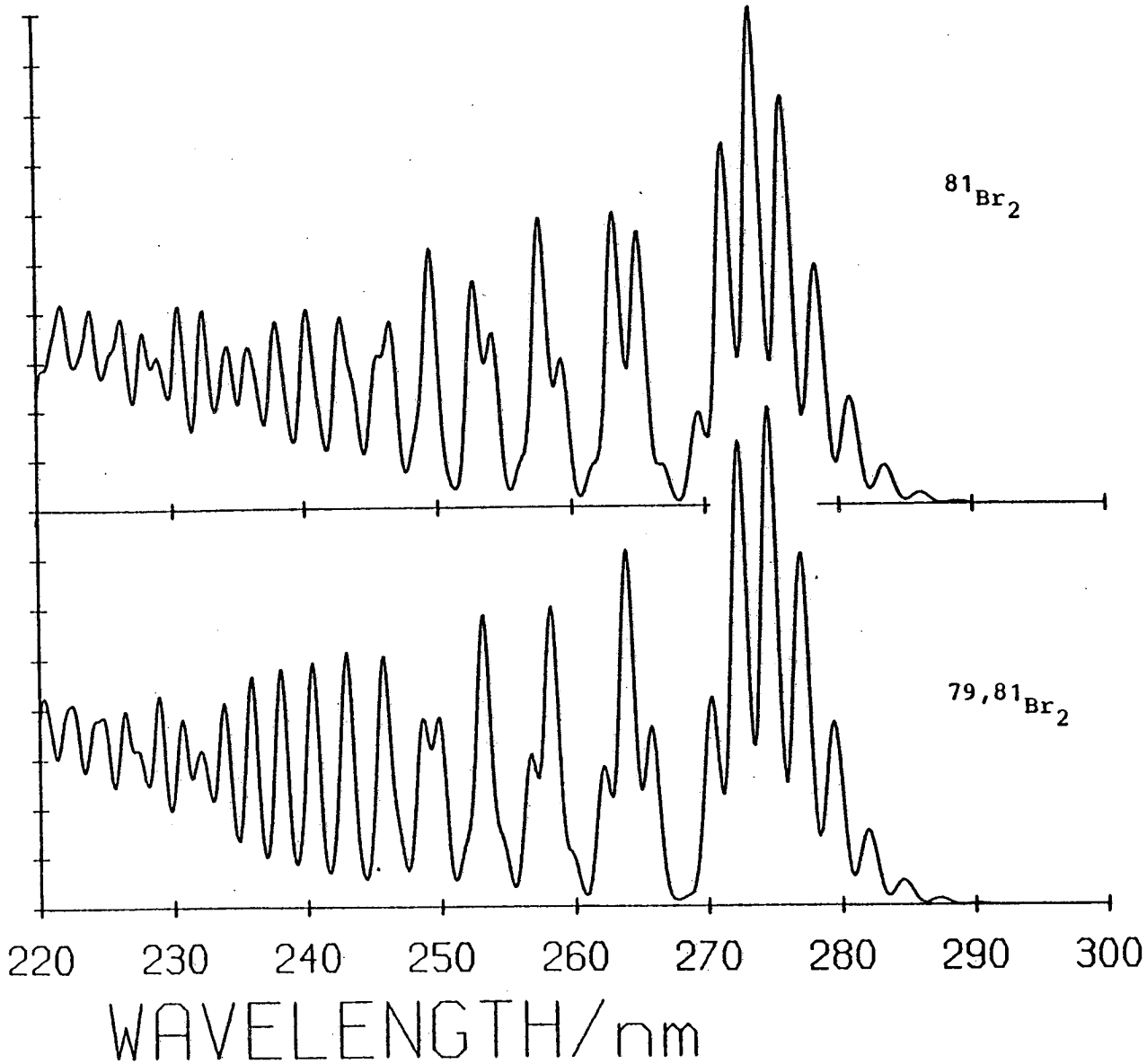

Figure 5.7 Simulation of the spectrum in Figure 5.5 for $^{79,81}Br_2$ (lower trace) and $^{81}Br_2$ (upper trace) using the Rittner potential given in Table 5.3.

The simulated spectrum (Figure 5.7) does not reproduce the feature at 248 nm in Figure 5.5. This feature corresponds to fluorescence at 7150 cm^{-1} above the dissociation energy of molecular bromine and can thus be explained as fluorescence from the outer turning-point of the upper state to the asymptote of a dissociative state leading to Br $^2P_{\frac{1}{2}}$ + Br $^2P_{\frac{1}{2}}$. The excitation energy of Br $^2P_{\frac{1}{2}}$ relative to $^2P_{3/2}$ is 3685 cm^{-1} (10).

Once the upper potential was fixed, simulations of the fluorescence spectra from each of the three isotopic pairs of Br_2 were run and the results compared. If one assumes equal absorption by each of the three isotopic pairs the result is that, under any reasonable resolution, the high frequency structure is completely washed away. This is because, by an unfortunate coincidence, each change of mass produces the same spectrum but shifted by half a wavelength of the high frequency structure. Now, as the relative abundance of each of the two isotopes of bromine is approximately 1:1, the medium weight (mixed) isotopic pair forms 50% of the Br_2 molecules and the light and heavy isotopic pairs form 25% each. However, the spectra of the light and heavy isotopic pairs are in phase with each other and exactly of the opposite phase to that of the mixed isotopic pair. Thus, if there was equal absorption by each isotopic pair the high frequency structure in the spectrum would be almost completely washed out. Judicious mixing of these three simulated spectra

and comparison with experiment gives satisfactory results with an equal mixture of $^{81}Br_2$ and $^{79,81}Br_2$, with very little $^{79}Br_2$ contributing to the fluorescence. The result of this mixture is shown in Figure 5.8. With a broad-band excitation source one would expect each of the isotopic pairs to be equally excited, but with a narrow band excitation source such as a F_2 laser ($\Delta\lambda$ = 0.05 nm) one would be surprised if each of the three isotopic pairs were equally excited.

The spectroscopic designation of this K state is unknown, but on the following evidence a guess can be made that it is the $^1\Sigma_u$ state of Br_2 correlating with $Br^-(^1S)$ + $Br^+(^3P_2)$. Only a single photon is required to excite this K state, thus it has to be of ungerade symmetry. The term value of the potential is $\sim$50,000 cm^{-1} implying that the diabatic dissociation products are $Br^-(^1S)$ + $Br^+(^3P_2)$. This state cannot be O_u^+ because this term has already been given to the D state dissociating to the same ionic states. Finally, $^2\Sigma_u$ is ruled out as $\Delta\Omega$ = 2 transitions are generally weak, whereas in this case both the absorption and fluorescence are strong. This only leaves a $^1\Sigma_u$ state for the K state designation.

Once the upper potential was fixed, effort was put into finding the lower state responsible for the fluorescence system running out to 350 nm. From the form of the spectrum it was assumed that the lower potential was purely repulsive and sufficiently steep that the

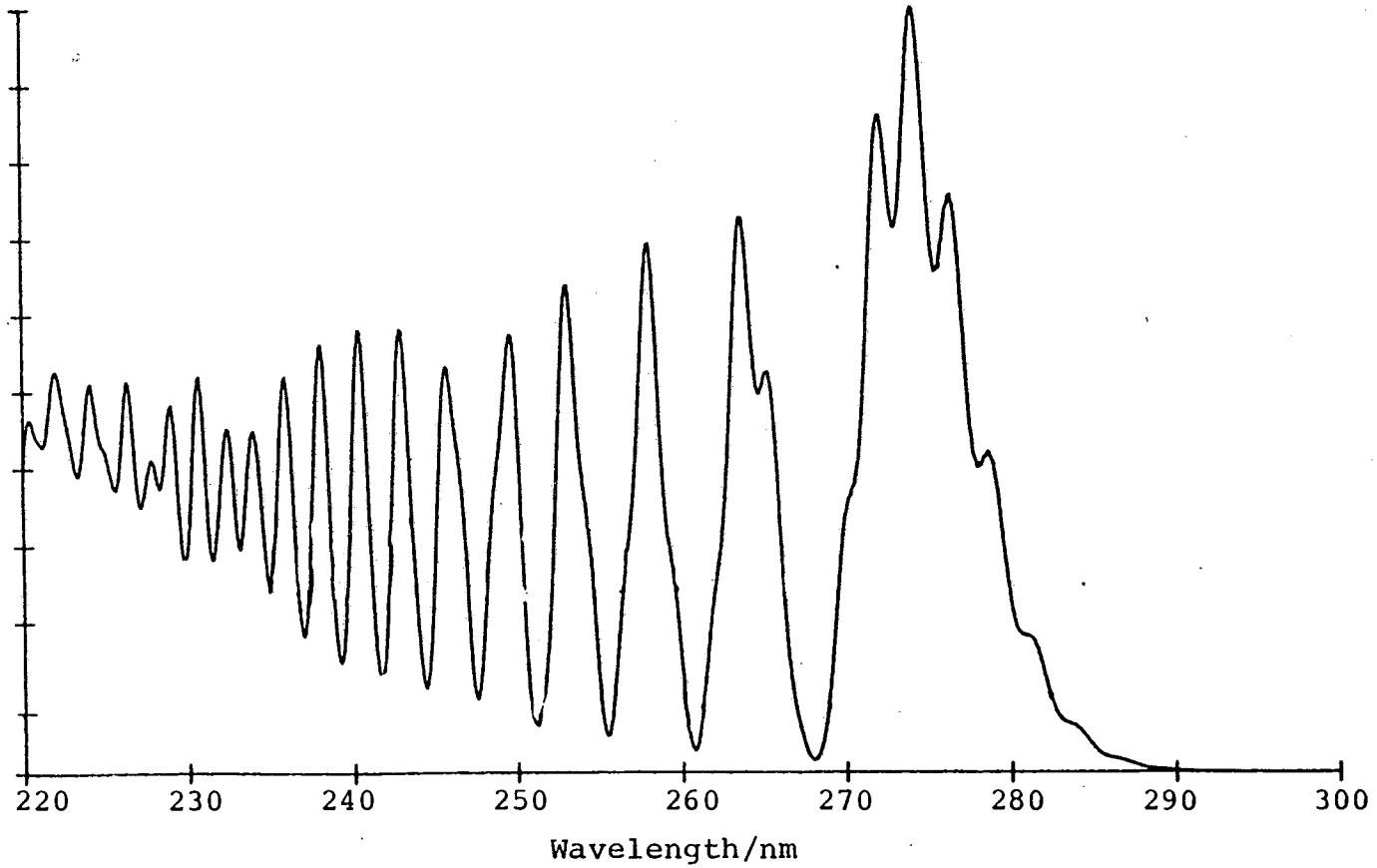

Figure 5.8 Simulation of the spectrum in Figure 5.5 for a 1:1 mixture of $^{79,81}Br_2$ and $^{81}Br_2$ using the Rittner potential given in Table 5.3.

difference potential was monotonic. On this basis a simple exponential form was assumed. As the fluorescence originates from the inner turning-point of the upper state, corresponding to the long wavelength fluorescence maximum of the spectrum, a point with the same bondlength as the upper state turning-point and with the correct energy to allow fluorescence at 355 nm was fixed. After this, the decay of the potential was varied until the best fit was obtained. The resulting potential was

$$U(r) = 9.632 \times 10^{7} \exp(-3.17\ r) + D_e(16057\ cm^{-1}) \qquad (5.3)$$

where energies are expressed in cm^{-1} and bondlengths are expressed in Å. The result of this simulation can be seen in Figure 5.9. It should be obvious from the figure that the potential given does not correctly describe the intensities of the peaks, although the peaks are well positioned. No monotonically decreasing dipole moment function, as allowed for in the simulation programme, gave a good fit for the peak intensities. For these to be fitted correctly the dipole moment function would have to rise sharply near the inner turning-point and then start to decay a few tenths of an angstrom later. All the potentials used are shown in Figure 5.10.

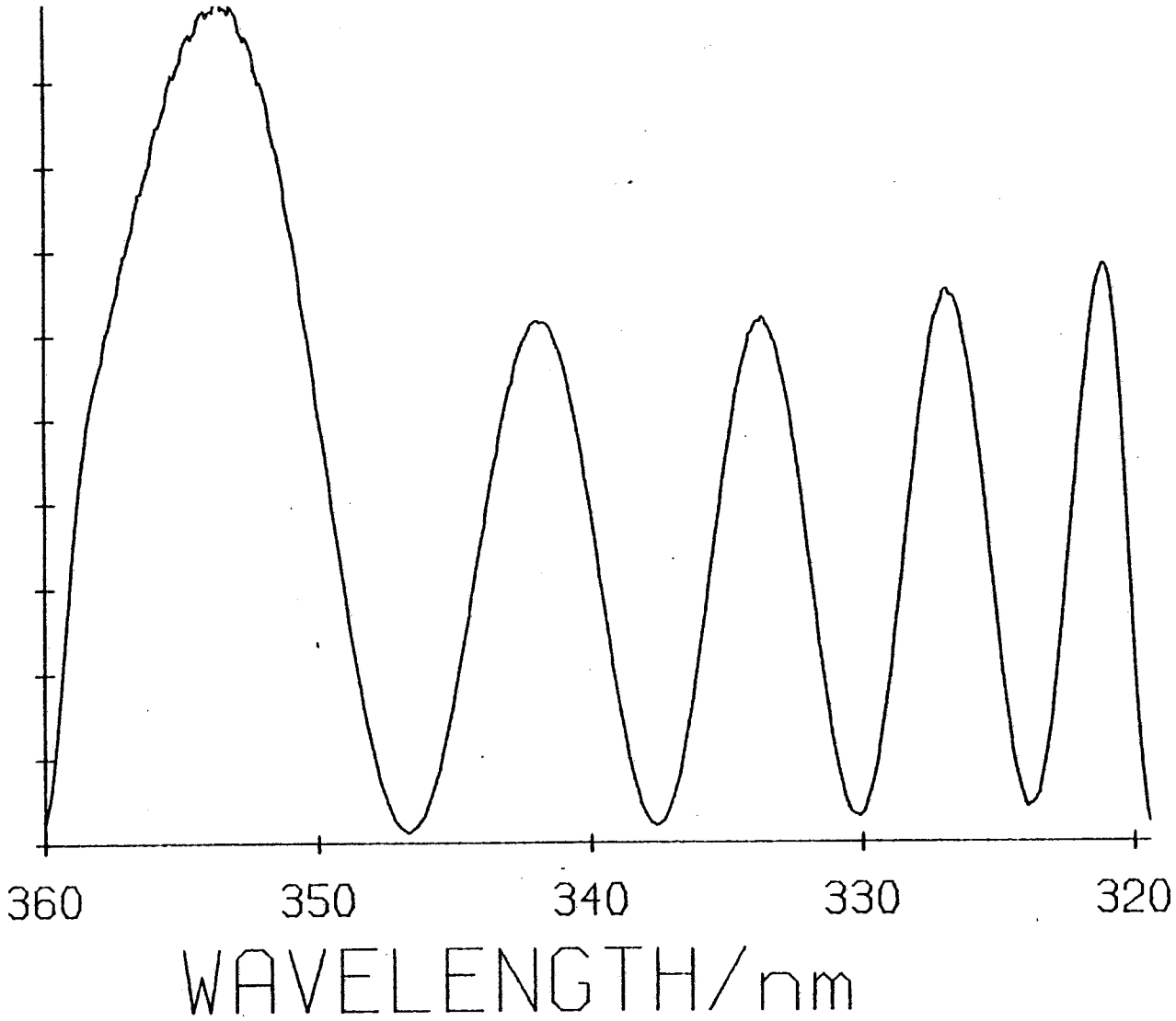

Figure 5.9 Simulation of the spectrum shown in Figure 5.6 using the Rittner potential described in Table 5.3 and the lower potential of equation 5.3. $^{79,81}Br_2$ was assumed.

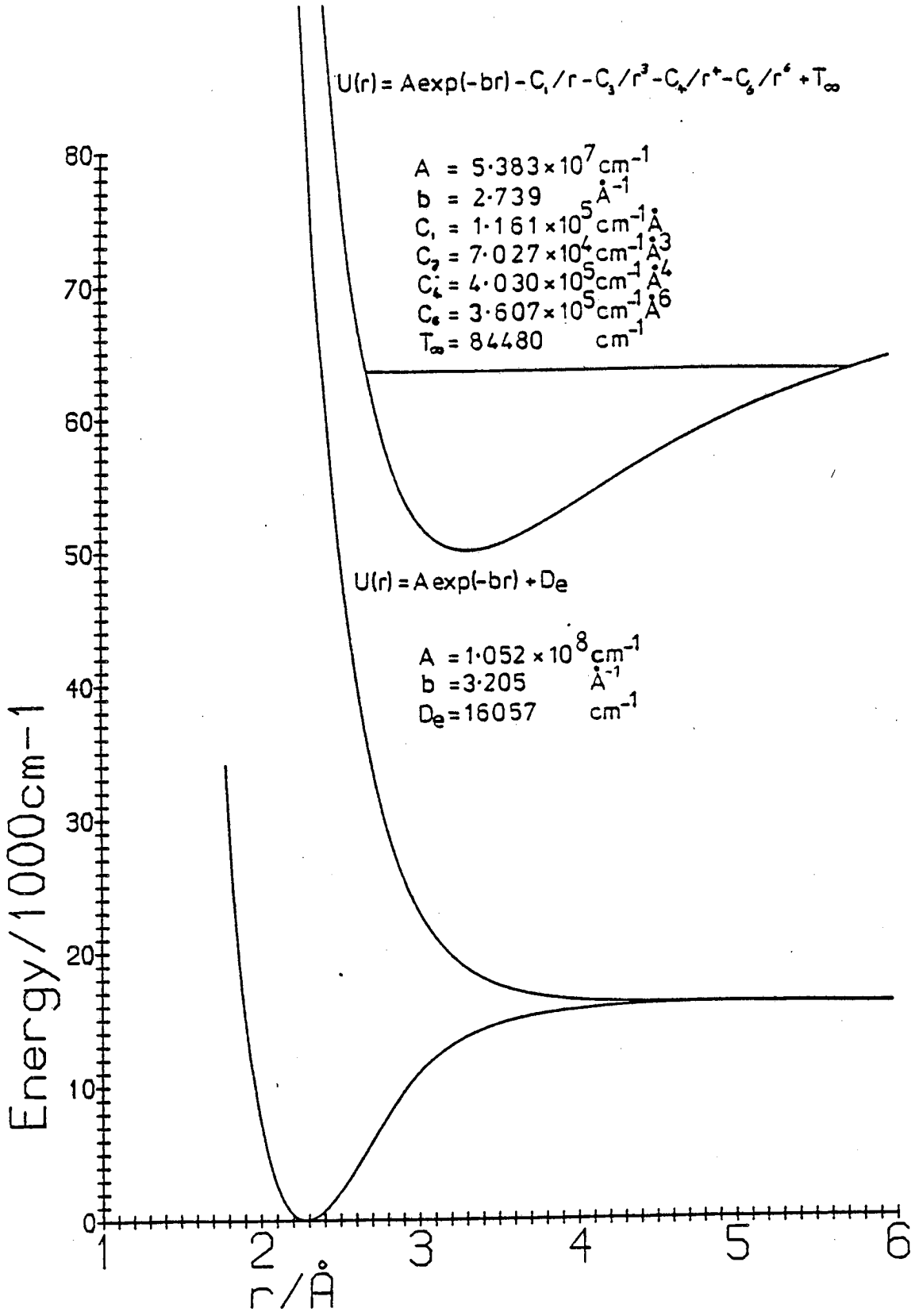

Figure 5.10 Diagram of the potentials used to simulate the recorded spectra. The definition of the ground state potential is described in the text.

5.7 Discussion

The information contained in the fluorescence spectrum only fixes the upper state in the region around the rainbow point. In Br_2 this is in the region around 3.5 Å bondlength. From this information the whole of the upper state must be extrapolated. This is relatively easy in going to longer bondlengths as the functional form of the potential and the asymptote are reasonably well known from theory, with the possible exception of the C_3 term. At ∿3.5 Å the Rittner potential is quite sensitive to this term (as well as to the other electrostatic terms) but it becomes less important as the bondlength is increased. Thus the outward extrapolation is well justified and probably accurate.

The main problem lies in inward extrapolation. This is shown by the inner turning-point of the extrapolated upper state potential occurring at 2.68 Å, while the minimum of the ground state occurs at 2.268 Å [9]. This is unrealistic as it means that any absorption would be extremely weak. The position of this inner turning-point is, unfortunately, insensitive to slight changes to the potential in the area responsible for the K → X fluorescence spectrum. As an example of this, the curvature of the difference potential was fixed at the rainbow point, to a value that gave a reasonable simulated spectrum, but its position (r) was allowed to vary and the effect on the inner turning-point noted. In moving the rainbow point from 3.1 to 4 Å, the

inner turning-point of the upper state only changed by 0.1 Å. Below 3.1 Å no reasonable potential could be found that conformed to the conditions set.

One reason for the difficulty in fixing the inner turning-point of the $Br_2(K)$ state is that the fluorescence spectrum is complex due to the problems involved in using isotopically impure Br_2. The simulation is not an exact fit to the data and there were problems in deciding how much of the structure was due to each of the individual isotopic pairs involved and how much was due to the potentials themselves. Thus, it is possible that the derived potential may not fit data obtained from F_2 (158 nm) laser induced fluorescence from a sample of isotopically pure Br_2. At the very least, there must be some doubt on the accuracy of the Rittner coefficients A and b. However, until experiments are carried out on isotopically pure bromine and in the absence of any evidence to the contrary it must be assumed that the derived K state potential fits the fluorescence data in the relevant bondlength region.

From the above, it can be concluded that a Rittner potential may not be a suitable form to model the repulsive wall of bromine ion-pair states. This means that the assumptions on which this potential is based have to be re-examined, in particular the assumption that the bond remains completely ionic over the full bondlength range.

The results imply that, for values of $r < r_e$, the ionic model has broken down and the r^{-1}, r^{-3} etc. terms should be modified or "switched off". This is probably reasonable as the electron clouds of the Br^+ and Br^- ions will start to overlap at short bondlengths (making the multipole expansion invalid). Also the higher moments may have to be modified first since they depend on $\langle r^n \rangle$ and overlap of the electron clouds will affect these at larger bondlengths. The reason why the Rittner potential works well for NaCl and the other alkali halides, for which it was developed, is that it need not include these terms (the ionic quadrupole moments are zero) and because the positively charged alkali metal ions are much smaller than the corresponding positively charged halide ions. Thus the overlap effects will occur at smaller bondlengths and will be less of a problem.

It is instructive to see which terms of the Rittner potential dominate in which regions of the potential. This is shown in Table 5.4.

The reason why outward extrapolation is so easy is that beyond the region of the rainbow point, the best known term (r^{-1}) dominates the potential, while conversely the reason why inward extrapolation is so difficult is that at 3.5 Å there is very little information on the repulsive part of the potential. There is certainly not enough information present to consider using a modified Rittner potential without considering the absorption spectra as well.

Table 5.4 The contribution of various terms in equation 5.2 to the total potential. All values of r are expressed in Å and all energies are in cm^{-1}

r	Aexp(-br)	$-C_1/r$	C_3/r^3	$-C_4/r^4$	$-C_6/r^6$	Total electro-static
2.268	1.08×10^5 (59%)	-5.12×10^4 (28%)	-6023 (3%)	-1.52×10^4 (8%)	-2650 (2%)	-7.507×10^4 (41%)
2.68	3.51×10^4 (39%)	-4.33×10^4 (48%)	-3651 (4%)	-7812 (9%)	- 973 (1%)	-5.574×10^4 (61%)
2.8	2.52×10^4 (33%)	-4.15×10^4 (54%)	-3201 (4%)	-6557 (8%)	- 749 (1%)	-5.201×10^4 (67%)
3.0	1.46×10^4 (24%)	-3.87×10^4 (65%)	-2603 (4%)	-4975 (8%)	- 495 (1%)	-4.502×10^4 (76%)
3.2	8415 (16%)	-3.63×10^4 (71%)	-2144 (4%)	-3843 (8%)	- 336 (1%)	-4.262×10^4 (84%)
3.316	6125 (13%)	-3.50×10^4 (75%)	-1928 (4%)	-3333 (7%)	- 271 (1%)	-4.053×10^4 (87%)
3.5	3700 (9%)	-3.32×10^4 (80%)	-1639 (4%)	-2686 (6%)	- 196 -	-3.772×10^4 (91%)
3.7	2140 (6%)	-3.14×10^4 (84%)	-1387 (4%)	-2150 (6%)	- 141 -	-3.508×10^4 (94%)
4.0	941 (3%)	-2.90×10^4 (89%)	-1098 (3%)	-1574 (5%)	- 88 -	-3.176×10^4 (97%)

This uncertainty in the form of the repulsive wall of the K state must also lead to uncertainty in the potential for the repulsive state responsible for the second system analysed. However, as in all oscillatory continua, the difference potential is more important than either of the individual potentials involved and any changes subsequently made in the upper potential will not have a serious effect on the calculated spectrum provided similar changes are also made to the lower potential.

In conclusion, the present work can be regarded as a preliminary study until better data are obtained using isotopically pure Br_2. However, these results do clearly show that the form of the Rittner potential will have to be adapted to pull the inner wall to smaller values of r, to be compatible with the observed absorption spectrum.

5.8 Quenching of the Upper State

It is known that halogen molecules excited into one of their ion-pair states will readily undergo collisional interstate transfer until the molecule finds itself in the lowest of the ion-pair states (2_g). This state, usually designated D', will then fluoresce strongly to the A'(2_u) state. Indeed it is this process and transition that is the basis of the F_2 laser (λ = 157.8 nm). In order to watch this process in Br_2 varying pressures of quenching gas (He, SF_6 and Ar) were added to the fluorescence cell.

With SF_6 this D' → A' emission, analysed by Sur and Tellinghuisen,[1] could be seen emerging with the addition of only 260 Nm^{-2} of gas.

For quenching by helium the general background signal tends to rise along with the D' → A' emission, suggesting that there is still significant continuum emission with fairly high pressures (5 kNm^{-2}) of gas present. At intermediate pressures of He (1.3-7 kNm^{-2}) two new peaks (303 nm and 385 nm) are observed in the fluorescence spectrum (Figure 5.11) implying that an intermediate state is populated in the cascade process leading to the D' state. A Stern-Volmer plot of the fluorescence at 340 nm (Figure 5.12) yields a quenching coefficient of 1.68 x 10^{-18} $cm^3 molecule^{-1}$. If a lifetime of 15 ns (I_2 $D(O_u^+)$ state) is assumed this corresponds to a rate constant of 1.12 x 10^{-10} $cm^3 molecule^{-1} s^{-1}$ (or a reactive cross section of 52.6 $\AA^2$). This efficiency of electronic transfer is very high, but not surprisingly so as it is comparable to that found for the other halogens (see Chapter 6 and reference 11) and because the ion-pair states are themselves very large and diffuse from their r^{-1} dependence.

When a similar experiment was carried out with SF_6 as the quenching gas, the D' → A' peak grew much narrower and more intense than it did with He. Also there was no evidence of intermediate states being involved with quenching by SF_6. The 290 nm peak (D' → A') became dominant by the time 2.4 kNm^{-2} of SF_6 was added. The peak continued

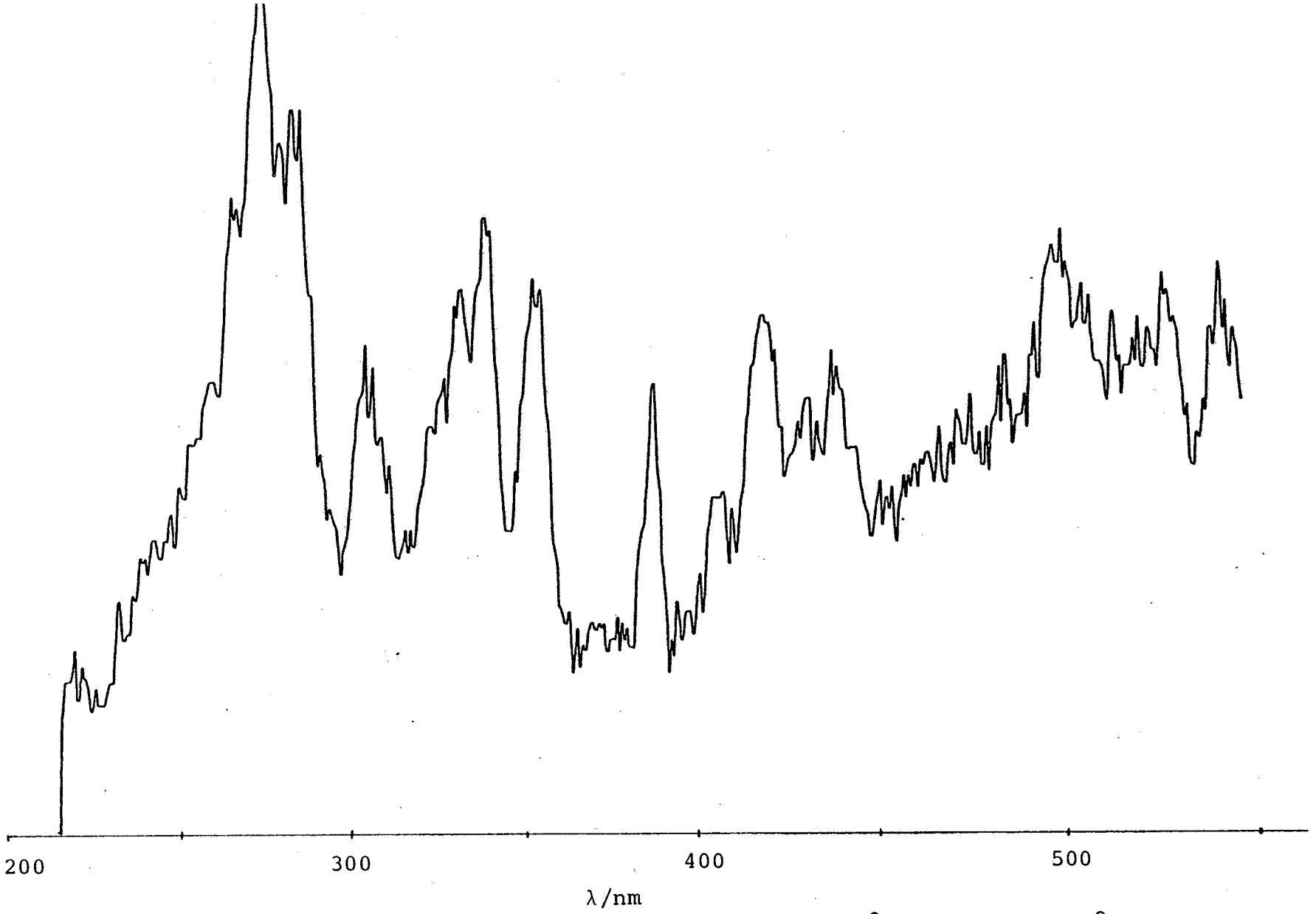

Figure 5.11 Low resolution spectrum of Br_2 (13.3 Nm^{-2}) + He (610 Nm^{-2}) recorded by averaging 5 shots of a Lambda Physik EMG200 laser onto a vidicon detector at 0.5 Hz. No filter was used but the detector has a poor response below 250 nm

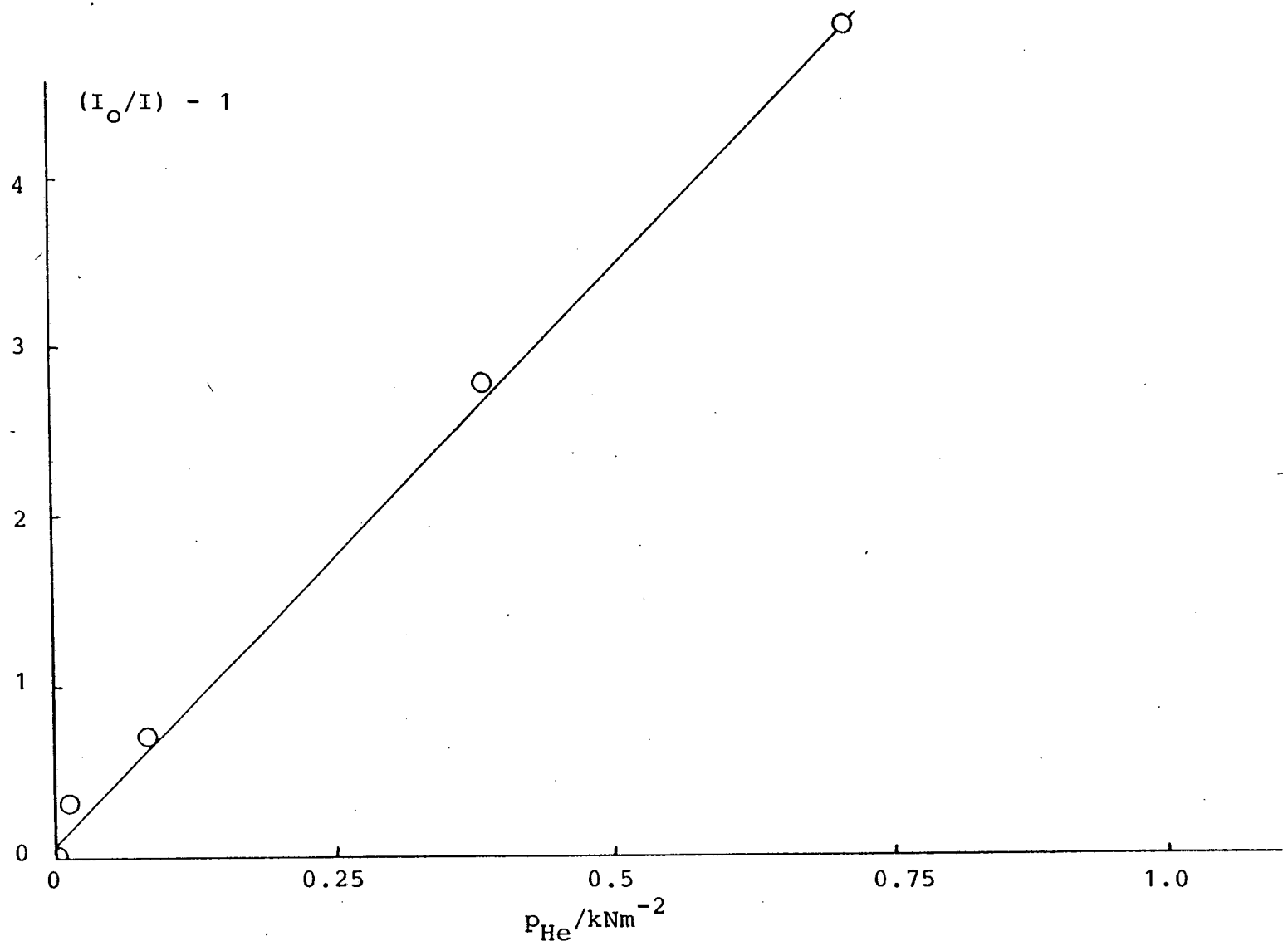

Figure 5.12 Stern-Volmer plot of quenching of Br_2 fluorescence at 340 nm with the addition of He.

to grow as more SF_6 was added and showed no sign of reaching a maximum intensity by the time 27 kNm^{-2} of SF_6 had been added. At a pressure of 13 kNm^{-2} of SF_6 the 290 nm band was almost two orders of magnitude more intense than any band in the unquenched spectrum. This is shown in Figure 5.13. This increase, especially below about 6.5 kNm^{-2} of SF_6, was due to the vibrational quenching of the D' state leading to a narrower D' → A' peak. Much of the increase in intensity with pressures above 6.5 kNm^{-2} of SF_6 could have been due to pressure broadening of the absorption. At pressures of about 13 kNm^{-2} of SF_6 there are also some weak emission at 303 and 350 nm (see Figure 5.13). This was probably also due to emission from the D'(2_g) state. A Stern-Volmer plot for the SF_6 data gave a quenching coefficient of 5.8×10^{-18} $cm^3 molecule^{-1}$. This yields a rate constant of 3.9×10^{-10} $cm^3 molecule^{-1} s^{-1}$ (or a cross section of 183 $Å^2$) if a lifetime of 15 ns is assumed.

Argon showed similar behaviour to SF_6 but the quality of the data recorded was poor. These data gave an approximate rate constant for quenching by Ar which was similar to that for SF_6.

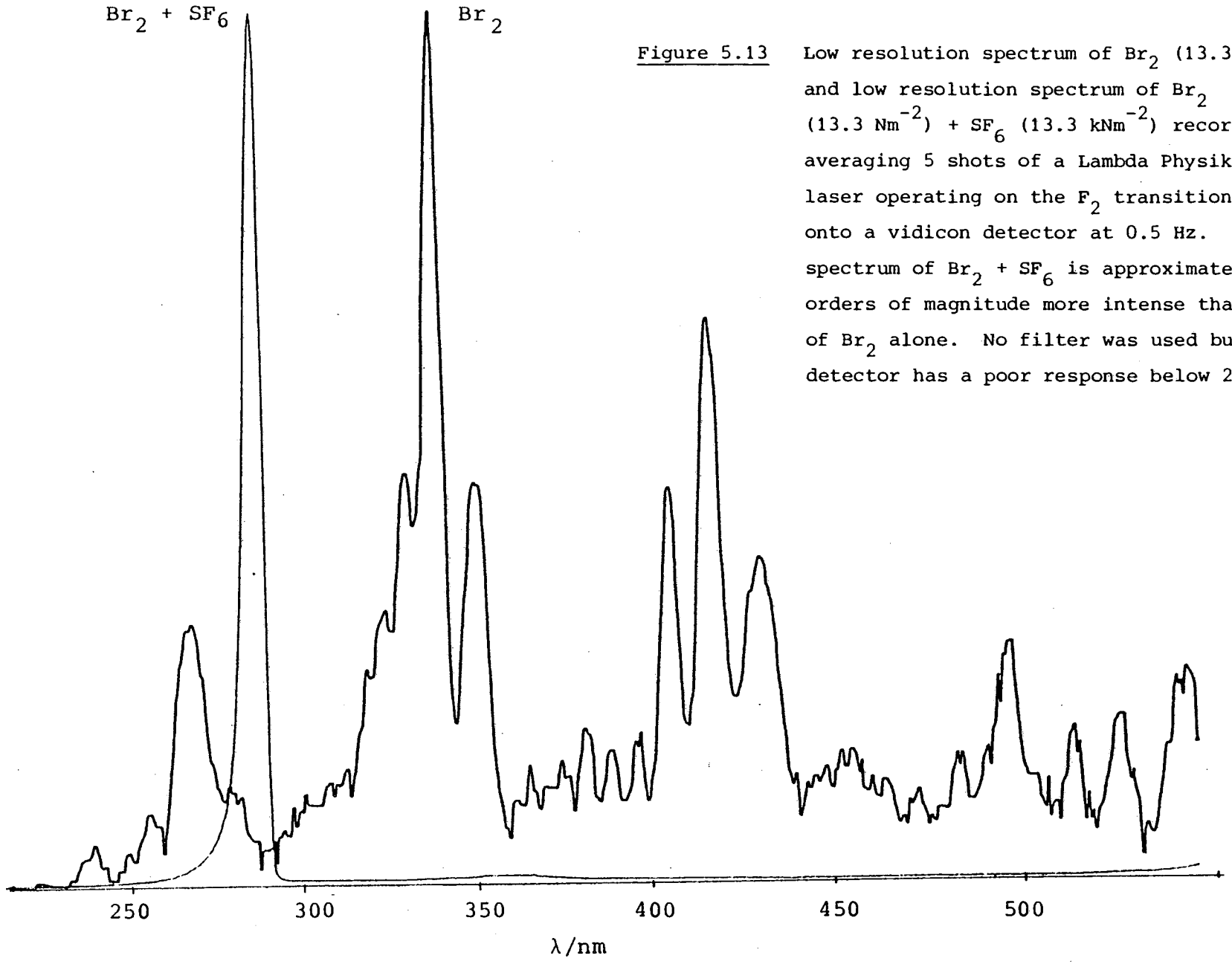

Figure 5.13 Low resolution spectrum of Br_2 (13.3 Nm^{-2}) and low resolution spectrum of Br_2 (13.3 Nm^{-2}) + SF_6 (13.3 kNm^{-2}) recorded by averaging 5 shots of a Lambda Physik EMG200 laser operating on the F_2 transition (157.8nm onto a vidicon detector at 0.5 Hz. The spectrum of Br_2 + SF_6 is approximately two orders of magnitude more intense than that of Br_2 alone. No filter was used but the detector has a poor response below 250 nm.

5.9 References

(1) A. Sur and J. Tellinghuisen, J.Mol.Spec., 88 (1981), 323.

(2) P. Berwanger, K.S. Viswanathan and J. Tellinghuisen, J.Mol.Spec., 91 (1982), 275.

(3) T. Shinzawa, A. Takunaga, T. Ishiwata, I. Tanaka, K. Kasatani, M. Kawasaki and H. Sato, J.Chem.Phys., 80 (1984), 5909.

(4) J.C.D. Brand, U.D. Deshpande, A.R. Hoy and S.M. Jaywant, J.Mol.Spec., 100 (1983), 143.

(5) T. Ishiwata, A. Tokunaga, T. Shinzawa and I. Tanaka, Bull. of Chem.Soc. Jpn., 57 (1984), 1469 (quoted in reference 3).

(6) T. Ishiwata, H. Ohtoshi and I. Tanaka, J.Chem.Phys., 81 (1984), 2300.

(7) P. Venkateswarlu, Can.J.Phys., 47 (1969), 2525.

(8) M. MacDonald, R.J. Donovan and M.C. Gower, Chem. Phys. Letts., 97 (1983), 72.

(9) J.A. Coxon, J.Quant.Spec.Rad.Trans., 11 (1971), 421.

(10) C.E. Moore, "Atomic Energy Levels", N.B.S. Monographs.

(11) R.J. Donovan, B.V. O'Grady, L. Lain and C. Fotakis, J.Chem.Phys., 78 (1983), 3727.

CHAPTER 6

Iodine Monobromide

Spectroscopy and Quenching of IBr(D)

6.1 Introduction

Little spectroscopic work has been done on the ion-pair states of IBr. Brand et al[1] have reported spectroscopic constants for the $E(0^+)$ and an $\Omega = 1$ state, correlating with $I^+(^3P_2) + Br^-(^1S)$, and the $f(0^+)$ state correlating with $I^+(^3P_0) + Br^-(^1S)$, while Diegelman et al[2] have estimated spectroscopic constants for the D'(2) state. The experiments by Brand et al used a pump-probe technique with a narrow band dye laser as the pump and a broad band probe (XeCl laser). The pump-probe transitions used in their study were E (or f) $\leftarrow$ B $\leftarrow$ X and $\Omega = 1 \leftarrow A \leftarrow X$. By polarising both lasers they were able to assign the E and f states as $\Omega = 0^+$ and identify the $\Omega = 1$ state mentioned above. R.K.R. analysis of the E and f states was also carried out, running out to 4.199 Å where the potential is dominated by the simple electrostatic r^{-1} term. It must be noted, however, that these experiments have only probed the lower vibrational levels ($v < 31$) of the states involved, whereas work described in this chapter involves absorption into what are expected to be highly excited vibrational levels of an IBr ion-pair state. The spectroscopic constants taken from the above papers are given in Table 6.1. Note the values from reference 2 were derived by fitting terms to a Rittner potential. These terms were estimated by extrapolation of values from the other halogens and inter-halogens where they were known. Thus these figures are not as accurate as those measured in reference 1.

Table 6.1 Known constants for some ion-pair states of IBr

State	Diabatic dissociation products	T_∞/cm^{-1}	T_e/cm^{-1}	$r_e/\AA$	ω_e/cm^{-1}	Ref.
D'(2)	$Br^-(^1S) + I^+(^3P_2)$	71,989	∿37,840	∿3.105	∿154	2
$E(0^+)$	$Br^-(^1S) + I^+(^3P_2)$	71,989	39,487	3.42	119.5	1
$\Omega = 1$	$Br^-(^1S) + I^+(^3P_2)$	71,989	∿39,520	∿3.4	∿120	1
$f(0^+)$	$Br^-(^1S) + I^+(^3P_0)$	78,440	45,383	3.40	128.8	1

Except for some limited data in a paper by Diegelman et al[2] there are no data on the physical or reactive quenching of the ion-pair states of IBr.

This chapter discusses the fluorescence observed from IBr excited at $\lambda \cong 190$ nm, but unlike the chapters on I_2 and Br_2 there is no attempt to invert these spectra to produce potentials. Physical quenching rate constants for the D state of IBr quenched by He, Ar and Xe have been measured and the reaction of Xe and IBr(D) to form XeBr(B) + I is discussed. Some of the work presented in this chapter has been published[3-5].

6.2 Experimental

In this chapter absorption and fluorescence spectra of IBr are presented. Two different instruments were used to record absorption spectra and two different experimental systems were used to record the fluorescence spectra.

A low resolution (0.25 nm) absorption spectrum of IBr from 190 nm - 200 nm was recorded at the S.E.R.C. Daresbury Laboratory using a Perkin-Elmer spectrophotometer (Model 554). The other absorption spectra were also recorded at the S.E.R.C. Daresbury Laboratory but used a McPherson 5 m monochromator attached to the Synchrotron Radiation Source.

To record fluorescence spectra two different systems were used, the simpler being a standard Perkin-Elmer 650-40 spectrofluorimeter. The other system employed used, as the excitation source, an ArF excimer laser either broad band (Lambda Physik EMG200) or line narrowed (Lambda Physik EMG150). The detection system was a Jobin-Yvon (HRS 2) 0.3 m monochromator with interchangeable gratings (giving low ($\sim$2.5 nm) and medium ($\sim$0.35 nm) resolutions), equipped with an EG&G optical multichannel analyser (OMA) at the exit port. Two detector heads were used: either a vidicon head (type 1254) or an intensified diode array head (type 1420). Figure captions will clearly state all the relevant experimental conditions.

To avoid contamination of the spectra by iodine, which also absorbs at $\lambda \sim 190$ nm an excess of bromine was added to the IBr; the pressures used were usually of the order of $P_{IBr} \cong P_{Br_2} \cong 200\ Nm^{-2}$, with the exact pressures being given in figure captions. Further details of the equipment used may be found in Chapter 2.

6.3 The Absorption Spectrum of IBr

The absorption spectrum of IBr between 190 nm and 200 nm was recorded on a Perkin-Elmer model 554 spectrophotometer at a resolution of 0.25 nm and is reproduced here as Figure 6.1. The E ← X Rydberg[6] absorption spectrum can be seen clearly. The peaks at 192.8 nm and 193.8 nm in the absorption spectrum may be important in the ArF (193 nm) laser induced fluorescence from IBr because the gain profile of the ArF laser covers the region 192.8 nm - 193.6 nm.

The absorption spectrum recorded, at 0.016 nm resolution, using the Synchrotron Radiation Source and the McPherson 5 m monochromator at Daresbury is shown in Figure 6.2. This shows that there are large areas of the absorption spectrum where Rydberg absorption is not strong. However, as discussed in the next section, the intensity of fluorescence does not seem to vary as the excitation wavelength is scanned across the absorption spectrum in this region. This leads to the conclusion that there is underlying absorption

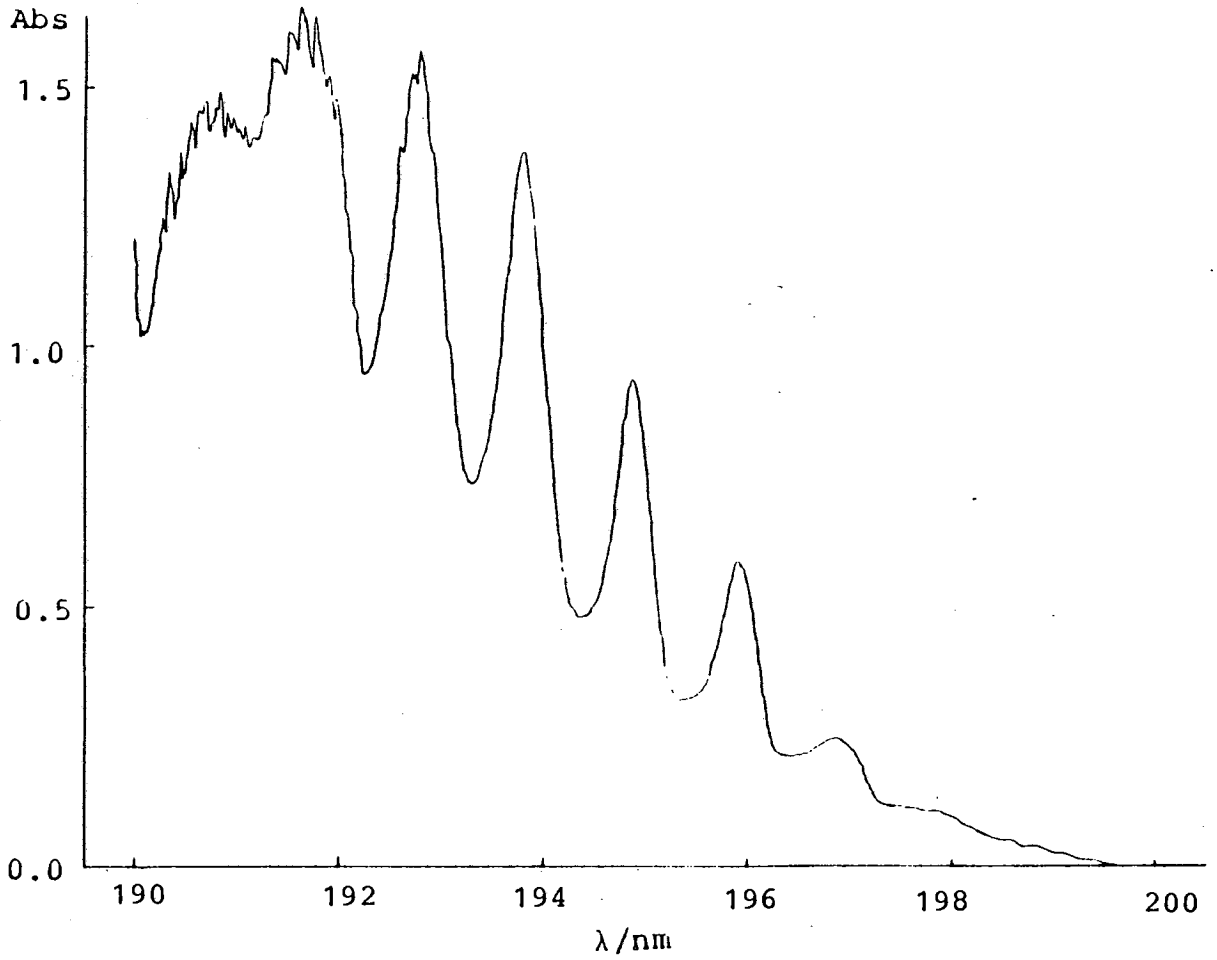

Figure 6.1 The absorption spectrum of IBr recorded at 0.25 nm resolution on a Perkin-Elmer model 554 spectrophotometer. This figure shows the E←X Rydberg absorption system of IBr.

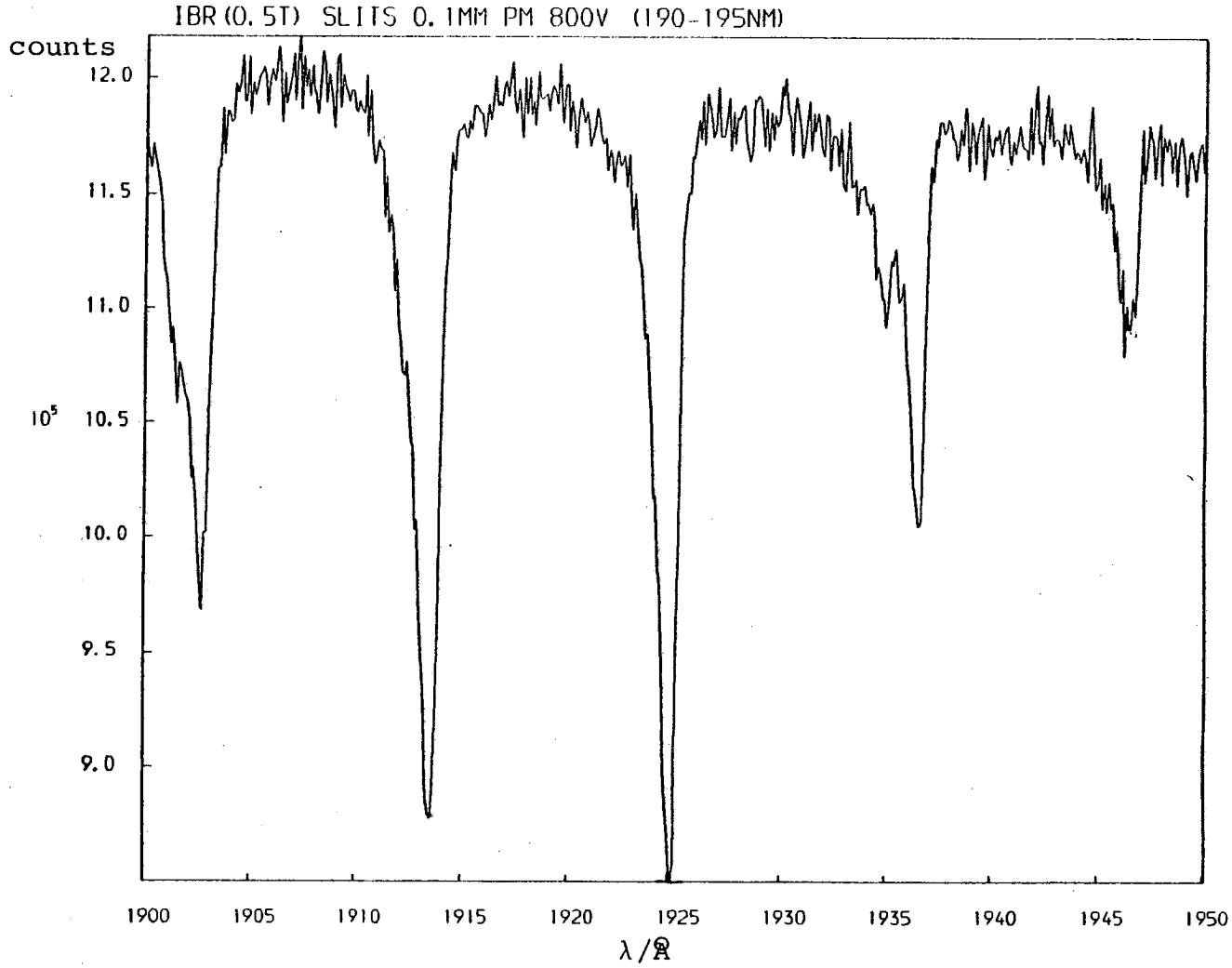

Figure 6.2 The absorption spectrum of IBr at 0.016 nm resolution recorded at the Synchrotron Radiation Source at Daresbury. Note the scale reads high by 2.8 Å. This figure shows there is a large area where little Rydberg absorption takes place.

to another state in this region. The absorption spectrum yields very little information on this underlying state as there is no clearly resolved structure to be seen between the Rydberg absorption peaks. The fluorescence and quenching behaviour of IBr excited in the region 190-200 nm implies that absorption to an ion-pair state occurs in this region.

Figure 6.3 is included to show the absorption spectrum in the range 160 nm - 200 nm. The various Rydberg absorption systems are marked.

6.4 The Fluorescence Spectrum of IBr Excited at $\lambda \cong 190$ nm

A low resolution fluorescence spectrum from IBr, excited by line narrowed ArF laser radiation is shown in Figure 6.4. This fluorescence spectrum remained virtually unchanged as the excitation wavelength was scanned across the gain profile of the ArF laser (192.8 - 193.6 nm) which includes the Rydberg absorption features mentioned previously and a region where Rydberg absorption is negligible. This implies that some other underlying absorption system is responsible for this fluorescence and not absorption to a Rydberg state. The idea that the absorbing state is an underlying ion-pair state is backed up by the fluorescence behaviour on the addition of a quenching gas. Figure 6.5 shows a spectrum of IBr taken under similar conditions to Figure 6.4 except that the excitation source was a broad band ArF laser (it was shown previously that the bandwidth did not affect the spectrum) and 7.45 kNm^{-2} of Ar had been

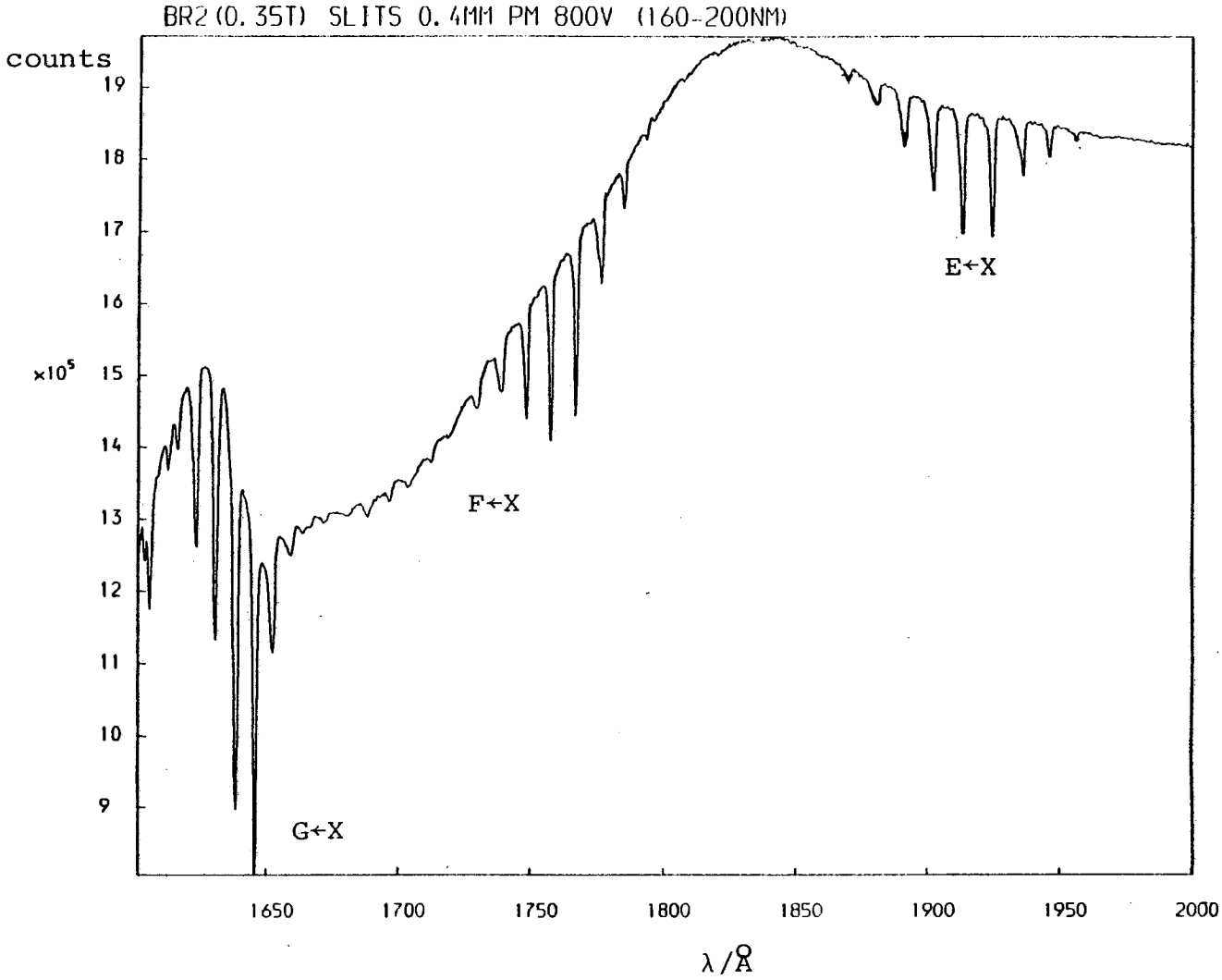

Figure 6.3 The absorption spectrum of IBr at 0.064 nm resolution recorded at the Synchrotron Radiation Source at Daresbury. This figure shows the various Rydberg absorption bands of IBr. Note the scale reads high by 2.8 Å.

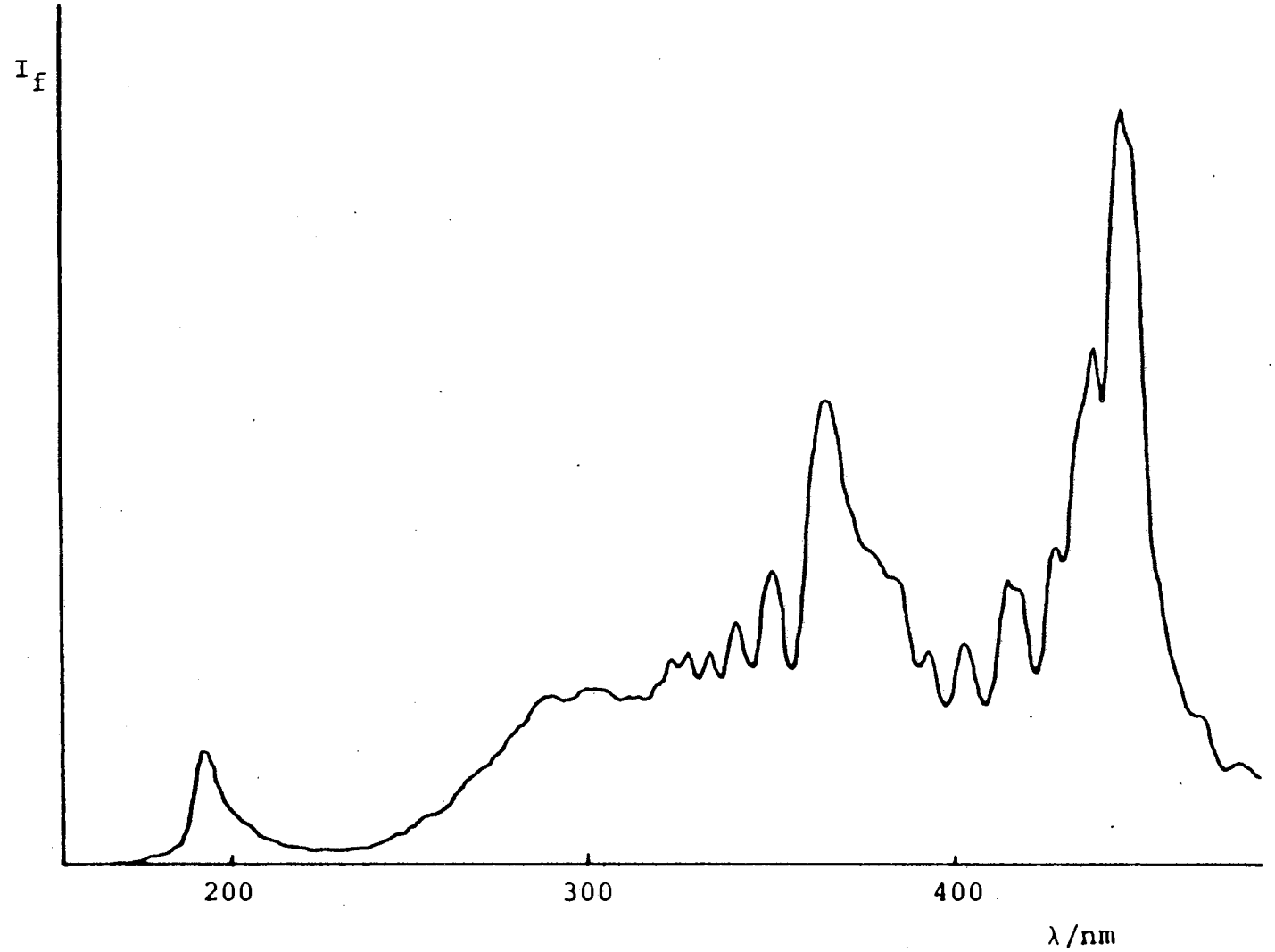

Figure 6.4 A low resolution spectrum of IBr excited with a line narrowed ArF laser. The spectrum was recorded by averaging 20 laser shots onto a diode array detector head of an O.M.A. $p_{IBr} = p_{Br_2} = 150\ Nm^{-2}$.

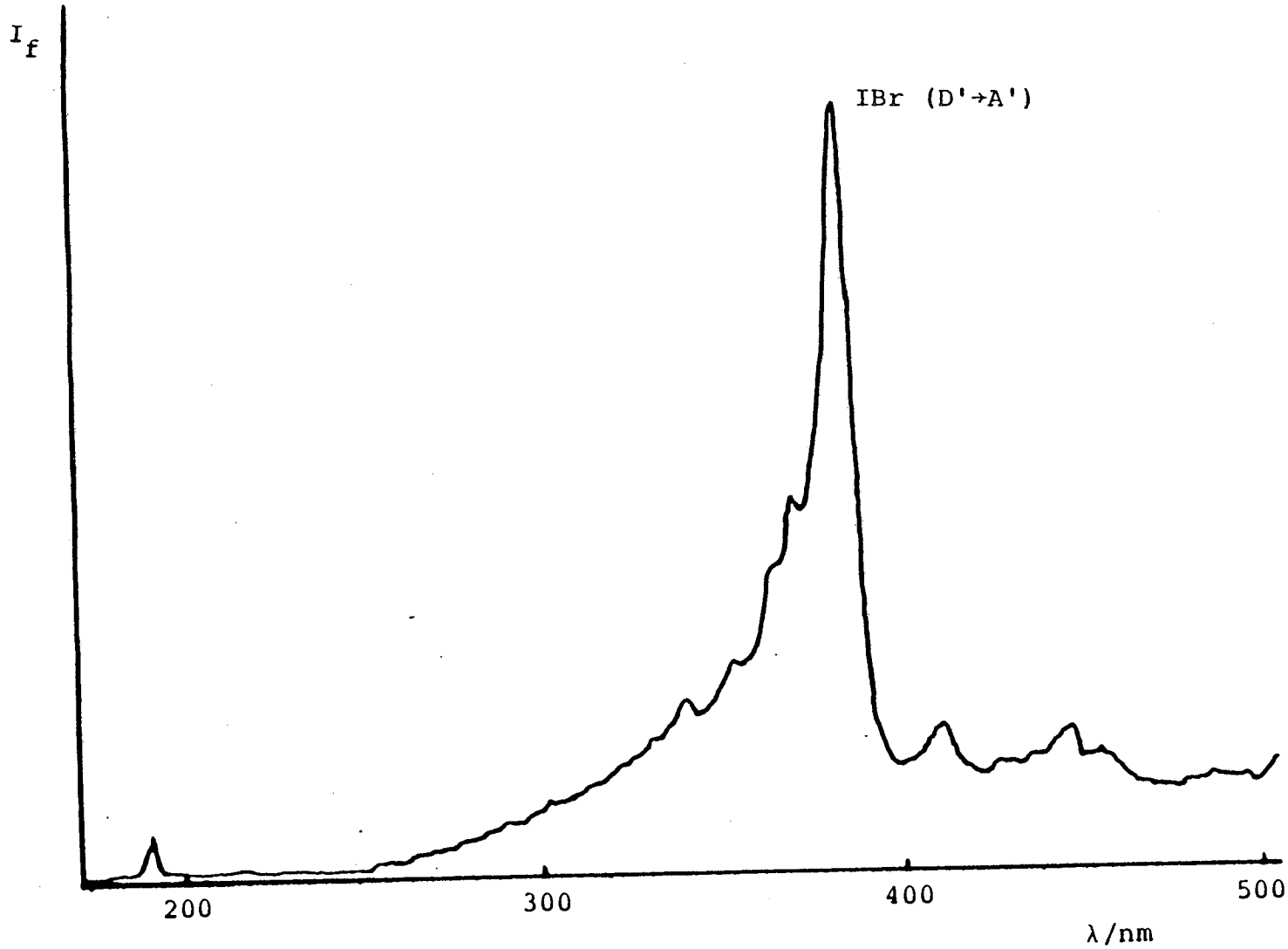

Figure 6.5 Fluorescence observed following excitation of IBr + Ar at 193 nm (Lambda Physik EMG200 laser). The spectrum was recorded by averaging 20 laser shots onto a diode array detector head of an O.M.A.
(p_{IBr} = 160 Nm^{-2}, p_{Br_2} = 147 Nm^{-2}, p_{Ar} = 7.45 kNm^{-2})

added to the sample. As can be seen, the spectrum now consists of one main peak at 385 nm which is degraded to the violet. This peak is in the right position[2] and is the correct shape to be the D' → A' peak from IBr. It is a property of these halogen ion-pair states that they are easily quenched, by inert gases, to the lowest energy ion-pair state (the D' state) and that in the process a considerable amount of vibrational energy is lost. Thus the rapid production of the D'→A' band originating from the lower vibrational levels of the D' state is indicative that the originally excited state is indeed an ion-pair state.

The spectrum shown in Figure 6.4 looks broadly similar to the spectra observed from I_2 and Br_2 (see Figures 4.3 and 5.3) and thus a tentative interpretation would be that the absorbing state is an ion-pair state, which because of the analogy with I_2 we call the D state, and that the majority of fluorescence is oscillatory continuum fluorescence.

The peak in Figure 6.4 at ∿200 nm is due partly to scattered laser light and partly to bound→bound transitions originating from the initially populated upper state and terminating on the lower few bound levels of the IBr ground state. The boundary between bound→bound and bound→free transitions for IBr excited at 193 nm lies at ∿270 nm and the emission on the long wavelength side of this limit resembles that of I_2 and Br_2. This is the reason for the interpretation that the structure from 270 nm to 370 nm consists of oscillatory continuum emission which is the equivalent of the

McLennan system of I_2. Taking this analogy with I_2 and Br_2 further, the second system between 380 nm and 460 nm can be interpreted as a second oscillatory continuum with a transition terminating on a repulsive lower state. In this interpretation of the data it would be expected that under higher resolution the 355 nm band head would resolve into a double frequency (McLennan) type of oscillatory continuum while the second system, peaking at 455 nm, would remain essentially unchanged by the increase in resolution.

Figures 6.6 and 6.7 show the medium resolution (0.35 nm) spectra from IBr excited with a line narrowed ArF laser. The first thing to note is that the system peaking at 355 nm does <u>not</u> have two frequencies of oscillation but instead seems to be a well behaved single frequency type of oscillatory continuum (the cut-off at 300 nm is due to the introduction of a pyrex filter). The second system, peaking at 450 nm, seems unusual in that it is composed of a series of regularly shaped "double peaks".

Work was then carried out using a spectrofluorimeter to examine how these bands behave as the wavelength of excitation is changed. The results of these experiments, shown in Figures 6.8 and 6.9, show that as the excitation wavelength is decreased, the wavelength of the last fluorescence peak in the 450 nm system also decreases. This is the opposite of what happens in I_2 and what would be expected from an oscillatory continuum originating from the inner turning-point of the upper ion-pair state. However if the system originated from the outer turning-point of

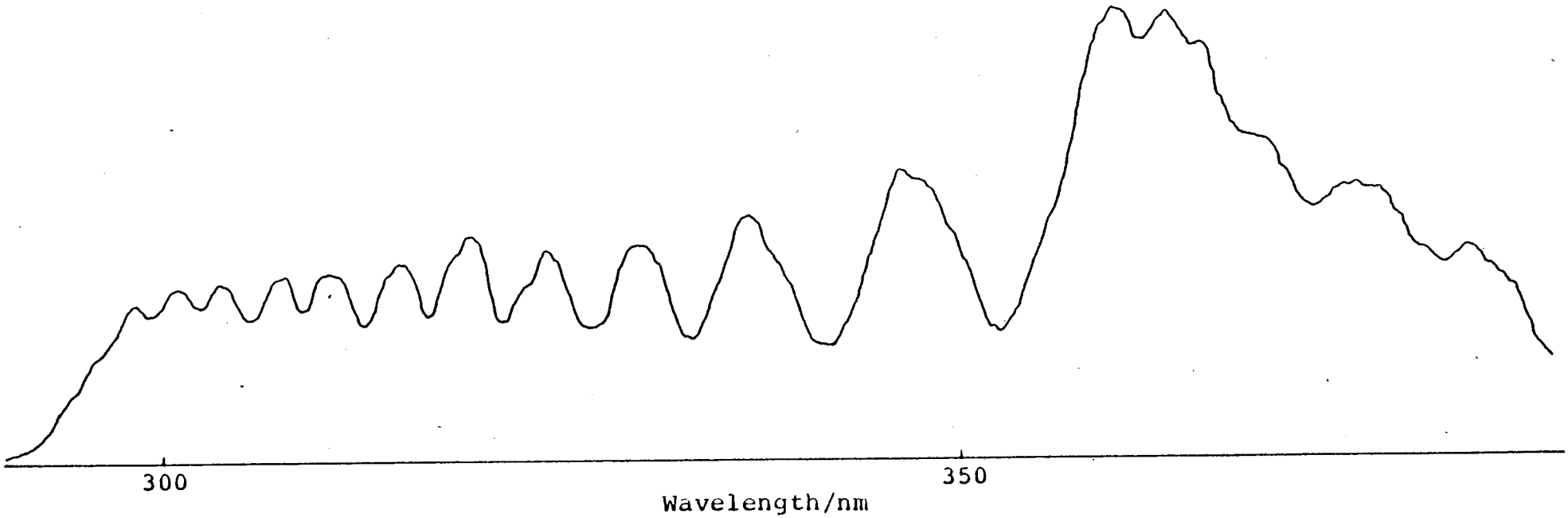

Figure 6.6 Medium resolution (0.3 nm) fluorescence spectrum of IBr recorded by averaging 20 shots of a line narrowed ArF laser (Lambda Physik EMG150) on a diode array detector of an O.M.A. The sample used was 200 Nm^{-2} IBr + 200 Nm^{-2} Br_2. A pyrex filter was used to remove light with $\lambda < 300$ nm.

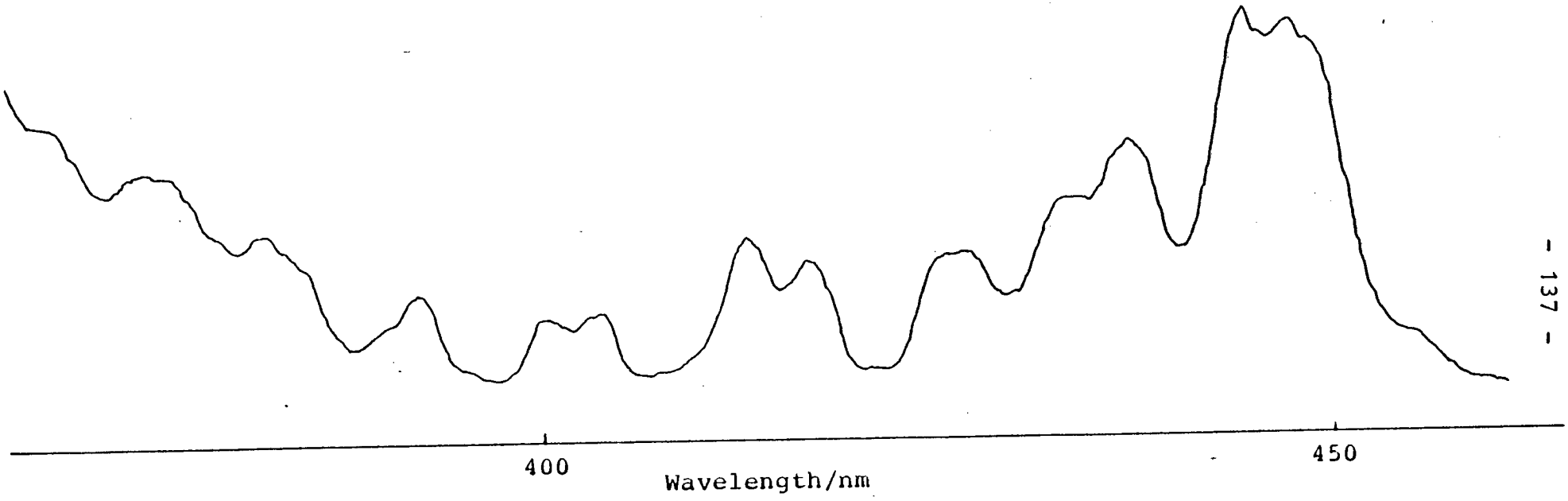

Figure 6.7 Medium resolution (0.3 nm) fluorescence spectrum of IBr recorded by averaging 20 shots of a line narrowed ArF laser (Lambda Physik EMG150) on a diode array detector of an O.M.A. The sample used was 200 Nm^{-2} IBr + 200 Nm^{-2} Br_2. A pyrex filter was used to remove light with $\lambda < 300$ nm.

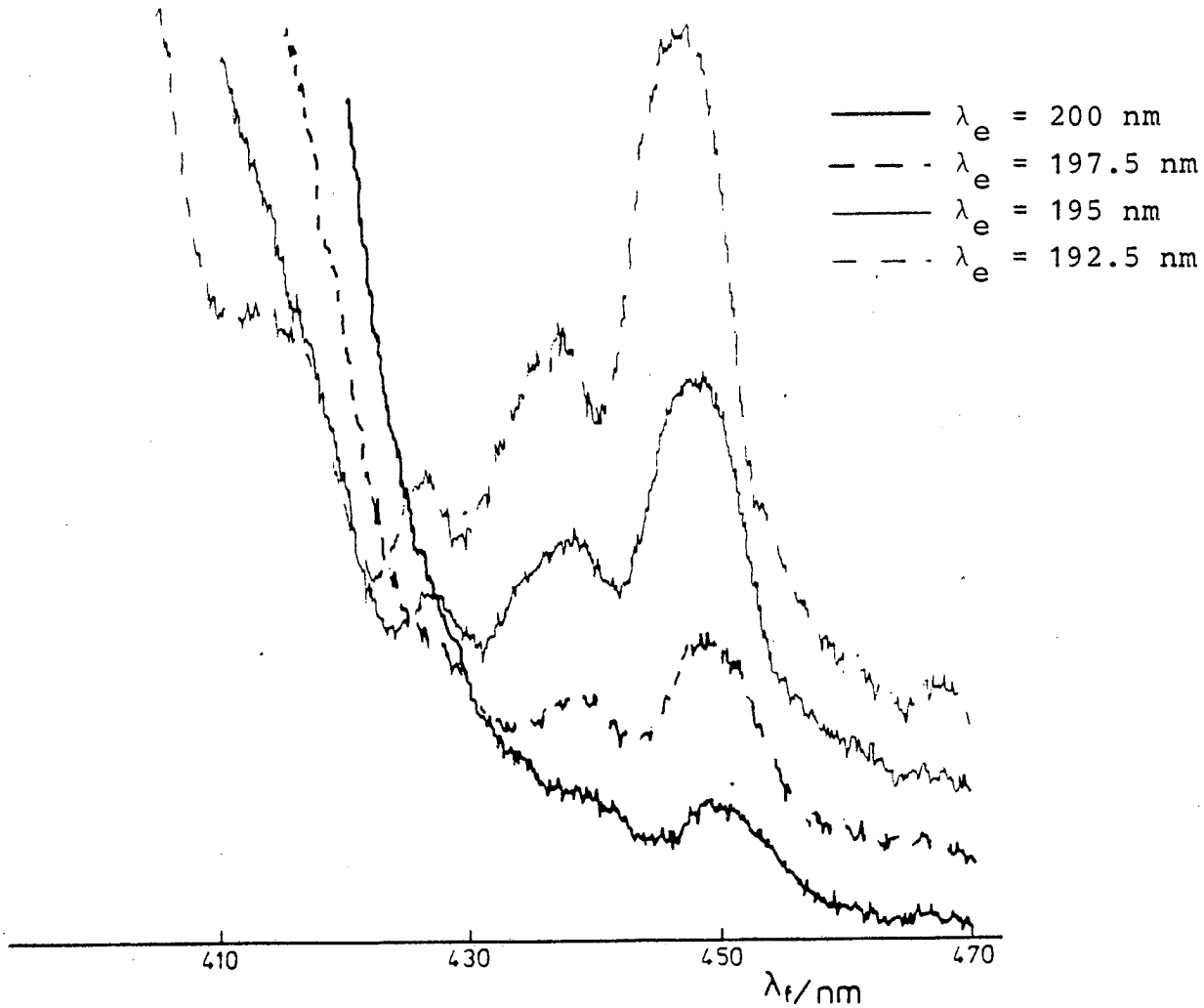

Figure 6.8 Fluorescence spectra of the 450 nm band system of IBr recorded at various excitation wavelengths, as indicated, using a Perkin-Elmer 650-40 spectrofluorimeter. The excitation monochromator was used in 2nd Order. The resolutions used in recording the spectra were; excitation 3.5 nm, fluorescence 3 nm. The sample used was 160 Nm^{-2} IBr + 160 Nm^{-2} Br_2. A pyrex filter was used to cut out fluorescence below 300 nm wavelength.

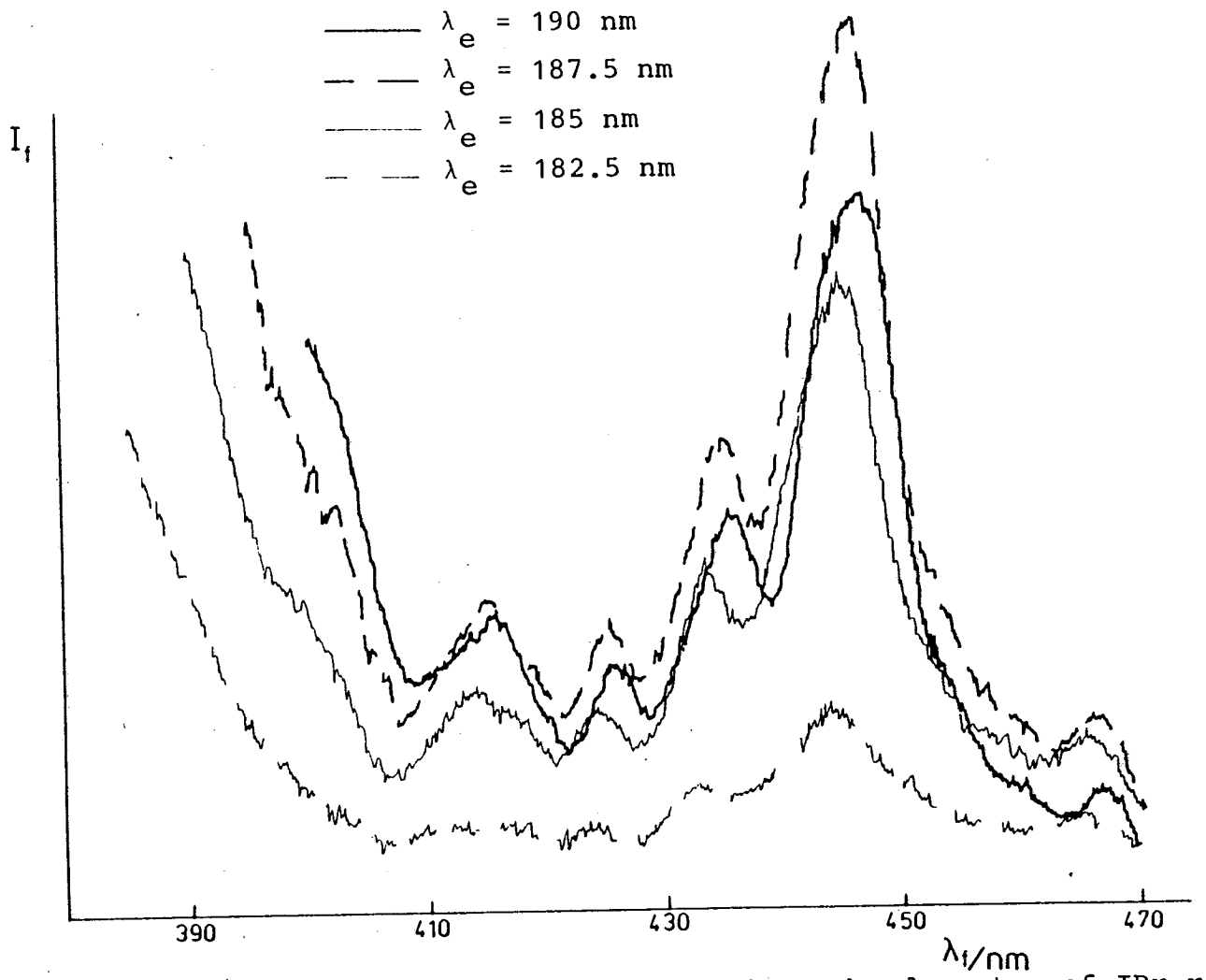

Figure 6.9 Fluorescence spectra of the 450 nm band system of IBr recorded at various excitation wavelengths, as indicated, using a Perkin-Elmer 650-40 spectrofluorimeter. The conditions were the same as for Figure 6.8 except that the sample consisted of 130 Nm^{-2} IBr + 130 Nm^{-2} Br_2

the IBr D state the shift in the peaks would be in the right direction but the main peak would be expected to be the first peak of the system instead of the last. A double frequency type of oscillatory continuum would not be expected to move with a change of excitation. Thus all that can be said is that at present we do not understand the nature of the 450 nm system of IBr.

The simpler of the two systems, peaking at 355 nm was also examined using the spectrofluorimeter (see Figure 6.10) and it was found that this sytstem remained unchanged as the excitation wavelength was altered between 200 nm and 212 nm. This is characteristic of a double frequency type of oscillatory continuum. Thus it appears that the high frequency structure has been "washed in" by the presence of the two isotopes of bromine. It may also be that the high frequency structure is too fine to be resolved in our experiments but this seems unlikely.

Further work on both oscillatory continuum systems of IBr is clearly needed. The best that can be done at present is to list the expected differences between IBr and I_2 and state that the explanation for the anomalies in the IBr oscillatory continuum fluorescence spectra is somehow related to these. The most important spectroscopic difference between I_2 and IBr is the lack of gerade-ungerade symmetry for IBr. One consequence of this is that the only relevant and strict one photon electronic selection rule for the heavy halogens breaks down. More electronic states

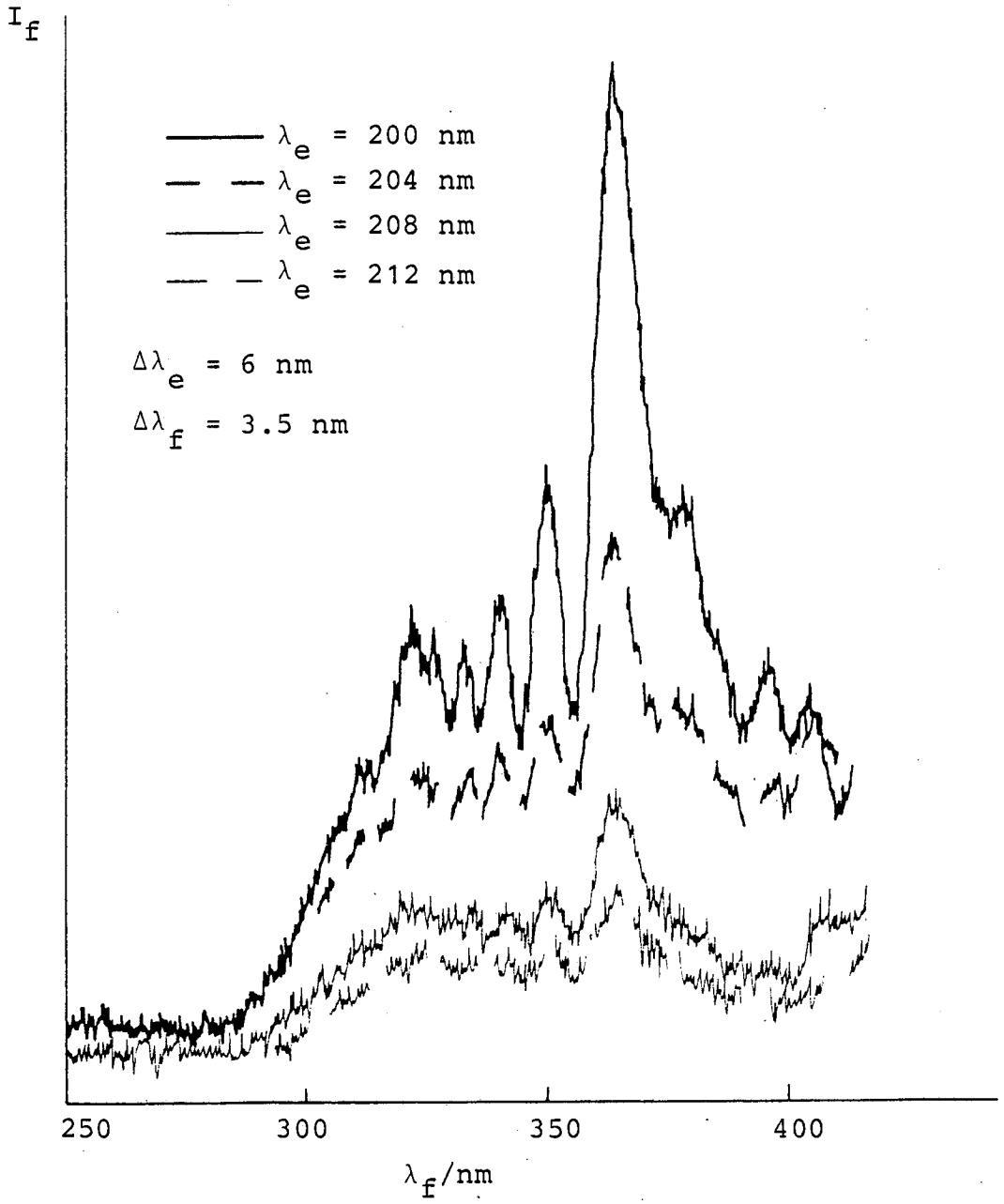

Figure 6.10 The fluorescence spectrum of IBr, in the region of 355 nm, recorded at various excitation wavelengths on a Perkin-Elmer 650-40 spectrofluorimeter. The excitation monochromator was used in 1st Order. The sample used was $p_{IBr} = P_{Br_2} = 150\ Nm^{-2}$. A pyrex filter was used.

are accessible with one photon and more fluorescence systems have to be considered in analysing the resulting fluorescence spectra from IBr. Another consequence of this lack of symmetry in IBr is that mixing between electronic states is more likely. This has two main consequences: firstly if a repulsive state mixes with a normal bound valence state the resulting mixture may produce a bound state with a large r_e and another state that is partially bound by the possession of a potential barrier, an example of this is seen with the B and B' states of IBr. This may be important as the origin of oscillatory continua lies in the difference in the r_e of the valence and ion-pair states. A second effect is that the lowest Rydberg states of IBr may mix with the ion-pair states in the region accessible with a 193 nm photon. In iodine the lowest Rydberg state (the 'a' state of Venkateswarlu)[7] is at an energy of $\sim$52,000 cm^{-1}, but since it is of gerade symmetry it is not seen in the absorption spectrum and cannot mix with the ungerade state populated. In IBr this mixing may have an effect on the single frequency type of oscillatory continua produced from the inner turning point of the upper state.

Another problem that exists for IBr but not for I_2 is that bromine has two naturally occurring isotopes of about equal abundance, ^{79}Br and ^{81}Br. This may lead to a degradation of the fluorescence spectrum of IBr. In order to find out exactly what effect this has, spectra should be recorded using isotopically pure IBr.

Although the fluorescence spectrum of IBr excited at approximately 190 nm is not understood yet, it is likely that the key to its understanding lies in the preceding two paragraphs. No attempt was made to simulate the spectra reproduced in this chapter because the first step in the process involves analysing the D→X bound→free transitions and this could not be done because of the problems mentioned above.

6.5 Physical Quenching of the D State of IBr

On quenching, the vibrationally excited ion-pair states of the halogens rapidly cascade to the lowest ion-pair state (the D' state) giving rise to strong D' → A' fluorescence. In IBr this D' → A' transition occurs at 381 nm and in common with the other halogens is degraded to the violet. In the work described in this section the quenching of the fluorescence from the excited D state of IBr upon the addition of various gases was examined. Because the D' → A' transition is degraded to the violet the fluorescence system peaking at 355 nm is lifted by the tail of the D' → A' peak and thus the quenching is difficult to measure. However, the system peaking at 450 nm is relatively free from these problems and is also reasonably free from contamination by I_2 fluorescence which has relatively little intensity beyond 420 nm. The 450 nm peak was therefore used to investigate the quenching behaviour of IBr. In these experiments a mixtures of IBr,

Br_2 and varying amounts of quenching gas were excited at 200 nm and the resulting fluorescence spectra recorded on a Perkin-Elmer 650-40 spectrofluorimeter. The intensity of the fluorescence peak at 450 nm was measured and a Stern-Volmer analysis was carried out.

Three main quenching gases were studied: He, Xe and Ar. Figure 6.11 shows the effect of adding varying pressures of argon to a standard mixture of 145 Nm^{-2} IBr plus 145 Nm^{-2} Br_2 and in particular that both the 355 nm and 450 nm systems of IBr lose intensity as argon is added, but the 355 nm system is lifted by the emergence of the D' → A' peak at 381 nm. Figure 6.12 shows that this peak continues to grow as more argon is added (up to at least 60 kNm^{-2}) and as the peak grows it narrows. This narrowing is produced because the vibrational population distribution in the D' state is being quenched into the lowest few vibrational levels. Part of the increase in intensity of this peak at the higher pressures may be due to pressure broadening of the absorption. The extra peak emerging at 340 nm in Figure 6.12 is fluorescence from the D' → A' transition in I_2. A Stern-Volmer plot was drawn from the data presented in Figure 6.11 and is shown as Figure 6.13. Analysis of this plot leads to a relative rate constant for the removal of the D state IBr by argon of 6.68×10^{-18} $cm^3 molecule^{-1}$. Quenching by argon seems to be a typical case of physical quenching.

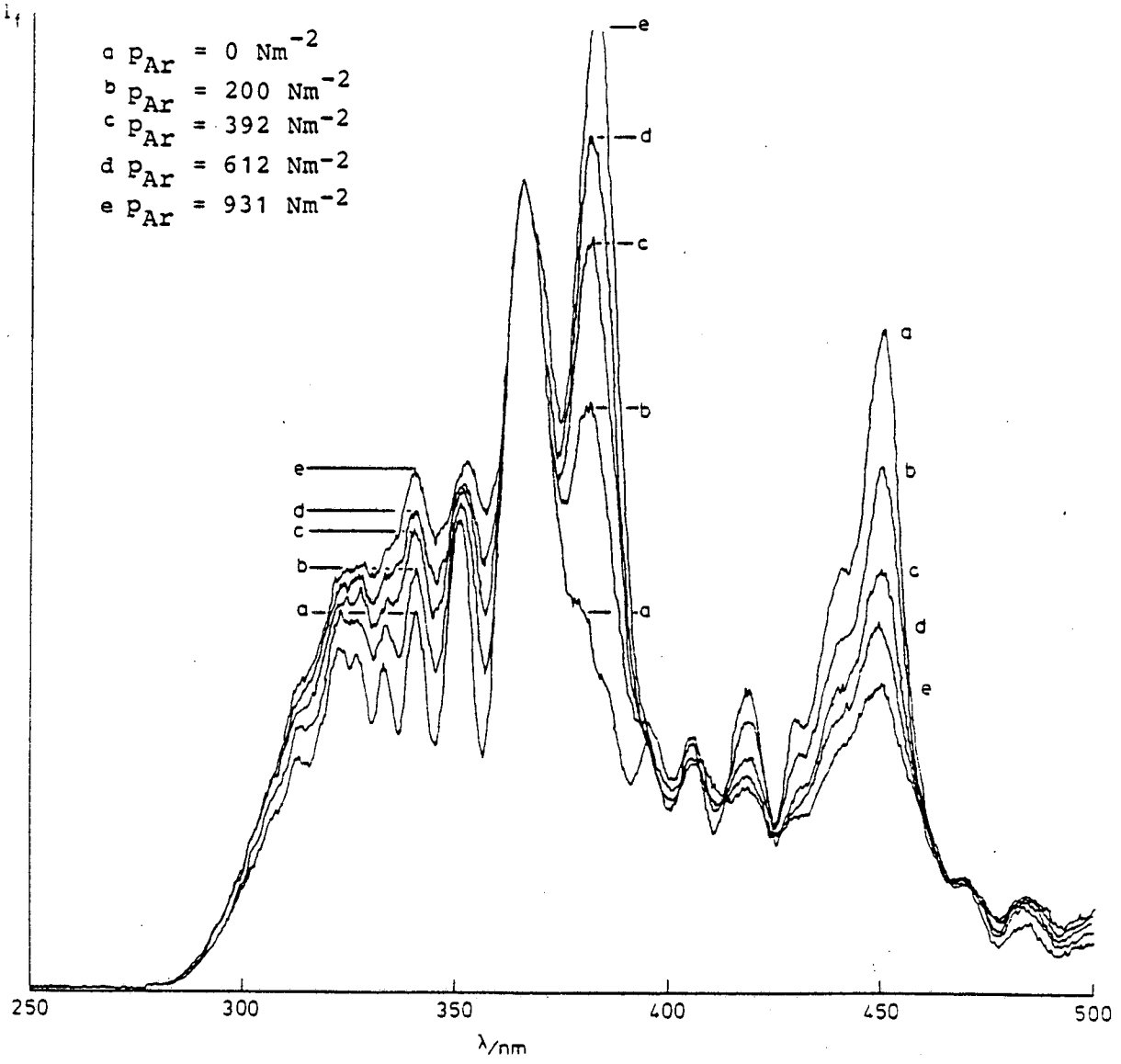

Figure 6.11 Fluorescence spectra of IBr excited at 200 nm using a Perkin-Elmer 650-40 spectrofluorimeter. The resolution of the excitation monochromator was 15 nm and the fluorescence monochromator 3 nm. A pyrex filter was used. p_{IBr} = 146 Nm^{-2}, p_{Br_2} = 146 Nm^{-2}, p_{Ar} as indicated.

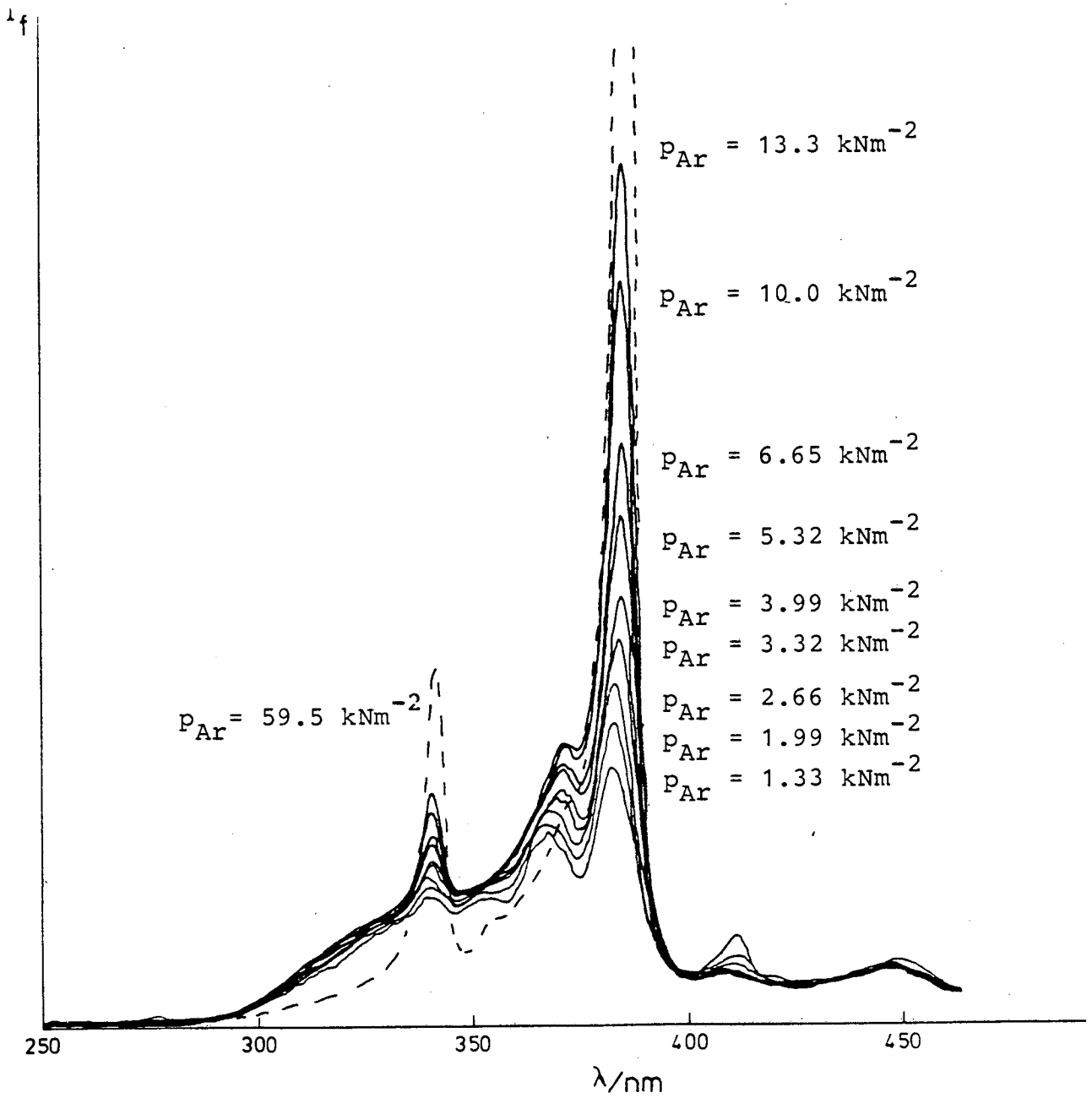

Figure 6.12 As Figure 6.11 but showing the rise of IBr D'→A' emission as the pressure of Ar is increased further.

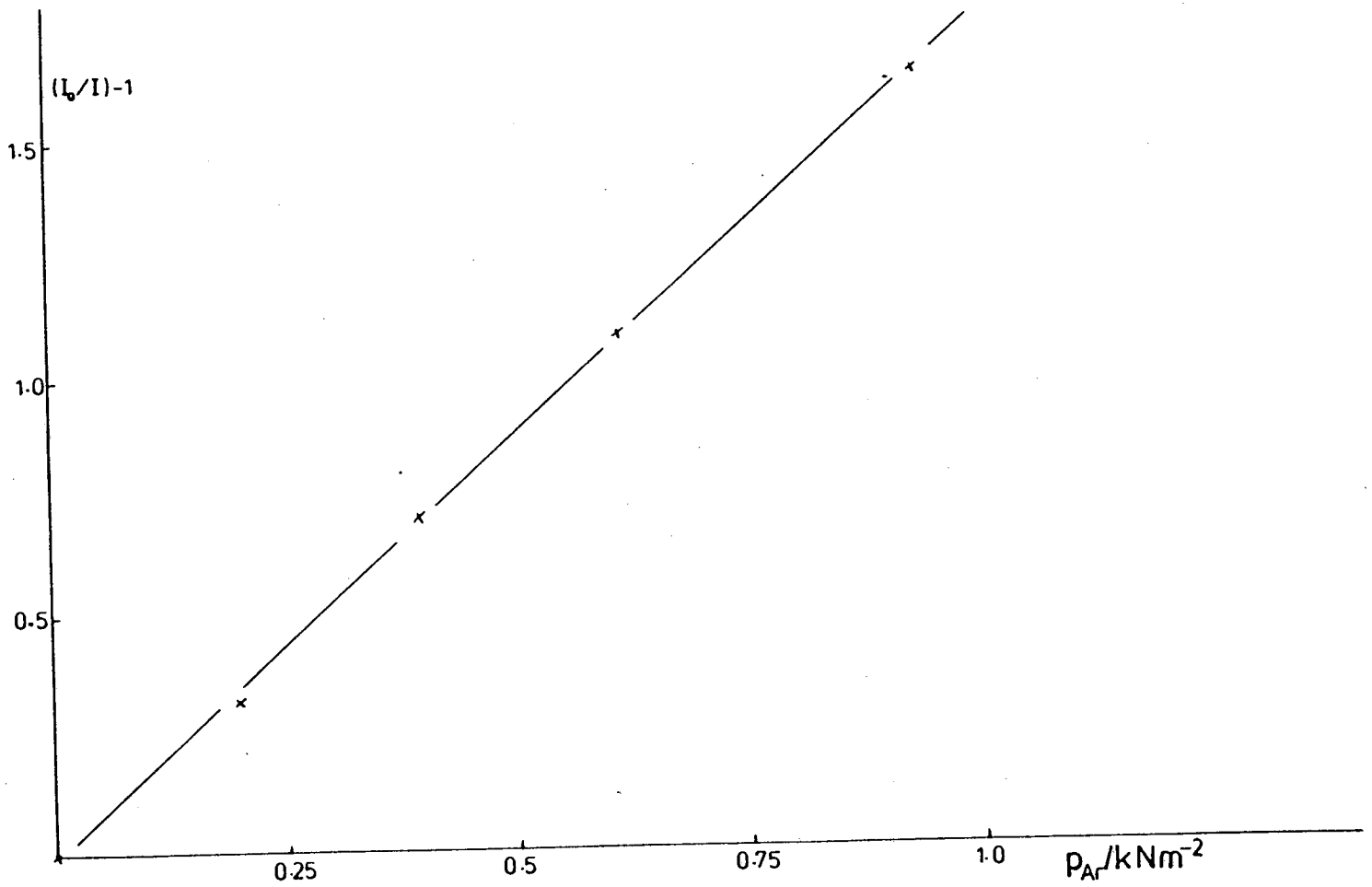

Figure 6.13 Stern-Volmer plot of the data from Figure 6.11.

Helium was the next gas studied. It behaved in a similar way to argon but there were some differences. The quenched spectra of IBr produced are shown in Figure 6.14 which again shows that both the 355 nm and 450 nm systems of IBr fluorescence are reduced in intensity and again shows the D' → A' peak appearing at 381 nm. However in this case the 381 nm peak is not so prominent or narrow as before. Also the overall intensity of fluorescence seems to decrease with the addition of helium implying that, as well as transferring population from the D state to the D' state, helium also transfers D state IBr into a state which does not fluoresce in the ultra-violet/visible region of the spectrum or it quenches the D' state. Figure 6.15 is a Stern-Volmer plot of the intensity at 455 nm with pressure of helium for the data contained in Figure 6.14. Analysis of this plot leads to a relative rate constant for the removal of IBr D state by helium of 4.18×10^{-18} $cm^3 molecule^{-1}$.

The final quenching gas studied was xenon. Quenching by xenon is not entirely physical quenching as a channel for the production of XeBr (B) is open for excitation wavelengths below 200 nm, but the results discussed here are for excitation at 200 nm and a 300 nm cut-off filter was used to block scattered excitation light appearing in the fluorescence spectrum in 2nd order which also blocked emission from XeBr(B) at 280 nm. This section will discuss the total quenching of the IBr D state by xenon while the next section (6.6) will be concerned with the production of XeBr (B).

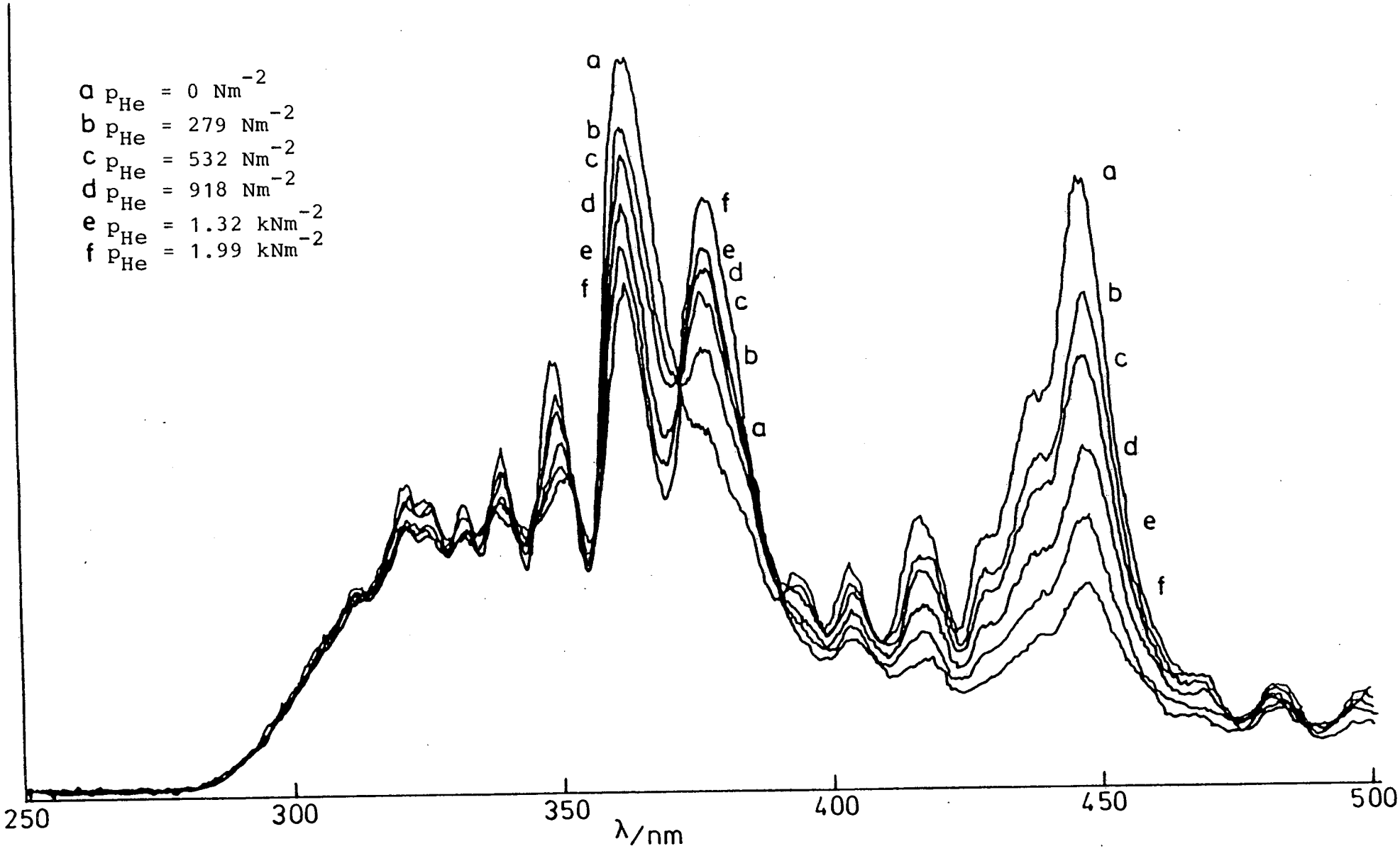

Figure 6.14 Spectrofluorimeter quenching study of IBr + He. The details are the same as for Figure 6.11 except that $p_{IBr} = p_{Br_2} = 200\ Nm^{-2}$. p_{He} as indicated.

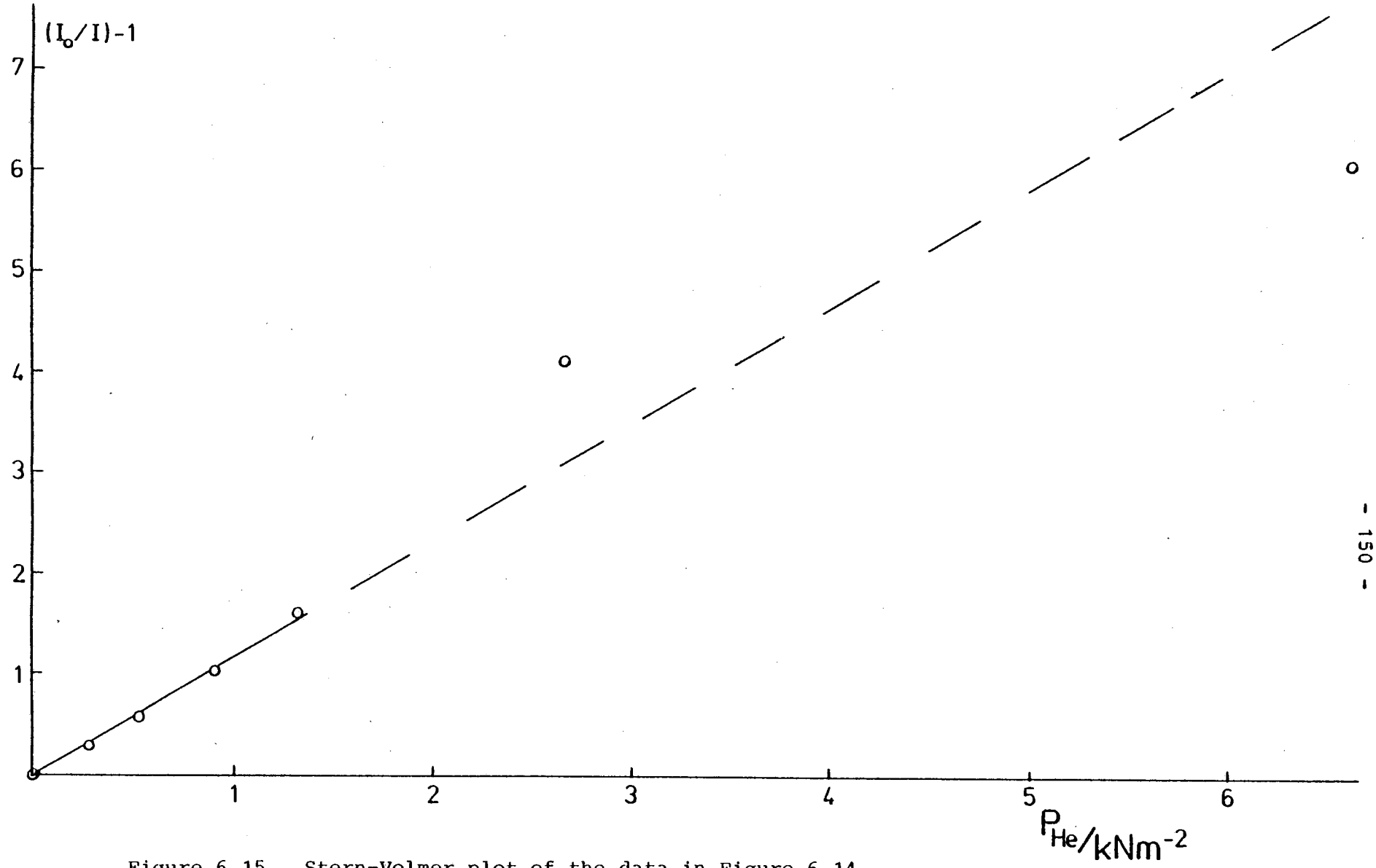

Figure 6.15 Stern-Volmer plot of the data in Figure 6.14.

Figure 6.16 shows the quenching of IBr(D) by xenon. A similar pattern is seen to that of argon and helium with the 450 nm and 355 nm fluorescence systems of IBr(D) being reduced in intensity and the 381 nm D'→A' transition increasing quite markedly although slightly less fast than the argon quenching. There is also evidence in Figure 6.16 for D'→A' emission from I_2 at 340 nm. Figure 6.17 shows a standard Stern-Volmer plot taken from IBr(D) fluorescence at 450 nm (data from Figure 6.16). The gradient of the slope of the best fit line leads to a relative rate constant for the removal of IBr(D) of 3.48×10^{-18} $cm^3 molecule^{-1}$.

In order to convert these relative rate constants to absolute quenching rate constants the lifetime of IBr(D) fluorescence in the absence of quenching gas but otherwise under the conditions used in the spectrofluorimeter experiments must be determined. To this end, experiments were carried out, with the help of a colleague, Mr. G. Gilbert, at the S.E.R.C. Daresbury Laboratory using the Synchrotron Radiation Source. For lifetime work the synchrotron was used in the "single bunch" mode, giving pulses of radiation 200 ps long with a time between pulses of 320 ns. The sample was irradiated at a wavelength of 188 nm (bandpass 3 nm) and the fluorescence lifetime was determined by measuring many times the interval between a photomultiplier pulse (after constant fraction discrimination) and the zero time reference signal from the

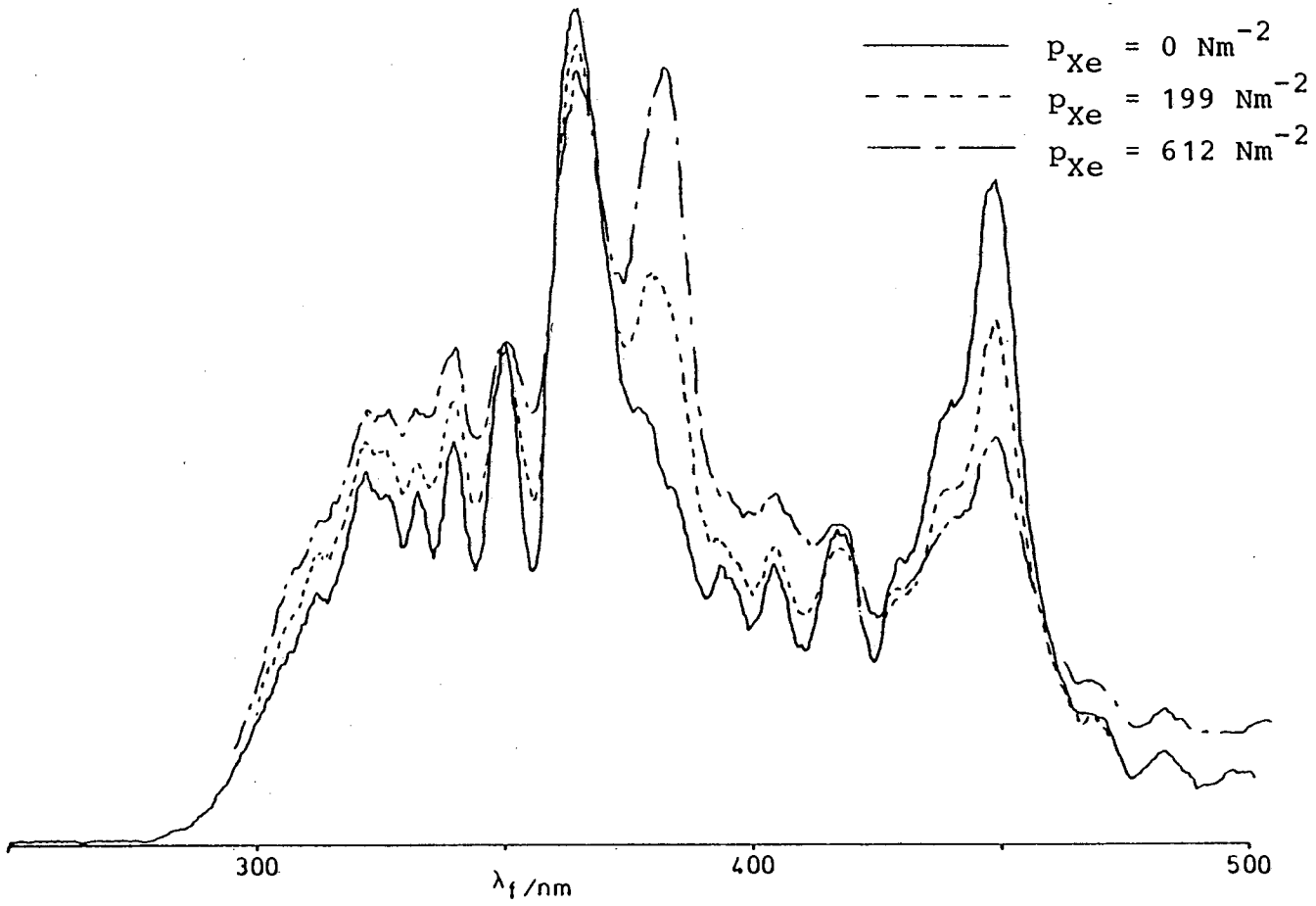

Figure 6.16 A spectrofluorimeter study of quenching of IBr(D) by Xe. The details are the same as for Figure 6.11 except p_{IBr} = 160 Nm^{-2}, p_{Br_2} = 160 Nm^{-2}, p_{Xe} as indicated.

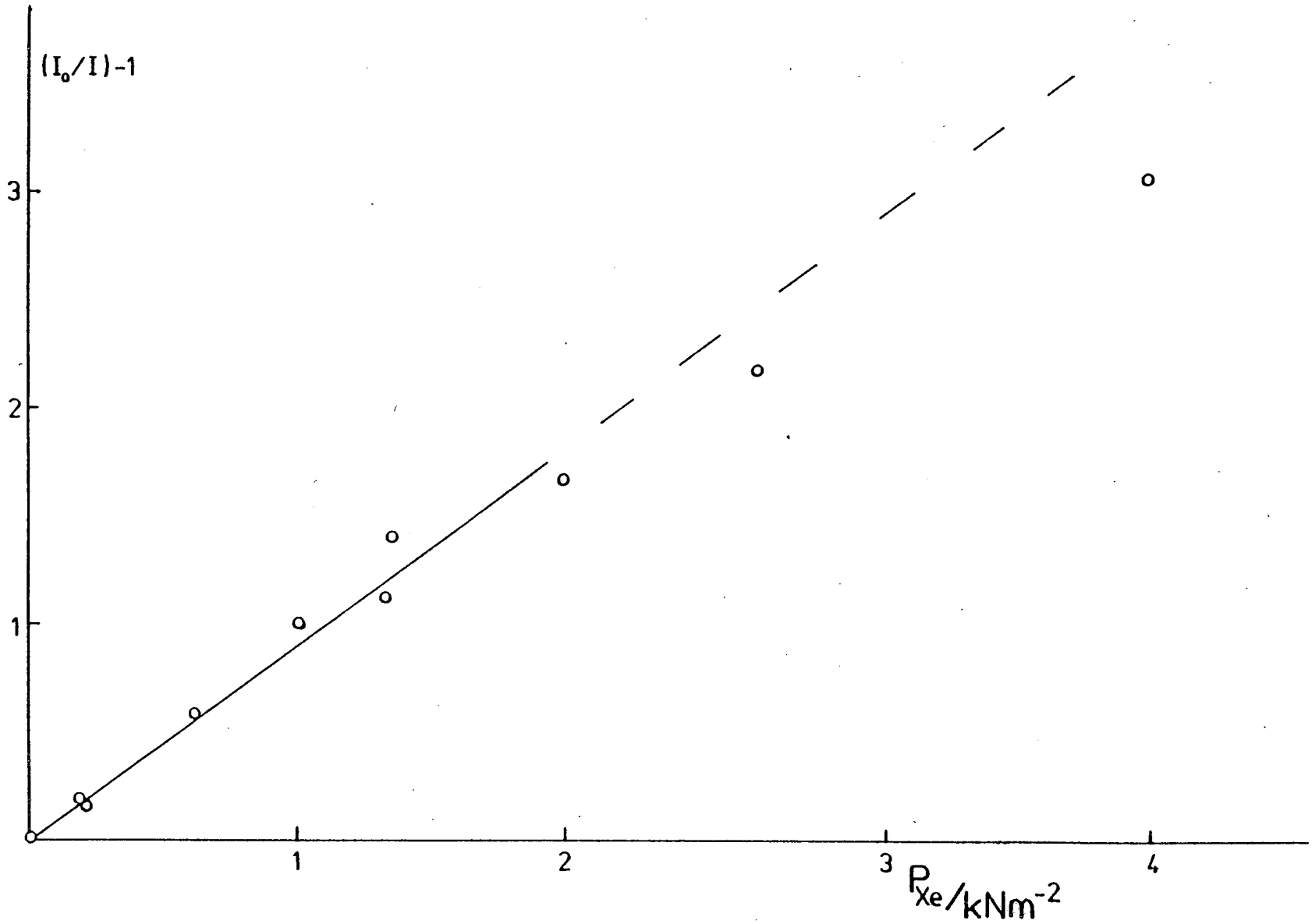

Figure 6.17 Stern-Volmer plot of the data in Figure 6.16 and other data measured in the same way.

storage ring using a time to amplitude converter (TAC). Output pulses from the TAC were accumulated on a multi-channel analyser and then passed to a local PDP 11/04 computer and then onto the AS7000 mainframe computer for analysis.

A fluorescence lifetime decay plot of IBr(D) fluorescence is shown as Figure 6.18 which shows that under the typical conditions used for the Stern-Volmer studies described here (e.g. $p_{IBr} = p_{Br_2} = 266\ Nm^{-2}$) the fluorescence lifetime is 12 ns ± 2 ns. A plot of IBr(D) fluorescence lifetime against P_{IBr} for 1:1 mixtures of IBr:Br_2 was obtained and was used to convert the relative quenching rate data above into absolute quenching rate data. In these experiments at Daresbury the purely radiative lifetime of IBr was obtained and was found to be 27 ± 4 ns. This is discussed more fully in reference 5.

The relative rate data given above were converted to absolute rate data using the measured IBr(D) lifetimes and the results are shown in Table 6.1 along with some data from G. Gilbert's work for physical quenching by the gases SF_6 and N_2 and for the reactive gases O_2, CH_4, C_2H_6, CH_3Cl and CF_3Cl.

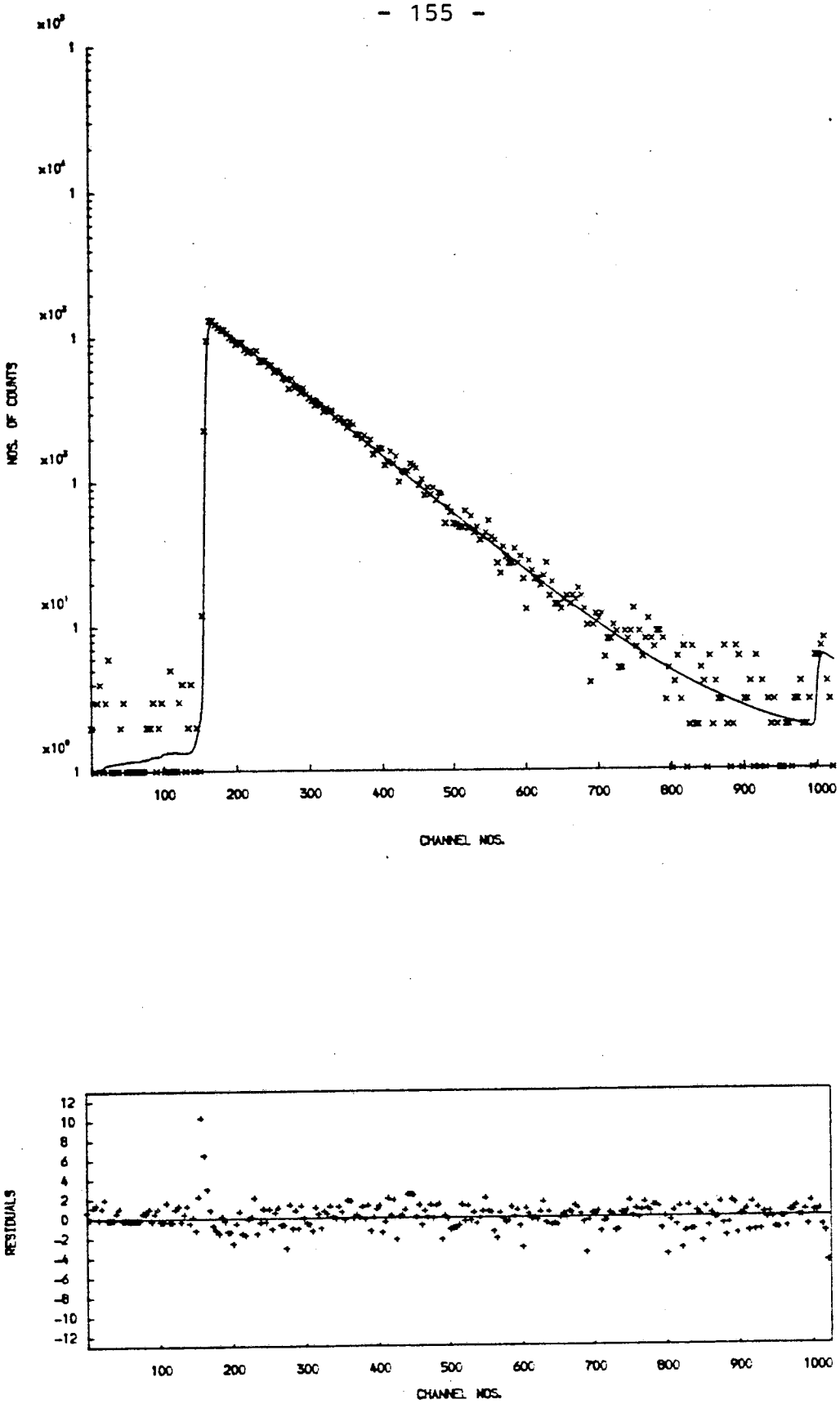

Figure 6.18 Decay of fluorescence from IBr (top trace) following excitation at 188 nm with pulsed synchrotron radiation (p_{IBr} = 133 Nm^{-2}; p_{Br_2} = 266 Nm^{-2}; time scale, one channel = 0.1132 ns
The bottom trace shows the residuals.

Table 6.1 Absolute rate constants for the removal of IBr(D) by various quenching gases

Quenching Gas	Rate constant k cm^3 $molecule^{-1}s^{-1}$
He	$3.3 \pm 0.6 \times 10^{-10}$
Ar	$4.4 \pm 0.3 \times 10^{-10}$
Xe	$2.7 \pm 0.4 \times 10^{-10}$
N_2	$2.9 \pm 0.6 \times 10^{-10}$
SF_6	$4.8 \pm 0.4 \times 10^{-10}$
O_2	$1.5 \pm 0.2 \times 10^{-10}$
CH_4	$5.5 \pm 0.6 \times 10^{-10}$
C_2H_6	$6.4 \pm 0.7 \times 10^{-10}$
CH_3Cl	$5.6 \pm 0.8 \times 10^{-10}$
CF_3Cl	$4.7 \pm 1.1 \times 10^{-10}$

6.6 The Formation of XeBr(B) from IBr(D) + Xe

Energetically, it is possible to react IBr excited into the D state by an ArF laser, with Xe to form XeBr(B) which then emits at a wavelength of 280 nm. This indeed has been observed. Figure 6.19 shows the fluorescence spectrum of IBr(D) quenched by xenon, showing in addition to the strong D'→A' emission at 385 nm a second strong feature at 280 nm. This is readily identified as the XeBr(B→X) exciplex emission and must result from the reaction of electronically excited IBr with ground state xenon atoms. Energy transfer from excited IBr to Xe followed by reaction of excited xenon atoms with ground state IBr can be ruled out as there is unsufficient energy available to populate even the lowest excited state of xenon. Reaction of translationally hot Br atoms formed following bound to free fluorescence can also be ruled out as again there is insufficient energy to form XeBr(B). The XeBr(B→X) peak grows along with the IBr D' → A' peak as the pressure of xenon is increased and as the IBr D state fluorescence is quenched, which implies that the reaction involved is as given in equation 6.1.

$$IBr(D\,^1\Sigma) + Xe \longrightarrow XeBr(B) + I \qquad (6.1)$$

The XeBr emission band is very narrow implying there is very little excess vibrational energy in the excited XeBr molecule, which is in agreement with the available thermodynamic data (i.e. the reaction is close to thermoneutral). To calculate the energetics of this reaction,

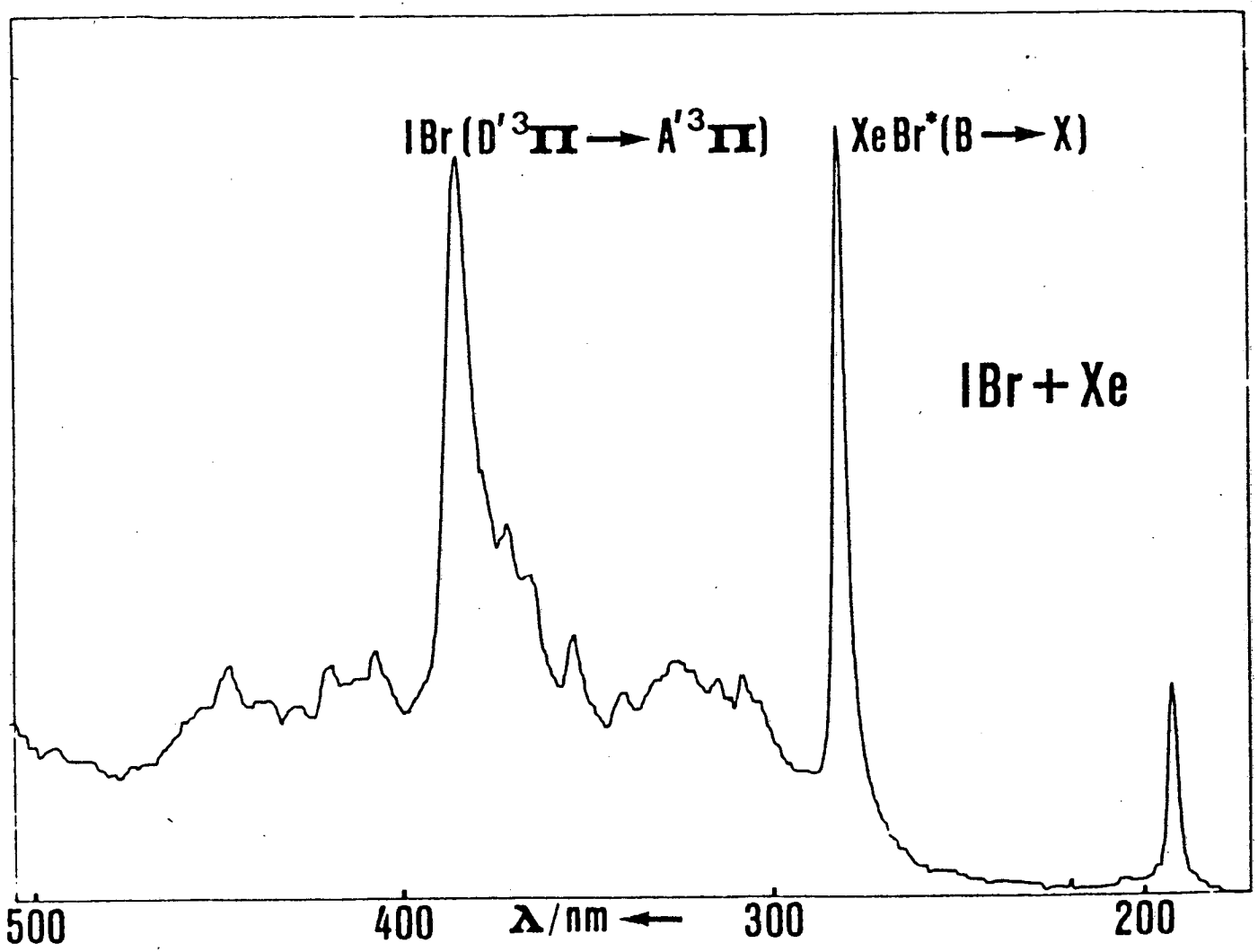

Figure 6.19 Fluorescence spectrum of IBr + Xe. The excitation source was a broad band ArF laser (Lambda Physik EMG200). To collect the signal 20 shots were averaged on a diode array detector head. No filter was used. The gas pressures were p_{IBr} = 173 Nm^{-2}, p_{Br_2} = 176 Nm^{-2} and p_{Xe} = 7.09 kNm^{-2}

it is assumed that after fluorescence XeBr separates to form Xe and Br with practically no kinetic energy, while in the reaction I is formed, again with no kinetic energy. Using these assumptions the minimum energy of a photon required to form XeBr(B) is simply the sum of the energy of a 280 nm photon plus the bond energy of IBr(X). This comes to a total energy of 50374 cm^{-1} which is equivalent to a photon of 198.5 nm wavelength.

To examine the photochemical threshold for the production of XeBr an excitation spectrum of 280 nm fluorescence from an $IBr/Br_2/Xe$ mixture was run. This is shown as Figure 6.20. It can be seen from this figure that allowing for the bandwidth of the exciting light the thermodynamic threshold comes to 198.5 ± 0.5 nm implying that the XeBr(B) does not have to be formed with any excess energy, i.e. there is no potential barrier in this reaction once it becomes energetically allowed.

When either the excitation slit on the spectrofluorimeter is widened or the excitation wavelength is reduced to below about 190 nm an extra small peak at 252 nm appears in the fluorescence spectrum of IBr quenched by xenon. This peak is shown in Figure 6.21. In order to find out if this peak could be due to XeI(B) which fluoresces at 253nm, an excitation spectrum of this peak was obtained, along with an excitation spectrum for fluorescence at 260 nm to act as a comparison. The excitation spectrum (Figure 6.22) shows that, after allowing for the band

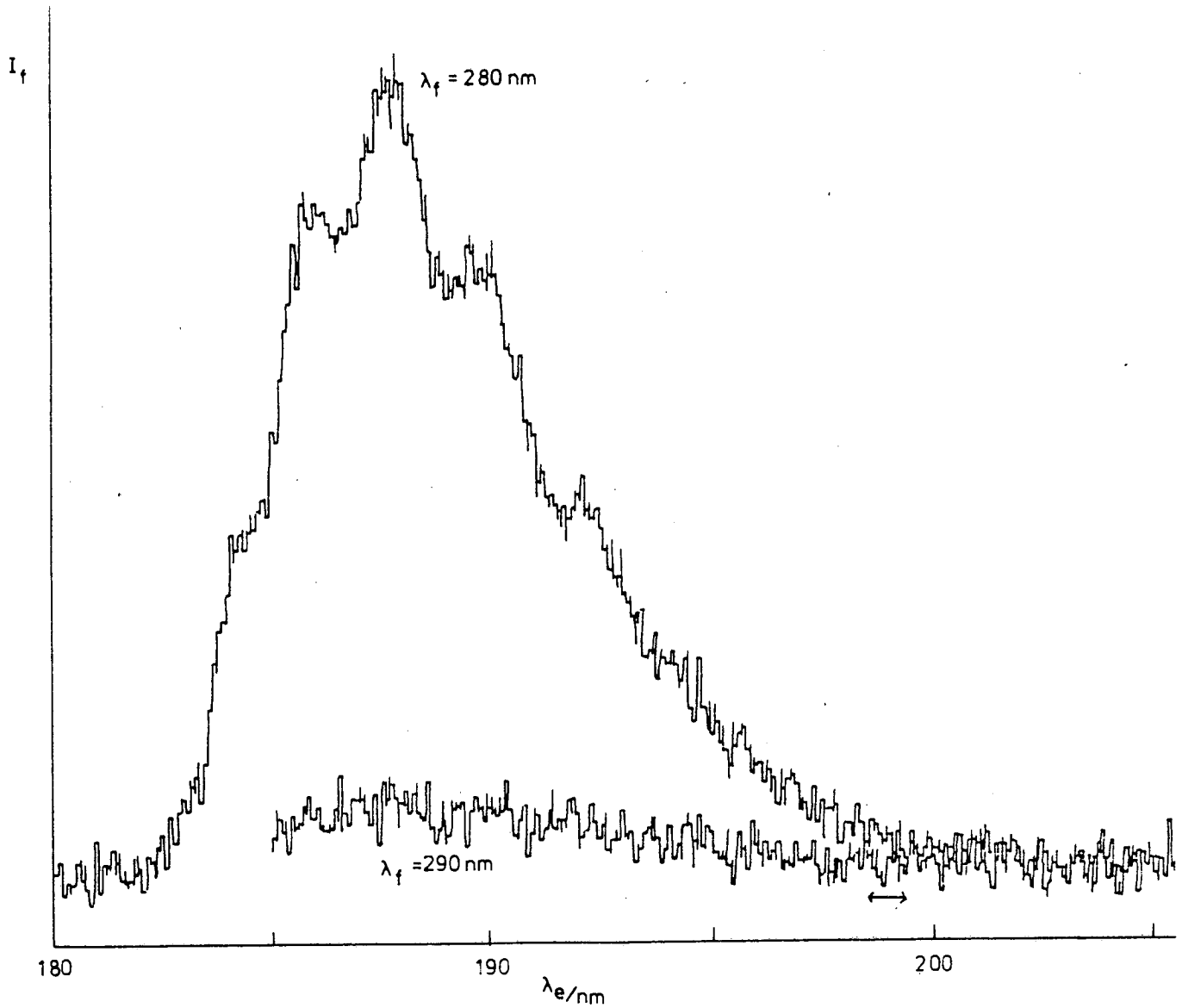

Figure 6.20 An excitation spectrum of XeBr emission. The fluorescence was detected at 280 nm ($\Delta\lambda$=3 nm) while the excitation was scanned from 180 - 205 nm in 2nd Order ($\Delta\lambda$=1 nm). The instrument used was a Perkin-Elmer 650-40 spectrofluorimeter. The gas pressures were $p_{IBr} = p_{Br_2} = 147\ Nm^{-2}$, $p_{Xe} = 12\ kNm^{-2}$. The marked area shows the photochemical cut-off for the production of XeBr(B).

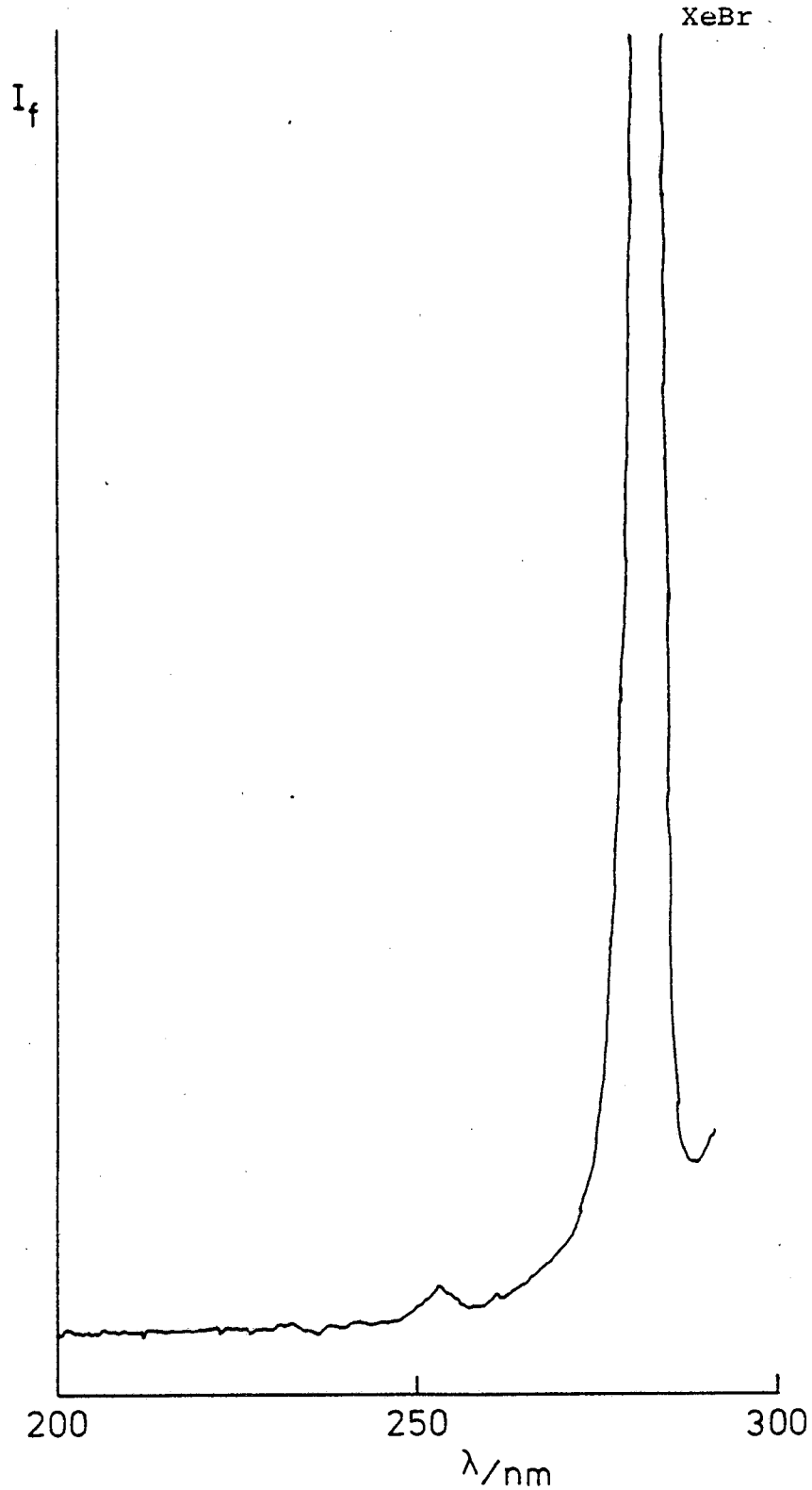

Figure 6.21 Fluorescence spectrum of IBr + Xe excited at 190 nm. The small peak at 253 nm was reproduceable. ($p_{IBr} = p_{Br_2} = 150\ Nm^{-2}$, $p_{Xe} = 27\ kNm^{-2}$). No filter was used.

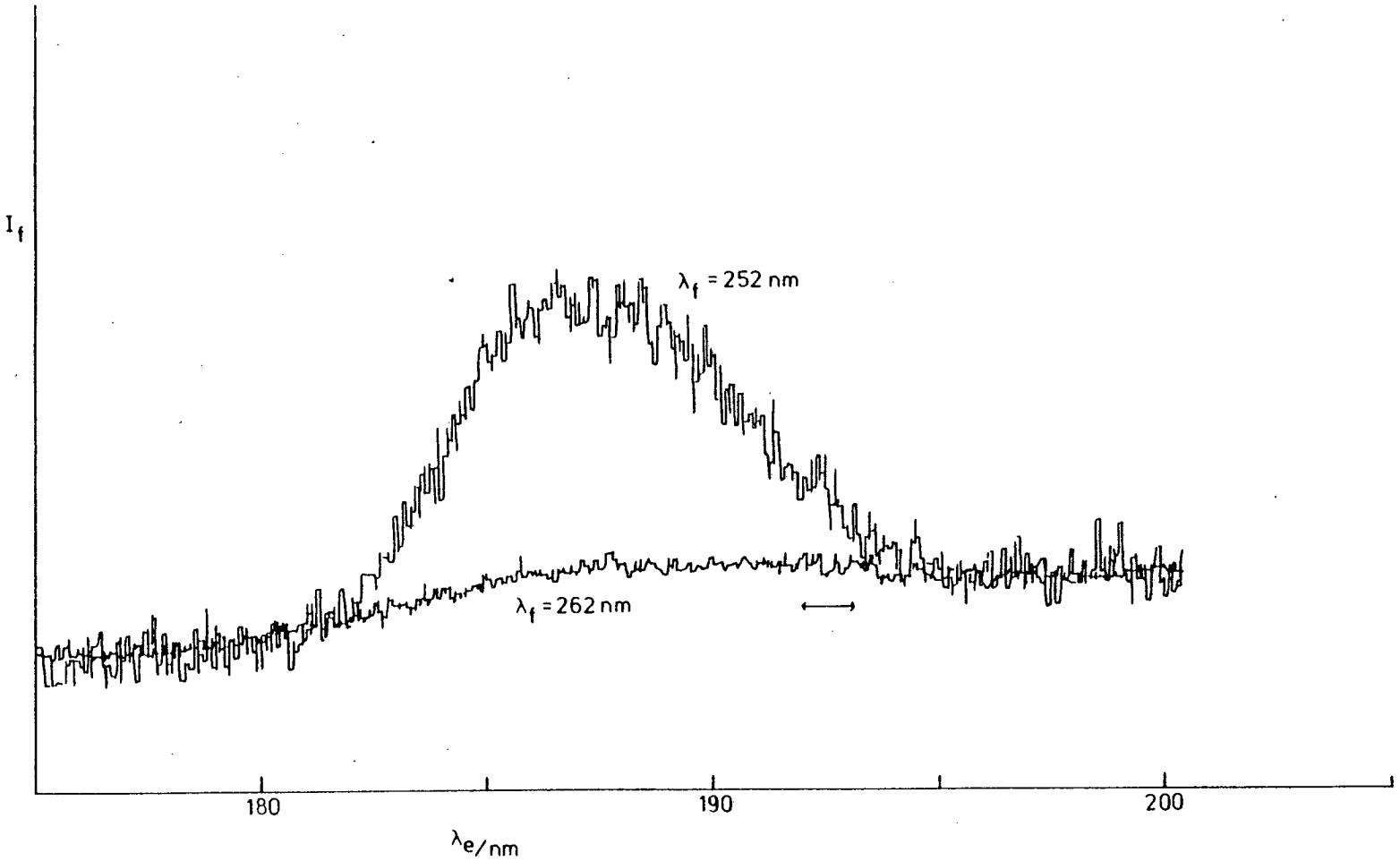

Figure 6.22 Excitation spectrum from the fluorescence of the peak at 253 nm in Figure 6.21. The excitation monochromator was used in 2nd Order at 4 nm resolution. Fluorescence was collected at 252 ($\Delta\lambda$=3nm). The instrument used was a Perkin-Elmer 650-40 spectrofluorimeter. The gas pressures were $p_{IBr} = p_{Br_2} = 147\ Nm^{-2}$, $p_{Xe} = 26.6\ kNm^{-2}$. The marked area shows the photochemical cut-off for the production of the 253 nm fluorescence peak.

width of excitation, the threshold wavelength of excitation for the production of this peak is 192.5 ± 1 nm. Now if one adds up the energy of a photon with a wavelength of 252 nm and the energy required to dissociate IBr(X) one finds that this comes to more than the energy of a 192 nm photon. In fact the energy required is 54342 cm^{-1} which is equivalent to a photon of wavelength 184 nm. Thus this extra peak can not be due to the reaction

$$IBr(D) + Xe \longrightarrow XeI(B) + Br \qquad (6.2)$$

The fluorescence must then be to either bound levels of IBr + Xe or to a metastable triatomic XeIBr, bound with respect to Xe + I + Br but not Xe + IBr. For this to be the case the XeIBr must be bound by at least 2,400 cm^{-1} (the energy difference between photons of wavelengths 192.5 nm and 184 nm).

A possible mechanism for the physical and reactive quenching of IBr is as follows. The first step is the formation of a short lived triatomic formed by IBr(D) and Xe. The internal energy of this complex is then rapidly redistributed and in the absence of any other exit channel the Xe atom is re-ejected with extra kinetic energy while the IBr is left in the D' state having lost some of its vibrational energy. Once a second exit channel opens up there is the possibility of the dissociation products of the short-lived triatomic complex being XeBr(B) and I and

it seems that this second exit channel, once open, is used. Finally, if the complex has enough energy (from the vibrationally excited IBr(D)) then it may emit a photon of 252 nm wavelength. The above scheme explains the rapid quenching to the D' state of IBr with the loss of vibrational energy involved and allows for the production of XeBr(B). In order to account for the fast quenching rates and large quenching cross sections, it must be assumed that the attractive limb of the complex potential is fairly long-range in character or that the minimum in the complex exists at a fairly large separation of xenon and IBr. This means that the transfer between electronic states in IBr probably occurs at large internuclear separation where the potentials of all the members of the lowest group of IBr ion-pair states are running close together.

This scheme may be extended to quenching by argon, which seems to have the same physical quenching behaviour as Xe, although it cannot undergo reaction with IBr for energetic reasons. Part of the behaviour of physical quenching by helium can also be explained by this scheme. At high helium pressures (70 kNm^{-2}) the D' → A' peak is broader than for Xe or Ar. This fits in with the above scheme when it is remembered that helium is far smaller than either Xe or Ar and will thus be less polarisable. Thus the binding energy of the collision complex will be less, meaning that there is less energy to partition among the collision partners and less for helium to carry off

after the reaction. Thus when the IBr D' state is formed it will have more vibrational energy than would be the case if the quenching partner were Xe or Ar. This in turn means that the D' → A' peak for helium quenching will be broader. Another reason for the lack of energy imparted to the He atom is that it is light, meaning that it would have to be ejected with very high velocity from the complex to contain the energy of a few vibrational quanta.

6.7 References

(1) J.C.D. Brand, U.D. Deshpande, A.R. Hoy, S.M. Jaywant and E.J. Woods, J.Mol.Spec., 99 (1983), 339.

(2) M. Diegelman, K. Hohla, F. Rebentrost and K.L. Kompa, J.Chem.Phys., 76 (1982), 1233.

(3) M. MacDonald, J.P.T. Wilkinson, C. Fotakis, M. Martin and R.J. Donovan, Chem.Phys.Letts., 99 (1983), 250.

(4) J.P.T. Wilkinson, M. MacDonald and R.J. Donovan, Chem.Phys.Letts., 101 (1983), 284.

(5) R.J. Donovan, G. Gilbert, M. MacDonald, I. Munro, D. Shaw and G.R. Mant, Chem.Phys.Letts., 109 (1984), 379.

(6) K.P. Huber and G. Herzberg,"Molecular structure and Molecular Spectra", Vol. 4, Constants of Diatomic Molecules, (Van Nostrand, Princeton, 1979).

(7) P. Venkateswarlu, Can.J.Phys., 48 (1970), 1055.

Appendix 1

An Annotated Copy of the Computer Programme used for Calculating Simulated Spectra

```
!        SPEC  Version 26
!        ~~~~~~~~~~~~~~~~
!   Written in IMP80
!   Plots wavelength
!   More general graphics
!   Allows graph output on any chosen scale
!   Takes account of continuum level spacing
!   Prompts for all input & defines streams internally
!   Outputs date automatically
!   Gives smooth B/F changeover
!   M.McD. & K.P.L.
!   10th January 1983
!
%BEGIN
! Fully interpolated potentials are read in on streams 3 (upper) and
! 4 (lower), from which eigenvalues, eigenvectors and, finally
! Franck-Condon Factors, S12, are calculated
!
! The reading list on stream 8 is :-
!        URMIN (Start of the upper potential in angstroms)
!        URMAX (End   "   "    "       "      "     "    )
!        MU    (Reduced mass of the diatomic in units of 10-24 g)
!        STEP  (The step length common to both potentials in A)
!        LRMIN (Start of the lower potential in angstroms)
!        LRMAX (End   "   "    "       "      "     "    )
!        E2    (Energy of the upper state relative to Te, nearest eigenvalue will be substituted )
!        TE    (Energyof min of upper state relative to min of ground state )
!        ACC   (The attenuation factor )
!        SSTART(Start of section of spectrum to be scanned in nm. )
!        SSTOP ( End  "     "   "      "    "  "     "   "  "  )
!        SIGMA (Monochromator resolution in nm. ,HWHM. Only if GRAPH selected.)
!        MONOSTEP(The distance the monochromator scans between pulses. Only if GRAPH selected.)
!        THRESHOLD(The fraction of gaussian height significant in final output. Only if GRAPH selected.)
!        GSCALE (The no of nm. per cm of graph paper for o/p. Only needed if GRAPH selected.)
!        HEIGHT (The height of the output graph,again only if GRAPH selected)
!
! Initialisation data is prompted for on stream 5 (define as .IN). All strings must be entered in double quotes.
!Output is writen onto LP20FILE on stream 7.
!
!
!
!

  %EXTERNALROUTINESPEC DEFINE(%STRING(63) S)
  %EXTERNALROUTINESPEC PROMPT(%STRING(15) S)
  %EXTERNALSTRINGFNSPEC DATE
  %EXTERNALSTRINGFNSPEC TIME
```

```
%LONGREAL URMIN,URMAX,MU,STEP,LRMIN,LRMAX,E2,TE,ACC,SSTART,SSTOP
%LONGREAL SIGMA,MONOSTEP,THRESHOLD,GSCALE,HEIGHT
%INTEGER NU,NL,PMULT
%STRING(63) STREAM,GRAPH; %STRING(255) TITLE
  DEFINE("7,LP20FILE"); SELECTOUTPUT(7)
  DEFINE("5,.IN"); SELECTINPUT(5)
  NEWLINES(4)
  PROMPT("Upper potl.:"); READSTRING(STREAM); DEFINE("3,".STREAM)
  PROMPT("Lower potl.:"); READSTRING(STREAM); DEFINE("4,".STREAM)
  PROMPT("Data stream:"); READSTRING(STREAM); DEFINE("8,".STREAM)
  PROMPT("Graph ? "); READSTRING(GRAPH)
  %IF GRAPH >= "Y" %THENSTART;                    ! If graph option selected
    PROMPT("Plotter O/P :"); READSTRING(STREAM); DEFINE("30,".STREAM); ! Give name of file on which the graph is to be held.
  %FINISH
  PROMPT("Number O/P :"); READSTRING(STREAM); DEFINE("9,".STREAM); ! Name of file for raw numerical output for
                                                  ! plotting later with different parameters
  PROMPT("Title:"); READSTRING(TITLE)
  SELECTINPUT(8)
  PROMPT("URMIN:"); READ(URMIN); PROMPT("URMAX:"); READ(URMAX)
  PROMPT("Reduced mass:"); READ(MU); PROMPT("Steplength/A:"); READ(STEP)
  PROMPT("LRMIN:"); READ(LRMIN); PROMPT("LRMAX:"); READ(LRMAX)
  PROMPT("E2:"); READ(E2)
  PROMPT("Te:"); READ(TE); PROMPT("Att. Fac.:"); READ(ACC)
  PROMPT("Scan start:"); READ(SSTART); PROMPT("Scan stop:"); READ(SSTOP)
  %IF GRAPH >= "Y" %THENSTART;                    ! Input for graphics data.
    PROMPT("HWHM RESN.:"); READ(SIGMA) ; SIGMA=SIGMA*2
    PROMPT("MONOSTEP:"); READ(MONOSTEP)
    PROMPT("Gaus. Thresh.:"); READ(THRESHOLD)
    PROMPT("GSCALE(nm/cm):"); READ(GSCALE)
    PROMPT("Max. height:"); READ(HEIGHT)
  %FINISH
  PRINTSTRING("**********************************"); NEWLINE
  PRINTSTRING("* "); PRINTSTRING(TIME); PRINTSTRING(" ** "); PRINTSTRING(DATE); PRINTSTRING(" *")
  NEWLINE
  PRINTSTRING("************************"); NEWLINES(2)
  PRINTSTRING(TITLE); NEWLINES(3)
  PRINTSTRING("Reduced mass = "); PRINT(MU,3,2); PRINTSTRING(" x10-24g")
  NEWLINES(2)
  PRINTSTRING("Upper potential runs from "); PRINT(URMIN,1,3)
  PRINTSTRING(" Angstroms to "); PRINT(URMAX,2,3)
  PRINTSTRING(" Angstroms ")
  NEWLINE
  PRINTSTRING("Lower    ""       ""    ""   "); PRINT(LRMIN,1,3)
  PRINTSTRING("     ""     ""  "); PRINT(LRMAX,2,3)
  PRINTSTRING("      ""     ")
  NEWLINE
  PRINTSTRING("The steplength ")
  PRINT(STEP,1,3); PRINTSTRING(" Angstroms")
```

```
  NEWLINES(2)
  PRINTSTRING("The term value is "); PRINT(TE,8,0)
  PRINTSTRING(" cm-1")
  NEWLINES(2)
  PRINTSTRING("Scanning from ")
  PRINT(SSTART,3,0); PRINTSTRING(" nm to ")
  PRINT(SSTOP,3,0); PRINTSTRING(" nm")
  NEWLINE
  NU = INTPT(((URMAX - URMIN) / STEP) + 1);      !No. of points in upper potential to be read in.
  NL = INTPT(((LRMAX - LRMIN) / STEP) + 1);      !No. of points in lower potential to be read in.
  NEWLINE
  PRINTSTRING("Attenuation factor - "); PRINT(ACC,1,1)
  NEWLINES(3)
%BEGIN
  %INTEGER IFIX,MIFIX,L,J,I,ITER,ITURN,OTURN,FLAG,A,NCYCLE,INB,P
  %INTEGER NB,NODE,NEIG,NMIN,NNPLOT,ISSTART,ISSTOP,IPEN,NK,NPTS0,WHERE,NLEVEL
  %INTEGER OWHERE
  %LONGREAL HH,FAC,EMIN,EMAX,EPS1,EPS2,NORM2,TRANS1,E1,XGRAF,VINF,NORM1,POSN
  %LONGREAL OPOSN
  %LONGREAL ATT,S1,S2,K,BIG,S12,OTEMP,TEMP,TEMP1,TEMP2,X00,PLOT1,K1
  %LONGREAL WINWIDTH,FRES,X0,DELX,CMSTART
  %LONGREALARRAY VD1,VEC1(1:NL)
  %LONGREALARRAY VD2,VEC2(1:NU)
  %LONGREALARRAY EIG1,EIG2(1:1500);              ! 1500 = Max vib. level allowed (bound or free)
  %LONGREALARRAY STORE(1:1500,1:4);              ! Storin data userd for output
  %ROUTINESPEC VECTOR(%LONGREALARRAYNAME X,F, %INTEGERNAME NODE,N,L,ITURN,OTURN, %LONGREALNAME EVAL)
  %ROUTINESPEC PERTURB(%LONGREALARRAYNAME F, %LONGREALNAME X, %INTEGER N)
  %ROUTINESPEC BISECT(%INTEGERNAME N,NEIG,NMIN,ITURN,OTURN,ITER, %LONGREALARRAYNAME F,EIG,
                      %LONGREALNAME EIGMIN,EIGMAX,EPS1,EPS2)
  %EXTERNALROUTINESPEC PLOTSPEC(%LONGREALARRAYNAME STORE, %LONGREALNAME SSTART,SSTOP,SIGMA,MONOSTEP,THRESHHOLD,
                        GSCALE,HEIGHT, %INTEGERNAME NPTS)
    HH = STEP ** 2
    FAC = 3.572 * MU * 0.01 * HH;               ! To convert to dimensionless units
    SELECTINPUT(3)
    %FOR I = NU - 1, - 1,1 %CYCLE;              ! Reading in upper potential
      READ(TEMP1)
      VD2(NU - I) = TEMP1 * FAC + 2;            ! Converting units & adding 2 for (dif)**2
    %REPEAT
    PRINTSTRING("Upper potential stops at ")
    PRINT(TEMP1,5,0); PRINTSTRING(" cm-1")
    SELECTINPUT(4)
    %FOR I = NL - 1, - 1,1 %CYCLE;              ! Reading in lower potential
      READ(TEMP1)
      VD1(NL - I) = TEMP1 * FAC + 2;            ! Again converting units and adding 2 for diff**2
    %REPEAT
    SPACES(5); PRINTSTRING("Lower potential stops at ")
    PRINT(TEMP1,5,0); PRINTSTRING(" cm-1")
    VD1(1) = 1012; VD1(NL) = 1012;              ! Infinite barriers at ends
```

```
      VD2(1) = 1012; VD2(NU) = 1012
      VINF = TEMP1 * FAC;                        !ENERGY OF BOUND/FREE BOUNDARY
      EMIN = 1 / (SSTART * 10 - 07);             ! Converting from na to cm-1
      EMAX = 1 / (SSTOP * 10 - 07)
      EMAX = (E2 + TE - EMAX) * FAC;             ! Corresponding energy limits
      EMIN = (E2 + TE - EMIN) * FAC;             ! of lower state in new units
      E2 = E2 * FAC
      EPS1 = FAC * 0.02;                         ! Required accuracy
      NEWLINES(3)
      BISECT(NU,IFIX,MIFIX,ITURN,OTURN,ITER,VD2,EIG2,E2,E2,EPS1,EPS2); ! To find nearest eigenval of upper state above E2
                                                 ! specified energy above Te
      PRINTSTRING("Upperstate eigenvalue = ")
      E2 = EIG2(IFIX);                           ! Energy of eigenstate
      PRINT(E2 / FAC,5,0); SPACES(2); PRINTSTRING("cm-1"); SPACES(9)
      VECTOR(VEC2,VD2,NODE,NU,L,ITURN,OTURN,E2); ! To calculate eigenfunction from eigenval.
      NORM2 = 0; J = 0; TEMP = 0; OTEMP = 0;     ! Setting counters and sums to zero before examining wavefunction
      ZFOR I = NU, -1,1 ZCYCLE;                  ! Cycle over entire wavefn primarily to get (area)**2 & hence normalise.
        NORM2 = NORM2 + VEC2(I) ** 2;            ! Sum of wavefn**2
        ZIF VEC2(I) ** 2 > TEMP ZTHEN TEMP = VEC2(I) ** 2 ZAND WHERE = I; ! To find posn of largest peak in wavefn**2
      ZREPEAT
      NORM2 = 1 / (NORM2 * STEP);                ! Corrected for step length of integration
      PERTURB(VEC2,TRANS1,NU - 1);               ! Gives 4th order perturbation
      PRINTSTRING("Perturbed Energy = ");        ! 1st Order pertbn. from 4th central dif.
      PRINT(TRANS1 * STEP * NORM2 / FAC,3,0); PRINTSTRING(" cm-1")
      NEWLINE
      PRINTSTRING("Turning points of upper state at ")
      PRINT(URMIN + (ITURN - 1) * STEP,2,2); PRINTSTRING(" And"); ! Inner & Outer turning points from VECTOR
      PRINT(URMIN + (OTURN - 1) * STEP,2,2); PRINTSTRING(" Angstroms")
      SPACES(8); PRINTSTRING("ITER = "); WRITE(ITER,4)
      NEWLINE; PRINTSTRING("Largest wavefn**2 is at r =")
      PRINT(URMIN + WHERE * STEP,1,3); PRINTSTRING(" Angstroms"); NEWLINE
      PRINTSTRING("No. of cycles = "); WRITE(L,2); SPACES(10)
      PRINTSTRING("N = "); WRITE(IFIX - 1,2); SPACES(3); ! N = vib. level
      PRINTSTRING("No. of nodes = "); WRITE(NODE,2); ! Actual number of nodes. Test on mesh size and programme.
      NEWLINES(3)
! Starting to examine lower state.
      BISECT(NL,NEIG,NMIN,ITURN,OTURN,ITER,VD1,EIG1,EMIN,EMAX,EPS1,EPS2); ! Asks for all eigenvals in energy range of interest.
      PRINTSTRING("Highest vib. state in lower elec. state "); WRITE(NEIG,4); NEWLINE
      PRINTSTRING("Inner t.p. of lower elec. state, N = ")
      WRITE(NEIG - 1,2); SPACES(2); PRINTSTRING("at")
      PRINT(LRMIN + (ITURN - 1) * STEP,1,3); PRINTSTRING(" Angstroms. Outer t.p. at ")
      PRINT(LRMIN + (OTURN - 1) * STEP,1,3); PRINTSTRING(" Angstroms.")
      NEWLINES(3)
      FLAG = 0;                                  ! To test and record if upper state or lower state starts first
      A = INTPT((LRMIN - URMIN) / STEP) + 1
      ZIF A (= 0 ZTHENSTART;                     ! If upper state starts first...
        FLAG = 1;                                ! Note upper state starts first.
        A = - A;                                 ! A = Pos. no. of steps difference between states
```

```
      %FINISH
      ACC = EXP( - ACC * STEP);                  ! Scaling attenuation factor to the steplength
      INB = 0; NCYCLE = 0; BIG = 0;              ! Setting counters to zero before working out overlaps & F.C.s
      X0 = (E2 - VINF) / FAC + TE;               ! X0 is waveno. of transition to the boundry
      CMSTART = (1 / SSTART) * 107;              ! Start of scan in wavenos.
      %IF CMSTART < X0 %THEN X0 = CMSTART;       ! To set first X0 to scan start if starting above boundry.
!
!****** Main cycle ******
      %FOR P = NMIN,1,NEIG %CYCLE;               ! To CYCLE over eigenvals of lower state
        NB = 0; TEMP = 0; OTEMP = 0;             ! Setting counters to zero before examining each eigenval
        E1 = EIG1(P);                            ! P is counter determining which eigenval we look at.
        VECTOR(VEC1,VD1,NODE,NL,L,ITURN,OTURN,E1); ! Calculates wavefn for eigenval P.
        %IF E1 < VINF %THEN NB = 1;              ! Bound (NB=1)
        %IF IMOD(P - NODE) > 1 %THENSTART;       ! Testing dif. between level counter & No. of nodes
          PRINTSTRING("Difficulty with node count at N =")
          PRINT(P,3,0)
          PRINTSTRING(" & No. of nodes = "); PRINT(NODE,3,0)
          NEWLINE
        %FINISH
        NCYCLE = NCYCLE + 1;                     ! Counter to neaten output
        %IF NB = 1 %THEN INB = NCYCLE;           ! Setting INB to level of boundry.
        XGRAF = (E2 - E1) / FAC + TE;            !The wavelength now in cm-1
        %IF FLAG = 1 %THENSTART
          J = 1;                                 ! To calculate FC's only from
          I = A;                                 ! the start of the overlap
        %FINISH;                                 ! of the two states.
        %IF FLAG = 0 %THENSTART
          J = A
          I = 1
        %FINISH
        NORM1 = 0; ATT = 1; S12 = 0;             ! Setting sums (& att. fac.) to zero before calc. overlaps.
        %IF NB = 0 %THENSTART;                   ! If free, normalise as follows...
          DELX = X0 - XGRAF;                     ! Artificial sepn. of free states
          K1 = 0.189 * SQRT(MU * (E1 - VINF) / FAC); !The asymptotic wave no. in reciprocal A
          NK = INTPT(NL - 2 * PI / (3 * K1 * STEP)); ! No. of points in 1/3 assym. wavelength.
          %IF NK < 1 %THENSTART;                 ! If 1/3 assym. wavelength > potential length
            NK = I;                              ! Reset NK
            PRINTSTRING("Too close to continuum onset?"); ! Print warning
            PRINTFL((E1 - VINF) / FAC,3);        ! and energy
            NEWLINE
          %FINISH
L22:      TEMP1 = VEC1(I);                       ! Area of overlap starts here. Calc will be sent back here
                                                 ! as long as two states overlap.
          S1 = TEMP1 * VEC2(J) * ATT;            ! Exponential attenuation factor
          %IF S1 ** 2 > OTEMP %THEN OTEMP = S1 ** 2 %AND OWHERE = I; ! To find max of overlap (including atten. fac.)
          TEMP2 = VEC1(I + 1);                   ! 2nd part of Simpson's Rule calcs.
          %IF I > NK %THENSTART;                 ! If less than 1/3 wavelength to go...
            TRANS1 = MOD(TEMP1);                 ! 1st Simpson
```

```
      %IF TRANS1 > NORM1 %THEN NORM1 = TRANS1 %AND WHERE = I; ! Find max (& posn.) of lower wavefn
      TRANS1 = MOD(TEMP2);                    ! 2nd Simpson
      %IF TRANS1 > NORM1 %THEN NORM1 = TRANS1 %AND WHERE = I + 1; ! Find max (& posn of max) of lower wavefn.
    %FINISH
    ATT = ACC * ATT;                          ! To get atten. fac. for 2nd Simpspon.
    S2 = TEMP2 * VEC2(J + 1) * ATT
    %IF S2 ** 2 > OTEMP %THEN OTEMP = S2 ** 2 %AND OWHERE = I + 1; ! To find max overlap for 2nd Simpson factor.
    S12 = S12 + 4 * S1 + 2 * S2;              ! Summing in pairs for Simpspons rule
    J = J + 2; I = I + 2;                     ! resetting parameters for next cycle.
    ATT = ACC * ATT;                          ! Resetting atten. fac. for next cycle.
    ->L22 %IF J (= NU - 1 %AND I (= NL - 1; ! If overlap at end of next cycle go back & calc overlap. If not...
    %IF I < NK %THEN I = NK;                  ! Set I to last 1/3 wavelength for finding assym. amplitude.
    %IF I < NL - 1 %THENSTART;                ! If not at end of potential from above calcs.
      %FOR L = I,1,NL %CYCLE;                 ! Cycle to end of potl. (from last 1/3 wavelength)
        TRANS1 = MOD(VEC1(L))
        %IF TRANS1 > NORM1 %THEN NORM1 = TRANS1 %AND WHERE = L; ! Note max & posn. of max of lower state
      %REPEAT
    %FINISH
    NORM1 = NORM1 * SQRT((XGRAF - (VD1(WHERE) - 2) / FAC) / (XGRAF - VINF)); ! To account for change in velocity.
    NORM1 = 1 / NORM1 ** 2
    S12 = S12 * STEP / 3;                     ! Simpson's Rule
    FRES = 2.998@10 * DELX;                   ! Sepn. of free state in inverse seconds
    S12 = S12 ** 2 * NORM1 * NORM2 * XGRAF ** 3 * 4 * MU * FRES / K1 / (1.054@ + 13); ! Free normalisation to be same
                                              ! as bound norm. (units of length).
    X0 = XGRAF;                               ! Resetting to get diff. of energy of free states.
  %FINISHELSESTART;                           !Bound normalisation starts here...
    %IF I > 1 %THENSTART;                     ! To normalise lower state up to
      %FOR L = I - 1, - 1,1 %CYCLE;           ! start of upper state.
        TEMP1 = VEC1(L)
        NORM1 = NORM1 + TEMP1 ** 2;           ! Sum of wavefn**2
        %IF TEMP1 ** 2 > TEMP %THEN TEMP = TEMP1 ** 2 %AND WHERE = L; ! Searching for max of wavefn**2
      %REPEAT
    %FINISH
L21:  TEMP1 = VEC1(I);                        ! Overlap starts here. Calc. will be sent back here as long as there is overlap.
    NORM1 = NORM1 + TEMP1 ** 2;               ! Still summing area
    S1 = TEMP1 * VEC2(J) * ATT;               ! Introducing exponential atten. fac.
    %IF S1 ** 2 > OTEMP %THEN OTEMP = S1 ** 2 %AND OWHERE = I; ! Searching for max of overlap
    TEMP2 = VEC1(I + 1);                      ! 2nd part of Simpson's Rule pair
    NORM1 = NORM1 + TEMP2 ** 2;               ! Still summing area.
    %IF TEMP1 ** 2 > TEMP %THEN TEMP = TEMP1 ** 2 %AND WHERE = I; ! Searching for max of wavefn**2
    %IF TEMP2 ** 2 > TEMP %THEN TEMP = TEMP2 ** 2 %AND WHERE = I + 1; ! searching for max of wavefn**2 in 2nd pair
    ATT = ACC * ATT;                          ! multiplying att. fac. for 2nd Simpson.
    S2 = TEMP2 * VEC2(J + 1) * ATT;           ! Overlap of 2nd Simpson
    %IF S2 ** 2 > OTEMP %THEN OTEMP = S2 ** 2 %AND OWHERE = I + 1; ! searcing for max overlap in 2nd Simpson
    S12 = S12 + 4 * S1 + 2 * S2;              ! Simpsons Sum for pair
    J = J + 2; I = I + 2;                     ! Resetting parameters for next time round loop.
    ATT = ACC * ATT;                          ! Resetting atten. fac. for next time round loop
    %IF J (= NU - 1 %AND I (= NL - 1 %THEN ->L21; ! If still in overlap at end of next loop go to L21 and calc overlap
```

```
        %IF I < NL - 1 %THENSTART;                  ! If lower state not finished by above calcs...
          %FOR L = I,1,NL - 1 %CYCLE;               ! Cycle to end of lower state
            NORM1 = NORM1 + VEC1(L) ** 2;           ! Still summing area.
            %IF VEC1(L) ** 2 > TEMP %THEN TEMP = VEC1(L) ** 2 %AND WHERE = L; ! To find max of wavefn**2 of lower state
          %REPEAT
          %FINISH;                                  ! Area & overlap of lower state caculated
          NORM1 = 1 / (NORM1 * STEP);               !Corrects for step length of integration
          S12 = S12 / 3 * STEP;                     ! Simpson's Rule
          S12 = S12 ** 2 * NORM1 * NORM2 * XGRAF ** 3; ! Normalisation for bound lower state including nu**3 from Einstein A
        %FINISH
        POSN = LRMIN + WHERE * STEP;                ! Converting posn. to Angstroms
        OPOSN = LRMIN + OWHERE * STEP
        STORE(NCYCLE,1) = S12;                      ! For output (intensity)
        STORE(NCYCLE,2) = XGRAF;                    !  "      "     (wavenumber)
        STORE(NCYCLE,3) = POSN;                     ! Max of wavefn**2
        STORE(NCYCLE,4) = OPOSN;                    !Max of overlap
        %IF S12 > BIG %THEN BIG = S12;              ! Normalising factor for graph.
      %REPEAT;                                      ! Go back and work out F.C.s for next level (P).
!****** End of main cycle ******
!
      PRINTSTRING("Normalisation factor for Fc = "); ! Main output of results starts here.
      PRINTFL(BIG,3); NEWLINE;                      ! Normalisation factor for calc. results before slitfn.
      NEWLINES(2)
      SPACES(2); PRINTSTRING(" N");                 ! Headings for tabulation of results
      SPACES(4); PRINTSTRING("Wavemax"); SPACES(4); PRINTSTRING("Omax")
      SPACES(6); PRINTSTRING("E1")
      SPACES(4); PRINTSTRING("Wavelength")
      SPACES(4); PRINTSTRING("FC")
      NEWLINE
      NLEVEL = NMIN;                                ! No. of first level to which fluoresence occurs
      %FOR I = 1,1,NCYCLE %CYCLE;                   ! To cycle over levels and output results for each level
        %IF I = INB + 1 %AND I # NCYCLE %THENSTART; ! If at boundry
          PRINTSTRING("-----------------------------------------------------"); ! print boudry indiactor.
          NEWLINE
        %FINISH
        WRITE(NLEVEL,4); SPACES(2);                 ! level to which fluoresence takes place.
        PRINT(STORE(I,3),2,3); SPACES(2);           ! posn of max wavefn.**2
        PRINT(STORE(I,4),2,3); SPACES(2);           ! Posn. of max overlap**2
        PRINT(E2 / FAC + TE - STORE(I,2),5,2); SPACE; ! Energy of lower state
        STORE(I,2) = 1.0 / STORE(I,2) * 1.007
        PRINT(STORE(I,2),3,2);                      ! Wavelength of flouresence in mm.
        SPACES(3); STORE(I,1) = STORE(I,1) / BIG; PRINTFL(STORE(I,1),4); ! Franck-Condon factor normalised to unity.
        SPACES(2)
        L = INTPT(STORE(I,1) * 70);                 ! To digitise intensity for block graph output.
        %IF L < 1 %THEN L = 1;                      ! If intensity is zero then print 1 '*' anyway.
        %FOR P = 1,1,L %CYCLE;                      ! Print P '*'s for output intensity.
          PRINTSTRING("*")
        %REPEAT
```

```
      NEWLINE;                                  ! Newline for next line of data
      NLEVEL = NLEVEL + 1;                      ! at next level.
    %REPEAT
    NEWLINE; WRITE(ITER,3); NEWLINES(2);        ! Write no of iterations required in getting last energy.
    SELECTOUTPUT(9);                            ! Write onto stream for numerical output for plotter prog.
    WRITE(NCYCLE - 1,3); NEWLINE;               ! No. of levels
    %FOR I = 1,1,NCYCLE - 1 %CYCLE;             ! For each level print...
      PRINT(STORE(I,2),3,2); SPACES(4); PRINT(STORE(I,1),1,4); ! Wavelength & intensity
      NEWLINE
    %REPEAT;                                    ! end of output for later use of slitfa. & plotter prog.
    %IF GRAPH >= "Y" %THENSTART;                ! For immediate use of this programme...
      NCYCLE = NCYCLE - 1
      PLOTSPEC(STORE,SSTART,SSTOP,SIGMA,MONOSTEP,THRESHOLD,GSCALE,HEIGHT,NCYCLE); ! Call programme writen in subroutine form.
    %FINISH
!
!
!
!
!
  %ROUTINE VECTOR(%LONGREALARRAYNAME X,F, %INTEGERNAME NODE,N,L,ITURN,OTURN, %LONGREALNAME EVAL)
! Calculates the eigenvector of the tridiagonal matrix F (which
! MUST HAVE ALL OFF-DIAGONAL ELEMENTS =-1) FOR A PREVIOUSLY
! determined eigenvalue EVAL. Gaussian elimination without
! interchanges is used and F must must be positive definite. L counts
! the number of back substitutions, limited to 4
!
    %INTEGER J,M,FLAG
    %LONGREAL DEV,NORM1,XJ,BJ,NORM,BJ1
    %LONGREAL XJ1
      M = 2 * N
    %BEGIN
      %LONGREALARRAY Y(1:M)
      %LONGREALARRAY B(1:N)
      %LONGREALARRAY C(1:N)
      %LONGREALNAME Y1T,YIS
        NORM = 0
        NODE = 0; L = 1; FLAG = 0
!                                               !B,X contain the iterated eigenvector at the Lth and (L+1)th
                                                ! stage of iteration respectively.  Y(odd) contains the diagonal
                                                ! entries of F-EVAL*I and Y(even) the reciprocal of the previous entry
!
      %INTEGER I
        Y(1) = F(1) - EVAL
        J = 2
        YIS == Y(2)
        YIS =  - 1 / Y(1)
        %FOR I = 3,2,M - 1 %CYCLE
```

```
          YIT == Y(I)
          YIT = YIS + F(J) - EVAL
          YIS == Y(I + 1)
          %IF MOD(YIT) < 1@ - 12 %THENSTART
            YIS = 1@12
            PRINTSTRING("DANGER IN PIVOTING")
            ->L3
          %FINISH
          YIS =  - 1 / YIT
L3:       J = J + 1
        %REPEAT
        B(N) =  - Y(N);                          !1st TRIAL EIGENVECTOR IS (1/L)*(011...110)
        BJ = 1
        %FOR I = N - 1, - 1,2 %CYCLE
          J = 2 * I
          BJ1 =  - (1 + BJ) * Y(J)
          %IF MOD(BJ1) > NORM %THEN NORM = MOD(BJ1)
          B(I) = BJ1
          BJ = BJ1
        %REPEAT;                                 ! First back substitution to produce 2nd approx to eigenvector
        B(1) =  - B(2) * Y(2)
        C(1) = B(1)
        %FOR I = 2,1,N %CYCLE
          J = 2 * I - 2
          C(I) =  - Y(J) * C(I - 1) + B(I)
        %REPEAT
        NORM = 1 / NORM
L1:     FLAG = 0; DEV = 0
        NODE = 0; NORM1 = 0
        X(N) =  - Y(M) * C(N) * NORM
        J = N
        XJ = X(N)
        %FOR I = M - 1, - 2,3 %CYCLE
          XJ1 =  - Y(I - 1) * (XJ + NORM * C(J - 1))
          %IF J > ITURN %AND J < OTURN %THENSTART
            %IF XJ > 1@ - 5 %AND XJ1 <  - 1@ - 5 %THEN NODE = NODE + 1
            %IF XJ <  - 1@ - 5 %AND XJ1 > 1@ - 5 %THEN NODE = NODE + 1
            %IF MOD(XJ1) > NORM1 %THEN NORM1 = MOD(XJ1)
          %FINISH
          X(J - 1) = XJ1
          XJ = XJ1
          J = J - 1
        %REPEAT
        L = L + 1
        X(1) =  - Y(2) * (X(2) + NORM * B(1))
        %IF L < 3 %THENSTART
          C(1) = X(1)
          %IF L = 2 %THEN ->L4
```

```
          %FOR I = 2,1,N %CYCLE
            J = 2 * I - 2
            C(I) = - Y(J) * C(I - 1) + X(I)
          %REPEAT
          NORM = 1 / NORM1
          FLAG = 1
        %FINISH
        %IF FLAG = 1 %THEN ->L1
L4:   %END
    %END
!
!
!
!
!
    %ROUTINE BISECT(%INTEGERNAME N,NEIG,NMIN,ITURN,DTURN,ITER, %LONGREALARRAYNAME F,EIG, %LONGREALNAME EIGMIN,
                    EIGMAX,EPS1,EPS2)
!
!The eigenvalues between EIGMIN and EIGMAX are stored in EIG(K)
! on exit.  F(I) contains the diagonal elements of the Hamiltonian
! matrix.  N is the dimension of the problem. NMIN and NEIG are
! locations of the nearest eigenvalues to EIGMIN and EIGMAX. EPS2
! is actual error and EPS1 required accuracy.
!
      %LONGREAL HH,Z1,UK,LK,XMIN,XMAX,EIT,FI,ST,DEN
      %LONGREALNAME EK
      %INTEGER I,J,K,M
      %LONGREALARRAY UPLIM,DNLIM(1:1500);          ! Arrays of upper & lower bounds to each energy.
        XMIN = EIGMIN;                             ! To start with temp lower bound = absolute lower bound.
        %IF EIGMAX > (F(2) - 2) %THENSTART;        ! If we are wanting information above inner turning point...
          PRINTSTRING("HIT THE WALL !");           ! Print a warning
          NEWLINE
          EIGMAX = F(2) - 2;                       ! And rescale limits.
        %FINISH
        Z1 = 10 - 12;                              ! Z1 is a name for a small number.
        XMAX = EIGMAX;                             ! Temp. upper bound = absolute upper bound
        HH = XMIN;                                 ! Temp. hold for XMIN.
        %IF HH + XMAX > 0 %THEN HH = XMAX
        EPS2 = (Z1 * HH) * 7 + (0.5 * EPS1);       ! Setting actual error.
        %FOR I = 1,1,1500 %CYCLE;                  ! Cycle over all posible levels...
          UPLIM(I) = XMAX;                         ! and initialise arrays with upper
          DNLIM(I) = XMIN;                         ! and lower bounds.
        %REPEAT
 ! Setting of the minimum eigenvalue
        J = 0;                                     ! Setting eigenval counter to zero.
        EIT = F(N) - EIGMIN;                       ! First term in recurence relation.
        %IF EIT < 0 %THEN J = J + 1;               ! If less than zero add one to counter.
        %IF MOD(EIT) < Z1 %THEN EIT = Z1;          ! Reset zero to a small No. to avoid catastrophie in division.
```

```
        N = 1;                                  ! ???
        %FOR I = N - 1, - 1,1 %CYCLE;           ! Examining whole potential.
          EIT = F(I) - EIGMIN - 1 / EIT;        ! Next term is recurence relation. ( P(i-1)/P(i) in Wilkinson.)
          %IF EIT < 0 %THEN J = J + 1;          ! Counting No. of times this is -ve. ( P(i) cahnages sign.)
          %IF MOD(EIT) < Z1 %THEN EIT = Z1;     ! Again to avoid dividing by zero.
        %REPEAT
        NMIN = J + 1;                           ! Eigenlevel = J + 1
        %IF EIGMIN = EIGMAX %THENSTART;         ! If only wanting one eigenvalue...
          DEN = EIGMIN / NMIN;                  ! Estimate density of states by (Energy/Vib. level)...
          NEIG = NMIN;                          ! set upper an lower levels to the same value...
          ->L4;                                 ! and go to label L4.
        %FINISH;                                ! If wantin more than one level...
        J = 0;                                  ! Reset counter...
        EIT = F(1) - EIGMAX;                    ! examine highest energy eigenval of interest...
        %IF EIT < 0 %THEN J = J + 1;            ! and re-calculate as before.
        %IF MOD(EIT) < Z1 %THEN EIT = Z1
        %FOR I = 2,1,N %CYCLE
          EIT = F(I) - EIGMAX - 1 / EIT
          %IF EIT < 0 %THEN J = J + 1
          %IF MOD(EIT) < Z1 %THEN EIT = Z1
        %REPEAT
        NEIG = J + 1;                           ! Position of upper eigenvalue
        DEN = (EIGMAX - EIGMIN) / (NEIG - NMIN); !The average density of states
L4:                                             !Main section
! The previous section used Sturm sequencing to get the density of stales.
! This section uses the density of states as a first approx. to get the energy of each state. This is done by
! Sturm sequencing and bisection.
        LK = EIGMIN;                            ! Set lower bound to absolute lower limit (for first cycle).
        %FOR K = NMIN,1,NEIG %CYCLE;            ! Cycle over each state to find its enersy.
          ITER = 0;                             ! Counter for number of iterations.
          EK == EIG(K);                         ! EK is a pointer and so is equivalent to EIG(K).
          EK = LK + DEN;                        ! Set first guess at energy as lower limit + one density of states.
L5:       J = 0;                                ! Set eigenvalue counter at zero. Calc gets sent back here if
                                                ! EK is not accurate enough.
          ITER = ITER + 1;                      !  Counter for No. of iterations to get reqd. accuracy.
!Formation of Sturm sequence
          EIT = F(1) - EK;                      ! As before, EK is guess at energy.
          %IF EIT < 0 %THEN J = J + 1;          ! Again J counts eigenvals at energy below EK.
          %FOR I = 2,1,N %CYCLE
            EIT = F(I) - EK - 1 / EIT;          ! Recurence relation is P(i-1)/P(i) in Wilkinson's book.
            %IF EIT < 0 %THEN J = J + 1
            %IF MOD(EIT) < Z1 %THEN EIT = Z1;   ! To avoin dividing by zero.
          %REPEAT;                              ! Sturm seqence completed.
! Resetting of upper and lower bounds...
          %IF J < K %THENSTART;                 ! If EK is below eigenvalue...
            LK = EK;                            ! Set lower limit at EK.
            %IF ITER = 1 %THENSTART;            ! If first iteration...
              EK = EK + 1 * DEN;                ! add one density of statses...
```

```
            ITER = 0;                          ! reset bisection counter
            ->L5;                              ! and try Sturm sequence and bisection again.
          ZFINISH
        ZFINISHELSESTART;                      ! If EK is above eigenval...
          UK = EK;                             ! set upper limit to EK.          J = J + 1
        ZFINISH
        EK = (UK + LK) * 0.5;                  ! Point of bisection, set EK to mid-point of range
        ZIF UK - LK > EPS1 ZTHEN ->L5;         ! and if error is to big start Sturm sequence again.
        ZIF K > NMIN ZTHENSTART;               ! If not first state...
          DEN = EK - EIG(K - 1);               ! density of states is difference of energy of previous two states.
        ZFINISH
        LK = EK;                               ! Lower limit of next state is eigenvalue of previous state.
      ZREPEAT;                                 ! Go to next level (eigenvalue)
! From here on in we are calculating turning points.
      UK = EIG(NEIG);                          ! For finding turning points, upper limit = highest eigenvalue.
      ZFOR I = 1,1,N ZCYCLE;                   ! Cycle over lower state to find inner turning point.
        ZIF F(I) - 2 < UK ZTHEN ->L10;         ! If energy is below UK jump out & record ITURN
      ZREPEAT
L10:  ITURN = I;                               ! Record inner turning point for output.
      OTURN = N - 1;                           ! Outer turning point = end of potential (unless reset later)
      ZIF F(N - 1) - 2 > UK ZTHENSTART;        ! If bound look for outer turning point.
L11:    I = I + 1
        ZIF F(I) - 2 > UK ZTHEN ->L12 ZELSE ->L11; ! If eneergy becomes greater than UK jump out and reset OTURN.
L12:    OTURN = I
      ZFINISH
  ZEND
!
!
!
!
!
!
  ZROUTINE PERTURB(ZLONGREALARRAYNAME F, ZLONGREALNAME X, ZINTEGER N)
    ZINTEGER I
    ZLONGREAL F1,F2,F3,F4,F5
      X = 0
      F1 = F(1)
      F2 = F(2)
      F3 = F(3)
      F4 = F(4)
      F5 = F(5)
      ZFOR I = 6,1,N ZCYCLE
        X = X + F3 * ( - F1 + 4 * F2 - 6 * F3 + 4 * F4 - F5)
        F1 = F2
        F2 = F3
        F3 = F4
        F4 = F5
        F5 = F(I)
```

```
        %REPEAT
        X = X / 12
    %END
!
!
!
!
!
  %END
%ENDOFPROGRAM
```

Appendix 2

Publications

Publications

(1) Analysis of the 350-400 nm oscillatory continuum from $I_2(D^1\Sigma_u^+)$.
K.P. Lawley, M.A. MacDonald, R.J. Donovan and Agust Kvaran, Chem.Phys.Letters, 92 (1982), 322.

(2) Oscillatory continuum emission from Br_2 following vacuum ultra-violet laser excitation.
M. MacDonald, R.J. Donovan and M.C. Gower, Chem.Phys. Letters, 97 (1983), 72.

(3) Oscillatory continuum emission from IBr.
M. MacDonald, J.P.T. Wilkinson, C. Fotakis, M. Martin and R.J. Donovan, Chem.Phys.Letters, 99 (1983), 250.

(4) Formation of electronically excited XeBr by reaction of excited IBr with ground-state xenon.
J.P.T. Wilkinson, M. MacDonald and R.J. Donovan, Chem.Phys.Letters, 101 (1983), 284.

(5) Determination of absolute quenching rates and fluorescence lifetime of IBr(D) using synchrotron radiation.
R.J. Donovan, G. Gilbert, M. MacDonald, I. Munro, D. Shaw and G.R. Mant, Chem.Phys.Letters, 109 (1984), 379.

ANALYSIS OF THE 350–400 nm OSCILLATORY CONTINUUM FROM $I_2(D\,^1\Sigma_u^+)$

K.P. LAWLEY, M.A. MACDONALD, R.J. DONOVAN
Department of Chemistry, University of Edinburgh, West Mains Road, Edinburgh EH9 3JJ, UK

and

Agust KVARAN
Science Institute, University of Iceland, Dunhaga 3, Reykjavik, Iceland

Received 15 July 1982; in final form 13 August 1982

The 350–400 nm oscillatory continuum, observed in emission when I_2 is excited to the $D\,^1\Sigma_u^+$ state (λ = 193 nm, $v' \approx$ 134), has been analysed. The lower potential state, which correlates with two ground-state I atoms, is found to be purely repulsive between 2.75 and 3.8 A, the range defined by the observed fluorescence. The band is partially overlapped by another system and there are two possible positions for the band origin, leading to very similar lower states.

1. Introduction

The study of the spectrum of molecular iodine has lead to numerous fundamental developments in our understanding of molecular spectroscopy. One recent example is the realisation by Mulliken [1] in 1971 that the diffuse bands of the I_2 system in the region of 320 nm (McLennan's diffuse bands) result from transitions between bound levels of the upper state ($D\,^1\Sigma_u^+$) and continuum regions of the ground state. These diffuse bands are therefore a structured continuum.

In the work reported here, we describe the analysis of a second structured continuum which lies in the 350–400 nm region and which originates from the same upper state as the 320 nm system. This new system is particularly well developed when I_2 is excited at 193 nm with an ArF laser [2,3]. The relatively broad output of the ArF laser ($\delta\lambda \approx 0.5$ mm) leads to the population of several (3–4) vibrational levels of the D state but, as will be seen, this does not appreciably degrade the structure in the fluorescence.

2. Preliminary analysis

The fluorescence observed in the 350–420 nm region, following excitation of I_2 at 193.3 nm with an ArF laser, is illustrated in fig. 1. The oscillatory struc-

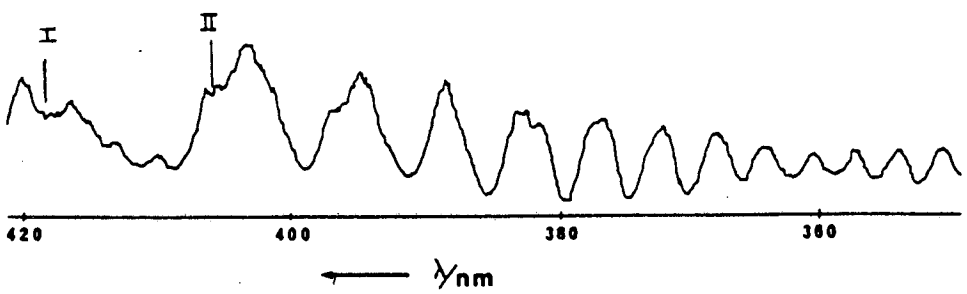

Fig. 1. The observed spectrum. The two possible positions for the band origin are indicated (I) and (II).

0 009-2614/82/0000–0000/$ 02.75

ture between 350 and 410 nm is the subject of the present analysis. To longer wavelengths (440–410 nm) lies a second system that remains to be analysed. It also appears to be a structured continuum.

The structure of the present system is that of a series of strong undulations converging to the blue with a peak spacing that falls from ≈600 to 300 cm^{-1}. The amplitude of the structure falls off slowly to shorter wavelengths. Superimposed on this structure is one of higher frequency and lower amplitude that dies out beyond 390 nm and may be the tail of the second structured continuum referred to above.

The essentially complete destructive interference at the minima is characteristic of Condon diffraction. In the present system there is no hint of a lower-frequency modulation to the envelope of the structure. This would arise if the difference potential $W(R)$ (= $[E(v') - V_1(R)] + V_2(R)$, where (1) ≡ upper, (2) ≡ lower) exhibited a maximum – examples are given by Tellinghuisen [4] and by Noda and Kato [5]. We thus conclude that $W(R)$ is monotonic. The band origin will then correspond to a transition near either the inner or outer turning point of the upper vibronic level. Since the progression is to shorter wavelengths, our band must originate at the inner turning point.

It is characteristic of high-frequency Condon structure near its origin that, if successive maxima and minima are indexed n and $n + \frac{1}{2}$ starting with $n = 0$ for the first maximum, then a plot of $\omega^{(n)} - \omega^{(0)}$ versus $(n + \frac{1}{4})^{2/3} - (\frac{1}{4})^{2/3}$ yields quite a good straight line. This result follows directly from linearising $V_1(R)$ and $V_2(R)$ near the inner turning point of the upper state, $R_0(v')$. The vibrational wavefunctions are then Airy functions and the 2/3 power plot – characteristic of the periodicity of the asymptotic form of Ai(x) – emerges after a little manipulation. More precisely, the peak spacing is found to be given by

$$\omega^{(n)} - \omega^{(0)} = (\tfrac{3}{2}\pi|V_2'|)^{2/3}(|V_1' - V_2'|/2\mu\hbar|V_1'|)^{1/3} \times [(n + \tfrac{1}{4})^{2/3} - (\tfrac{1}{4})^{2/3}], \quad (1)$$

where V_i' are the constant potential gradients. We have analysed several simulated spectra from realistic potentials using eq. (1). The upper state has been taken as known and the gradient of the lower state near $R_0(v')$ derived from the initial gradient of the 2/3 power plot. It is found that, when $W(R)$ is a fairly slowly varying function, $V_2(R_0(v'))$ can be recovered to within 10% but tends to be on the low side. With a simple exponential form for the lower state and a slowly varying difference potential, the initial gradient of V_2 is obtained to within 2–3% for values in the range (3–5) × 10^4 cm^{-1} $Å^{-1}$. We regard the lower-state potential gradient obtained from eq. (1) as useful in assigning initial parameter values in a trial potential preliminary to a pointwise iterative fitting of the spectrum.

This peak index plot is illustrated in fig. 2 for two choices of the band origin (see below). The near linearity of the plot over 3000 cm^{-1} is at first sight surprising in view of the fact that the classical point of transition, R_c, moves through roughly 1 Å in traversing the fluorescence band and neither potential can be expected to be linear over such a range. These near linear plots have been found for a range of simulated structured continua for different systems. The explanation seems to be that the phase difference between the upper and lower state wavefunctions, upon which the structure depends, is most sensitive to the shift in inner turning point of the lower-state motion with energy E_2. These $R_0(E_2)$ values typically change by only 0.1 Å and linearisation is more realistic over this range. The peak heights of the fluorescence structure are given in the semi-classical limit by (see, e.g. ref. [6])

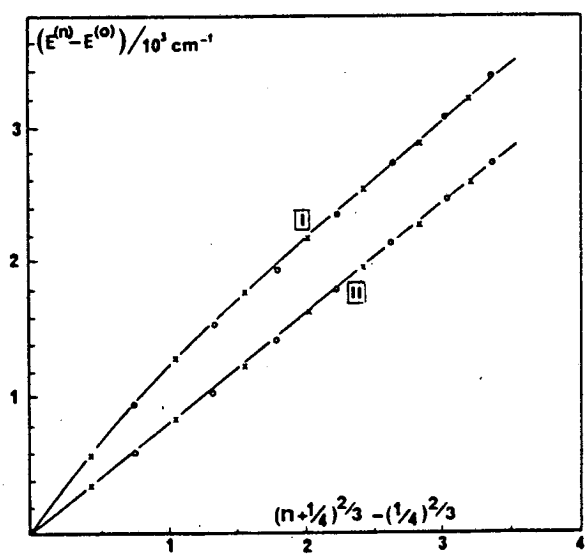

Fig. 2. The peak position plots for the two assignments. o = maximum, × = minimum.

$$I(\omega^{(n)}) \propto (\omega^{(n)})^5 \mu_{21}^2(R_c^{(n)})/k(R_c^{(n)})\, W'(R_c^{(n)}) , \quad (2)$$

where $k(R) = \{2m[E_2 - V_2(R)]\}^{1/2}/\hbar$, when V_1 and V_2 are linearised around the classical point of transition $R_c^{(n)}$ appropriate to the particular value of ω. However, peak heights are less useful than positions in fitting because of their dependence on the wavelength resolution of the detector and because of the influence of the largely unknown transition dipole moment function $\mu_{21}(R)$.

3. Results: detailed fitting

Throughout the fitting, the potential of the D state was taken for numerical purposes to be (all energies in cm^{-1}, R in Å)

$$V_1(R) = 4.77848 \times 10^6 \exp(-R/0.55023) - 1.71407 \times 10^5/(R - 0.004) + 8.200 \times 10^4 , \quad (3)$$

which is essentially the potential used in ref. [4] (see also ref. [7]), slightly modified by us to improve the fitting of the McLennan bands.

$\mu_{21}(R)$ was assumed to be a slowly varying function of the form $\exp(-bR)$. The band origin is hard to locate because of the superimposed secondary structure. The first assignment (I) was $\lambda^{(0)} = 417.5$ nm, but this may be an unresolved group of peaks of the secondary system. The alternative assignment (II) is to take the origin at the more prominent peak at 404.2 nm. Using assignment (I), the initial gradient of the $(n + \frac{1}{4})^{2/3}$ plot indicated a value of 42000 cm^{-1} $Å^{-1}$ for the gradient of the lower state potential at 2.75 Å. The line frequency gave a value for the lower state potential at this separation of 14852 cm^{-1} and thus the two parameters in a preliminary exponential fit to the lower state potential can be assigned. Franck–Condon factors were then calculated from this pair of potentials using a discretized continuum method outlined in ref. [8]. The envelope of the Condon diffraction structure can be seen from eq. (2) to depend on four factors. If $k(R_c)$ and $W(R_c)$ are only slowly varying functions of R_c, then the peak heights fall slowly with increasing n mainly due to the increasing relative velocity near R_c [proportional to $k(R_c)$]. Thus, the first assignment with $I^{(0)} < I^{(1)}$ implies somewhat unusual behaviour in $W(R)$ or in

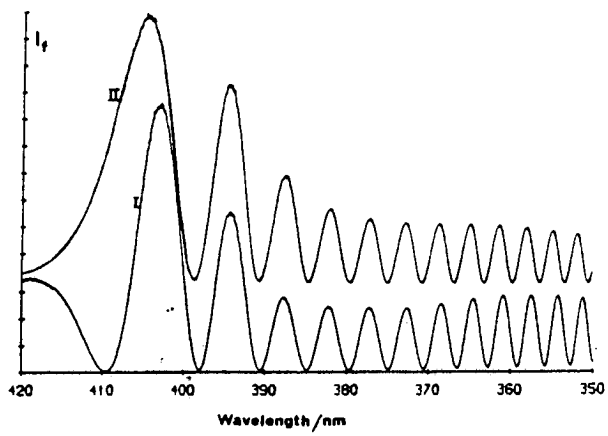

Fig. 3. The two simulated spectra.

$\mu_{21}(R)$ around the inner turning point of the upper state – either $\mu_{21}(R)$ must decrease rapidly or $W(R)$ must increase rapidly [this is also indicated by the greater curvature of the 2/3 power plot for assignment (I)].

With this assignment the best stimulated spectrum is shown in fig. 3 and the corresponding potential of the lower state is listed in table 1 in a form suitable for spline interpolation and is plotted in fig. 4. It is characterised by a rather rapid steepening at around $R = 2.75$ Å in order to reproduce the peak heights. Peak positions are reproduced to ±5 Å and the rapid change in the lower-state potential gradient around

Table 1
Potential V_2 for assignment (I)

R (Å)	V_2 (10^3 cm^{-1})
2.6500	35.98
2.8113	25.7884
3.0110	20.1166
3.2141	17.0838
3.3273	15.8840
3.3934	15.1848
3.4543	14.6406
3.5114	14.1930
3.5731	14.8482
3.6243	13.5472
3.6831	13.3385
3.7366	13.2238
3.7841	13.1020
3.8271	13.0190
4.6000	12.5480
4.6001	12.5480

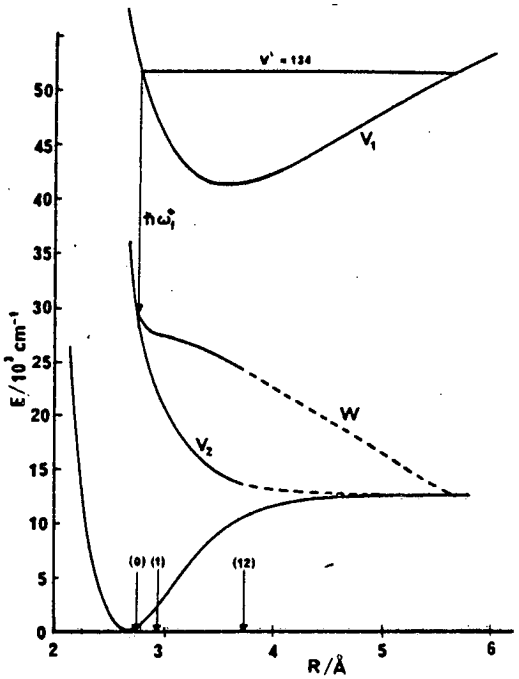

Fig. 4. The upper state, lower state and difference potentials for assignment (I) (V_2 and W for assignment (II) are barely distinguishable on this scale). The separations labelled (n) are the classical points of transitions for the corresponding peaks in the spectrum, $R_c^{(n)}$. The classical position of the band origin at ω^* is also indicated.

2.8 Å is responsible for the marked discrepancy between the lower-state potential gradient at $R_0(v')$ derived from eq. (1) and that of the best fit potential, $\approx 47500\ \mathrm{cm}^{-1}$. It proved impossible to fit this potential satisfactorily by either a single exponential or the form $Ae^{-\alpha R} + CR^{-6}$, though the main cause of this is the slight elbow in the potential at around 3.8 Å. Transitions in this region are beginning to overlap the McLennan system and it is just here that there should be a van der Waals minimum.

Turning to the second possible assignment, $\lambda^{(0)} = 404.2$ nm, the initial potential gradient from the 2/3 power plot yielded an initial gradient of 36800 cm^{-1} $\mathrm{Å}^{-1}$ at $R \approx 2.75$ Å. Fitting proceeds as before and after optimisation yields the simulated spectrum shown in fig. 3. The peak positions are again reproduced to ± 5 Å, with the exception of the first peak which is hard to locate to within 10 Å in the actual spectrum. Fitting this optimised lower state potential by a single exponential $V_2(R) = C_0 \exp(-aR)$ yields

Table 2
Potential V_2 for assignment (II)

R (Å)	$V_2(10^3\ \mathrm{cm}^{-1})$
2.6500	32.1400
2.8453	23.9650
3.0802	18.5904
3.2534	16.3464
3.3731	15.2444
3.4664	14.4703
3.5422	14.0627
3.6090	13.7304
3.6624	13.5561
3.7203	13.3838
3.7678	13.3838
3.7678	13.2420
3.8108	13.1450
4.704	12.5480
4.7041	12.5480

$C_0 = 1.79 \times 10^7\ \mathrm{cm}^{-1}$, $a = 2.582\ \mathrm{Å}^{-1}$, but with a rather poor standard deviation $\sigma = 229\ \mathrm{cm}^{-1}$. Adding a term C_6R^{-6} and optimising all three parameter values yields $C_0 = 1.531 \times 10^7\ \mathrm{cm}^{-1}$, $a = 2.315\ \mathrm{Å}^{-1}$, $C_6 = -5.0 \times 10^6\ \mathrm{Å}^6\ \mathrm{cm}^{-1}$, $\sigma = 65\ \mathrm{cm}^{-1}$. This potential is listed in table 2, and the initial gradient of 37500 cm^{-1} $\mathrm{Å}^{-1}$ at 2.75 Å is within 2% of the value derived above from the 2/3 power plot.

4. Effect of pump laser bandwidth

Classically, the band origin of the type of structure discussed above corresponds to a transition at the inner turning point of the upper state vibration. Denoting this fluorescent frequency by ω_f^* (see fig. 4),

$$\hbar\omega_f^* = V_1(R_0(v')) - V_2(R_0(v')), \qquad (4)$$

differentiation with respect to the upper state energy E_1 [$= V_1(R_0(v_1'))$] yields

$$\partial\omega_f^*/\partial E_1 = \hbar^{-1}[1 - V_2'(R_0(v'))/V_1'(R_0(v'))] \qquad (5)$$

for the shift of ω_f^* with E_1 and hence with the pump laser photon energy. Semi-classically, ω_f^* corresponds to the point of maximum gradient on the low-frequency side of $\omega_f^{(0)}$. If the potential gradients were constant over the whole range of R covered by the fluorescence, eq. (5) would give the shift in energy of any feature of the spectrum caused by a change in E_1.

Model quantum calculations indicate that (5) gives an upper limit to such shifts, the shift in $\omega^{(n)}$ decreasing with increasing n for a given change in E_1. In the present case, we can substitute the initial gradients of the potentials derived above into (5). The vibrational level spacing of the upper state is rougly 50 cm^{-1} and we find that each peak in the fluorescence spectrum is shifted by 5 cm^{-1} or less for a change $\Delta v' \approx \pm 1$. This is confirmed by detailed calculations and indicates that there is no appreciable broadening of the structure with the laser linewidth used which corresponds to $\Delta v' \approx \pm 2$. Excitation of I_2 molecules from $v'' = 1$ leads to a similar broadening of the structure and thus has no significant effect.

5. Conclusions

The observed spectrum can be reproduced by either of two very similar lower-state potentials depending upon whether or not the peak at ≈417 nm (which is clearly overlaid by another structured continuum) belongs to the band under consideration. The two potentials are both monotonically repulsive and the observed spectrum defines them between roughly 2.75 and 3.8 Å. They differ mainly in their behaviour around 2.7–2.8 Å. A transition dipole moment function of exponential form with exponent 0.4 ± 0.2 $Å^{-1}$ is needed to account for the general decrease in intensity of the band at higher frequencies, not unlike the function proposed by Tellinghuisen for the D → X band.

Although the second of the two potentials presented is the smoother, a decision between them can really only be made by observing fluorescence from higher vibrational levels of the D state thereby probing smaller values of R_c at the band origin.

References

[1] R.S. Mulliken, J. Chem. Phys. 55 (1971) 309.
[2] H. Hemmati and G.J. Collins, Chem. Phys. Letters 75 (1980) 488.
[3] M. Martin, C. Fotakis, R.J. Donovan and M.J. Shaw, Nuovo Cimento 63 (1981) 300.
[4] J. Tellinghuisen, Chem. Phys. Letters 29 (1974) 359.
[5] C. Noda and H. Kato, Chem. Phys. Letters 86 (1982) 415.
[6] M.S. Child, Molecular collision theory (Academic Press, New York, 1973).
[7] J. Tellinghuisen, M.R. McKeever and A. Sur, J. Mol. Spectry. 82 (1980) 225.
[8] K.P. Lawley and R. Wheeler, J. Chem. Soc. Faraday Trans. II 77 (1981) 1133.

OSCILLATORY CONTINUUM EMISSION FROM Br_2 FOLLOWING VACUUM ULTRAVIOLET LASER EXCITATION

M. MACDONALD, R.J. DONOVAN
Department of Chemistry, University of Edinburgh, West Mains Road, Edinburgh EH9 3JJ, UK

and

M.C. GOWER
SERC Rutherford Appleton Laboratory, Didcot, Oxfordshire, OX11 0QX, UK

Received 25 February 1983

Laser-induced fluorescence from Br_2 following excitation at 158 nm (F_2 laser) is reported. The most intense emission features are associated with three bound–free transitions (oscillatory continua) in the region 210–440 nm. Efficient collisional interstate transfer, by SF_6, N_2 and He, is observed and the possibility of constructing an optically pumped Br_2 laser is noted.

1. Introduction

There has been considerable recent interest in the ion-pair states of the halogen molecules. Transitions to most of these states, from the ground electronic state, are forbidden for single-photon excitation as they are based mainly on doubly excited electronic configurations [1]. Two-photon excitation of such states is allowed and recent interest has been centred around the use of lasers to induce either sequential or simultaneous (coherent) two-photon transitions in these molecules [2].

A well-known [1] exception in the case of I_2 is the intense $D\,^1\Sigma_u^+ \leftarrow X\,^1\Sigma_g^+$ transition which is observed by single-photon absorption in the region ≈170–200 nm. The $I_2(D\,^1\Sigma_u^+)$ state can be efficiently transferred to other close-lying ion-pair states by collisions with a wide variety of gases including the inert gases [3,4]. Thus emission from ion-pair states that are not otherwise readily accessible can be observed and their collisional properties studied. Quenching to states outside the ion-pair manifold appears to be inefficient, except when chemical reaction is possible, while interstate transfer within the manifold is generally very efficient. These properties are of importance in the construction of efficient optically pumped laser systems [5] and for the study of the chemistry of halogen ion-pair states [6].

In previous work we have concentrated attention on the ion-pair states of I_2. We now extend this work and report observations on the ion-pair states of Br_2. In the present communication we report the first observation of laser-induced fluorescence from the K state [7] of Br_2 (equivalent to the $D\,^1\Sigma_u^+$ state of I_2) following vacuum ultraviolet excitation with an F_2 laser (λ = 157.8 nm). We also show that collisional transfer to the lower $D'\,^3\Pi_{2g}$ ion-pair state is rapid and efficient.

2. Experimental

The experimental arrangement was of conventional design [3], the main novelty being in the use of an F_2 laser (λ = 157.8 nm; $\Delta\lambda \leqslant 0.05$ nm) [8]. The output from the laser (Lambda Physik EMG201) was directed along the axis of a cylindrical cell which had an MgF_2 entrance window and a spectrosil quartz side window for viewing the fluorescence. The fluorescence was dis-

0 009-2614/83/0000–0000/$ 03.00

persed using a Jobin Yvon 0.3 m monochromator equipped with interchangeable gratings (medium-resolution ≈0.35 nm; low-resolution ≈2.6 nm). Light was detected at the exit port of the monochromator with an optical multichannel analyser (Princeton Applied Research/EG & G, O.M.A. with interchangeable silicon-diode array and intensified vidicon heads).

Typical laser pulse energies were in the range 0.5–5 mJ, and had a duration of ≈10 ns. The rear reflector in the laser was an aluminium-coated (internal to the laser cavity) quartz flat and the output coupler a CaF_2 flat. The coating on the rear reflector was observed to deteriorate slowly, due to attack by F_2, over a period of a few days and this limited the performance (energy) of the system. The optical path between the laser head and the fluorescence cell was carefully purged, with Ar or N_2, for ≈30 min before and also during experimental runs.

In addition to the ultraviolet output from the F_2 laser the well-known red line emissions [9] from atomic fluorine were observed. The relative intensity of these lines is known to vary markedly with the pressure and composition of the laser gas mixture [9]. Addition of Ne to the laser gas mixture is known to suppress the red lines and 20 kN m^{-2} of Ne was therefore added to laser mixtures used for this work. The importance of these lines to the present work is the possible coincidence between one of them and visible absorption by Br_2 which could lead to optical pumping of the A or B states. It would be difficult, if not impossible, to optically filter these red lines without affecting the 158 nm output of the laser, however their intensity can be further reduced by using spatial filtering: the red lines formed a wide divergent beam (spontaneous emission) while the 158 nm laser beam was well collimated. Furthermore, fluorescence from Br_2 was recorded for a range of different fillings of laser gas, such that the relative intensities of the red lines changed significantly, and the effects of any optical pumping would have been apparent. All but one of the Br_2 spectra, recorded following this procedure, appeared to be identical: the one exception proved to be non-reproducible.

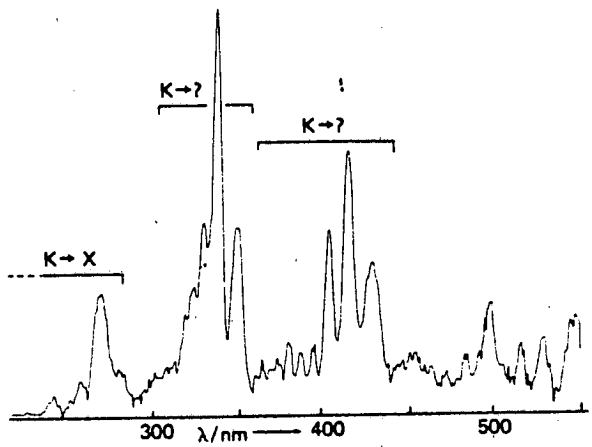

Fig. 1. Low-resolution spectrum of the fluorescence observed from Br_2 following excitation at 158 nm (F_2 laser): P_{Br_2} = 13.3 N m^{-2}; recorded with silicon-diode array head.

3. Results and discussion

3.1. Spectroscopic observations

A low resolution spectrum of the fluorescence produced when 13.3 N m^{-2} of Br_2 was excited by the F_2 laser line is shown in fig. 1. Three distinct spectral systems are clearly present and these are summarised in table 1. The shortest wavelength system extends from the atmospheric cut-off at ≈180 nm up to ≈290 nm (maximum at 275 nm). A second system is observed between 300 and 360 nm and a third system between 360 and 440 nm.

Table 1
Emission systems observed following F_2 laser (158 nm) excitation of Br_2

Designation	Wavelength range	Comments
$K \rightarrow X\ ^1\Sigma_g^+$ (system 1)	180–290 nm	bound to bound emission below 210 nm and bound to free emission between 210 and 290 nm
K → ? (system 2)	300–360 nm	bound to free emission: lower state is probably purely repulsive
K → ? (system 3)	360–440 nm	bound to free emission: lower state is probably purely repulsive

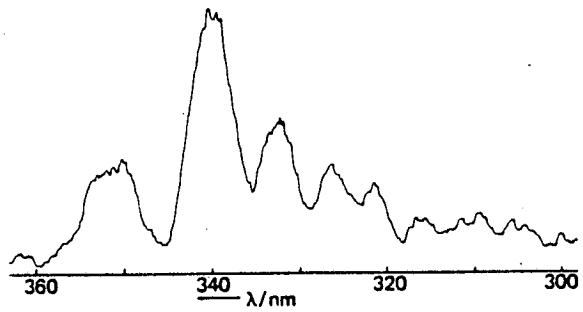

Fig. 2. Medium-resolution spectrum of the 300–360 nm oscillatory continuum: P_{Br_2} = 13.3 N m^{-2}; recorded with intensified vidicon head.

The short wavelength system consists of two distinct regions: between 180 and 210 nm the fluorescence arises from transitions between bound upper and lower states, while above 210 nm the emission involves transitions to unbound regions of the lower state (i.e. it is an oscillatory or structured continuum). This system is thus analogous to the well-known McLennan system of I_2, i.e. $I_2(D\,^1\Sigma_u^+ \rightarrow X\,^1\Sigma_g^+)$, where both bound–bound and bound–continuum emission is also observed [1,3]. Both high- and low-frequency oscillatory structure is observed in this system, again paralleling the structure seen in the McLennan bands of I_2, however, the entire system is shifted to shorter wavelengths for Br_2, as expected. This system is designated as Br_2(K → X) following the current nomenclature in the literature [7], however, we emphasise that the K state of Br_2 appears to be directly equivalent to the better known $D(^1\Sigma_u^+)$ state of I_2.

The two new systems at longer wavelengths both appear to be structured continua. The 300–360 nm system is reproduced under higher resolution in fig. 2. Unlike the K → X system, only a single low-frequency oscillation is superimposed on the continuum. It closely resembles a system that we have recently analysed for I_2 and which lies on the long wavelength side of the McLennan bonds [10], between 350 and 400 nm. Thus both of the new Br_2 systems discussed so far appear to be the direct counterparts of known systems in I_2.

The third system (360–440 nm) is similar to the second and again exhibits only a single low-frequency oscillatory structure although the amplitude is less regular than that for the second system. This may well prove to be the counterpart of an intense system observed from I_2, located between 400 and 450 nm, which has proved difficult to analyse [3,10]. From its appearance the Br_2 system should prove to be more readily analysable. It is important to note in this context that the line width of the F_2 laser ($\lesssim$ 20 cm^{-1}) is at least one order of magnitude less than that of the ArF laser used to study fluorescence from I_2 and thus only a single vibronic level of Br_2 should be excited. This could well result in the simplification of some of the fluorescence features in the case of Br_2. Unfortunately the presence of two isotopes of Br could introduce a complexity that was absent for I_2, which has only one stable isotope, and studies using an isotropically pure sample of Br_2 may be necessary to counter this.

Other weaker fluorescence may well be present in our spectra but it is difficult to be certain of this with the present data. Work at higher resolution and with better signal-to-noise ratios will be required to resolve this point.

Tellinghuisen et al. [11] have also reported a number of fluorescence systems from Br_2 in the region 200–400 nm, however, their spectra were excited with a weak tesla discharge (both in the presence and absence of Ar) and were accounted for in terms of transitions from states that lie in close proximity to the $D'\,^3\Pi_{2g}$ state. It was proposed that the upper states were in local thermal equilibrium with an effective temperature of 360 K. We should not therefore expect any of these emissions to correspond with those reported here, except for the 290 nm band originating from $Br_2(D'\,^3\Pi_{2g} \rightarrow A'\,^3\Pi_{2u})$, which is discussed below.

3.2. *Collisional energy transfer*

As noted earlier the $D(^1\Sigma_u^+)$ state of I_2 readily undergoes interstate transfer and the ensuing electronic cascade process ultimately terminates in what is thought to be the lowest ion-pair ($^3\Pi_{2g}$) state. We therefore investigated the effect of added SF_6, N_2 and He on the Br_2(K) fluorescence discussed above. Addition of SF_6 leads to efficient transfer out of the initially populated state and the intense bands at 270, 335 and 420 nm are almost entirely eliminated for pressures of SF_6 > 1.3 kN m^{-2}. They are replaced by an intense narrow band at 291 nm and a much weaker band at 300 nm (see fig. 3). The 291 nm emission is $\approx 10^2$ times more intense than any of the systems displayed in fig. 1. This band is readily assigned to the $Br_2(^3\Pi_{2g} \rightarrow {}^3\Pi_{2u})$ transition which has been analysed by Sur and Tellinghuisen [12].

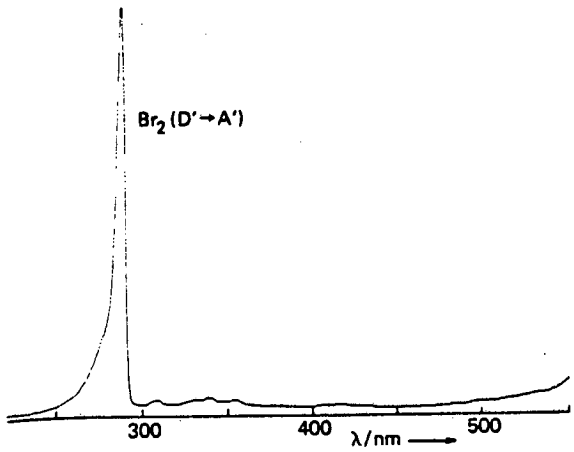

Fig. 3. Low-resolution spectrum of the fluorescence observed from Br_2 (P = 13.3 N m^{-2}) in the presence of SF_6 (P = 2.52 kN m^{-2}) following excitation at 158 nm (recorded with silicon-diode array head). Note that the fluorescence at 291 nm is approximately two orders of magnitude more intense than any of the systems shown in fig. 1.

Addition of N_2 induced similar collisional transfer processes and the end result, namely population of the $^3\Pi_{2g}$ state, was the same. However, with N_2 there was evidence for the participation of intermediate states in the transfer process and features were observed at wavelengths other than those of the initial and final emitting states. Studies at higher resolution will be needed to clarify this point.

Addition of He again resulted in the efficient removal of the initially pumped state, but the 291 nm band did not appear until quite high pressures were achieved (≈10 kN m^{-2}). Intermediate states appear weakly as the pressure is raised but there is also a broad semi-continuous background fluorescence. This may be due to unstructured fluorescence from a wide range of vibronic states and requires further investigation. It is significant that emission from the $^3\Pi_{2g}$ state at low He pressures is broader and blue shifted, by a few nanometers, relative to its appearance at higher pressures and this is consistent with emission from higher vibrational levels of the $^3\Pi_{2g}$ state being important under these conditions.

4. Conclusion

Optical excitation of Br_2 at 158 nm, with an F_2 laser, produces fluorescence from three electronic systems. The dominant fluorescence is from a bound upper state to unbound regions of the lower states which produces a characteristic oscillatory structure superimposed on the continua. The new fluorescence systems for Br_2 correspond closely with known systems of I_2 originating from the $D\,^1\Sigma_u^+$ state.

Collisional interstate transfer from Br_2(K) closely parallels the behaviour of $I_2(D\,^1\Sigma_u^+)$ and leads to efficient population of the lowest ion-pair ($^3\Pi_{2g}$) state. This suggests that the construction of an optically pumped laser, similar to that described [5] for I_2, should be feasible. Further spectroscopic work at higher resolution is planned.

Acknowledgement

We thank the SERC for the provision of laser facilities at the Rutherford Appleton Laboratory and J. Szechi for assistance with the equipment.

References

[1] R.S. Mulliken, J. Chem. Phys. 55 (1971) 288.
[2] D.L. Rousseau and P.F. Williams, Phys. Rev. Letters 33 (1974) 1368;
G.W. King, I.M. Littlewood and J.R. Robins, Chem. Phys. 56 (1981) 145;
F.W. Dalby, G. Petty-Sil, M.H.L. Pryce and C. Tai, Can. J. Phys. 55 (1977) 1033;
J.C.D. Brand, K.J. Cross and N.P. Ernsting, Chem. Phys. 59 (1981) 405;
J.C.D. Brand and A.R. Hoy, Can. J. Phys. 60 (1982) 1209;
K. Kasatani, Y. Tanaka, K. Shibuya, M. Kawasaki, K. Oki, H. Sato and I. Tanaka, J. Chem. Phys. 74 (1981) 895;
H.P. Grieneisen and R.E. Francke, Chem. Phys. Letters 88 (1982) 585;
A.D. Williamson, Chem. Phys. Letters 60 (1979) 451;
K. Chen, L.E. Steenhoek and E.S. Yeung, Chem. Phys. Letters 59 (1978) 222;
U. Heemann, H. Knockel and E. Tiemann, Chem. Phys. Letters 90 (1982) 17;
T. Ishiwata, I. Fujiwara and I. Tanaka, Chem. Phys. Letters 89 (1982) 527;
G.W. King, I.M. Littlewood, R.G. McFadden and J.R. Robins, Chem. Phys. 41 (1979) 379.
[3] M. Martin, C. Fotakis, R.J. Donovan and M.J. Shaw, Nuovo Cimento 63B (1981) 300.
[4] H. Hemmati and G.J. Collins, Chem. Phys. Letters 67 (1979) 5.

[5] M.J. Shaw, C.B. Edwards, F. O'Neill, C. Fotakis and R.J. Donovan, Appl. Phys. Letters 38 (1980) 346.
[6] R.J. Donovan, B.V. O'Grady and L. Lain, J. Chem. Phys., to be published.
[7] P. Venkateswarlu, Can. J. Phys. 47 (1969) 2525.
[8] H. Pummer, K. Hohla, M. Diegelmann and J.P. Reilly, Opt. Commun. 28 (1979) 104.
[9] T.R. Loree and R.C. Sze, Opt. Commun. 21 (1977) 255.
[10] K.P. Lawley, M.A. MacDonald and R.J. Donovan, Chem. Phys. Letters 92 (1982) 322.
[11] J. Tellinghuisen, P. Berwanger, J.G. Ashmore and K.S. Viswanathan, Chem. Phys. Letters 84 (1981) 528.
[12] A. Sur and J. Tellinghuisen, J. Mol. Spectry. 88 (1981) 323.

OSCILLATORY CONTINUUM EMISSION FROM IBr

M. MACDONALD, J.P.T. WILKINSON, C. FOTAKIS *, M. MARTIN ‡ and R.J. DONOVAN
Department of Chemistry, University of Edinburgh, West Mains Road, Edinburgh EH9 3JJ, UK

Received 23 May 1983

Optical excitation of IBr at 193 nm (ArF laser) leads to strong fluorescence in the region 280–460 nm. This fluorescence is dominated by two oscillatory continua resulting from bound–free radiative transitions.

1. Introduction

A number of oscillatory emission continua [1,2] have been observed from diatomic halogen molecules [3–6] and these have recently been employed to derive interatomic potentials [2,6].

Two oscillatory continua have been observed previously from discharges through IBr and less complete data have been obtained using optical excitation [7,8]. However, the agreement between these studies was not good, probably due to the wide range of vibrational levels populated in the discharge studies which results in the overlapping of many individual spectra. We have shown previously that selective excitation, using laser lines or other discrete excitation sources, results in good quality spectra which can then be used to derive interatomic potentials. In the present work we show that excitation of IBr with the output of an ArF laser (193 nm) produces two oscillatory continuum systems in the region 460–320 nm.

2. Experimental

IBr vapour was optically excited at 193 nm by an ArF laser. The resulting fluorescence was observed at right angles to the laser beam and dispersed with a Jobin–Yvon (HRS 2) 0.3 m monochromator (resolution ≈2.6 nm), equipped with an EG&G optical multichannel analyser (OMA) at the exit port [4]. Two types of OMA head were employed: for work above 400 nm an intensified vidicon detector (type 1254 SIT) was used: wider spectral coverage was obtained with an intensified silicon photodiode array head (type 1420).

IBr was prepared by addition of equimolar amounts of Br_2 to I_2. The reaction to form IBr is rapid and leads to an equilibrium mixture which is predominantly IBr (90%) but contains small amounts of I_2 and Br_2. In order to reduce further the I_2 present, which leads to strong fluorescence in the same region as IBr, excess Br_2 was added to most of the samples used to record spectra in this work.

3. Results and discussion

The oscillatory continuum emissions, excited the ArF laser line at 193 nm, from both IBr and I_2, in the region 390–490 nm, are compared in fig. 1. Even small pressures of I_2 (≈26 N m^{-2}) give rise to intense fluorescence [4] and it is necessary to suppress the I_2, present in equilibrium with IBr, to obtain good spectra. This can be readily achieved by adding an excess of Br_2 to the equilibrium mixture as fluorescence from Br_2, excited at 193 nm, is very much weaker than that from either IBr or I_2.

By examining the fluorescence from a range of equilibrium mixtures and from pure I_2 and Br_2, over

* Present address: Department of Physics, University of Crete, Iraklion, POB 470, Crete, Greece.
‡ Present address: CSIC, Instituto de Quimica Fisica, "Rocasolano", Serrano 119, Madrid 6, Spain.

0 009-2614/83/0000–0000/$ 03.00

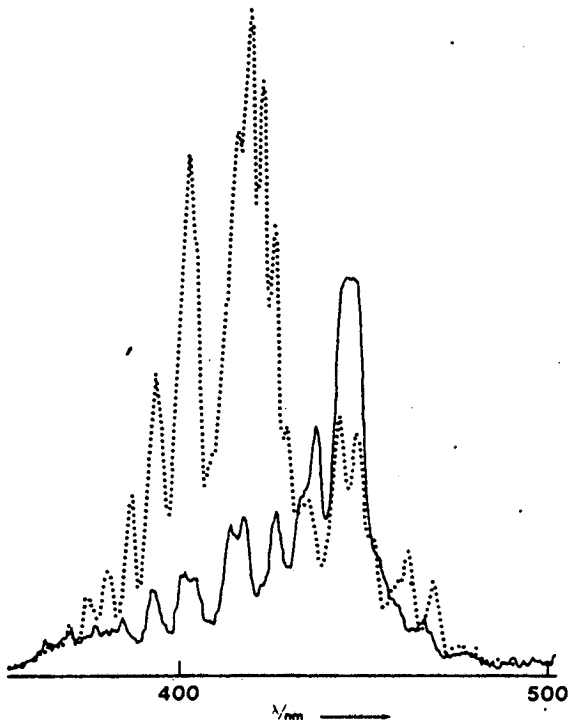

a range of total pressures, we have shown that the oscillatory continua shown in fig. 2 are due to IBr (the solid line in fig. 1 is predominantly due to IBr but contains some fluorescence due to residual I_2).

Starting with the shortest-wavelength emission (fig. 2) the broad peak at 200 nm is assigned to bound–bound fluorescence originating from the initially populated upper state and terminating on bound levels of the ground electronic state. There is also a component of scattered light from the laser (193 nm) at this wavelength and work at higher resolution will be needed to derive any further useful information from the spectrum in this region. The boundary between bound–bound and bound–free

◀ Fig. 1. Oscillatory continuum emission from IBr (solid line: $P_{IBr} = 400$ N m^{-2}) and I_2 (dotted line: $P_{I_2} = 26$ N m^{-2}) following excitation at 193 nm (ArF laser). The spectrum has not been corrected for detector response which decreases very rapidly below 390 nm. It should be noted that there is some slight contamination of the IBr spectrum by fluorescence from residual I_2.

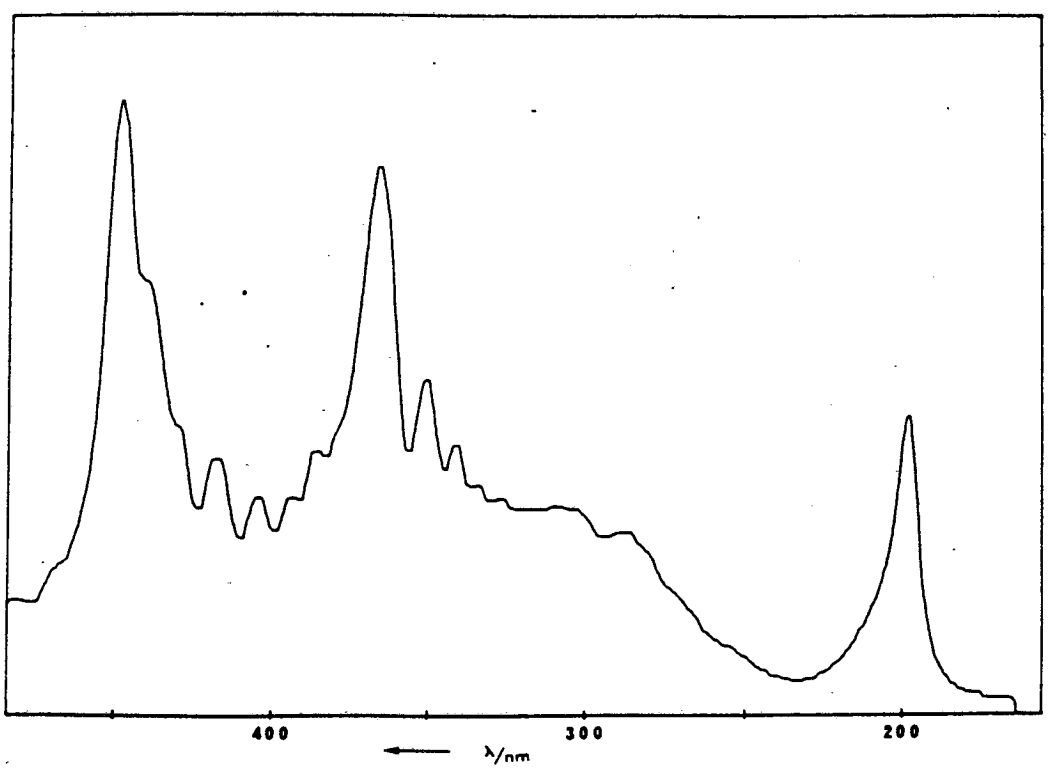

Fig. 2. Fluorescence from IBr following excitation at 193 nm.(ArF laser). The spectrum has not been corrected for detector response ($P_{IBr} = 5.3$ N m^{-2}; $P_{Br_2} = 290$ N m^{-2}).

fluorescence lies at ≈270 nm and the emission on the long-wavelength side of this limit resembles that observed previously [2–4] from I_2 and leads to the characteristic broad oscillatory (structured) continuum in the region 320–380 nm. The system must be the equivalent of the McLennan system of I_2 and will thus be of great value in providing a means by which the *upper* state potential, associated with this fluorescence, can be obtained [2,6].

Between 390 and 460 nm a second oscillatory continuum is observed (figs. 1 and 2) and by analogy with I_2 we assign this to a transition terminating on a repulsive lower state [6]. Once the upper state potential has been derived, using the spectrum below 380 nm, the *lower* (repulsive) state, associated with the 390–460 nm oscillatory continuum, can be determined [6].

Up to this point we have tacitly assumed that the upper state associated with the observed oscillatory continua is an ion-pair state similar to the $D\,^1\Sigma_u^+$ state of I_2. However, the dominant absorption feature in the spectrum of IBr at 193 nm is associated with a transition to a low vibrational level of a Rydberg state [9,10]. This type of state could not give rise to the extensive oscillatory continua observed here, although it could yield bound–bound fluorescence to low vibrational levels of the ground electronic state and possibly some narrow regions of continuum emission. No such emissions could be identified from our spectra and it appears that the fluorescence yield from this Rydberg state is low. The broad emission systems shown in fig. 2 are characteristic of transitions from high vibrational levels of a broad ion-pair state and, by analogy with I_2 and Br_2, we would expect absorption to such a state to occur at 193 nm. The highly congested structure associated with absorption to ion-pair states of the halogens makes their observation at low resolution very difficult and only broad "continuous" absorption, underlying the Rydberg features, would be apparent under such observational conditions. Further work at high resolution is thus needed if the absorption spectrum of IBr, in the region below ≈200 nm, is to be fully characterised.

In the absence of a high-resolution spectrum, we have adopted a different approach in order to confirm the involvement of an ion-pair state in the absorption process at 193 nm. By using the 184.9 nm line of Hg, which does not coincide with any of the Rydberg absorptions of IBr, we have been able to produce analogous oscillatory continua to those shown in figs. 1 and 2. Furthermore, the monochromated output from a xenon continuum lamp at 200 nm ($\Delta\lambda$ = 5 nm) also leads to similar fluorescence spectra, although with much weaker overall intensity (due to very weak absorption in the tail of the system). It is clear from these observations that an absorption system underlying the longest-wavelength Rydberg bands of IBr is responsible for the excitation process which leads to the fluorescence systems described above. This work is continuing and will be reported in greater detail elsewhere.

Acknowledgement

We thank the SERC for an equipment grant, for the use of the ultraviolet laser facility at the Rutherford Appleton Laboratory, and for a fellowship for MM. We also thank the British Council for a travel grant for CF.

Rerefences

[1] R.S. Mulliken, J. Chem. Phys. 55 (1971) 309.
[2] J. Tellinghuisen, Chem. Phys. Letters 29 (1974) 359.
[3] H. Hemmati and G.J. Collins, Chem. Phys. Letters 75 (1980) 488.
[4] M. Martin, C. Fotakis, R.J. Donovan and M.J. Shaw, Nuovo Cimento 63 (1981) 300.
[5] M. MacDonald, R.J. Donovan and M.C. Gower, Chem. Phys. Letters 97 (1983) 72.
[6] K.P. Lawley, M.A. McDonald, R.J. Donovan and A. Kvaran, Chem. Phys. Letters 92 (1982) 322.
[7] R.K. Asundi and P. Venkateswarlu, Indian J. Phys. 21 (1947) 76;
P. Venkateswarlu and R.D. Verma, Proc. Ind. Acad. Sci. A47 (1958) 150.
[8] A. Filippov, Z. Physik 50 (1928) 861.
[9] K.P. Huber and G. Herzberg, Molecular structure and molecular spectra, Vol. 4. Constants of diatomic molecules (Van Nostrand, Princeton, 1979).
[10] R.J. Donovan and D. Husain, Trans. Faraday Soc. 64 (1968) 2325.

FORMATION OF ELECTRONICALLY EXCITED XeBr BY REACTION OF EXCITED IBr WITH GROUND-STATE Xe

J.P.T. WILKINSON, M. MacDONALD and R.J. DONOVAN
Department of Chemistry, University of Edinburgh, West Mains Road, Edinburgh, EH9 3JJ, UK

Received 28 July 1983

Reaction between *ground-state* Xe and electronically excited IBr (optically excited at 193 nm) is shown to yield electronically excited $XeBr^*(B)$, which is observed in fluorescence at 280 nm.

1. Introduction

The reactions of electronically excited rare gas atoms with halogen and halogen containing molecules [1,2], e.g.

$$Ar^* + Cl_2 \rightarrow ArCl^* + Cl \quad (1)$$

have been studied extensively due to the importance of excited rare gas halide molecules in the development of high-power laser systems. It has also been shown that reaction of electronically excited halogen molecules with *ground-state* rare gas atoms can lead to the formation of excited rare gas halide molecules, e.g.

$$Cl_2^* + Kr \rightarrow KrCl^* + Cl. \quad (2)$$

In one case synchrotron radiation, in the vacuum ultraviolet (≈135 nm), was employed to excite molecular chlorine [3]. The excitation of $XeCl_2$ collision complexes using vacuum ultraviolet laser radiation (158 nm) has also been employed [4]. In a third example laser multiphoton excitation of Br_2 was used to produce excited XeBr [5].

In the present work we show that $XeBr^*$ can be readily produced by reaction of optically excited IBr (λ = 193 nm) with ground-state Xe atoms. This is a far simpler experimental method than any of those described previously.

2. Experimental

IBr was excited using the 193 nm output of an ArF laser (Lambda Physik EMG 201) [6]. The fluorescence was dispersed with a small optically fast monochromator (0.3 m, Jobin–Yvon HRS-2) and detected with an optical multi-channel analyser (Princeton Applied Research/EG&G, OMA2). The signal-to-noise ratio was sufficient to record a full spectrum from a single laser pulse but in general several (≈20) pulses were averaged, on the detector head, to ensure that weaker features were clearly observed. IBr was prepared and handled as described previously [6]. Ar (B.O.C. high purity grade) and Xe (B.O.C. spectroscopic grade) were used directly as received.

3. Results and discussion

The fluorescence from IBr following excitation at 193 nm is illustrated in fig. 1a. The main features have been described [6]. Briefly, two oscillatory continua are seen between 300–380 nm and 390–460 nm. Below ≈270 nm the spectrum is discrete but is not resolved with our present instrumentation. The spectrum shown in fig. 1a was recorded at slightly higher resolution than the spectrum reported previously [6] and distinct structure is now observable on the short-wavelength side of the intense band at 450 nm. Structure is also now apparent on the long-wavelength edge of the

0 009-2614/83/0000–0000/$ 03.00

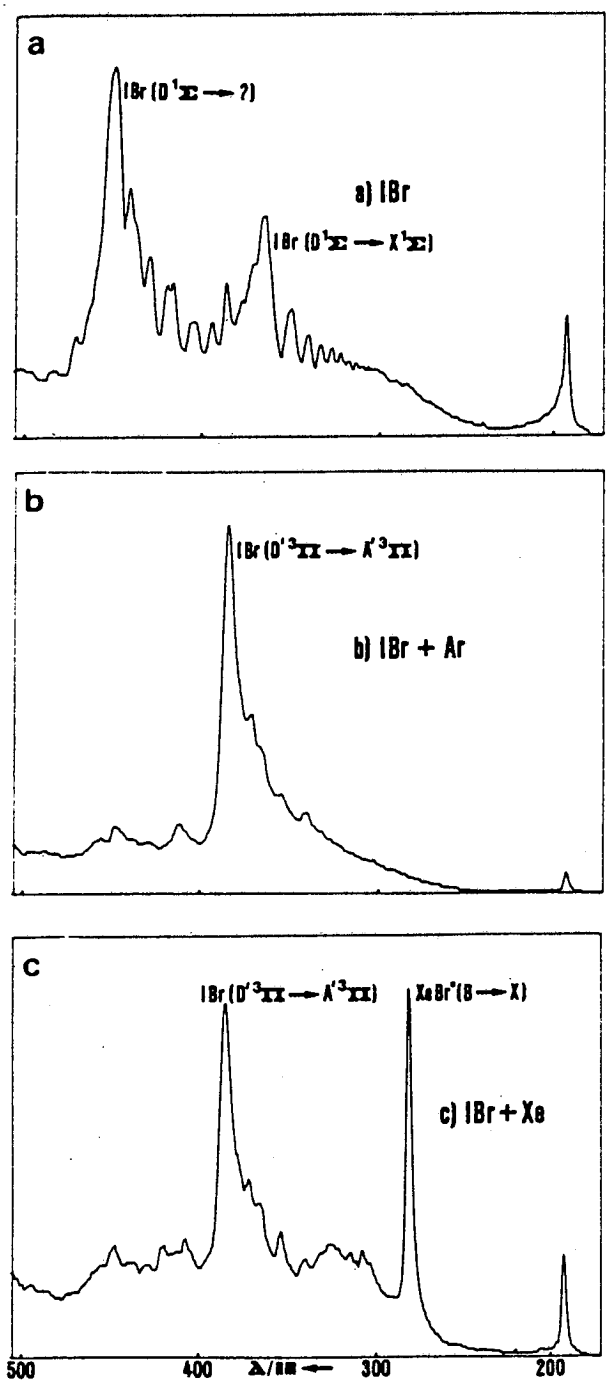

Fig. 1. Fluorescence observed following excitation of IBr at 193 nm (ArF laser) (a) IBr (P_{IBr} = 173 N m^{-2}, P_{Br_2} = 176 N m^{-2}), (b) IBr + Ar (P_{IBr} = 160 N m^{-2}, P_{Br_2} = 147 N m^{-2}, P_{Ar} = 7.45 kN m^{-2}), (c) IBr + Xe (P_{IBr} = 173 N m^{-2}, P_{Br_2} = 176 N m^{-2}, P_{Xe} = 7.09 kN m^{-2}).

band centred at 370 nm and the oscillatory structure' extending to shorter wavelengths (360–300 nm) is more fully developed.

As IBr exists in equilibrium with both I_2 and Br_2, and because I_2 gives rise to intense fluorescence when excited at 193 nm, an excess of Br_2 was added to suppress I_2: the partial pressures used were $P_{IBr} \approx P_{Br_2} \approx$ 170 N m^{-2}.

Addition of Ar to this system results in efficient interstate transfer and strong fluorescence from the D' state (i.e. D' $^3\Pi \rightarrow$ A' $^3\Pi$) at 385 nm. This is illustrated in fig. 1b. As the pressure of Ar is raised from 1 to 80 kN m^{-2} the D' $\rightarrow$ A' system sharpens considerably due to vibrational relaxation within the D' state. Quenching into the D' state of IBr by Ar is very efficient in contrast to its removal which is extremely inefficient, except for radiative processes. This behaviour is directly analogous to that observed for $I_2(D\,^1\Sigma_{u^+})$ and its collisional transfer into the close lying D' $^3\Pi_{2g}$ state [7]. Clearly an optically pumped IBr laser, analogous to the efficient I_2 laser system reported previously [8], could be readily constructed.

Quenching of excited IBr by Xe is illustrated in fig. 1c. In addition to the D' $\rightarrow$ A' emission at 385 nm a second strong emission feature is observed at 280 nm. This is readily identified as due to XeBr*(B $\rightarrow$ X) exciplex emission [9] and must result from the reaction of electronically excited IBr with ground-state Xe atoms. Energy transfer from IBr* to Xe followed by reaction of excited Xe atoms with ground-state IBr can be excluded as there is insufficient energy available to populate even the lowest excited state of Xe. We can also exclude reaction of translationally hot Br atoms, formed following bound-free fluorescence, as the energy available is again insufficient to reach the observed emitting state of XeBr*. We therefore conclude that XeBr(B) is formed by reaction of electronically excited IBr with ground-state Xe atoms. Furthermore, as the XeBr(B) fluorescence increases in parallel with the IBr(D' $\rightarrow$ A') emission, while the initial IBr fluorescence (fig. 1a) is quenched, we can assign the state involved in this reaction as IBr(D $^1\Sigma$), i.e.

$$IBr(D\,^1\Sigma) + Xe \rightarrow XeBr(B) + I. \qquad (3)$$

From the available thermodynamic data it is clear that reaction (3) is close to thermoneutral and the narrow emission band observed confirms that XeBr(B) is formed with very little excess vibrational energy. The overall

quantum efficiency from formation of XeBr(B) appears to be quite high (≈30%), however, further quantitative studies are required to define this figure more precisely. Never the less it suggests that optical pumping of IBr with an ArF laser provides a relatively efficient method for achieving laser action from $XeBr^*$ at 280 nm.

Acknowledgement

We thank S.E.R.C. for the provision of laser facilities at the Rutherford Appleton Laboratory.

References

[1] M.F. Golde and B.A. Thrush, Chem. Phys. Letters 29 (1974) 486.
[2] J.E. Velazco and D.W. Setser, J. Chem. Phys. 62 (1975) 1990.
[3] M.C. Castex, J. Le Calvé, D. Haaks, B. Jordan and G. Zimmerer, Chem. Phys. Letters 70 (1980) 106; Nuovo Cimento 63B (1981) 265.
[4] H.P. Grieneisen, H. Xue-Jing and K.L. Kompa, Chem. Phys. Letters 82 (1981) 421.
[5] D.J. Erlich and R.M. Osgood, J. Chem. Phys. 73 (1980) 3038.
[6] M. MacDonald, J.P.T. Wilkinson, C. Fotakis, M. Martin and R.J. Donovan, Chem. Phys. Letters 99 (1983) 250.
[7] M. Martin, C. Fotakis, R.J. Donovan and M.J. Shaw, Nuovo Cimento 63B (1981) 300.
[8] M.J. Shaw, C.B. Edwards, F. O'Neill, C. Fotakis and R.J. Donovan, Appl. Phys. Letters 37 (1980) 346.
[9] K. Tamagake, D.W. Setser and J.H. Kolts, J. Chem. Phys. 74 (1981) 4286.

DETERMINATION OF ABSOLUTE QUENCHING RATES AND FLUORESCENCE LIFETIME FOR IBr(D) USING SYNCHROTRON RADIATION

R.J. DONOVAN, G. GILBERT, M. MACDONALD
Department of Chemistry, University of Edinburgh, West Mains Road, Edinburgh EH9 3JJ, UK

and

I. MUNRO, D. SHAW and G.R. MANT
SERC Daresbury Laboratory, Daresbury, Warrington WA4 4AD, UK

Received 11 June 1984

The fluorescence lifetime for the first optically accessible ion-pair state of IBr ($E \approx 50000$ cm^{-1}) has been determined using pulsed synchrotron radiation (single bunch mode: $\Delta t = 200$ ps). These data are used to convert relative rate data for quenching by N_2, O_2 and CH_4 into absolute data.

1. Introduction

The ion-pair states of the halogens ($E \approx 50000$ cm^{-1}) exhibit a number of interesting chemical and physical properties. Chemically they are very aggressive, reacting readily with hydrocarbons [1,2] and attacking even perfluorinated hydrocarbons [3]. It has also been shown that they can react with rare-gas atoms to yield electronically excited rare-gas halide molecules [4].

The ion-pair states of the halogens are also interesting spectroscopically as their main fluorescence systems are generally structured (oscillatory) continua [5–10].

We are currently engaged in a systematic study of the spectroscopy, physical quenching and chemical behaviour of the ion-pair states of I_2 and IBr. During the course of this work, we have determined a number of relative quenching efficiencies using steady-state fluorescence techniques. In order to convert these relative data into absolute quenching rate constants, we require the fluorescence lifetime of IBr under the conditions of our experiments. The fluorescence lifetime is expected to be of the order of a few nanoseconds, and thus fast excitation and detection systems are essential for this measurement. In this communication we describe the use of pulsed synchrotron radiation in conjunction with single-photon counting to determine the fluorescence lifetime of IBr. This provides an ideal method for this type of determination.

2. Experimental

Synchrotron radiation from the electron storage ring at the SERC Daresbury Laboratory was used for the time-resolved studies reported here. The storage ring was operated in single bunch mode, giving 200 ps duration light pulses with a repetition time of 320 ns. The radiation, dispersed by a Spex 1500 SP Czerny–Turner monochromator, excited samples of IBr contained in a Spectrosil cell mounted in a sample chamber. An excitation wavelength of 188 nm (bandpass 3 nm) was used in these studies. Fluorescence, after passage through an LF30 filter ($\lambda > 300$ nm), was detected by a Mullard XP2020Q photomultiplier at right angles to the excitation beam. The fluorescence lifetime was determined by measuring successive time intervals between photomultiplier pulses (after constant fraction discrimination) and the zero time reference signal from the storage ring, using a time to amplitude converter

(TAC). Output pulses from the TAC were accumulated in a multichannel analyser. Time spectra were recorded locally on a PDP 11/04 and also transferred to the AS7000 mainframe computer at Daresbury for data storage and analysis.

Relative fluorescence quenching data were obtained using a Perkin–Elmer 650/40 fluorimeter. A standard 1 cm^2 Spectrosil fluorescence cell was fitted with a greaseless tap and filled from a conventional vacuum line.

3. Results and discussion

The fluorescence from IBr, excited at 200 nm, is illustrated in trace (a) of fig. 1. Two oscillatory continuum systems are observed as described previously [7]. Care must be taken to suppress I_2, which exists in equilibrium with IBr, as I_2 also gives rise to strong fluorescence in this same region. Suppression in I_2, to an acceptable level, can be achieved by adding excess Br_2 and in the work reported here an equal pressure of Br_2 was added to all samples of IBr: this reduced the I_2 partial pressure to approximately 1% of that for IBr.

Addition of a quenching gas reduces the oscillatory continuum emission (fig. 1) however some interstate transfer is observed and emission from the D′ state of IBr occurs at 383 nm [4]. With CH_4 and O_2 as quenching gases the D′ state is also rapidly quenched and the peak at 383 nm is only observed weakly at intermediate pressures (see traces (b) and (c) of fig. 1). With N_2 the emission from the D′ state increases steadily with increasing pressure and eventually dominates the spectrum. The behaviour with N_2 is directly analogous to that observed previously for quenching by Ar [4].

By careful measurement of the decrease in the oscillatory continuum emission from IBr, as a function of the pressure of added quenching gas, relative quenching rates are readily derived (Stern–Volmer method). These relative rates can be placed on an absolute basis if the fluorescence lifetime of IBr (under the conditions used for the Stern–Volmer studies), is known. By analogy with I_2 the radiative lifetimes of the ion-pair states of IBr are expected to be of the order of 10 ns. This is a difficult time regime to work in with conventional instrumentation, particularly as the required excitation wavelength is <200 nm. However, the task is relatively

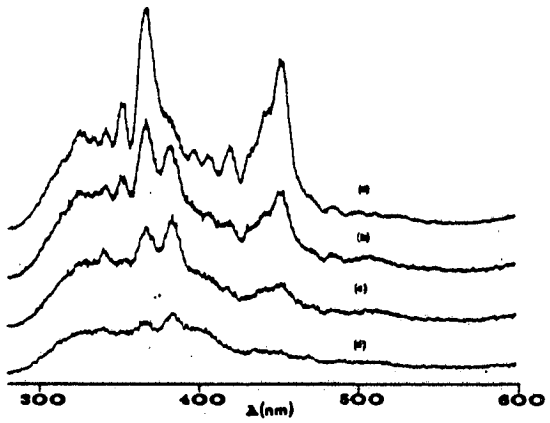

Fig. 1. Quenching of electronically excited IBr by CH_4. Trace (a) shows the oscillatory continuum emission observed in the absence of CH_4. Traces (b)–(d) show the effect of increasing pressure of CH_4: (b) P_{CH_4} = 280 N m^{-2}, (c) P_{CH_4} = 1.3 kN m^{-2}, (d) P_{CH_4} = 6.7 kN m^{-2}; in all traces $P_{IBr} = P_{Br_2}$ = 120 N m^{-2}.

straightforward using pulsed (single bunch) synchrotron radiation and we have therefore used this technique for the present study.

The decay of IBr fluorescence following excitation at 188 nm ($\Delta\lambda$ = 3 nm), with pulsed synchrotron radiation, is shown in fig. 2. These data give an excellent fit to an exponential decay over two and a half decades and the fluorescence lifetime can be obtained with high *precision*. The greatest uncertainty in these experiments arises from the handling of halogen molecules at low pressure where wall adsorption becomes a problem. From experience with a wide range of other experiments we would place an uncertainty of ±15% on the measured partial pressures for the halogens. This is the main limitation in the *accuracy* of the rate data reported here.

We have observed the decay of IBr fluorescence over a range of conditions and by extrapolating plots of the observed fluorescence lifetimes to zero pressure we obtain a pure *radiative lifetime* of 27 ± 4 ns. Under the typical conditions used for the Stern–Volmer studies (e.g. $P_{IBr} = P_{Br_2}$ = 266 N m^{-2}) the fluorescence lifetime was determined as 12 ± 2 ns. Quenching by IBr and/or Br_2 is clearly very efficient and we propose to study this in more detail in the future.

For our present purposes, we require the lifetime under the conditions for the Stern–Volmer studies in order to convert the relative rate data into absolute

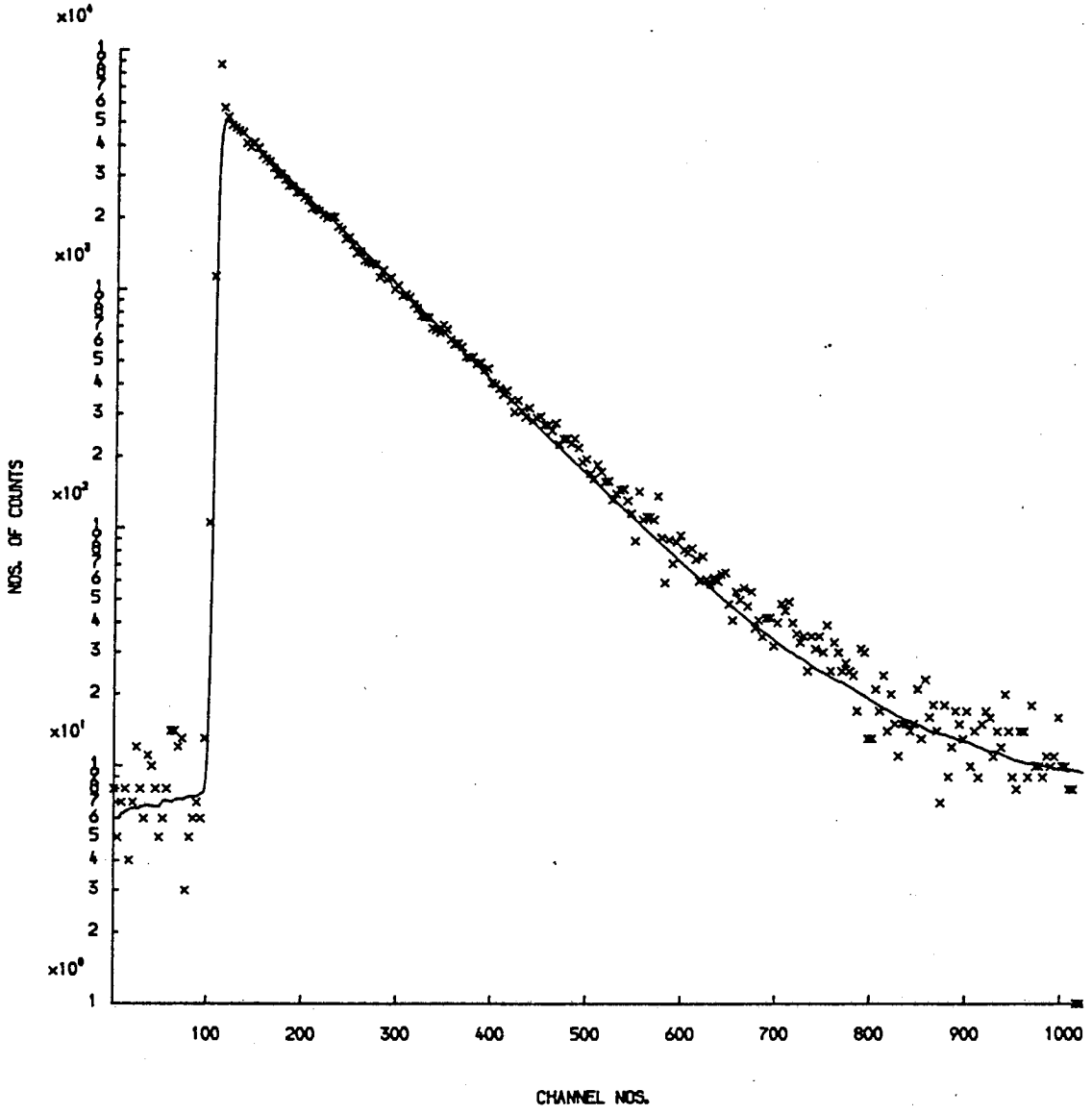

Fig. 2. Decay of IBr fluorescence following excitation at 188 nm with pulsed synchrotron radiation ($P_{IBr} = P_{Br_2} = 133$ N m^{-2}: time scale, 1 channel = 0.1132 ns).

data. Table 1 gives values for the absolute rate constants for quenching of IBr by O_2, N_2 and CH_4 determined in this way. Quenching by all three gases is clearly very efficient and the rate constants are comparable to those observed for quenching of the D 0_u^+ ion-pair states of I_2 [2]. However, they are in sharp contrast with the much lower efficiencies observed for the low-lying valence states of the halogens [11]. Quenching

Table 1
Absolute rate data for quenching of eletronically excited IBr

Quenching gas	k (cm^3 molecule^{-1} s^{-1})
N_2	$(5.0 \pm 1.0) \times 10^{-10}$
O_2	$(2.1 \pm 0.3) \times 10^{-10}$
CH_4	$(9.4 \pm 1.0) \times 10^{-10}$

of $I_2(D\,0_u^+)$ by CH_4 and O_2 is known to lead to bond cleavage and it will be interesting to see if similar reactions occur with the ion-pair states of IBr. The main channel in the quenching of electronically excited IBr by N_2 appears to be transfer into the lowest (D′) ion-pair state from which fluorescence to the A′ state is the main decay process.

Further work on the chemical and physical quenching of the ion-pair states of IBr is in progress.

Acknowledgement

We thank the SERC for use of the synchrotron radiation facility at the Daresbury Laboratory.

References

[1] L.C. Glasgow and J.E. Willard, J. Phys. Chem. 77 (1973) 1585.
[2] R.J. Donovan, B.V. O'Grady, L. Lain and C. Fotakis, J. Chem. Phys. 78 (1983) 3727.
[3] Zhang Yun-Wu, W. Fuss and K.L. Kompa, J. Photochem. 23 (1983) 311.
[4] J.P.T. Wilkinson, M. MacDonald and R.J. Donovan, Chem. Phys. Letters 101 (1983) 284.
[5] R.S. Mulliken, J. Chem. Phys. 55 (1971) 309.
[6] J. Tellinghuisen, Chem. Phys. Letters 29 (1974) 359.
[7] M. MacDonald, J.P.T. Wilkinson, C. Fotakis, M. Martin and R.J. Donovan, Chem. Phys. Letters 99 (1983) 250.
[8] M. MacDonald, R.J. Donovan and M.C. Gower, Chem. Phys. Letters 97 (1983) 72.
[9] K.P. Lawley, M. MacDonald, R.J. Donovan and A. Kvaran, Chem. Phys. Letters 92 (1982) 322.
[10] M. Martin, C. Fotakis, R.J. Donovan and M.J. Shaw, Nuovo Cimento B63 (1981) 300.
[11] J.I. Steinfeld, JILA Information Centre Report No. 24, University of Colorado, Boulder, Colorado (1984).

Appendix 3

Conferences and Lectures Attended

Lectures Attended

In accordance with the regulations of the University of Edinburgh, the Department of Chemistry, the following lectures and lecture courses were attended during the past three years.

1. Fortran 77 Computing Course
2. Microcomputers - 1 week course.
3. Lasers in Chemistry
4. The Chemistry of the Photographic Process
5. Least Squares Methods
6. R.K.R. Theory

In addition, many of the regular departmental seminars and all research group meetings were attended.

Conferences Attended

1. 7th International Symposium on Gas Kinetics (August 1982).
2. Two day conference on diatomic molecules to mark the retiral of R.F. Barrow, Oxford (April 1983).
3. 8th International Symposium on Gas Kinetics (July 1984).